

University of Nottingham
UK | CHINA | MALAYSIA

Department of Molecular Therapeutics and Formulation

School of Pharmacy

Non-covalent polymer and drug complexes as targeted delivery system for pulmonary delivery

Huitong (Lucy) Li, MPharm

Thesis submitted to the University of Nottingham

for the degree of Doctor of Philosophy

September 2020

"Have the courage to follow your heart and intuition. They somehow know what you truly want to become."

Steve Jobs

Abstract

Pulmonary delivery is increasingly seen as an attractive, non-invasive route for the delivery of forthcoming protein therapeutics. However, the lung presents specific barriers for macromolecular/protein therapeutics. Susceptibility to enzymatic degradation, poor absorption across epithelial barrier, as well as lung induced immunogenicity are significant challenges to be addressed if this approach is to be adopted as a viable alternative for protein delivery. In this context, nanomedicine and, in particular, polymer therapeutics (PT) is emerging as a powerful alternative strategy to overcome these limitations. To this aim, in the present PhD project we utilised non-covalent polymer-protein nanocomplexes to allow reversible complexations of protein formulation and investigate their potential to protect and release them at the target site following pulmonary administration. It has been recognised that nanocarriers conjugated with specific ligands can increase the interaction with epithelial cells which makes ligand targeted delivery a very attractive area for in-depth research.

In Chapter 3, we describe protein complexes with a new 'complexing excipient' - vitamin B_{12}-targeted poly(ethylene glycol)-*block*-poly(glutamic acid) (PEG-*b*-pGA) copolymer. Native B_{12} was first activated at the 5'-hydroxyl group of the ribose moiety using 1,1'-carbonyldiimidazole (CDI) followed by the addition of α-

dibenzocyclooctyne-amine giving α-dibenzocyclooctyne-vitamin B_{12}. The product was precipitated, purified by preparative TLC and characterised by mass spectrometry ready to react with azide-terminated linear PEG-*b*-poly(glutamic acid) *via* copper-free azide-alkyne cycloaddition to afford the desired targeted B_{12}-PEG-*b*-pGA copolymers. The synthesis of azide-terminated linear PEG-*b*-pGA started from a commercially available azide-PEG-amine 3500 precursor acting as a macroinitiator for NCA polymerisation. Following click reaction, a purification step by dialysis yielded the desired B_{12}-PEG_{3k}-*b*-pGA copolymer. These form complexes in sub-200 nm size with a model protein interacting *via* ionic interaction, suitable for cellular targeting and intracellular delivery. Initially we confirmed expression of vitamin B_{12}-internalisation receptor (CD320) by Calu-3 cells of the *in vitro* lung epithelial model used and demonstrated enhanced B_{12} receptor-mediated cellular internalisation of B_{12}-targeted complexes, relative to non-targeted counterparts or protein alone. The nanocomplexes were spray-dried into inhalable particles with aerodynamic diameter within the suitable range (<5 μm) for lower airway deposition. *in vivo* lung tolerance studies of copolymer-protein complexes demonstrated that repeated administration of formulated dry powders over a 3 week period in healthy BALB/c mice induced no significant toxicity or indications of lung inflammation, as assessed by cell population count and quantification of IL-1β, IL-6, and TNF-α pro-inflammatory

markers. Importantly, the *in vivo* data appear to suggest that B_{12}-targeted polymer complexes administered as dry powder enhance lung retention of their protein payload, relative to protein alone and non-targeted counterparts.

Next, to test the versatility of this formulation approach, we sought to investigate the inclusion of different targeting ligands detailed in Chapter 4 and 5. Studies have suggested a potential use of another essential vitamin – biotin – as an endocytosis ligand. Biotin receptor was found overexpressed in cancer cells, relatively more than folate or vitamin B_{12} receptors, and investigated as ligand for targeted delivery of nano-systems and prodrugs. Furthermore, this vitamin is a promoter of cell growth in many cell types which does not limit this delivery system only to target cancer cells. To this aim we synthesised biotin-terminal PEG_{2k}-*b*-poly(glutamic acid) linear copolymers using commercially available biotin-PEG_{2k}-amine suitable to act as a macroinitiator for *N*-carboxyanhydrides (NCA) ring opening polymerisation using the same strategy utilised previously for the B_{12} targeted B_{12}-PEG-*b*-pGA polymer synthesis. These also form complexes in sub-200 nm size with a model protein lysozyme. Flow cytometry data demonstrated statistically significant increased cellular internalisation by biotin receptor positive A549 cells of biotin-PEG_{2k}-*b*-$GA_{10/30}$:lysozyme nanocomplexes relative to untargeted mPEG_{2k}-*b*-GA_{30}:lysozyme control complexes or 'free' Cy5-lysozyme. By fluorescently labelling lysozyme and tagging

biotin targeted copolymers after cellular internalisation with Alexa Fluor™ 488 conjugated streptavidin, co-localisation analysis of the two fluorescently labelled polymer and protein using Pearson's correlation analysis was performed on several confocal images. An average *r* value of ~ 0.5 was obtained, suggesting that at 1 h after the complexes were applied to, and internalised by A549 cells, lysozyme and biotin-PEG_{2k}-*b*-GA_{10} copolymers were co-localised.

These promising preliminary results encouraged us for further *in vitro* investigation in understanding the cellular internalisation mechanism that might be responsible for targeted polymer-protein complex uptake. Therefore, work was carried out to probe the mechanisms of entry into the cells of targeted biotin-PEG_{2k}-*b*-pGA:lysozyme nanocomplex, and whether it significantly differs to free lysozyme or non-targeted mPEG_{2k}-*b*-GA_{30}:lysozyme nanocomplexes. In this respect, a panel of pharmacological inhibitors was used to investigate which endocytic mechanisms were responsible for cellular uptake of our targeted nanoparticles. Dynamin which plays a vital role in vesicular trafficking processes by facilitating vesicle pinching of membranes of cells and organelles was found to play a major role in the uptake of all 3 samples, with lysozyme predominantly taken up *via* the clathrin mediated pathway while mPEG_{2k}-*b*-GA_{30}:lysozyme and biotin-PEG_{2k}-*b*-$GA_{10/30}$:lysozyme preferred the caveolae-mediated pathway;

inhibiting the caveolae pathway had higher impact on the uptake of biotin-PEG_{2k}-*b*-$GA_{10/30}$:lysozyme nanocomplexes.

The use of targeted PEG-*b*-pGA copolymer delivery systems to successfully complex and deliver model protein lysozyme to epithelial cells *in vitro* and *in vivo* pave the way for further investigations, wherein the PEG-*b*-pGA copolymer can be used to deliver protein or peptide therapeutics and maintain or improve the therapeutic effect. Furthermore, it was envisaged that the PEG-*b*-pGA copolymer delivery system can potentially be applied not only to proteins but also small molecule therapeutics formulated in nano-sized entities, which became the focus of the final chapter of this thesis.

Finally, in Chapter 6, antibiotic cationic peptide colistin was successfully formulated into nanocomplexes with $mPEG_{2k}$-*b*-GA_{30} copolymer and complexation was confirmed by agarose electrophoresis and transmission electron microscopy. Colistin:$mPEG_{2k}$-*b*-GA_{30} *r* = 1:2 nanocomplexes possess enhanced bacteriostatic effect in non-pathogenic *E. coli* XL1 and bactericidal activity in pathogenic *E. coli* E2348/69 compared to free colistin applied at the same concentration. It should be noted that colistin:$mPEG_{2k}$-*b*-GA_{30} *r* = 1:2 formulation showed enhanced bactericidal effect in EPEC E2348/69 infected of HeLa cells, compared to free colistin by killing extra 2 logs of EPEC after 2 h

treatment. This result strongly indicates that PEG-*b*-pGA delivery system can be utilised widely aiding the delivery of proteins and small molecule drugs.

Acknowledgements

I would like to take this opportunity to express my profound appreciation to all the people who have supported, inspired and helped me throughout my Ph.D.

First and foremost, I offer my sincerest gratitude to my supervisors Prof. Snow Stolnik, Assoc. Prof. Giuseppe "Beppe" Mantovani, Drs Gemma Keegan and Nick Childerhouse.

Snow, thank you for your energy and enthusiasm for research. Your wisdom and support have helped me through the tough times during the PhD. Together with your guidance and the opportunities to explore the work in my own way, I have developed both professionally and personally. Beppe, thank you for your kind patience and invaluable advice throughout the PhD, your dedication to research is inspirational which greatly encouraged me to get the most out of my work.

Gemma and Nick, thank you for your meaningful insight into the project and advice. In addition, I greatly appreciated your support with conferences and placement during my PhD. Also, I would like to extend my thanks and appreciation to my internal assessor Assoc. Prof. Frankie Rawson for his very helpful advices and opinion on the project.

Throughout my PhD, I have been blessed with a friendly and cheerful group of fellow students who has been a source of not only fun but also science discussion and help with the project. In particular I would like to thank Patricia, Rosa, Rebe, Gordon, Ruggero, Thais Rob… and especially Alejandro for introducing me to the project and for making my 1st year of PhD so enjoyable and Shelly for her friendship and banter over the past four years.

I want to acknowledge the Department of Pharmacy in providing me with the support and equipment I needed to produce and complete my thesis and also Vectura Group plc for funding my studies.

And finally, my sincerest gratitude and upmost respect goes to my family and friends for their never-ending love and encouragement throughout my life.

Table of contents

Abstract I

Acknowledgements VIII

Table of contents IX

Abbreviations XVI

Chapter 1. Literature review and project overview 1

1.1 Protein therapeutics 1

1.2 Potential routes for mucosal delivery 6

1.2.1 Oral 6

1.2.2 Nasal 7

1.2.3 Pulmonary 7

1.2.4 Other mucosal routes 8

1.3 Pathways for crossing the mucosal surface 9

1.4 Pulmonary delivery of protein 9

1.4.1 Anatomy of the respiratory system 9

1.4.2 Advantages of pulmonary delivery 12

1.4.3 Barriers of pulmonary delivery 13

1.4.3.1 Mucus barrier 14

1.4.3.2 Lung clearance mechanisms 16

1.5 Commonly employed methods to improve mucosal delivery 22

1.5.1 Bio-adhesive polymers 23

1.5.2 Surfactant and tight junction modulating agents 24

1.5.3 Receptor-mediated drug delivery 25

1.6 Polymer therapeutics 26

1.6.1 Concept and classification 26

1.6.2 Rational design of polymeric nanosystems 34
1.6.3 Advantages of polymeric nanosystems 34
1.6.4 Disadvantages of polymeric nanosystems 35
1.6.5 Polymer-drug conjugates 36
1.6.5.1 Covalent polymer-protein conjugates 40
1.6.5.2 Electrostatic interactions 41
1.7 Project overview 42
Chapter 2. Materials and general methods 44
2.1 Materials 44
2.1.1 Cells, culture media, media components and cell solutions 44
2.1.2 Plasticware and glassware 45
2.1.3 Cell toxicity assay reagents 45
2.1.4 Chemicals and reagents 45
2.2 Methods 47
2.2.1 Maintenance of cells 47
2.2.1.1 Maintenance of cells in culture flasks 47
2.2.1.2 Frozen storage of cells 49
2.2.1.3 Cell revival 50
2.2.1.4 Culture of cells on transwells 50
2.2.1.5 Measurement of TEER 52
2.2.2 Synthesis 53
2.2.2.1 γ-Benzyl-L-glutamate N-carboxyanhydride (NCA) 53
2.3 Statistical Analysis 54
Chapter 3. B_{12} targeted PEG-*b*-poly(glutamic acid) complexes for inhalation protein delivery to the lung 55

3.1 Introduction 55
3.2 Methods 58
3.2.1 Synthesis of cyanocobalamin fluorescent probe pyr- B_{12} 58
3.2.1.1 Pyranine methyl ester (i) 58
3.2.1.2 Carboxyl pyranine (ii) 59
3.2.1.3 Amino cyanocobalamin (B_{12}-NH_2) 60
3.2.1.4 Pyranine B_{12} fluorescent probe (pyr-B_{12})..... 60
3.2.2 Synthesis of mPEG$_{2k}$-*b*-pGA copolymer 61
3.2.2.1 Hydrolysis of benzyl ester repeating units 62
3.2.3 Synthesis of targeted B_{12}-PEG$_{3.5k}$-*b*-GA$_{30}$ copolymer ... 64
3.2.3.1 Synthesis of azide-PEG$_{3.5k}$-*b*-GA$_{30}$ 64
3.2.3.2 α-dibenzocyclooctyne-vitamin B_{12} (DBCO-B_{12})..... 65
3.2.3.3 Conjugation of α-dibenzocyclooctyne-vitamin B_{12} to azide-PEG$_{3.5k}$-*b*-GA$_{30}$ polymer 66
3.2.4 Preparation of polymer-protein complexes 66
3.2.5 cDNA synthesis and quantitative PCR analysis of B_{12} receptor in Calu-3 cells 68
3.2.6 Cellular uptake of pyr-B_{12} fluorescent probe 69
3.2.7 Cellular internalisation of polymer-protein complexes applied as suspension 70
3.2.8 Formulation of complexes as dry powders by spray-drying 71
3.2.9 *In vivo* evaluation of the complexes formulated as dry powders 72
3.2.9.1 Animals and husbandry conditions 72

3.2.9.2 Characterisation of dry powder formulations emitted by the dry powder insufflator 72
3.2.9.3 Local pulmonary tolerance of the complexes 73
3.2.9.4 In vivo pulmonary deposition and retention. 75
3.3 Results and Discussion 77
3.3.1 Expression of mRNA and function of B_{12} receptors 77
3.3.2 Synthesis of $mPEG_{2k}$-*b*-pGA copolymers 82
3.3.3 Synthesis of targeted B_{12}-$PEG_{3.5k}$-*b*-GA_{30} copolymer ... 86
3.3.4 Targeted PEG-*b*-pGA:lysozyme complexes 90
3.3.5 Cellular internalisation of B_{12}-targeted protein-polymer complexes *in vitro.* 92
3.3.6 Local pulmonary tolerance of polymer-protein complexes based dry powder formulations in healthy mice. 96
3.3.7 *In vivo* pulmonary deposition and retention of polymer-protein complexes based dry powder formulations in healthy mice 101
3.4 Conclusions 104
Chapter 4. Biotin targeted PEG-*b*-poly(glutamic acid) copolymer for delivery of proteins 106
4.1 Introduction 106
4.2 Methods 108
4.2.1 Biotin-PEG_{2k}-*b*-GA_{10} and biotin-PEG_{2k}-*b*-GA_{60} synthesis 108
4.2.2 Lysozyme fluorescent labelling 109
4.2.3 Complexation of biotin-PEG-*b*-pGA to lysozyme 110
4.2.4 Agarose gel electrophoresis 111

4.2.5 Cell culture 112
4.2.6 Determination of cells metabolic activity by MTS assay... 112
4.2.7 Cellular uptake biotin-PEG$_{2k}$-*b*-pGA:lysozyme nanocomplexes 113
4.2.8 Confocal Microscopy 114
4.3 Results and discussion 116
4.3.1 biotin-PEG$_{2k}$-*b*-GA$_{10}$ and biotin-PEG$_{2k}$-*b*-GA$_{60}$ synthesis... 117
4.3.2 Biotin-PEG$_{2k}$-*b*-pGA:lysozyme complexation 120
4.3.3 Cellular internalisation of biotin-PEG$_{2k}$-*b*-pGA:lysozyme nanocomplexes *in vitro* 122
4.3.4 Live confocal microscope imaging of biotin-PEG$_{2k}$-*b*-GA$_{10/30}$: lysozyme complexes cellular internalisation. 128
4.3.5 Confocal microscope imaging of biotin-PEG$_{2k}$-*b*-GA$_{10/30}$: lysozyme complexes in fixed cells 130
4.4 Conclusions 137
Chapter 5. Endocytosis Mechanism of Biotin-PEG-*b*-pGA protein nanocomplexes 140
5.1. Introduction 140
5.2. Methods 145
5.2.1. Complexation of biotin-PEG-*b*-pGA to lysozyme 145
5.2.2. Cell culture 145
5.2.3. Cytotoxicity of endocytosis inhibitors (MTS assay) ... 146
5.2.4. Assessment of transferrin and cholera toxin subunit B cellular uptake by A549 cells. 147
5.2.5. Investigate mechanism of endocytosis of lysozyme and biotin-PEG$_{2k}$-*b*-GA$_{10/30}$:lysozyme nanocomplexes 148

5.3. Results 149
5.3.1. Effect of inhibitor on A549 metabolic activity *via* MTS assays 149
5.3.2. Effect of inhibitors on cholera toxin β and transferrin uptake into A549 cells 153
5.3.3. The effect of endocytosis inhibitors on the uptake of biotin-PEG_{2k}-*b*-$GA_{10/30}$:lysozyme nanocomplexes into A549 cells 157
5.3.3.1. Role of clathrin-mediated endocytosis (chlorpromazine and concanavalin A) 157
5.3.3.2. Role of endocytosis pathway involving dynamin (dynasore) 160
5.3.3.3. Tyrosine kinase and caveolae dependent pathway (genistein) 161
5.3.3.4. Caveolae mediated endocytosis (filipin) 163
5.3.3.5. Role of cholesterol (nystatin and MβCD) 164
5.3.3.6. Macropinocytosis (EIPA and cytochalasin) 167
5.4. Discussion 170
5.4.1. Mechanisms of Cellular Internalisation of lysozyme and polymer:lysozyme complexes 170
5.5. Conclusions 182
Chapter 6. Complexations and antibacterial effects of colistin:$mPEG_{2k}$-*b*-GA_{30} polymer nanocomplex 184
6.1 Introduction 184
6.2 Methods 189
6.2.1 Preparation of colistin-polymer nanocomplexes 189
6.2.2 Agarose gel electrophoresis 190
6.2.3 Assessing complex dissociation 191

6.2.4 Cell culture conditions and sample preparations 192
6.2.5 Determination of the metabolic activity by MTS assay 193
6.2.6 Antibacterial activity of colistin:mPEG$_{2k}$-*b*-GA$_{30}$ nanocomplexes 194
6.2.7 Time-kill bactericidal activity assay 196
6.2.8 Enteropathogenic Escherichia coli infection treatment..... 197
6.3 Results and discussion..... 198
6.3.1 Colistin:mPEG$_{2k}$-*b*-GA$_{30}$ polymer complexation 198
6.3.2 Assessing complex dissociation..... 202
6.3.3 MTS toxicity assay of complexes on A549 cells 207
6.3.4 E. coli XL1 bacteria growth curve in the presence of nanocomplexes 209
6.3.5 E. coli XL1 growth curve by colonies counting..... 213
6.3.6 Enteropathogenic Escherichia coli killing curve 218
6.3.7 Enteropathogenic Escherichia coli infection treatment..... 220
6.4 Conclusions..... 224
Chapter 7. General discussions and future work 245
Appendix 245
Supporting information..... 245
Chapter 3 245
Chapter 4 250
Chapter 6 253
References..... 255

Abbreviations

Asp	Aspartic acid
ATCC	American Type Culture Collection
CFU	Colony forming units
CM	Cytoplasmic membrane
CMS	Colistimethate sodium
Đ	Molecular weight dispersity
DCM	Dichloromethane
DI	Deionised
DLS	Dynamic light scattering
DMEM	Dulbecco's modified eagle medium
DMF	Dimethylformamide
DMSO	Dimethyl sulfoxide
DMTMM	4-(4,6-dimethoxy-1,3,5-triazin-2-yl)-4-methylmorpholinium chloride
DPAP	2,2-dimethoxy-2-phenylacetophenone
DPBS	Dulbecco's phosphate buffer saline
DPI	Dry powder inhaler
ED	Emitted dose
EDTA	Ethylendiaminetetraacetic acid
EPEC	Enteropathogenic *Escherichia coli*
ESI-MS	Electrospray ionisation mass spectrometry
Et_2O	Diethylether
Et_3N	Triethylamine
EtOAc	Ethyl acetate
FBS	Foetal bovine serum

FDA	Food and drug administration
FPF	Fine particle fraction
FT-IR	Fourier transform infrared spectroscopy
GA	Glutamic acid
GI	Gastrointestinal
h	Hour
HBSS	Hank's balanced salt solution
HPLC	High performance liquid chromatography
K_d	Equilibrium Dissociation Constant
LB	Luria-Bertani
LDH	Lactate dehydrogenase
LDP	Labelled dry powders
Lin	Linear
LPS	Lipopolysaccharide
MeOD	Deuterated methanol
MeOH	Methanol
mM	Millimolar
M_n	Number average molecular weight
M_p	Peak molecular weight
M_r	Molecular mass
MTS	3-(4,5-dimethyl-2-yl)-5-(3-carboxymethoxyphenyl)-2-(4-sulfophenyl)-2H-tetrazolium, inner salt
M_w	Weight average molecular weight
MWCO	Molecular weight cut-off
NCA	*N*-carboxyanhydride
NMR	Nuclear magnetic resonance

OD	Optical density
OM	Outer membrane
PB	Phosphate buffer
PBS	Phosphate buffer saline
PEG	Poly(ethylene glycol)
PI	Propidium iodide
pMDI	Pressured metered dose inhaler
Ppm	Parts per million
r	Relative molar charge ratio
SD	Standard deviation
SEC	Size exclusion chromatography
SEM	Scanning electron microscopy
TAE	TRIS-acetate-EDTA
TEER	Transepithelial Electrical Resistance
TEM	Transmission electron microscopy
THF	Tetrahydrofuran
TLC	Thin layer chromatography
Trp	Tryptophan
UDP	Unlabelled dry powders
UV	Ultraviolet
$VitB_{12}$ or B_{12}	Vitamin B_{12}, cyanocobalamin
w/v	Weight/Volume
λ_{em}	Emission wavelength
λ_{ex}	Excitation wavelength

Chapter 1. Literature review and project overview

1.1 Protein therapeutics

Proteins are one of the most dynamic and diverse classes of biological macromolecules (Lodish *et al.* 2000): they catalyse countless biochemical reactions, transport and store small molecules, support intracellular and extracellular scaffolding, and can also act as receptors and channels in cell membranes (Cooper 2000). Abnormal protein structures has been associated with many diseases and conditions, including diabetes and cancer (Valastyan and Lindquist 2014; Mukherjee *et al.* 2015). Currently, the Unites States Food and Drug Administration (FDA) has approved more than 1190 proteins or peptides for clinical use, and many more are in development (Santos *et al.* 2017).

Most of these protein drugs are administered parenterally, as they often suffer from poor bioavailability. They are unable to withstand the harsh gastrointestinal (GI) environment, which leads to protein degradation, and to inefficient transport through the gut epithelial barriers (Pisal *et al.* 2010). However, parental route can cause discomfort for the patients and treatments are often expensive due to labour intensive, high administration cost. Thus, research into non-invasive alternative ways of administering this class of

therapeutics is much needed. Increasing commercial progress has been made in the past several years, selected examples of commercially available drugs for non-invasive routes of administration are listed in **Table 1.1**.

There are some additional potential benefits offered by delivering drug *via* mucosal routes namely: high surface area for absorption (e.g. intestinal and pulmonary routes), rapid absorption (nasal, pulmonary, sublingual and vaginal routes) and avoidance of first pass (hepatic) metabolism. Nevertheless, mucosal administration presents unique challenges for the delivery of 'fragile' macromolecules such as protein therapeutics and these will be discussed in the following sections.

Table 1.1. *Selected examples of commercially available drugs for non-invasive routes of administration, adapted from Bajracharya et al. (2019)*

Product	Drug	Route	Indications
Minirin®	Desmopressin	Oral, Nasal	Cranial diabetes insipidus or nocturia associated with multiple sclerosis
Sandimmune®	Cyclosporine A	Oral	Immunosuppressants
Colomycin®	Colistin	Oral	Intestinal infection (caused by sensitive Gram-negative organisms)
Cytorest®	Cytochrome C	Oral	Leucopenia
Cachexon®	Glutathione	Oral	AIDS- related cachexia
Ceredist®OD	Taltirelin	Oral	Spinocerebellar ataxia
Anginovag®	Tyrothricin	Oral	Pharyngitis
Vancocin®	Vancomycin	Oral	Infection, clostridium difficile-associated diarrhea
Oral-Lyn™	Insulin	Buccal	Diabetis mellitus
Suprifact™	Buserelin	Nasal	Prostate cancer, endometriosis

Product	Drug	Route	Indications
Suprecur®	Buserelin	Nasal	Prostate cancer, endometriosis
Synarel®	Nafarelin	Nasal	Endometriosis
Kryptocur®	LHRH	Nasal	Cryptorchism
Miacalcin®	Salmon calcitonin	Nasal	Hypercalcemia or osteoporosis
Fortical®	Salmon calcitonin	Nasal	Hypercalcemia or osteoporosis
Desmospray®	Desmopressin	Nasal	Cranial diabetes insipidus or nocturia associated with multiple sclerosis
Syntocinin™	Oxytocin	Nasal	Indicated for the initiation or improvement of uterine contractions
Antepan®	Protirelin	Nasal	Hypothyroidism and acromegaly
FluMist® Quadrivalent	Vaccine	Nasal	Influenza

Product	Drug	Route	Indications
Eylea®	Aflibercept	Ocular	Wet age-related macular degeneration (WAMD), Diabetic macular edema (DME) or Diabetic retinopathy (DR) in DME, Macular edema following retinal vein occlusion (MEtRVO)
Lucentis®	Ranibizumab	Ocular	WAMD, DME or DR in DME, MEtRVO, Myopic choroidal neovascularization (mCNV)

1.2 Potential routes for mucosal delivery

1.2.1 Oral

Oral route is associated with convenience and low cost, but as mentioned above, the unfavourable acidic environment together with the presence of proteolytic enzymes in the GI tract can destroy most proteins and peptides. (Peppas and Carr 2009; Bruno *et al.* 2013; Yamanaka and Leong 2008). Even if the therapeutic can withstand harsh physiological conditions, it will encounter further barriers. Firstly, the solid dosage form of the drug must dissolve in the contents of the intestinal lumen before passing through a protective mucus layer at the surface of the epithelial cells, where it meets the epitopal barrier. After crossing the epithelial cells, the therapeutic reaches the capillaries. Due to the lipid-based plasma membrane structure lining the capillaries, entry into blood circulation *via* partitioning and diffusion process are almost impossible for hydrophilic macromolecules (e.g. most protein therapeutics). The epithelial cell barrier appears as an almost continuous sheet rendering its effectiveness at limiting the absorption of proteins; the high proximity between adjacent epithelial cells owing to the presence of epithelial tight junctions. The small pore diameter of the tight junctions restricts the intercellular passage of molecules larger than 1000 Da (Stolnik and Shakesheff 2009).

1.2.2 Nasal

Nasal mucosa delivery is another attractive and widely studied therapeutic option (Meredith *et al.* 2015). Nasal olfactory epithelium has relatively large surface area (200–400 mm^2), highly vascularised submucosa, lower enzymatic activities compared to the GI tract; and the possibility of avoiding first pass metabolism (Illum 2000; Ugwoke *et al.* 2001). However, absorption is typically low due to rapid mucociliary clearance and a low molecular weight cut-off of approximately 1 kDa for molecules to cross the mucosa (Lochhead and Thorne 2012; Kissel and Werner 1998; Ugwoke *et al.* 2001).

1.2.3 Pulmonary

Pulmonary delivery possesses all the advantages of nasal delivery, such as avoidance of first pass metabolism and minimal enzymatic activities in the lungs (Peppas and Carr 2009). In addition, lungs have very large surface areas (approximately 140 m^2) for drug absorption (Owens *et al.* 2003) and epithelial lining of lungs present minimal barriers to drug transport (Peppas and Carr 2009). Section 1.3 will discuss in detail the anatomy of the respiratory system and both advantages and potential problems with pulmonary delivery route.

1.2.4 Other mucosal routes

Utilising the large surface area for absorption and extensive vascular network of support, the **buccal** administration route can also be considered. This route benefit from the avoidance of first pass metabolism by the liver, however the presence of saliva whose role is the defence against foreign agents, posing as a physiological barrier to drug transport (Morales *et al.* 2017).

Less common routes for transmucosal protein delivery are *via* the rectal, vaginal and ocular mucosal surfaces (Owens *et al.* 2003; Agarwal *et al.* 2016). **Rectal** mucosal presents relatively small surface area for drug delivery but the environment in the rectum is considered relatively constant and stable and has low enzymatic activity in comparison to other sections of the gastrointestinal tract. Rectally delivered drug can be directly absorbed by the lymphatic system bypass liver degradation. Potential problems associated with this approach include longer transit/dissolution times in the colon milieu, bacterial activity and interference from faecal matter (Hua 2019). Low and variable absorption associated with the **ocular** and **vaginal** routes, even in the presence of absorption enhancers, and localised adverse reactions hinder the used of both these routes for drug or protein delivery (Peppas and Carr 2009; Owens *et al.* 2003).

1.3 Pathways for crossing the mucosal surface

Depending on the size and physiochemical properties of the molecules crossing the mucosal surface, there are 3 main routes available. i) Small, amphipathic molecules have the ability to partition into and out of lipid bilayer membranes (apical and basolateral) allowing them to readily enter and leave the epithelial cells without a specific transport system; ii) smaller hydrophilic macromolecules can pass the epithelial tight junction paracellularly and iii) larger macromolecules and nano-sized particles can be transported across the cells *via* transcytosis route most likely through highly regulated selective transport mechanism (Mostov *et al.* 2003). As proteins and macromolecule drugs are unlikely fit into categories i and ii, this chapter will mainly focus on route iii.

1.4 Pulmonary delivery of protein

1.4.1 Anatomy of the respiratory system

The respiratory tract can be anatomically divided into upper and lower respiratory systems **(Figure 1.1)**; with the upper consisting of the oropharynx, the nasopharynx, the pharynx and associated structures; and the latter including the larynx, trachea, bronchi and lungs (Itoh *et al.* 2004). The diameter of the respiratory tubes decrease gradually and the cells lining the respiratory walls change from bigger and more organised cells to smaller flattened squamous

cells **(Figure 1.2)** along the respiratory tract allowing efficient oxygen transport into the blood (Patwa and Shah 2015).

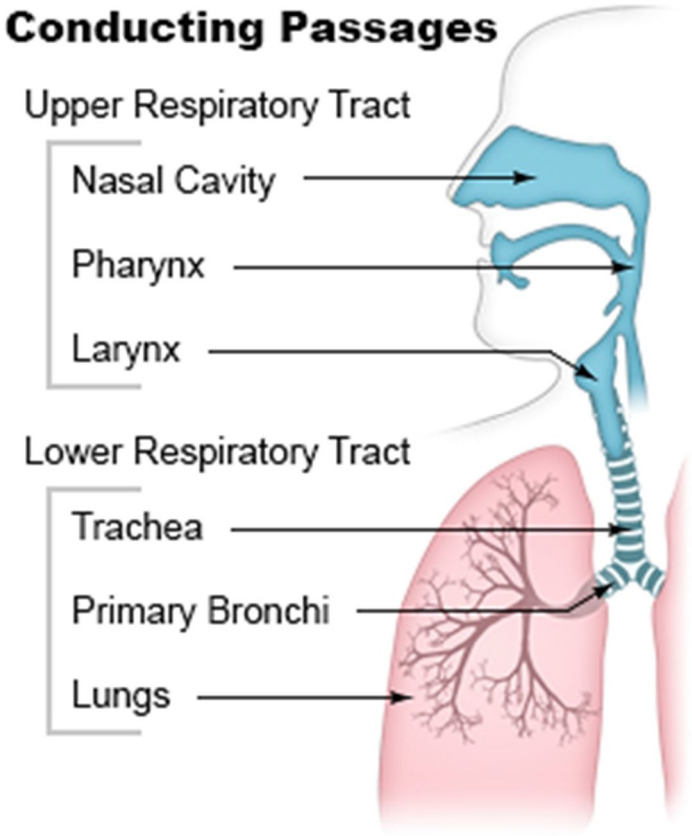


Figure 1.1. *Illustration of the respiratory system. Adopted from National-Cancer-Institute (2017).*

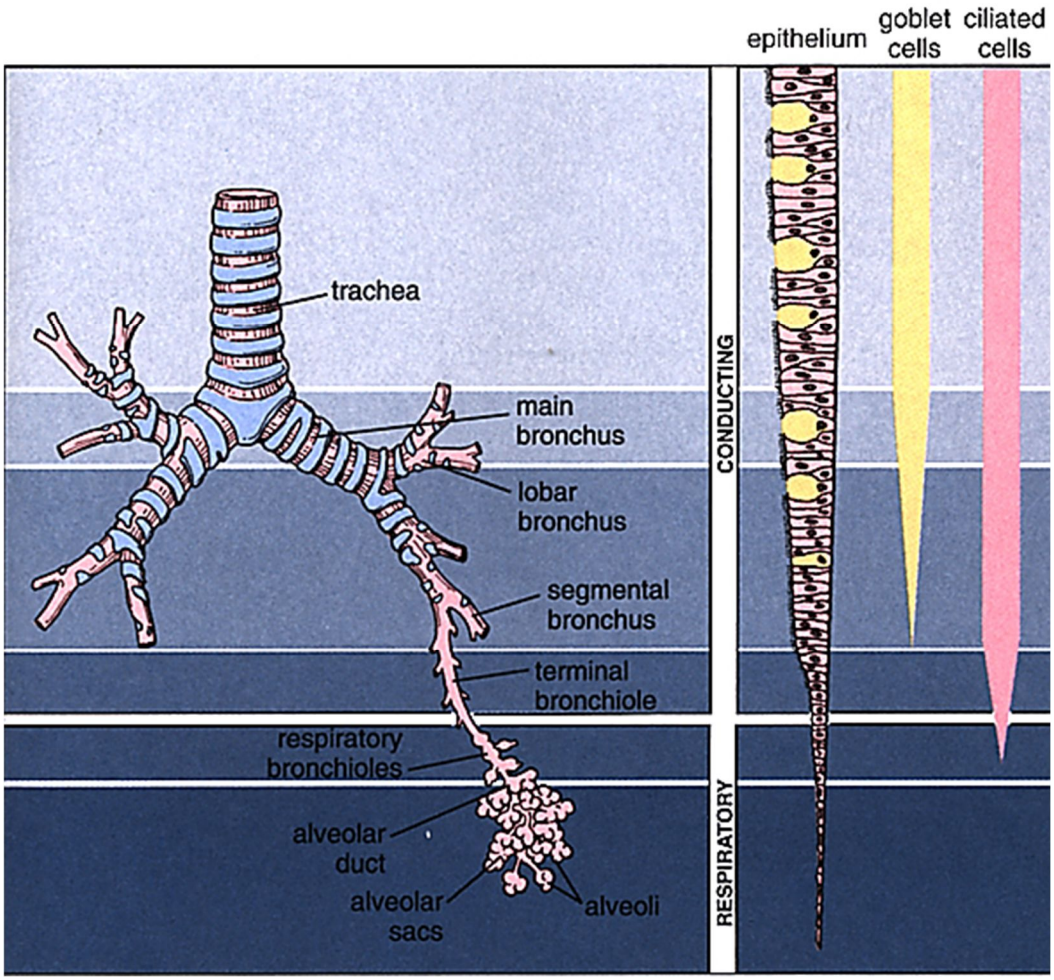


Figure 1.2 *Structural features of the respiratory tract from trachea to alveoli. Adopted from Rohatagi et al. (2000).*

As illustrated in **Figure 1.2**, the epithelium composition evolves along the respiratory tract. In the upper airway, the epithelium is composed of basal goblet and ciliated cells. Goblet cells produce mucus to clear entrapped particles entering the lungs, the beating ciliated cells move the mucus sheet in an escalator-like fashion towards the pharynx where the trapped material is swallowed or expectorated. Ciliated cells are present up to the bronchioles, whereas goblet cells are only present in the trachea and bronchi. There are two types of cells in the alveoli epithelium: type I and type

II pneumocytes. Type I pneumocytes cover about 95% of the total area of the lungs, which are uniform and liable to make gas exchange. Type II cells synthesise, store, and secrete pulmonary surfactant, which decrease the surface tension in the alveoli and stabilise alveolar units for efficient gas exchange (Zhao *et al.* 2010).

As a part of the host innate defence, macrophages are present in the alveoli (around five to seven per alveolus in lungs of non-smokers) (Stone *et al.* 1992), the main function of which is to ingest inhaled particles and microorganisms and other foreign particles. In addition, macrophages are able to secrete enzymes and inflammation mediators (Hickey 2003).

1.4.2 Advantages of pulmonary delivery

As mentioned in Section 1.2.3, pulmonary administration is a very attractive way for non-invasive protein delivery. Several proteins and peptides (e.g. cyclosporine A to treat asthma, interleukin-2 (IL-2) to treat pulmonary metastases of renal cell carcinoma) (Rohatagi *et al.* 2000; Merimsky *et al.* 2004) have been investigated both for local drug delivery. The high permeability of the very thin alveolar epithelium (around 0.1-0.5 μm thick), the large absorptive surface area of lungs (approximately 70-140 m^2 in adult humans) and the great blood supply permitting rapid drug absorption of systemic therapies, are all very desirable features associated with lung delivery (Groneberg *et al.* 2003; Bailey and Berkland 2009). Further

advantages of pulmonary administration include the comparatively low enzymatic activities in lungs, hence less unwanted protein degradation; and the capacity for overcoming first-pass metabolism (Cefalu 2004).

1.4.3 Barriers of pulmonary delivery

Despite the numerous advantages offerd by pulmonary delivery, there are several challenges the respiratory system poses as barriers to decrease the deposition and absorption of therapeutic agents in the lungs. Physiological barriers such as presence of mucus and the existence of tight junctions paracellularly greatly effect drug absorption (Hussain *et al.* 2004). The main mechanisms effecting deposition and promoting particle clearance are the mucociliary escalator, the presence of alveolar macrophages and proteolytic enzymes **(Figure 1.3)**. The restrictions of mucosal absorption presented by mucus and the specific clearance mechanisms present in lungs: mucocilary escalator, alveolar macrophages and lung proteases are discussed in detail below.

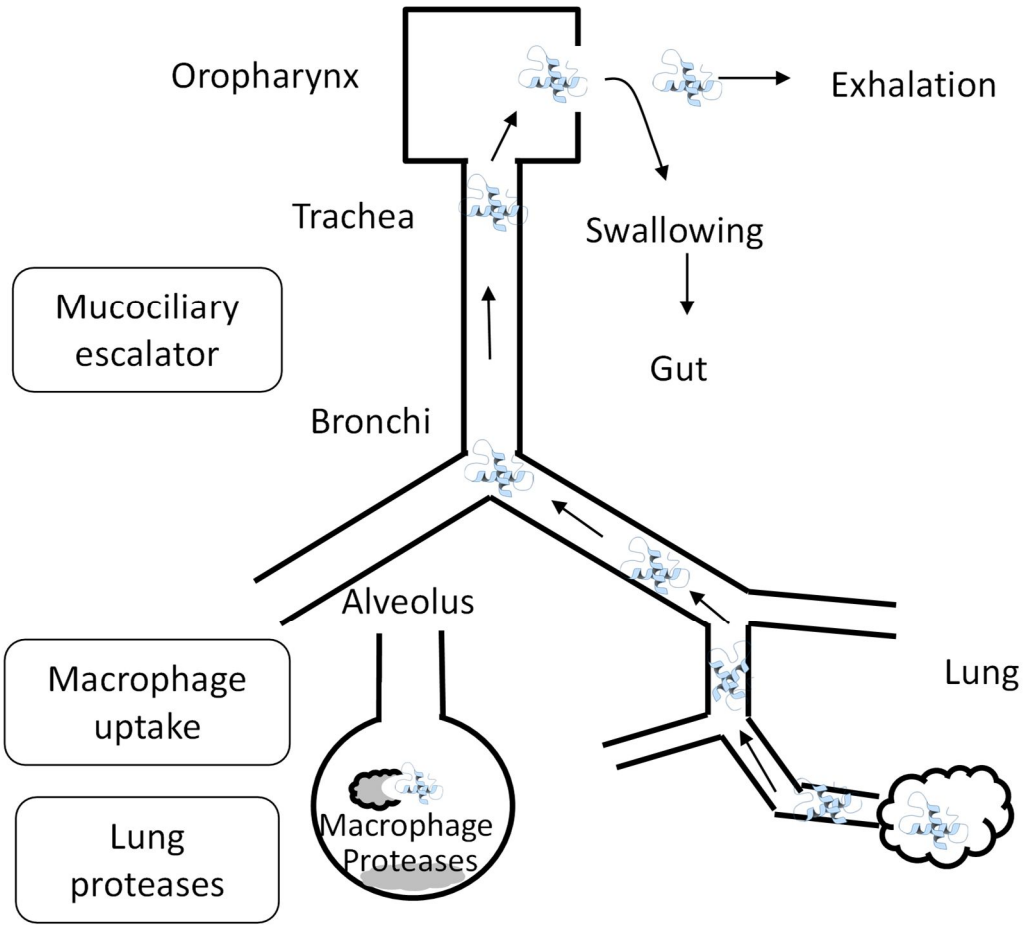


Figure 1.3 *Schematic representation of the main mechanisms for protein clearance after pulmonary protein administration: mucociliary clearance, macrophage uptake and proteolytic degradation. Adopted from (Depreter et al. 2013).*

1.4.3.1 Mucus barrier

Mucus is a selective barrier to particles and molecules; crucial for preventing invasion of foreign agents such as bacteria, viruses, allergens and irritants to the epithelial surface of mucosal tissues. During homeostasis, the airway epithelium contains a protective continuous mucus layer, with a thickness of 5–15 μm in the nasal cavity (Beule 2010), 10–30 μm in the trachea and 2–5 μm in the bronchi (Sanders *et al.* 2009; Wine 1999). Normal mucus in the lung

compose of 97% water and 3% solids (mucins, non-mucin proteins, salts, lipids, and cellular debris); it has gel-like consistency with properties of both a soft (deformable), elastic solid and a viscous fluid (Fahy and Dickey 2010). Mucin, the primary non-aqueous component of mucus, is polymers carrying a complex and heterogeneous structure with domains that undergo a variety of molecular interactions, such as hydrophilic/hydrophobic, hydrogen bonds and electrostatic interactions (Leal *et al.* 2017). Mucus as a barrier impedes transport of drugs and other molecules, and its physicochemical properties such as pore size, viscoelasticity, pH, ionic strength, and charges can impact the success of drug delivery systems in mucosal tissues.

Various attempts have been made to enhance mucosal permeability of drugs, including nanoparticle-based formulations, permeation enhancers, nanoemulsions, mucoadhesive and mucopenetrating systems, polymers, enzymes, liposomes, and peptides. It has been demonstrated that poly(lactic-co-glycolic acid) (PLGA) and polystyrene particles functionalised with mucus inert polymers such as poly(ethylene glycol) (PEG) enhanced mucus transport in human respiratory mucus (Schuster *et al.* 2013). The same study has found that 100 and 200 nm diameter PEG-coated particles rapidly penetrated respiratory mucus, at rates exceeding their uncoated counterparts by approximately 15- and 35-fold, respectively.

1.4.3.2 Lung clearance mechanisms

Mucociliary clearance

Mucociliary clearance is the primary innate defence mechanism of the lung. It consists of 2 main functional components: protective mucous layer covering airway surface that entraps inhaled particles and foreign pathogens as mentioned in Section 1.4.3.1 and the cilia on the surface of ciliated epithelial cells for efficient mucus clearance *via* mechanism of ciliary beating (Bustamante-Marin and Ostrowski 2017). Mucus are produced by goblet cells in trachea and bronchi; inhaled molecules and foreign particles are trapped within and diverted to the pharynx and eventually swallowed to the gastrointestinal tract (Hoiby *et al.* 2010). This mechanism can remove insoluble particles larger than 6 μm within 24 h, whilst smaller particles can reach the bronchial epithelium or be directly deposited in the alveolar region (Möller *et al.* 2006). In healthy lungs, the production of mucus is around 10-20 mL per day (Toremalm 1960; Foster *et al.* 1980). However, the rate of mucociliary clearance is reduced in older people and can be affected by lung diseases (Lowery *et al.* 2013; Labiris and Dolovich 2003)

Alveolar macrophages

Alveolar macrophages are part of the immune response in the alveolar spaces to remove foreign particulates. They are able to neutralise the invading pathogens or recruit neutrophils and other

mononuclear cells, or simply transport them to the mucociliary escalator and the lymphatic system (Lombry *et al.* 2004; Zhang *et al.* 2011; Nicod 2005). Alveolar macrophages also have important bactericidal activities capable of killing a wide variety of bacteria by producing lysozyme or defensins and cationic proteins (Kisich *et al.* 2001; Biggar and Sturgess 1977). In the lungs, particles between 1.5 and 3 μm are easily recognised by macrophages, whilst particles below 70 nm are usually not phagocytised (Azarmi *et al.* 2008; Yang *et al.* 2008; Oberdorster *et al.* 2005).

Lung proteases

Proteases produced by lung parenchyma and inflammatory cells play a key role in healthy and diseased lungs (Chakraborti *et al.* 2017). In the healthy lung, proteases fulfil basic homeostatic roles and regulate processes such as regeneration and repair (Chakraborti *et al.* 2017). Together with pulmonary peptidases, they are involved in specific clearance mechanisms for peptides and proteins found in humans and other mammals (Van Der Walle 2011; Giannoni *et al.* 2006; Janoff *et al.* 1983; Wall and Lanutti 1993; Fujita *et al.* 1990). For inhaled biological therapies, including proteins, peptides and antibodies; lung proteases play an important role in their stability and pharmacokinetics (Agu *et al.* 2001). For example, peptide therapeutics have been demonstrated to undergo significant, rapid degradation (half-life = ~6.5 min) upon incubation with lung

homogenates, which contain high pulmonary peptidase concentrations (Youn *et al.* 2008). However, as peptidases are widely distributed among human tissues and body fluids; their amount in lungs is still significantly lower than that in the gastrointestinal tract which provides opportunities for pulmonary protein delivery (Patton *et al.* 2004). It is important to note that the amount of metabolic enzymes differs from patients and depending on disease states. For example, lung of smoker have higher production of enzymes than non-smokers, which can have an effect on the fate and efficacy of inhaled protein and peptide therapeutics (Thorley and Tetley 2007). Individuals with chronic airways diseases such as cystic fibrosis, chronic obstructive pulmonary disease or asthma can have excessive protease activity in lungs; the dysregulated expression or activity of the protease can adversely impact on the inflammatory process (Rubin and Williams 2014).

The addition of exogenous proteases inhibitors have been investigated to discourage protease activity, however their use could lead to destabilisation of the natural balance of airway surface liquid homeostasis (Garcia-Verdugo *et al.* 2010). However, despite these potential challenges, there are a few successes in the field of inhaled biologics. **Table 1.2** shows some of the inhaled biological treatments currently on the market or in clinical developments for local or systemic applications.

Table 1.2 *Inhaled biological treatments currently on the market or in clinical developments for local or systemic applications. Adapted from Morales et al. (2017).*

Drug	Clinical application	Development status
Locally acting inhaled products		
Pitrakinra (recombinant human interleukin-4)	Asthma	Phase II (Bayer Corp (phase 1 SC) and Aerovance (all other studies)
Granulocyte-macrophage colony-stimulating factor (GM-CSF)	Pulmonary alveolarproteinosis	Phase II (Niigata University Medical and Dental Hospital Japan)
DAS181	Influenza virus	Phase II (Ansun Biopharma, Inc.)
INF-γ	Cystic fibrosis, pulmonary fibrosis	Phases I and II for cystic fibrosis (InterMune), phase II for *Mycobacterium avium* complex infections (National Institute of Allergy and Infectious Diseases (NIAID and InterMune))
Interleukin-2 (IL-2)	Cancer	Phase I (University of Southern California), phases I and II (M.D. Anderson Cancer Center), phase I (Max Kade Foundation (New York)

Sargramostin	Metastatic cancer, sarcoma—interfere with tumor growth in lungs before and after surgery	Phase II (Children's Oncology Group)
α1-Antitrypsin	Fibrosis	Phase II/III (ongoing) (Kamada)
Beractant (SP-B and SP-C) (trade name Survanta (r)—intrathecal use only)	Infant RDS	Approved (Abbot)
Vasoactive intestinal peptide	COPD, asthma	Phase II (COPD) (Medical University of Vienna) preclinical (asthma)
Glutathione	Cystic fibrosis	Phase II (completed) (Mukoviszidose Institut GmbH)
Systemic acting inhaled products		
Insulin (Exubera®) (Nektar/Pfizer)	Type I/II diabetes	Approved (discontinued 2007)
Insulin (AIR system) (Alkermes/ Eli Lilly)	Type I/II diabetes	Phase III (discontinued 2008)
Insulin (Afrezza®) (MannKind)	Type I/II diabetes	Approved
Insulin (AERxIDMS) (Aradigm)	Type I/II diabetes	Phase III (discontinued 2008)

Insulin (Dance 501®)	Type I/II diabetes	Phase III (Dance BioPharm)
Human parathyroid hormone (PTH)	Osteoporosis, hormone replacement therapy	Pilot clinical trial (MannKind)
Interleukin-2 (IL-2)	Tumor therapy (pulmonary metastases) and immunodeficiency including HIV	Phase I (terminated) (NCI)
Human growth hormone (hGH)	Growth hormone deficiency	Phase I completed (Alkermes/Eli Lilly)
EPO-Fc	Anemia	Phase I completed (Syntonix/BI)
DAS181 Fludase® (Ansun)	Influenza	Phase I (Ansun BioPharma, Inc)
Heparin	Prevention of thrombosis; treatment of inhalation smoke injury	Phase I (Danish Lung Association) (phase II trial terminated)
Calcitonin	Osteoporosis, Paget's disease	Phase I completed (Dura Pharm.)
Leuprolide (Lupron®)	Hormone-responsive cancers, estrogen-dependent conditions, precocious puberty, and *in vitro* fertilization	Approved TAP Pharmaceuticals, Abbott Laboratories (AbbVie)
Glucagon-like peptide-1 (GLP-1)	Type II diabetes	Phase I completed, 2008; phase II ongoing (MannKind)
Oxytocin (GSK)	Treatment of postpartum hemorrhage	Phase I completed, 2016 (GlaxoSmithKline)

1.5 Commonly employed methods to improve mucosal delivery

In order to overcome the challenges mentioned above, several drug delivery systems have been investigated to improve the absorption and bioavailability of mucosal delivered protein therapeutics (**Figure 1.4**). These strategies include the use of mucoadhesive polymers to prolong the contact time of the drug with the mucosal surfaces **(Figure 1.4a)**; surfactant like agents to destabilise cell membrane and increase cell permeation **(Figure 1.4b)**; and compounds that open the epithelial tight junctions **(Figure 1.4c)** (Laffleur and Bernkop-Schnurch 2013). Uptake-enhancing strategies such as receptor-mediated transcytotic pathways **(Figure 1.4d)** have also been investigated for their potential in transmucosal delivery of protein therapeutics and will be discussed in details later on in Section 1.5.3. In addition, to improve mucosal drug access to epithelium and stability of the administered protein drug, agents such as mucolytics and proteolytic enzyme inhibitors, respectively, can also be employed (Vllasaliu 2010).

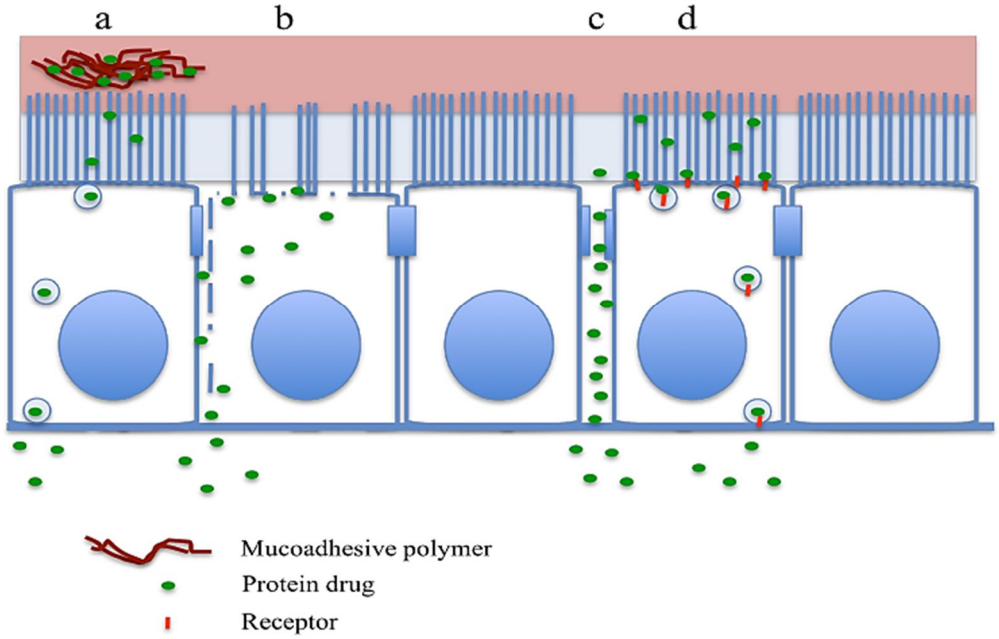


Figure 1.4 *Common strategies investigated for improvement of mucosal absorption of protein therapeutics. a) Mucoadhesive polymers prolonging the residence time of the complexed protein drug at the mucosal surface, b) Surface-active permeability enhancers compromising cell membrane integrity, whereby otherwise membrane-impermeable protein drug crosses the epithelial barrier, c) Tight junction opening where the paracellular space is increased, improving the paracellular access of protein molecules, and d) Exploiting epithelial transcytotic mechanisms by conjugating the drug (or a drug carrier nanoparticulate system) to a ligand (not shown) that is transported transepithelially via this route. Adopted from Vllasaliu (2010)*

1.5.1 Bio-adhesive polymers

Mucoadhesion mainly occur between polymer interacting with negatively charged mucus and other secondary forces such as hydrogen bonds and Van der Waals interactions (Laffleur and Bernkop-Schnurch 2013). Positively charged polymers, such as chitosan, can bind to mucins *via* electrostatic interactions with the negatively charged sialic acid moieties. However, polymers with negatively charged groups such as poly(acrylic acid), poly(methacrylic acid), and others bearing carboxyl groups have

been shown to exhibit better bioadhesion than cationic or neutral polymers, supporting other mechanisms including hydrophobic interactions, hydrogen bonding, and van der Waals' interactions, are also possible, which probably involve other parts of the mucin molecules (Salamat-Miller *et al.* 2005). The problem with this method is the challenge to retain the drug at the desired mucosal region (Kompella and Lee 2001); The residence time of dosage forms is limited by the mucin turnover time, which has been calculated to range between 12–24 h in humans (Forstner 1978). Therefore, this system is susceptible to sloughing of the mucosa and displacement by mucus excretion (Lehr *et al.* 1990; Pathak and Malviya 2020).

1.5.2 Surfactant and tight junction modulating agents

Other approaches include enhancing the absorption by either transiently disrupting cell membranes **(Figure 1.4b)** or opening the epithelial tight junctions **(Figure 1.4c).** Most commonly used absorption enhancers are surfactants, because of their ability to disrupt the lipid bilayer and improve transcellular transport (Alama *et al.* 2019). Tight junctions are known to be regulated by extracellular calcium; depletion of calcium can cause tight junctions to open (Zihni *et al.* 2016) and increase bioavailability. However, many studies showed the disruptions to cell membrane are often permanent and can cause mucociliary arrest (Gizurarson *et al.*

1990), hence limiting their applications. Polymer based nanocarrier systems could overcome these limitations if they can take advantage of efficient epithelial transcytosis mechanisms.

1.5.3 Receptor-mediated drug delivery

Receptor-mediated cellular uptake involving inward budding of the plasma membrane (invagination) has become increasingly attractive as a method for drug delivery and has been exploited for designing of site-specific delivery systems. Ligand mediated active targeting has emerged as a novel paradigm in targeting either vascular compartment (first-order), cellular (second-order), or intracellular (third-order) levels (Vyas *et al.* 2001; Michael and Curiel 1994). Most carrier systems or bioconjugates explored so far can potentially be used as cargo units for the site-specific presentation and delivery of various bioactive using biorelevant ligands, including viral proteins, antibodies, polypeptides, oligosaccharides (carbohydrates), and molecules of endogenous origin. The biological transport systems targeted by these drug delivery systems are diverse and can include blood carbohydrate (lectin) receptors, Fc receptors, complement receptors, interleukin receptors, lipoprotein receptors, transferrin receptors, scavenger receptors, receptors/epitopes expressed on tumour cells, and cell adhesion receptors (Vyas *et al.* 2001). Of particular interest in this thesis, is the use of ligand-targeted nanocomplex systems for the delivery of

biotherapeutics to the lung, which will be discussed across the chapters.

1.6 Polymer therapeutics

Polymer therapeutics are amongst the most successful first generation of nanomedicines, with 15 products in routine clinical use and 2 compounds reaching the US Top 10 selling drugs list; examples are the immunomodulatory polymeric drug glatiramer acetate for the treatment of multiple sclerosis (Copaxone®, Teva Pharm; $3.7 billion), and the polyethylene glycol (PEG) modified form of the recombinant human granulocyte colony-stimulating factor (G-CSF) analogue filgrastim for the treatment of neutropenia (Neulasta®, Amgen; $3.6 billion) (Atkinson *et al.* 2018; Duncan 2014).

1.6.1 Concept and classification

The term "polymer therapeutics" was firstly used to describe hybrid nanoconstructs, consisting of bioactive agent combined with polymer (Duncan 2003). Later on, polymer therapeutics were categorised in five different groups: complex multicomponent polymeric drugs, polymer-protein conjugates, polymer-drug conjugates, multicomponent polyplexes which are being developed as non-viral vectors and polymeric micelles where the drug is attached through covalent bonds to relevant polymers **(Figure 1.5)**. These nano-sized medicines in the 5-100 nm diameter range

are considered as new chemical entities from an industrial standpoint, they can alter drug pharmacokinetics at both the whole organism and subcellular level through improvement in solubility hence therapeutic effects (Greco and Vicent 2009).

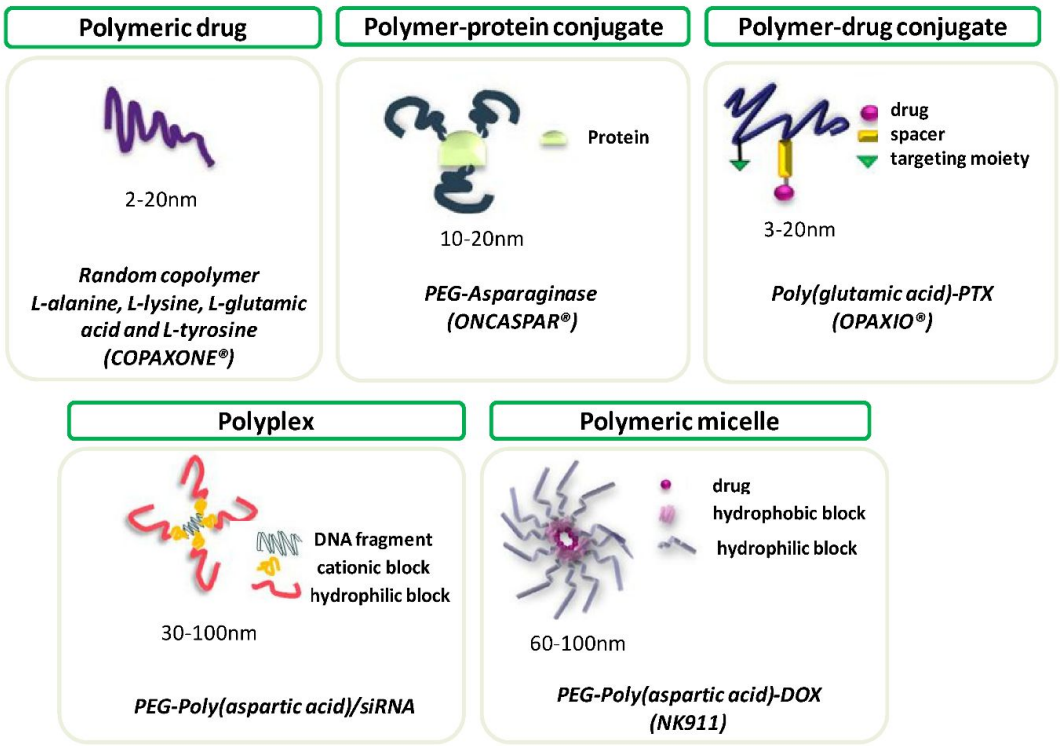


Figure 1.5 *Schematic representation of the Polymer Therapeutics family. Adopted from Duro-Castano et al. (2014)*

Polymer therapeutics have been well established over the years, some of the current polymer therapeutics on the market is listed in **Table 1.3**; **Table 1.4** lists the formulations that are currently in clinical development. Early products were mainly developed as anticancer agents, however recent advancement have been made for a broader range of disease indications and different routes of administration, for example PEGylated-anti-TNF Fab Cimzia® for

rheumatoid arthritis and the PEG-aptamer Macugen® for age related macular degeneration (Duncan 2011; Sanchis *et al.* 2010).

Table 1.3 *First generation marketed polymer therapeutics. Adapted from ref (England et al. 2012; Duncan and Gaspar 2011; Duro Castaño 2015; Duncan 2011)*

Product name	Technology	Indication	Route of Admin	Information source
		Polymer-protein conjugates		
Zinostatin stimalmer®	Styrene maleic anhydride neocarzinostatin (SMANCS)	Cancer-hepatocellular carcinoma	Local via hepatic artery infusion	Yamanouchi Japan
Oncaspar®	PEG-asparaginase	Cancer-acute Lymphocytic leukemia	i.v./i.m.	Enzon
PEGIntron®	PEG-Interferon alpha 2b	Hepatitis C	s.c.	Schering-Plough
Pegasys®	PEG-Interferon alpha 2a	Hepatitis C	s.c.	Roche
Neulasta™	PEG-hrGCSF	Chemotherapy-induced neutropenia	s.c.	Amgen
Adagen®	PEG-adenosine deaminase	Severe combined immune deficiency syndrome	i.m.	Enzon
Somavert®	PEG-HGH antagonist	Acromegalia	s.c.	Pfizer
Mircera®	PEG-EPO (polyethylene glycol-epoetin beta)	Treatment of anemia associated with chronic kidney disease	i.v./ s.c.	Roche

Cimzia™ (certolizumab pegol)	PEG-anti-TNF Fab	Rheumatoid arthritis Crohn's disease	s.c.	UCB
Puricase®	PEG-uricase	Gout	i.v.	Savient Pharmaceuticals
		Polymer-aptamer conjugate		
Macugen®	PEG-aptamer (apatanib)	AMD	i.v	OSI-Eyetech
		Polymer-drug conjugate		
Movantik™/Moventig® (NKTR-118)	PEG-naxolol	Opiod-induced constipation	Oral	AstraZeneca/ Daiichi Sankyo Co, Ltd.
		Polymeric drugs		
Copaxone®	Glu, Ala, Tyr copolymer	Multiple sclerosis	s.c.	Teva
Renagel®	Phosphate binding polymer	End stage renal failure	Oral	Genzyme (Daiichi Co, Ltd. Licensed)
Welchol®	Cholesterol binding polymer	Type 2 diabetes	Oral	Genzyme
VivaGel®	Lysine-based dendrimer	Microbiocide	Topical	Starpharma

**Ala: Alanine, ALL: Acute lymphoblastic leukemia, AMD: Age-related Macular Degeneration, EPO: Epoetin beta; Fab: Fragment antigen-binding, HGH: Human Growth Hormone, hrGCSF: human recombinant Granulocyte-Colony Stimulating Factor, i.m.: intramuscular, i.v.: intravenous, s.c.: subcutaneous, Tyr: Tyrosine, TNF: Tumor Necrosis Factor.*

Table 1.4 *Examples of polymer therapeutics in clinical development. Adapted from ref (England et al. 2012; Duncan and Gaspar 2011; Duro Castaño 2015)*

Product name	Technology	Indication	Route	Stage	Information source
		Polymer-protein conjugates			
ADI-PEG 20	PEG-arginine deaminase	Cancer-hepatocellular carcinoma, melanoma	i.v.	Phase III	Polaris Group
Hemospan® MP40X	PEG-hemoglobin	Delivery of O2 in post-surgery and trauma patients	i.v.	Phase III	Sangart
CDP 791	PEG-anti VEGFR-2- Fab	Cancer-NSCLC	i.v.	Phase II	UCB Pharma
		Polymer-aptamer conjugates			
ARC1779	PEG-anti-platelet-binding function of von Eillebrand Factor	Thrombotic microangiopathies	i.v.	Phase II	Archemix
E10030	PEG-anti-PDGF aptamer combination with Lucentis®	AMD	Local intravitreal	Phase III	Ophthotech
		Polymeric drugs			
AMG 223	Phosphate binding polymer	Hyperphosphatemia in CKD patients on hemodialysis	Oral	Phase II	Amgen

Polymeric Drug-Conjugates

CT-2103; Xyotax; Opaxio	Poly-glutamic acid (PGA)-paclitaxel	Cancer-NSCLC, ovarian, various other cancers and combinations	i.v.	Phase III	Cell Therapeutics Inc
Prolindac®	HPMA-copolymer- DACH platinate	Cancer-melanoma, ovarian	i.v.	Phase III	Access Pharmaceuticals
FCE 28068 (PK1)	HPMA-copolymer-DOX	Breast, lung and colon cancer	i.v.	Phase II	Pfizer
FCE 28069 (PK2)	HPMA-copolymer-DOX	Hepatocellular carcinoma	i.v.	Phase I/II	Pfizer
PEG-SN38	Multiarm PEG-camptothecan	Cancer-various	i.v.	Phase II/III	Enzon Inc
CRLX101	CD-PEG-camptothecin	Cancer-various	i.v.	Phase I/II	Cerulean Pharma
CRLX301	CD-PEG-Docetaxel	Solid tumors	i.v.	Phase I	Cerulean Pharma
DEP™ Docetaxel	Dendrimer-Docetaxel	Solid tumors	i.v.	Phase I	Starpharma/ AstraZeneca
NKTR-181	PEG-naloxone	Chronic pain	Oral	Phase III	Nektar
NKTR-171	PEG-Na+ channel blocker	Neuropathic pain	Oral	Phase I	Nektar
NKTR-102	PEG-irinotecan	Cancer-various	i.v.	Phase II/III	Nektar
XMT-1001 (Fleximer® based)	Polyacetal-camptothecin	Cancer-various	i.v.	Phase I/II	Mersana

XMT-1107	Polyacetal-fumagillin	Solid tumors	i.v.	Phase I	Mersana/Teva
		Micelles			
SP1049C BiotransportTM	Pluronic® formulation of DOX	Cancer-upper GI, NSCLC colorectal	i.v.	Phase III	Supratek Pharma Inc
NK 105 (Nanocarrier® technology)	Paclitaxel block copolymer micelle	Breast cancer	i.v.	Phase III	Nippon Kayaku Co
NC-6004, NanoplatinTM	Cisplatin block copolymer micelle	Cancer-various	i.v.	Phase I/II	NanoCarrier Co./ Orient Neuropharma
NC-4016 (Nanocarrier® technology)	Oxaliplatin block copolymer micelle	Solid Tumors	i.v.	Phase I	NanoCarrier Co
NC-6300 (K-912)	Epirubicin bock copolymer micelle	Solid Tumors	i.v.	Phase I	NanoCarrier Co./Kowa

**CD: Cyclodextrin, CKD: Chronic Kidney Disease, DACH: 1,2-diaminocyclohexane, GI: Gastro-Intestinal, NSCLC: Non-Small Cell Lung Cancer, PDGF: Platelet Derived Growth Factor, VEGF: Vascular Endothelial Growth Factor.*

1.6.2 Rational design of polymeric nanosystems

Polymeric nanosystems can be separated into two categories: polymer-protein and polymer-drug conjugates. When delivering proteins, one mainly seeks to improve protein stability after application and to reduce immunogenicity. With drugs that possess lower molecular weight, the system primarily aims to influence pharmacokinetics at whole organism and at cellular level. The following design rationale can be shared by both polymer-protein and polymer-drug conjugates: improving ability to cross biological barriers, recognition of specific targets, hence decreasing non-specific toxicities, controlling drug release rate and enhancing its therapeutic value (Duro Castaño 2015).

1.6.3 Advantages of polymeric nanosystems

Polymer therapeutics offer several advantages including: i) improve aqueous solubility of poorly soluble drugs such as cisplatin and paclitaxel; ii) decrease kidney clearance by increasing hydrodynamic volume, resulting in longer plasma half-life; iii) prevent or reduce aggregation by offering steric hindrance; iv) protection against proteolytic enzymes, help to avoid immunogenicity and antigenicity; v) with targeted delivery system, it can also help to decrease unspecific cellular uptakes (Dyawanapelly *et al.* 2014; Duncan 2011). Other advantages can include higher internalisation in specific cells and decrease in toxicity. Nanoparticles coated with hydrophilic

polymers such as PEG and chitosan improve protein transport through preferential mucoadhesion (Tobio *et al.* 2000; Vila *et al.* 2002). PEG-coated nanoparticles also offer greater stability against aggregations, lower toxicity and minimisation of immunogenicity (Liechty *et al.* 2010).

Interestingly, in lungs, nanomedicines with appropriate design can also help to avoid the mucociliary escalator mechanism, and escape phagocytosis of alveolar macrophages (Bailey and Berkland 2009).

1.6.4 Disadvantages of polymeric nanosystems

Despite these advantages, several challenges in the use of nanomedicines for pulmonary delivery need to be considered. In the case of liposomes, although they have great potentials in drug delivery, their physical and chemical stability – e.g. their tendency to be disrupted or to aggregate - can limit their applications *in vivo* . Another example is the solid lipid nanoparticles which showed poor capacity to load drug, and premature release of drug which can occur during storage (Ramteke K.H 2012). Within this context, polymeric nanosystems are gaining popularity, as they could potentially overcome many of the limitations presented by the other nanocarrier systems. Polymeric materials can slow down the degradation of their protein cargoes. While this is often desirable, it could also promote the accumulation of protein/polymer in the body and eventually cause long term toxicity (Sivadas *et al.* 2008; Lee *et al.* 2015).

Studies have also found that positively charged polymers can lead to higher toxicity on different cells and tissues compared to negatively and neutral polymers (Fischer *et al.* 2003; Lv *et al.* 2006). Thus, special attention must be paid to limit these undesirable effects *in vivo*. For pulmonary delivery, *in vitro* toxicity studies with appropriate lung models should be performed to address their effect on cell metabolic activity, the release of inflammatory mediators and the membrane integrity of cells after exposures to nanocarriers.

1.6.5 Polymer-drug conjugates

This pharmaceutical formulation strategy emerged as a potential solution to evade many of the limitations presented by peptide/protein/antibody therapies that have limited water stability, short circulation half-life, poor therapeutic outcomes as well as possible immunogenic responses (Duncan *et al.* 2006).

Notably, linear polymers with random-coil conformations are most commonly used to synthesise polymer therapeutics in the clinic. These include natural polymers (dextran (α-1,6 polyglucose), dextrin (α-1,4 polyglucose), hyaluronic acid, cyclodextrin); and synthetic polymers, such as polyethylene glycol (PEG), *N*-(2-hydroxypropyl) methacrylamide (HPMA) copolymers, polyacetals and poly-L-glutamic acid (PGA) (Duncan and Vicent 2013).

PEG for protein conjugation has exhibited the greatest clinical success thus far (Davis 2002). PEGylation technology is the use of

PEG building block to conjugate with protein drug which has been approved by the FDA (Food and Drug Administration) (Alconcel *et al.* 2011) with various examples already in clinical use **(Table 1.3)**. PEGylation increases protein drug solubility and stability in circulation; it can also help reduce immune recognition and prolongs plasma half-life by avoiding rapid excretion through reticulum endothelium system, overall yielding better patient compliance (Abuchowski *et al.* 1977).

One of the first FDA approved PEG–protein formulation (Adagen®) was in 1990, used as an enzyme replacement therapy for adenosine deaminase deficiency in patients with severe combined immunodeficiency (Hershfield *et al.* 1987). While the PEGylated Factor VIII (Jivi®) to treat Haemophilia A was the most recently approved following clinical success of the technology (Ekladious *et al.* 2019).

As shown in **Table 1.3** and **Table 1.4**, the product on the market and in development are mainly administered by intravenous injections and this is far more common compared to pulmonary administration due to the barriers presented in lungs as mentioned in previous sections. However, polymeric nanosystems containing proteins and small molecule drugs are gaining more interest through pulmonary delivery systems in the 21st century (Menon *et al.* 2014; Loira-Pastoriza *et al.* 2014; Sivadas *et al.* 2008; Pirooznia *et al.*

2012; Al-Qadi *et al.* 2012; Paranjpe and Müller-Goymann 2014; Velino *et al.* 2019).

Small molecule drug tobramycin was encapsulated in particles based on poly(d,l,-lactide-co-glycolide) (PLGA) and poly(ethylene glycol)-co-poly(d,l,-lactide-co-glycolide) diblock (PEG-PLGA) with spherical shaped particle sizes of 225-231 nm possessing negative zeta potentials to overcome the biofilm barrier of *P. aeruginosa* and *B. cepacia* effect of the formulated tobramycin was strongly enhanced under fluidic experimental conditions as well as under static conditions in artificial mucus without cytotoxicity *in vitro* in human lung epithelial cells (Ernst *et al.* 2018). An example of pulmonary protein delivery was the insulin-loaded poly(DL-lactic-*co*-glycolic acid) nanospheres granulated with mannitol, which also had a stronger and prolonged pharmacological effect compared to the inhalation of insulin solution (Yamamoto *et al.* 2007).

Closely related to pulmonary delivery, intranasal administration of polymer-protein conjugate was also demonstrated by entrapping basic fibroblast growth factor in solanum tuberosum lectin-targeted polyethylene glycol-polylactide-polyglycolide (PEG-PLGA) nanoparticles. The nanoparticles had negative zeta potential and were designed to selectively bind to *N*-acetylglucosamine on the nasal epithelial membrane for brain delivery (Zhang *et al.* 2014a). Upon intranasal administration in rats, solanum tuberosum lectin targeted PEG-PLGA basic fibroblast growth factor nanoparticle

formulation (STL-bFGF-NP) had highest brain distribution compared to non-targeted nanoparticles, free fibroblast growth factor and the same formulation administered *via* intravenous route. The increased concentration of basic fibroblast growth factor delivered in the brain also corresponded to significant improvement in the spatial learning and memory of Alzheimer's disease rats in STL-bFGF-NP group, compared with Alzheimer's disease model group (Zhang *et al.* 2014a).

The success of polymer therapeutics show that with appropriate design, polymers can protect incorporated proteins from extreme environmental conditions such as proteolytic enzymes and increase the bioavailability of drugs at the target sites (Anand *et al.* 2007; Hamid Akash *et al.* 2015; Bertrand *et al.* 2014). However, this effect cannot be taken for granted, careful attentions are needed to investigate the stability and the toxicological profile of polymeric systems case-by-case. Studies have reported lung accumulation of polymeric materials with slow degradation profiles resulting in long-term toxicity (Sivadas *et al.* 2008; Armstrong *et al.* 1996; Lee *et al.* 2015). Surface charge is also important in respect to biological effect namely cellular trafficking and biodistribution profile of formulations. For instance, neutral or negatively charged surfaces usually avoid non-specific uptakes and positively charged surfaces are prone to tubular reabsorption in the kidneys (Scheinberg *et al.* 2010). Studies have also indicated the higher cytotoxicity produced by positively

charged polymers on different cells and tissues (Fischer *et al.* 2003; Lv *et al.* 2006). All these issues must be considered when choosing the appropriate polymer carrier for the desired application.

1.6.5.1 Covalent polymer-protein conjugates

Proteins can be covalently conjugated to a range of natural and synthetic polymers *via* different synthetic approaches (Klok 2005; Van Rijn 2013). As mentioned in Section 1.6.5, covalently linked polymer-drug conjugates possess the ability to improve therapeutic outcomes: this conjugation can improve protein stability in plasma, increase circulation half-life and reduce immunogenicity; and for small molecules, renal glomerular filtration rates can be effected (Mero *et al.* 2009). However, due to covalent bonding between polymer and drug conjugate, key amino acids responsible for the protein bioactivity could be irreversibly modified in the process; steric shielding of the protein active site could also occur rendering the inactivation of the therapeutic agent, leading to poor clinical outcome. (Zhang *et al.* 2014b; Greenwald *et al.* 2003; Kalaydina *et al.* 2018). In addition, several synthetic and purification steps may be needed to afford the final polymer-drug conjugate (Gauthier and Klok 2010), and other than the extra costs involved, damages to the fragile formation of protein therapeutics could also occur (Frokjaer and Otzen 2005).

1.6.5.2 Electrostatic interactions

To overcome the challenges posed by covalent polymer conjugation, non-covalent conjugation strategies have been explored. Research mainly focussed on conjugation through hydrophobic polymer-protein interactions (Salmaso *et al.* 2012; Ambrosio *et al.* 2016; Salmaso *et al.* 2014), lectin-glycopolymer recognition (Antonik *et al.* 2016), and electrostatic complexation (Harada and Kataoka 1998; Tsiourvas *et al.* 2012; Coue and Engbersen 2011; Lee *et al.* 2008). Among the non-covalent polymer-drug/protein complexation strategies, ionic interacting complexes have received special attention and have been increasingly investigated as alternatives to covalent conjugation (Kurinomaru *et al.* 2014). The complexation model relies on interaction between polymers presenting multiple copies of charged repeating units, and oppositely charged residues such as amine groups of amino acids at the surface of drug molecules or proteins. The pH of the reaction and storage media can greatly affect both the assembly process, and stability of the resulting polymer-protein complexes, as the complex formation is dependent on the protonation/deprotonation of ionisable residues (Kurinomaru and Shiraki 2015; Mueller *et al.* 2012).

Ionic complexation offers two main advantages over covalent conjugates: i) polymer-protein/drug complexes are achieved by simple mixing of protein/drug and polymer solutions. Thus, often complex synthetic routes for the attachment of end-functionalised

polymers to proteins or drugs and subsequent characterisation of conjugates are not required. ii) The intrinsically reversible nature of these interactions can allow complex disassembly under specific conditions - e.g. those found in the proximity of the intended biological target - which can offer therapeutic advantages.

Stable complexes in nanometre size range have been assembled between PEG-polyanion/polycation copolymers and charged macromolecules including proteins (Harada and Kataoka 1998) and DNA (Harada-Shiba *et al.* 2002). Protein nanocomplexes with an average diameter of around 50 nm were produced from lysozyme and PEG-*b*-poly(aspartic acid) (Harada and Kataoka 1998), lysozyme and PEG-*b*-poly(glutamic acid) (Nieto-Orellana *et al.* 2017). A detailed review on this topic was recently published by Cabral *et al*. (Cabral *et al.* 2018). However, despite these pioneering studies, the field of non-covalent polymer conjugation is still in its infancy; more advanced delivery method of such system for instance, targeted delivery, remains still largely unexplored.

1.7 Project overview

In summary, pulmonary protein delivery is a promising non-invasive route of drug administration. Importantly, the field of non-covalent protein-polymer conjugation is still in its infancy, this is a promising

field to be investigated and explored further as lung delivery systems.

The work presented in this thesis is predominantly to develop ligand targeted non-covalent polymer protein complexes suitable for inhalation delivery to the lungs. Work initially focussed on the assessment of Calu-3 cells' suitability as lung epithelial model to study the vitamin B_{12} transport pathway. Followed by synthesis of B_{12}-targeted anionic PEG-*b*-poly(glutamic acid) copolymers, investigating the potential of b_{12} receptor mediated cellular uptake of protein-polymer complexes in lung models. Next, to expand the applicability of the novel ligand targeted non-covalent polymer-protein complexes delivery system, biotin targeted anionic PEG-*b*-poly(glutamic acid) polymers were synthesised and the polymer-protein complexes were investigated upon cellular internalisation by A549 cells for their intactness in cells and followed by investigation into the mechanisms of cellular uptake of the biotin-PEG-*b*-poly(glutamic acid):lysozyme nanocomplexes in A549 cells. Finally, the ability of the PEG-*b*-poly(glutamic acid) copolymers to interact *via* electrostatic interaction with lower molecular weight drug for the treating pulmonary infections were examined using bacteria cultures to assess its antibacterial efficacy.

Chapter 2. Materials and general methods

2.1 Materials

2.1.1 Cells, culture medium, medium components and cell solutions

Caco-2 cells were obtained from the European Collection of Cell Cultures (ECACC) and used at passages 30-60. Calu-3 and A549 cells were obtained from the American Type Culture Collection (ATCC) and used between passages 20-35. Dulbecco's Modified Eagles Medium (DMEM) with or without phenol red, Hanks Balanced Salt Solution (HBSS) without phenol red, 2.5% Trypsin/EDTA solution, Phosphate buffer saline (PBS) tablet, foetal bovine serum (10%), L-glutamine (200 mM), antibiotic solution (100 U/mL penicillin and 0.1 mg/mL streptomycin) and non-essential amino acids (100%) were purchased from Sigma Aldrich. Cell medium DMEM was supplemented with penicillin, streptomycin and amphotericin at final concentrations of 100 units/mL, 0.1 mg/mL and 0.25 µg/mL, respectively, plus L-glutamine and non-essential amino acids (Fisher Scientific). FBS at a final concentration of 10% v/v made with deionised water and sterilised.

2.1.2 Plasticware and glassware

Polystyrene transwell® permeable supports, referred to in this thesis as 'filters' or 'transwells', of 12 mm diameter, 0.4 µm pore size (with a surface area of 1.1 cm^2) were obtained from Corning Life Sciences (Holland). Cell culture flasks (75 cm^2, canted neck with vented caps), 96-well polystyrene microplates (black or clear, noncell culture treated) and sterile pipettes, used routinely for the maintenance of cells, were also purchased from Corning Life Sciences (Holland). Clear, tissue culture treated 96-well plates, black 96-well microplates (used for fluorescence measurement) and sterile cryovials (1 mL capacity) were supplied by Nunc. Sterile centrifuge tubes (of 15 ml and 50 ml volume capacity) were purchased from Greiner (USA).

2.1.3 Cell toxicity assay reagents

3-(4,5-dimethylthiazol-2-yl)-5(3-carboxymethonyphenol)-2-(4-sulfophenyl)-2H-tetrazolium-(MTS) reagent (commercially known as 'CellTiter 96 AQueous One Solution Cell Proliferation Assay') was purchased from Promega (UK).

2.1.4 Chemicals and reagents

L-Glutamic acid γ-benzyl ester (≥99.0%), allyl bromide (97%), cysteamine hydrochloride (≥98%), 4-(4,6-dimethoxy-1,3,5-triazin-

2-yl)-4-methylmorpholinium chloride (DMTMM), *p*-toluenesulfonyl chloride (≥99.0%), trimethylamine (≥ 99.0 %), sodium bicarbonate, sodium azide (≥99.0%), cyanocobalamin (vitamin B_{12}, ≥98.0%), 1,1'-carbonyldiimidazole (CDI), dibenzocyclooctyne-amine, sodium phosphate dibasic (99.9%), sodium phosphate monobasic dehydrate (≥99.0%), L-leucine, D-(+)-trehalose dehydrate, 1-butanol, 1M ammonium hydroxide solution, acetonitrile (anhydrous, 99.8%), dichloromethane (anhydrous, ≥99.8%), tetrahydrofuran (THF, anhydrous, ≥99.9%), triphosgene 98.0%, methanol (MeOH, anhydrous, 99.8%), dimethyl sulfoxide (DMSO, anhydrous, ≥99.9%), Triton X-100, Tris-acetate-EDTA (TAE) buffer, mounting medium, deuterated chloroform ($CDCl_3$, 99.8 atom % D), deuterium oxide (D_2O, 99.9 atom % D) and deuterated methanol (CD_3OD, 99.8 atom % D) were purchased from Sigma Aldrich. Methyl 3,4,5-trihydroxybenzoate (98.0%), potassium carbonate anhydrous (≥99.0%), sodium hydroxide (≥97.0%), 2,2-dimethoxy-2-phenylacetophenone (DPAP) (99.0%), hydrochloric acid, magnesium sulphate dried, toluene, methanol, diethyl ether anhydrous, propan-2-ol and petroleum ether were supplied by Fisher Scientific. Lysozyme molecular biology grade was purchased from Alfa Aesar. *O*-(2-aminoethyl)polyethylene glycol 3.0 kDa and cyanine 5 NHS ester were supplied by Iris Biotech and Lumiprobe, respectively. All the chemicals were used as received without further

purification. Anhydrous solvents were used as received and stored under dry and inert atmosphere. Thin layer chromatography (TLC) was carried out on pre-coated TLC sheets ALUGRAM®SIL G/UV254 purchased from Macherey-Nagel. TLCs were visualized by exposure to UV light (254 nm) followed by staining with $KMnO_4$. Transferrin Alexa Fluor® 488 Conjugate (T*f*) and cholera toxin B subunit Alexa Fluor® 488 Conjugate (CTß) were purchased from Fisher scientific (UK). Agarose powder was obtained from MP Biomedicals (USA). Pharmacological inhibitors: concanavalin A, chlorpromazine, dynasore, genistein, MßCD, nystatin, filipin, EIPA and cytochalasin D were obtained from Sigma-Aldrich (UK). All other chemicals were obtained from Sigma Aldrich.

2.2 Methods

2.2.1 Maintenance of cells

2.2.1.1 Maintenance of cells in culture flasks

All cell lines were routinely cultured in 75 cm^2 flasks at 5% CO_2, 95% relative humidity and 37°C until confluence (in this work confluence was considered as approximately 75-95% coverage of the flask surface by cells). Cell culture medium was replaced every other day by aspirating the old culture medium from the flasks, followed by

the addition of 10 mL of fresh medium, pre-warmed to 37°C. Cell growth was monitored regularly by viewing the cells under an optical microscope. Once confluent, cells were passaged using the following procedure: culture medium was removed (aspirated) from the flask and cells washed with PBS (6 ml, pre-warmed to 37°C), which was added to the flask and the flask gently swirled. Fresh PBS was used to remove any dead cells remaining in the flask and traces of medium; it was important to perform this step prior to the addition of trypsin/EDTA solution to cells since FBS present in the cell culture medium inhibits the action of trypsin. PBS was then aspirated and replaced with 3 ml of pre-warmed (37°C) 2.5% trypsin/EDTA solution. The flask was gently swirled to ensure that trypsin/EDTA solution covered the cells and then transferred to the incubator at 37°C. The flask was observed at regular intervals for cell detachment from the tissue culture flask plastic. The period of incubation with trypsin/EDTA solution was dependent on the cell line and the extent of confluence. Generally, for Caco-2 and A549 cells an incubation period of approximately 10 min was sufficient for complete cell detachment from the flask plastic. On the other hand, Calu-3 cells required no less than 15 min incubation with trypsin/EDTA for complete detachment. Following cell detachment, approximately 9 ml of pre-warmed (37°C) culture medium was added to the flasks in order to dilute the cell suspension and deactivate trypsin (different

medium were used for each cell line, as will be described later). The resulting cell suspension was transferred to a sterile centrifuge tube and the cells centrifuged (pelleted) at 180 x g for 5 min. Trypsin-containing supernatant was aspirated and pre-warmed culture medium (37°C, 5-10 ml) added to the cell pellet to create a cell suspension. A proportion of the resulting cell suspension was transferred to a new flask (containing pre-warmed culture medium appropriate for the cell line) for further culturing. Split ratios between 1:3 and 1:5 were normally used for Calu-3 cells, while higher ratios between 1:6 and 1:10 were typically used for both A549 and Caco-2 cells.

2.2.1.2 Frozen storage of cells

Cells were cultured to confluence and then detached from the flask as described previously (section 2.2.1.1). Following centrifugation of the cell suspension, the supernatant was aspirated, and the cell pellet re-suspended in 1 mL of complete culture medium containing sterile DMSO. The concentration of DMSO used was 5% v/v for Calu-3, Caco-2 cells and A549 cells. The cell suspension was added to a sterile cryovial (clearly labelled with the cell type, passage number, user name and date), which was placed into a freezing container ('Mr Frosty') in a - 80°C freezer for a gradual, controlled temperature decrease. Cells were stored at – 80°C for up to 4 weeks. Thereafter,

cells were transferred into a liquid nitrogen cell storage tank. Half of cells from a single confluent monolayer in one 75 cm2 tissue culture flask were transferred and stored frozen in a single cryovial; multiple flasks of cells were routinely detached and transferred into the equivalent number or sterile cryovials for frozen storage.

2.2.1.3 Cell revival

Cryovials containing frozen cells were removed from the liquid nitrogen-containing storage tank and thawed by placing the cryovial in the incubator at 37°C for approximately 5 min. DMSO-containing medium was removed by transferring the cell suspension into a centrifuge tube containing approximately 8 ml of warm (37°C) culture medium, centrifuging the resulting suspension at 180 x g for 5 min and aspirating the supernatant. The cell pellet was thereafter suspended in approximately 2 mL of culture medium and transferred into a 25 cm^2 flask containing approximately 3 mL of fresh, warmed (37°C) culture medium. Cells from one cryovial were revived and transferred into one tissue culture flask.

2.2.1.4 Culture of cells on Transwell®

Calu-3 cells

Calu-3 cells were cultured to confluence in 75 cm^2 flasks at 5% CO_2 and 37°C. Cells were then detached from the flasks using the

method described above (Section 2.2.1.1). Transwell® filters were incubated with DMEM (250 µl and 1.5 ml on the apical and basolateral chambers, respectively) at 37°C for approximately 15 min prior to the addition of cells. This was performed in order to coat the surface of the filter plastic with proteins present in the culture medium (serum), to encourage cell attachment to plastic. It should be noted that polystyrene transwell filters were used for all experiments in this thesis, as opposed to polycarbonate filters due to better attachment by cells. Cells were counted using a haemocytometer and the volume of the cell suspension containing the required number of cells was calculated. These volumes were subsequently added to the donor compartments of the transwell. The number of cells added ('seeding density') was $1x10^6$ cells cm^{-2} on Transwell® inserts (12 mm diameter, 0.4 µm pore size; Corning Life Sciences, USA). The apical chamber volume was made up to 500 µL by adding warmed DMEM. After seeding on filters, cells were maintained at 5% CO^2 and 37°C with DMEM. Cells were cultured using air-interface culture (AIC) conditions known to promote mucus secretion, starting from day 2 post-seeding on Transwell® inserts. Cells were cultured on transwells with medium (0.5 mL) present in the basolateral chamber only. Calu-3 cells were typically cultured on filters for 14 days with medium replacement every two days prior to their use in experiments as confluent and polarised cell layers.

Hereafter, the term 'polarised' is used to define fully differentiated, filter-cultured cell layers.

Caco-2 cells

Caco-2 cells were seeded on filters in a similar way to Calu-3 cells, except that a density of $2x10^5$ cells/cm^2 was used. Caco-2 cells were cultured using liquid covered culture (LCC) conditions, with DMEM as the culture medium (0.5 mL top + 1.5 mL bottom) and were routinely grown on filters for 14 days (with culture medium replaced every other day) prior to their use in experiments as confluent, polarised cell monolayers.

2.2.1.5 Measurement of TEER

Transepithelial electrical resistance (TEER) is a convenient, reliable and non-destructive method to monitor the growth of epithelial tissue cultures *in vitro*, with the added benefit of determining cell layer integrity and assed for the presence and the tightness of the cellular tight junctions (TJs) (Chen *et al.* 2015). By measuring the resistance to ion flux across an epithelial layer linking to tight junction disruption, it can also provide an indication of cellular viability (Narai *et al.* 1997). TEER can be conveniently measured using a portable ohmmeter (EVOM, World Precision Instruments), comprising a set of "chopstick" electrodes. The chopstick electrodes

were firstly pre-sterilised by immersing in absolute ethanol for approximately 30 min prior to their use. The electrodes were then washed with PBS and carefully placed in the culture medium bathing the cell layers; the shorter electrode was submerged in the medium present in the apical chamber, while the longer electrode was placed in the basal medium. Cell confluence and cell layer integrity before treatments with test samples was confirmed by transepithelial electrical resistance (TEER) measurements (EVOM voltohmmeter, World Precision Elements, USA). Prior to the application of test samples to cells, the culture medium was removed, cells washed with PBS and HBSS (warmed to 37°C; pH 7.4) added to both sides of the cell layers and were allowed to equilibrate for at least 30 min, followed by TEER measurements. Cells included in the experiments always had values higher than 550 Ω cm^{-2}.

2.2.2 Synthesis

2.2.2.1 γ-Benzyl-L-glutamate N-carboxyanhydride (NCA)

Synthesised previously in the group (Nieto-Orellana *et al.* 2017) and descried here briefly. L-Glutamic acid γ-benzyl ester (13.7 g, 57.8 mmol) was added to a dry round bottomed flask. Anhydrous THF (200 mL) and triphosgene (6.8 g, 23 mmol) were then added under nitrogen atmosphere. The mixture was heated at 50 °C under stirring. The reaction mixture turned clear in about 1 h. The solution

was then cooled down to room temperature and bubbled with nitrogen for 2 h to remove traces of gaseous co-products (during this process the outlet was connected to a NaOHaq trap). The solution was then concentrated under vacuum to a ~10 mL volume, precipitated with petroleum ether, filtered, washed with petroleum ether and recrystallised from THF : petroleum ether 1 : 1 (v/v) at 0 °C to give the desired product as crystalline solid.

2.3 Statistical Analysis

Statistical comparisons (for a maximum of two data sets in any given comparison) were performed by Student's t-test. Values of $p<0.05$ were considered statistically significant. One-way analysis of variance (ANOVA) was applied for comparison of group means of three or more groups with normal distribution date sets. P values of < 0.05 were considered statistically significant. *, **, *** and **** indicate $p<0.05$, $p<0.01$, $p<0.001$ and $p<0.0001$, respectively. 'ns' indicates non-significant.

Chapter 3. B_{12} targeted PEG-*b*-poly(glutamic acid) complexes for inhalation protein delivery to the lung

3.1 Introduction

Pulmonary delivery is increasingly investigated as an alternative route for the delivery of bio-therapeutics, including proteins (Patil and Sarasija 2012). Several proteins and peptides - e.g. cyclosporine A to treat asthma, and interleukin-2 to treat pulmonary metastases of renal cell carcinoma (Rohatagi *et al.* 2000; Merimsky *et al.* 2004) have been investigated for delivery to the lung. In 2014, an inhaled insulin preparation Afrezza was approved by the US Food and Drug Administration (Klonoff 2014), and is a currently available option in diabetes treatment. However, the lung presents specific barriers for macromolecular/protein therapeutics. Susceptibility to enzymatic degradation, poor absorption across the epithelial barrier, as well as lung induced immunogenicity are significant challenges to be addressed if this approach is to be adopted as a viable alternative for protein delivery (Baker *et al.* 2010; Hussain *et al.* 2004). Covalent attachment of PEG (generally referred to as PEGylation) has been widely utilised to increase protein resistance to enzymatic degradation and reduced immunogenicity (Turecek *et al.* 2016). PEGylation has been shown to enhance protein absorption following

nasal administration through prolongation of protein action time (Youn *et al.* 2008; Kim *et al.* 2012), and several studies showed promising delivery of PEGylated therapeutics to both the upper and lower respiratory tract for either systemic or local therapeutic effects (Croyle *et al.* 2008; Sahib *et al.* 2011).

To date, chemical conjugation to a therapeutic protein has been used in the vast majority of PEGylation studies (Kataoka *et al.* 2000; Dozier and Distefano 2015). However, a potential disadvantage of this approach is the decrease in the protein's therapeutic effect due to irreversible modification/steric shielding of its active site (Rodriguez-Martinez *et al.* 2008). Non-covalent PEGylation, i.e. formation of protein–polymer non-covalent complexes has been explored as a potentially suitable alternative. In a seminal work from Kataoka's group, stable complexes in nanometre size range were assembled from PEG-*b*-polyanion or PEG-*b*-polycation copolymers and charged macromolecules, including proteins (Harada and Kataoka 1998). Non-covalent PEGylated complexes were also produced from insulin and oligolysine or oligoarginine type peptide polymers functionalised with PEG (Tsiourvas *et al.* 2012). An alternative to non-covalent PEGylation based on electrostatic interactions between PEG-*b*-polyelectrolyte copolymer and selected protein, PEG bearing a terminal cholanic moiety ($mPEG_{5k}$-cholane) was utilised to generate polymer conjugates through non-covalent hydrophobic interactions with a range of protein and peptides,

including recombinant human granulocyte colony stimulating factor (rh-G-CSF) (Salmaso *et al.* 2012), palmitoylated vasoactive intestinal peptide (VIP) (Ambrosio *et al.* 2016), and recombinant human growth hormone (rh-GH) (Salmaso *et al.* 2014). These non-covalent protein-polymer complexes can be assembled by simply mixing protein and polymer components under optimised conditions, avoiding the often-complex conjugation chemistries required for covalent PEGylation. The intrinsically reversible nature of these interactions potentially allows complex disassembly under specific conditions - e.g. those found in the proximity of the intended biological target - which addresses the potential disadvantages of covalent conjugation discussed above.

In this work, we present a further development in the non-covalent PEGylation approach, by engineering ligand-targeted non-covalent complexes which exploit cell-specific transport pathways for the intracellular delivery of therapeutic protein. Accordingly, we synthesised cyanocobalamin (vitamin B_{12}) ligand-targeted complexes based on B_{12}-PEG-*block*-poly(glutamic acid) (B_{12}-PEG-*b*-pGA), using lysozyme as a model protein cargo. B_{12}-PEG-*b*-pGA copolymers were synthesised and used as 'complexing excipient' to assemble nano-sized complexes with the model protein, which can then be spray-dried into inhalable dry powders for inhalation delivery to the lung epithelium. In *in vitro* studies, Calu-3 cells were chosen as lung epithelial model and were grown as polarised layers in air-

liquid interface culture (AIC) conditions to promote mucus secretion, normally considered to mimic lung physiological conditions (Grainger *et al.* 2006). Data show enhanced cellular internalisation of targeted complexes, relative to non-targeted counterparts or 'free' protein. *In vivo* lung tolerability assessment shows no significant signs of lung inflammation on repeated administration of formulated dry powders to healthy mice. *In vivo* lung deposition data illustrate ability of the complexes formulated as dry powders to deposit and retain model protein cargo in the lung tissue following pulmonary administration.

3.2 Methods

3.2.1 Synthesis of cyanocobalamin fluorescent probe pyr- B_{12} (Figure 3.2)

*3.2.1.1 Pyranine methyl ester **(i)***

8-Hydroxypyrene-1,3,6-trisulfonic acid trisodium salt (pyranine, 1.00 g, 1.91 mmol, 1 eq.) was added to methanol (60 mL) and heated to reflux (65 °C) under stirring to ensure full dissolution, protected from light. Methyl bromoacetate (1.11 g, 7.24 mmol, 3.8 eq.) and DIPEA (*N,N*-diisopropylethylamine, 0.690 g, 5.32 mmol, 2.8 eq.) were dissolved in methanol (6.0 mL) in a separate flask, and the resulting solution added portion wise - a third of the total volume every 1.5 h, to the refluxing solution of pyranine. The resulting yellow mixture was further refluxed for 3 h, still protected from light,

and then left stirring at room temperature (22 °C) overnight before precipitation in 200 mL isopropanol. The solid was then collected by centrifugation at 3,400 x g for 15 min (Megafuge™, Thermo Scientific™), residual traces of solvent were removed under reduced pressure, and the resulting crude product **(i)** used for the next step without further purification. Yield: 938 mg, 82 %.

^{1}H NMR (400 MHz, methanol-d_4) δ 9.44 (s, 1H, C$H_{aromatic}$), 9.28 (d, J = 9.7 Hz, 1H, C$H_{aromatic}$), 9.26 (d, J = 9.7 Hz, 1H, C$H_{aromatic}$), 9.18 (d, J = 9.8 Hz, 1H, C$H_{aromatic}$), 8.75 (d, J = 9.6 Hz, 1H, C$H_{aromatic}$), 8.32 (s, 1H, C$H_{aromatic}$), 5.21 (s, 2H, OCH_2), 3.87 (s, 3H, OCH_3). ESI-TOF mass spectrometry: expected m/z [M – Na^+] 618.89, found 618.90.

*3.2.1.2 Carboxyl pyranine **(ii)***

Pyranine methyl ester **(i)** (200 mg, 0.336 mmol, 1 eq.) was dissolved in deionised water (5.0 mL) containing sodium hydroxide (16 mg, 0.40 mmol, 1.2 eq.), and the resulting solution was stirred at 60 °C for 30 min. After cooling to room temperature, the solution was neutralised with aqueous hydrochloric acid, and the desired product was precipitated in isopropanol. The orange precipitate was collected by vacuum filtration, and residual traces of solvent were removed under reduced pressure, to give the intermediate **(ii)** as an orange solid. Yield: 104 mg, 53%.

^{1}H NMR (400 MHz, methanol-d_4) δ 9.44 (s, 1H, C$H_{aromatic}$), 9.28 (d, J = 9.7 Hz, 1H, C$H_{aromatic}$), 9.26 (d, J = 9.7 Hz, 1H, C$H_{aromatic}$), 9.18 (d, J = 9.8 Hz, 1H, C$H_{aromatic}$), 8.79 (d, J = 9.6 Hz, 1H, C$H_{aromatic}$), 5.16 (s, 2H, OCH_2. ESI-TOF mass spectrometry: expected m/z [M – Na^+] 604.88, found 604.88.

3.2.1.3 Amino cyanocobalamin (B_{12}-NH_2)

Carbonyldiimidazole (CDI) (144 mg, 0.890 mmol, 4 eq.) was added to cyanocobalamin (0.300 g, 0.221 mmol, 1 eq.) previously dissolved in anhydrous dimethyl sulfoxide (DMSO) (10 mL). The mixture was stirred for 2 h at 30°C. 2,2'-(Ethylenedioxy)bis(ethylamine) (132 mg, 0.890 mmol, 4 eq.) was then added, and the mixture stirred at room temperature for further 24 h. The mixture was poured into 200 mL ethyl acetate, and the resulting precipitate was isolated by centrifugation at 3,400 x g for 15 min (Megafuge™, Thermo Scientific™) and purified by silica column chromatography (mobile phase: 30:45:4:21 2-propanol: *n*-butanol: $ammonia_{aq}$ (1M) : water vol:vol:vol:vol) and then lyophilized. Yield: 68 mg, 21%. ESI-TOF mass spectrometry: expected m/z [M^+] 1529.68, found 1529.67.

3.2.1.4 Pyranine B_{12} fluorescent probe (pyr-B_{12})

Carboxypyranine **(ii)** (16 mg, 0.028 mmol, 2eq.) and 4-(4,6-dimethoxy-1,3,5-triazin-2-yl)-4-methylmorpholinium chloride (DMTMM) (8 mg, 0.06 mmol, 4 eq.) were dissolved in methanol, in separate flasks (2 mL of methanol per flask). The DMTMM solution

was added to the carboxypyranine solution dropwise, and the resulting solution was left to stir for 1 h at room temperature, followed by addition of a solution of B_{12}-NH_2 (20 mg, 0.014 mmol, 1 eq.) in methanol (5 mL). The resulting mixture was left to stir overnight at room temperature, concentrated under reduced pressure, and the product purified by preparative thin layer chromatography (TLC) (30:40:4:26 2-propanol: *n*-butanol: ammonia (1M) : water vol:vol:vol:vol), extracting the desired fluorescent pyr-B_{12} probe from the relevant TLC band with methanol (yield: 7.7 mg, 54%). ^{1}H NMR (400 MHz, MeOD, δ, ppm): the appearance of the peaks between 9.5-8.5 which corresponded to the aromatic groups within the pyranine structure confirmed the success of conjugation. ESI-TOF mass spectrometry: expected m/z [M^+] 2024.58, found 2024.60.

3.2.2 Synthesis of mPEG$_{2k}$-*b*-pGA copolymer

mPEG$_{2k}$-*b*-GA_{30} copolymer was prepared using a method described previously by our group (Nieto-Orellana *et al.* 2017). Briefly, methoxypolyethyleneglycol amine (mPEG-NH_2) 2 kDa (48 mg, 0.024 mmol) was dissolved in toluene (20 mL), and solvent was evaporated under reduced pressure. This process was repeated three times to remove residual water potentially present in the mPEG-amine starting material. The residue was then dissolved in anhydrous THF (50 mL) and the resulting solution cooled to 0^{o}C. In a separate flask,

γ-benzyl-L-glutamate NCA (274 mg, 1.04 mmol, 43 eq.) was also dissolved in THF (20 mL) and cooled to 0°C before being transferred to the flask containing mPEG-amine initiator. The reaction was left to stir in ice bath under inert atmosphere (N_2) for 5 days and used in the next step without purification. The conversion at 5 days were about 70% as determined by ^{1}H NMR analysis, by comparing the areas of the signals for the α-CH groups at around 5.2 ppm, with the polymer signal located downfield compared to that of the NCA monomer **(Figure 3.4)**.

The same copolymer with different number of glutamic acid repeating units were also synthesised.

mPEG$_{2k}$-*b*-GA$_{10}$

Reaction conditions. Methoxypolyethyleneglycol amine 2kDa (50.0 mg, 0.0250 mmol); γ-benzyl-L-glutamate NCA (92.1 mg, 0.350 mmol, 129 eq.). THF 20ml, conversion 86%

mPEG$_{2k}$-*b*-GA$_{90}$

Reaction conditions. Methoxypolyethyleneglycol amine 2kDa (48.5 mg, 0.0243 mmol); γ-benzyl-L-glutamate NCA (823 mg, 3.13 mmol, 129 eq.). THF 50ml, conversion 81%

3.2.2.1 Hydrolysis of benzyl ester repeating units

Following on from mPEG$_{2k}$-*b*-GA$_{30}$ synthesis in previous section, 2.6 mL of 1M sodium hydroxide solution (2.5 equivalent of NaOH per

benzyl group) were added slowly to the flask containing $mPEG_{2k}$-*b*-GA_{30} under vigorous stirring on day 5 to hydrolyse the benzyl ester groups in the polymer repeating units. The reaction was left to stir at room temperature for a further two days, then the solvent was evaporated under reduced pressure. Deionised water (5 mL) was then added to dissolve the residue, and the resulting solution was dialysed (SnakeSkin™ Dialysis Tubing, 3.5K MWCO) for 2 days against deionised water (10 L, with 3 changes of water per day) before being freeze-dried and analysed by ^{1}H NMR. $M_{n,NMR}$ was determined by comparing the area of the signal at 4.38-3.99 ppm (Hα peak of GA repeating unit), and that of OCH_2CH_2 of the mPEG block at 3.70-3.27 ppm.

$mPEG_{2k}$-*b*-GA_{10} 64.3 mg, 78%. ^{1}H NMR (400 MHz, D_2O, δ, ppm): 4.38-3.99 (m, 14H, HNC*H*CO), 3.70-3.47 (s, 1770H, OCH_2 of PEG), 3.3 (s, 3H, CH_3O of PEG), 2.4-1.6 (m, 77H, CH_2CH_2COOH). $M_{n,NMR}$ = 3.3 kDa

$mPEG_{2k}$-*b*-GA_{30} 171 mg, 95%. ^{1}H NMR (400 MHz, D_2O, δ, ppm): 4.38-3.99 (m, 39H, HNC*H*CO), 3.70-3.47 (s, 165H, OCH_2 of PEG), 3.3 (s, 3H, CH_3O of PEG), 2.4-1.6 (m, 161H, CH_2CH_2COOH). $M_{n,NMR}$ = 7.0 kDa

$mPEG_{2k}$-*b*-GA_{90} 249 mg, 60%. ^{1}H NMR (400 MHz, D_2O, δ, ppm): 4.38-3.99 (m, 14H, HNC*H*CO), 3.70-3.47 (s, 1770H, OCH_2 of PEG),

3.3 (s, 3H, C*H*$_3$O of PEG), 2.4-1.6 (m, 77H, C*H*$_2$C*H*$_2$COOH). $M_{n,NMR}$ = 17 kDa

3.2.3 Synthesis of targeted B_{12}-$PEG_{3.5k}$-*b*-GA_{30} copolymer

3.2.3.1 Synthesis of Azide-$PEG_{3.5k}$-b-GA_{30}

Firstly, azide-polyethyleneglycol amine (N_3-PEG-NH_2) 3.5 kDa as a free base was isolated from its commercially available TFA salt. N_3-$PEG_{3.5k}$-NH_2·TFA(0.100 g) was dissolved in dichloromethane (10 mL). Amberlyst A-21 basic resin was added and the suspension stirred at room temperature for 30 minutes. The mixture was then filtered, and the resin was washed with additional dichloromethane. The organic fractions were pooled, and the solvent was evaporated under reduced pressure. The removal of the TFA salt was confirmed by the absence of signals in the ^{19}F NMR spectrum (N_3-PEG-NH_2·TFA starting material gave a single peak at -75.5 ppm). N_3-PEG-NH_2 free base (48 mg, 0.024 mmol) was then dissolved in toluene (20 mL) and solvent was evaporated under reduced pressure to remove traces of residual water. This procedure was repeated three times. The residue was then dissolved in anhydrous THF (50 mL) and cooled to 0°C. Benzyl-L-glutamate NCA (274 mg, 1.04 mmol, 45 eq.) was separately dissolved in THF (20 mL) and cooled to 0°C before being transferred to the flask containing the N_3-$PEG_{3.5k}$-NH_2 initiators. The reaction was left to stir in ice bath under inert atmosphere (N_2) for 5 days (~ 70%

conversion) and used in the next subsequent deprotection step without purification.

A sodium hydroxide aqueous solution (1 M, 3.1 ml, 2.5 equivalent of NaOH per benzyl group) were then added dropwise to the flask under vigorous stirring to hydrolyse the benzyl ester groups in the polymer repeating units. The reaction was left to stir at room temperature for further two days, after which solvent was evaporated under reduced pressure. Deionised water was then added to dissolve the residue, and the resulting solution was dialysed for 2 days against deionised water. After freeze-drying, azide-PEG$_{3.5k}$-*b*-GA$_{30}$ was then isolated as a white powder.

Azide-PEG$_{3.5k}$-*b*-GA$_{30}$. 130 mg, 54%. ^{1}H NMR (400 MHz, D_2O, δ, ppm): 4.34-4.19 (m, 39H, HNC*H*CO), 3.70-3.47 (s, 300H, OC*H*$_2$ of PEG), 2.27-1.78 (m, 149H, C*H*$_2$C*H*$_2$COOH). $M_{n,NMR}$ = 7.0 kDa

3.2.3.2 α-dibenzocyclooctyne-vitamin B$_{12}$ (DBCO-B$_{12}$)

Cyanocobalamin (vitamin B_{12}, 135 mg, 0.0995 mmol, 1 eq.) was dissolved in anhydrous DMSO (10 mL) under inert atmosphere. 1,1'-carbonyldiimidazole (CDI) (32.2 mg, 0.199 mmol, 2 eq.) was added to round bottom flask, and the reaction was stirred at 30°C for 1.5 h prior to addition of a solution of dibenzocyclooctyne-amine (100 mg, 00.362 mmol, 3.65 eq.) in DMSO (5 mL). The resulting solution was stirred at room temperature protected from light for 24 h. The mixture was then precipitated in diethyl ether, centrifuged at 3,400

x g for 15 min (Megafuge™, Thermo Scientific™), and the solid residue was dissolved in methanol and purified by preparative-TLC (^{i}PrOH : *n*-BuOH : H_2O : NH_4OH 30:45:21:4). The product was extracted from the relevant TLC band using methanol, then the resulting suspension was filtered, and after solvent removal under reduced pressure DBCO-B_{12} was isolated as a pink-red solid. Yield: 31 %. Expected m/z [M-Na^{++}] theor. 851.85, found 851.32.

3.2.3.3 Conjugation of α-dibenzocyclooctyne-vitamin B_{12} to Azide-PEG$_{3.5k}$-b-GA$_{30}$ polymer

Azide-PEG$_{3.5k}$-*b*-GA$_{30}$ (50 mg, 0.0057 mmol, 1 eq.) was dissolved in deionised water (1.5 mL). α-dibenzocyclooctyne-vitamin B_{12} (19 mg, 0.011 mmol, 2 eq.) was dissolved in DMSO (1.5 mL) and then added to the round bottom flask containing the copolymer to form B_{12}-PEG$_{3.5k}$-*b*-GA$_{30}$ copolymer. The mixture was stirred overnight at room temperature, protected from light. The solution was then dialysed (MWCO 3.5 kDa) for 2 days against deionised water, again protected from light, and finally freeze-dried (yield 28%, efficiency of attachment 66.5%).

3.2.4 Preparation of polymer-protein complexes

mPEG$_{2k}$-*b*-GA$_{30}$:lysozyme complexes were prepared at relative molar charge ratios r = 2.5 where r is the charge ratio between the number of glutamic acid residues in the copolymer (negatively charged at physiological pH), and the 17 lysine and arginine residues (positively

charged at physiological pH) of lysozyme. Polymers and protein were separately dissolved in phosphate buffer (PB, 10 mM, pH 7.4) and appropriate aliquots were mixed to achieve r = 2.5. For example, to make 1 mL of complexes at 70 µg/mL protein concentration, 21 µg of $mPEG_{2k}$-*b*-GA_{30} and 70 µg of lysozyme were mixed in 1 mL of 10 mM PB. Specific protein and polymer concentrations are reported in the description of individual experiments below. To prepare targeted polymer-protein complexes, $mPEG_{2k}$-*b*-GA_{30} and B_{12}-$PEG_{3.5k}$-*b*-GA_{30} copolymers were mixed at relative molar ratios of 85:15 (mol:mol), respectively. Polymers mixture and lysozyme were then mixed at relative molar charge ratio of 2.5.

To monitor protein cellular uptake, lysozyme was fluorescently labelled with sulfo-cyanine5 (Cy5) succinimidyl (NHS) ester (Lumiprobe), according to manufacturer protocol (Lumiprobe 2018). Accordingly, 3 equivalents of the fluorescent dye per lysozyme molecule were utilised. Cy5 dye (1.00 mg, 1.29 µmol 3 eq.) and lysozyme (6.00 mg, 0.42 µmol 1 eq.) were dissolved in 0.10 M sodium phosphate buffer at pH 8.4, stirred while protected from light for 4 h at room temperature, and extensively dialysed for 24 h at 4°C against 10 mM pH 7.4 phosphate buffer solution, again protected from light. Protein concentration and degree of labelling were determined using Tech Tip #31 Calculate dye:protein (F/P)molar rations (Scientific 2011) equations after dialysis.

$$\text{Protein concentration (M)} = \frac{A_{280} - (A_{max} \times CF)}{\varepsilon} \times \text{dilution factor}$$

ε = protein molar extinction coefficient (M^{-1} cm^{-1}), ε for lysozyme is 38,940 cm^{-1} M^{-1}

Amax = Absorbance (A) of a dye solution measured at the wavelength maximum (λ_{max}) for the dye molecule, Amax for sulfo-Cy5 is at λ = 646 nm

CF = Correction factor; adjusts for the absorbance at 280 nm caused by the dye, CF for sulfo-Cy5 is 0.04

Dilution factor = the extent (if any) to which the protein:dye sample was diluted for absorbance measurement

$$\text{Moles dye per mole protein} = \frac{A_{max} \text{ of the labeled preotin}}{\varepsilon' \times \text{protein concentration (M)}} \times \text{dilution factor}$$

ε’ = molar extinction coefficient of the fluorescent dye

ε' of sulfo-cy5 dye is 271000 $L \cdot mol^{-1} \cdot cm^{-1}$

3.2.5 cDNA synthesis and quantitative PCR analysis of B_{12} receptor in Calu-3 cells

Total RNA was extracted using RNeasy Mini Kit (Qiagen, Hilden, Germany) according to manufacturer’s instructions assisted by Dr Cíntia Júnia Monteiro. RNA concentration and purity were assessed using NanoDrop spectrophotometer (Thermo Scientific, Wilmington, DE). 500 nanograms of total RNA were reverse transcribed to

complementary DNA (cDNA) by QuantiTect Reverse Transcription Kit (Qiagen). Genomic DNA elimination was carried out twice, during RNA extraction and before the cDNA synthesis. qPCR reactions were performed in 96-well white-walled plates using 2x Brilliant II SYBR® Green QPCR Master Mix (Agilent) with the following primer sets: cubilin forward primer: 5′-CGTGGAACACACAAACTTTAGG-3′ and reverse primer: 5′-CCAGTGAGGGGATCTGATTG-3′; TCN2 receptor (CD320) forward primer: 5′-CACCCACCAAGTTCCAGTGCCG-3′ and reverse primer: 5′-GTTCCACAGCCGAGCTCGTCG-3′; TCN2 forward primer: 5′-GCTGGTTGTGGCACAGTA-3′ and reverse primer: 5′-AGGTCCACAGGCCATCAAT-3′. Glyceraldehyde-3-phosphate dehydrogenase (GAPDH) was used as a standardisation control (forward primer: 5′-AGGTGAAGGTCGGAGTCAAC-3′ and reverse primer: 5′-GATGACAAGCTTCCCGTTCT-3′). ΔΔCq method was used to calculate relative gene expression.

3.2.6 Cellular uptake of pyr-B_{12} fluorescent probe

Calu-3 and Caco-2 cells were cultured on Transwell® inserts over 14 days, under air-liquid or liquid-liquid interface respectively. Culture medium was removed from filter-cultured cells and replaced with Hank's Balanced Salt Solution (HBSS) in both Transwell® compartments for TEER measurements. Following the measurement of TEER, pyr-B_{12} probe was dissolved in DMEM medium without phenol red at concentration of 200 µg/mL, and 500 µL of this solution

was added to the apical chamber of the Transwell® insert. Cells were then incubated at 37°C for 3 hours and analysed by flow cytometry (Beckman Coulter Astrios EQ) in at least triplicate experiments, with more than 5,000 cells measured in each sample.

The effect of a competitive ligand on receptor-mediated cellular internalisation of fluorescent pyr-B_{12} probe was studied in the presence of an excess of free vitamin B_{12}; 500 µL of a 1.0 mg/mL solution of cyanocobalamin (B_{12}) in DMEM medium was added to the apical chamber of Transwell® inserts. Cells were subsequently incubated at 37°C for 30 min, then the medium was replaced with a stock solution of fluorescent pyr-B_{12} probe (500 µL, final probe concentration 200 µg/mL) plus free vitamin B_{12} at a concentration of 1.0 mg/mL. Cells were incubated at 37°C for 3 hours, fixed with formaldehyde and analysed by flow cytometry (Beckman Coulter Astrios EQ). Experiments were made in at least triplicates, with more than 5,000 cells measured in each sample.

3.2.7 Cellular internalisation of polymer-protein complexes applied as suspension

Calu-3 and Caco-2 cells were cultured on Transwell® inserts over 14 days as previously described in Chapter 2. Following a routine measurement of TEER, culture medium was removed from wells and replaced with DMEM medium without additional supplements. Polymer-protein nanocomplexes prepared as previously described

were suspended in medium at protein concentration of 10 µg/mL and the nanocomplex suspension (0.5 mL) was added to the apical chamber of the Transwell® insert. Cells were then incubated at 37 °C for 3 h and fixed with 2% formaldehyde followed by analysis by flow cytometry in at least triplicate experiments on separate occasions, with more than 5,000 cells measured in each sample.

The effect of a competitive ligand on receptor-mediated uptake of B_{12} targeted complexes was studied in the presence of an excess of free cyanocobalamin (vitamin B_{12}). Firstly, 500 µL of a 1.0 mg/mL solution of cyanocobalamin in medium was added to the apical chamber of Transwell® inserts. Cells were then incubated at 37°C for 30 min following addition of targeted polymer-protein nanocomplex suspension (500 µL, final protein concentration 10 µg/mL). Cells were incubated again at 37°C for 3 h, washed, fixed and analysed by flow cytometry.

3.2.8 Formulation of complexes as dry powders by spray-drying

All the dry powder work was carried out by Dr Alejandro Nieto-Orellana with assistance from Dr David Coghlan at project sponsor site Vectura group Plc, Chippenham, UK. Results are included and briefly discussed in this chapter for completeness.

The complexes were formulated into dry powders following procedures optimised previously (Nieto-Orellana *et al.* 2018). The

composition of dry powders was: 0-10 % (w/w) protein-polymer complexes, 10 % (w/w) leucine, 6.6 % (w/w) phosphate buffer salts, and trehalose as bulking agent (up to 100 % (w/w)).

3.2.9 *In vivo* evaluation of the complexes formulated as dry powders

In vivo experiments were carried out by our collaborators Drs Remi Rosière, Nathalie Wauthoz and Karim Amighi at the Free University of Brussels (Belgium). Results are discussed here for the sake of completeness.

3.2.9.1 Animals and husbandry conditions

Female BALB/c mice (Charles River, Arbresle, France) were kept under conventional housing conditions (22 ± 2°C, 55 ± 10 % humidity, and 12-hour day/night cycle). All studies and manipulations were approved by the CEBEA ethical committee of the Faculty of Medicine, ULB (Commission d'Ethique du Bien-Etre Animal, Université libre de Bruxelles, Belgium) (Ethical protocol N°585N). The laboratory federal agreement number is LA 1230568.

3.2.9.2 Characterisation of dry powder formulations emitted by the dry powder insufflator

Aerosol particles generated from Dry Powder Insufflator™ model DP4-M® (Penn-Century®, Philadelphia, USA) were confirmed to be suitable for endotracheal administration into the mice by using a

Spraytec® laser diffractometer. The emitted aerosol, created using Dry Powder Insufflator™ model DP4-M®, was presented dispersed in air directly and perpendicular to the laser beam for size measurement. For all formulations tested (Table 1) a loading powder mass of 2 mg was evaluated (n=10). High emitted mass values (> 80%), particle size D50 ≤ 5 µm and RSD values ≤ 25% for emitted masses were considered suitable for the administration of dry powder formulations to the mice**.**

3.2.9.3 Local pulmonary tolerance of the complexes

Solution of lipopolysaccharide (LPS) and dry powder formulations (detailed in the next paragraph) were administered by the non-invasive endotracheal route using an aerosolising system (Microsprayer™ model IA-1C®) or a dry powder insufflator designed for mice (Dry Powder Insufflator™ model DP4-M®, Penn-Century), respectively, as described elsewhere (Bivas-Benita *et al.* 2005; Rosiere *et al.* 2016).

Composition of formulations tested is shown in **Table 3.1**. Five groups were compared: (i) non-treated mice negative control (i.e. group baseline, n=6), (ii) mice treated with unlabelled dry powder (denoted as UDP) (control dry powders, with no protein nor copolymers, excipients only) (n=5), (iii) mice treated with unlabelled dry powder-protein (UDP-P) (dry powders containing lysozyme, but not polymers) (n=5), (iv) mice treated with unlabelled dry powder

containing protein-targeted complexes (UDP-TC) (dry powders containing 85:15 [mPEG$_{2k}$-*b*-GA$_{30}$/B$_{12}$-PEG$_{3k}$-*b*-GA$_{30}$]-lysozyme complexes) (n=5), and (v) mice treated with a lipopolysaccharide (LPS) solution (single administration of 1 µg dose) as positive control (n=6). Mice were treated with 2 mg dose of dry powders three time a week for three consecutive weeks.

Bronchoalveolar lavage fluids (BALFs) were analysed in terms of cell composition (total and differential cell count) and pro-inflammatory markers concentration (cytokines IL-1β, IL-6, and TNF-α), as previously described (Rosiere *et al.* 2016). Mice were euthanised by a lethal intraperitoneal injection of 12 mg sodium phenobarbital (Nembutal®, Ceva Santé Animale, Brussels, Belgium) 8 h (for the LPS group) or 24 h (for the dry powder inhaler groups) after the last inhaled administration. BALFs were collected using a 20-gauge cannula (Surflo® catheter, Terumo, Leuven, Belgium) with 3 flushes of 0.7 mL cold PBS and conserved on ice until total cell count analysis (Z2™ Coulter Counter®, Beckman Coulter, Suarlée, Belgium). BALF were centrifuged at 160 x g at 4°C, supernatants were collected and conserved at -80°C for cytokine quantification. Differential cell counts were performed on cytospin preparations after staining with May Grünwald and Giemsa (Sigma-Aldrich). A total of 200 cells were counted per slide and were referred to as alveolar macrophages, lymphocytes or polymorphonuclear neutrophils according to their morphology. Cytokine concentrations were determined by ELISA for

mouse IL-1 β, IL-6, and TNF-α (DuoSet® ELISA, RnD Systems) according to the manufacturer's protocols. The limits of quantification for the techniques used were 15.6 pg/mL for IL-1β and IL-6, and 31.3 pg/mL for TNF-α.

3.2.9.4 In vivo pulmonary deposition and retention.

The deposition of the dry powder formulations was evaluated after pulmonary delivery. Lysozyme-Cy5-containing DPI formulations (LDP-P, LDP-TC and LDP-NT, composition in Table 1) were administered to mice (2 mice *per* group) by the endotracheal route, as described above. After 0, 3 and 14 hours, mice were sacrificed using sodium pentobarbital, the lungs were collected and blocked using Optimum Cutting Temperature (OCT) solution (Tissue-Tek® OCT compound, Sakura). Five non-serial cryo-sections of 7 µm *per* lung were prepared and mounted on SuperFrost™ slides (Thermo Fischer Scientific) using a DAPI solution (DAPI Counterstain, Abott Laboratories, Des Plaines, IL, USA) and finally covered with a coverslip. The slides were observed under a Leica SP8 confocal microscope (Leica Microsystems, Diegem, Belgium) with filters (Zeiss, Germany) at λ = 546 nm (bandwidth 12 nm) and λ = 610 nm (bandwidth 65 nm) used for excitation and emission, respectively, for Cy5-labelled protein. Due to sub-optimal spectral overlap, prolonged exposure (1000 ms) was needed to acquire images. A DAPI filter (Zeiss) was used for DAPI. The images were processed (i.e. fluorescence intensity, mean grey values) using

ImageJ Software (National Institutes of Health, USA). Quantitative data are presented as the ratio of average of the grey mean values of Cy5 to DAPI areas (n=5 tissue slices), as described in Dawson *et al* (Dawson *et al.* 2009).

Table 3.1 *Composition of dry powder formulations used in the in vivo studies.*

	Formulation code	Lysozyme/ Complexes (w/w)	Excipients		
			Leucine (% w/w)	Buffer salts (% w/w)	Trehalose (% w/w)
unlabelled dry powder (UDP)	UDP	0 % complexes	10	6	Up to 100
	UDP-P	5 % lysozyme	10	6	Up to 100
	UDP-TC	10 % targeted complexes[a]	10	6	Up to 100
Cy5 labelled dry powder (LDP)	LDP-P	5 % lysozyme	10	6	Up to 100
	LDP-TC	10 % targeted complexes[a]	10	6	Up to 100
	LDP-NT	10 % non-targeted complexes	10	6	Up to 100

[a] *corresponding to ~ 5 % w/w of lysozyme.*

UDP-P denotes dry power containing unlabelled protein, UDP-TC denotes dry power containing unlabelled protein complexes with B_{12}-targeted polymer, LDP-TC denotes dry powder containing labelled protein complexes with B_{12}-targeted polymers, LDP-NT denotes dry powder containing labelled protein with non-targeted polymer.

Unlabelled dry powder formulations were used for local pulmonary tolerance studies, and Cy5-labelled protein dry powder formulations were used for pulmonary deposition and retention studies.

3.3 Results and Discussion

Delivery of therapeutic macromolecules into, or across cells forming epithelial barrier is a recognised therapeutic challenge. Potential solutions include approaches that exploit normal biological pathways of cellular internalisation and transcytosis of nutrients, vitamins, as well as macromolecules (Russell-Jones *et al.* 1995; Tuma and Hubbard 2003). In our previous study, we demonstrated that vitamin B_{12} can i) be used as a ligand to enhance internalisation of model sub-200 nm polystyrene particles by epithelial cells, ii) influence their intracellular trafficking pathways, and iii) enhance transport of decorated nanoparticles across Calu-3 cell layer (Fowler *et al.* 2013a; Fowler *et al.* 2013b). Here, we exploited the B_{12} directed cellular internalisation and transport to achieve targeted delivery of polymer-protein complexes *in vitro* and *in vivo*. Accordingly, we synthesised targeted B_{12}-$PEG_{3.5k}$-*b*-GA_{30} copolymers and utilised this to generate polymer-protein complexes *via* ionic, non-covalent interactions between polymer and model protein charged functionalities.

3.3.1 Expression of mRNA and function of B_{12} receptors

The presence of components involved in vitamin B_{12}-specific transport pathways has been widely confirmed in intestinal epithelium models, such as *in vitro* cultures of Caco-2 cells (Dix *et al.* 1990). B_{12} receptors have been successfully targeted for intestinal

delivery of proteins (Russell-Jones *et al.* 1999; Chalasani *et al.* 2007), and *in vitro* transport of nanoparticles across intestinal epithelium. In the latter, B_{12} transport can occur through two different receptors: cubilin and transcobalamin receptor (CD320, or TCN2R) (Kozyraki and Cases 2013). Evidence of vitamin B_{12} transport mechanisms in the lung epithelium and *in vitro* cell models, are scarce. We have previously demonstrated, using a combination of molecular biology and immunostaining techniques, that Calu-3 bronchial cell line expresses the B_{12}-IF receptor (cubilin), the transcobalamin receptor ('TCN2 receptor', CD320), and the transcobalamin II transport protein ('TCN2') (Fowler *et al.* 2013a). The present work confirms **(Figure 3.1a)** at mRNA level, expression of cubilin (human CUBN gene), transcobalamin receptor (CD320 gene) and transcobalamin II protein (human TCN2 gene). mRNA expression of the cubilin receptor was found to be very low, relative to control gene expression. It should be noted that the mechanism of vitamin B_{12} uptake *via* cubilin receptor requires the initial complexation of B_{12} with Intrinsic Factor (IF, or Gastric Intrinsic factor, GIF), a glycoprotein that is produced by parietal cells in the stomach (Green *et al.* 2017). Thus, it may not be surprising that cubilin-dependent transport pathway would be downregulated in Calu-3 cells, which originate from the lung tissue. Conversely, transcobalamin receptor (CD320)-mediated transport requires initial binding of vitamin B_{12} to TCN2 carrier protein, followed by uptake of

the resulting complex by CD320 (transcobalamin) receptor-mediated endocytosis (Gherasim *et al.* 2013; Benoit *et al.* 2018). The TCN2 protein in this complex is eventually degraded in the lysosomes, releasing cobalamin (vitamin B_{12}) which is further processed intracellularly (Gherasim *et al.* 2013). In this work, expression of mRNA for transcobalamin II protein in Calu-3 cell culture was confirmed by qPCR **(Figure 3.1a)** while in a previous study we have shown TCN2 protein expression in Calu-3 cells in a qualitative manner, by immunostaining (Fowler *et al.* 2013a). Taken together, our results indicate that Calu-3 cell model used in this study possess all the functional components required for cellular internalisation of cobalamin (vitamin B_{12}) molecules *via* transcobalamin (CD320) receptor-mediated transport.

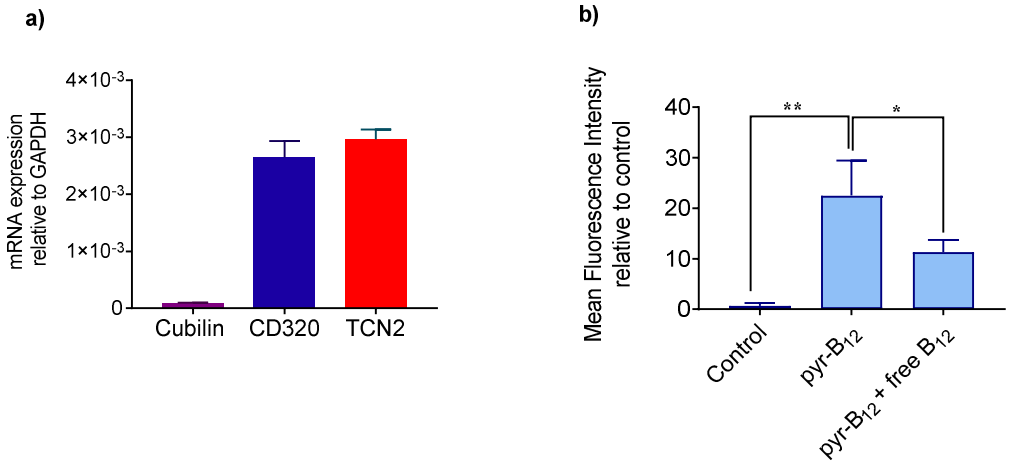


Figure 3.1 *a)mRNA expression of cubilin, CD320 and TCN2 relative to GAPDH (as housekeeping gene) by Calu-3 cells. b) Cellular internalisation of pyr-B_{12} fluorescent probe by Calu-3 cells in the presence or absence of free vitamin B_{12} competitive ligand. Control: untreated Calu-3 cells. One-way ANOVA was used for statistical analysis. *P ≤ 0.05, **P ≤ 0.01, ***P ≤ 0.001, **** P ≤ 0.0001. Flow cytometry conducted at λ_{ex} 401 nm and λ_{em} 421 nm. The error bar shown is the standard deviation of the mean. (N=3, n=3).*

To confirm functional, endocytic activity of vitamin B_{12} receptors in Calu-3 epithelial model employed in this study, we designed a low molecular weight B_{12}-fluorescent probe, pyr-B_{12}. This *O*-alkyl pyranine-based fluorescent compound was selected due to its structural similarity to Lucifer Yellow, which is known to have low cell membrane permeability, while possessing functionalities appropriate for conjugation to vitamin B_{12}. Accordingly, *O*-alkyl pyranine blue-fluorescent dye with narrow Stokes shift (λ_{ex} = 401 nm, λ_{em} = 421 nm), was linked to the 5' hydroxyl group of the ribose ring of cyanocobalamin, in a similar way to the approach followed for the synthesis of DBCO-B_{12}, in four steps, starting from 8-hydroxypyrene-1,3,6-trisulfonic acid trisodium salt (pyranine), and cyanocobalamin (B_{12}) **(Figure 3.2)**. For comparative purposes, in another experiment cellular internalisation of pyr-B_{12} by the established cell model expressing both cubilin and TCN2 B_{12} receptors, intestinal Caco-2 cell line (Bose *et al.* 1997; Aseem *et al.* 2013), was also assessed and shown in Appendix. Data in **Figure 3.1b** show a significant reduction of pyr-B_{12} cellular internalisation in the presence of an excess of 'free' vitamin B_{12} competitive ligand. This indicates a prominent, but not exclusive, role of B_{12}-specific transport in the cellular internalisation of pyr-B_{12} probe, likely occurring through TCN2 receptor mediated transport.

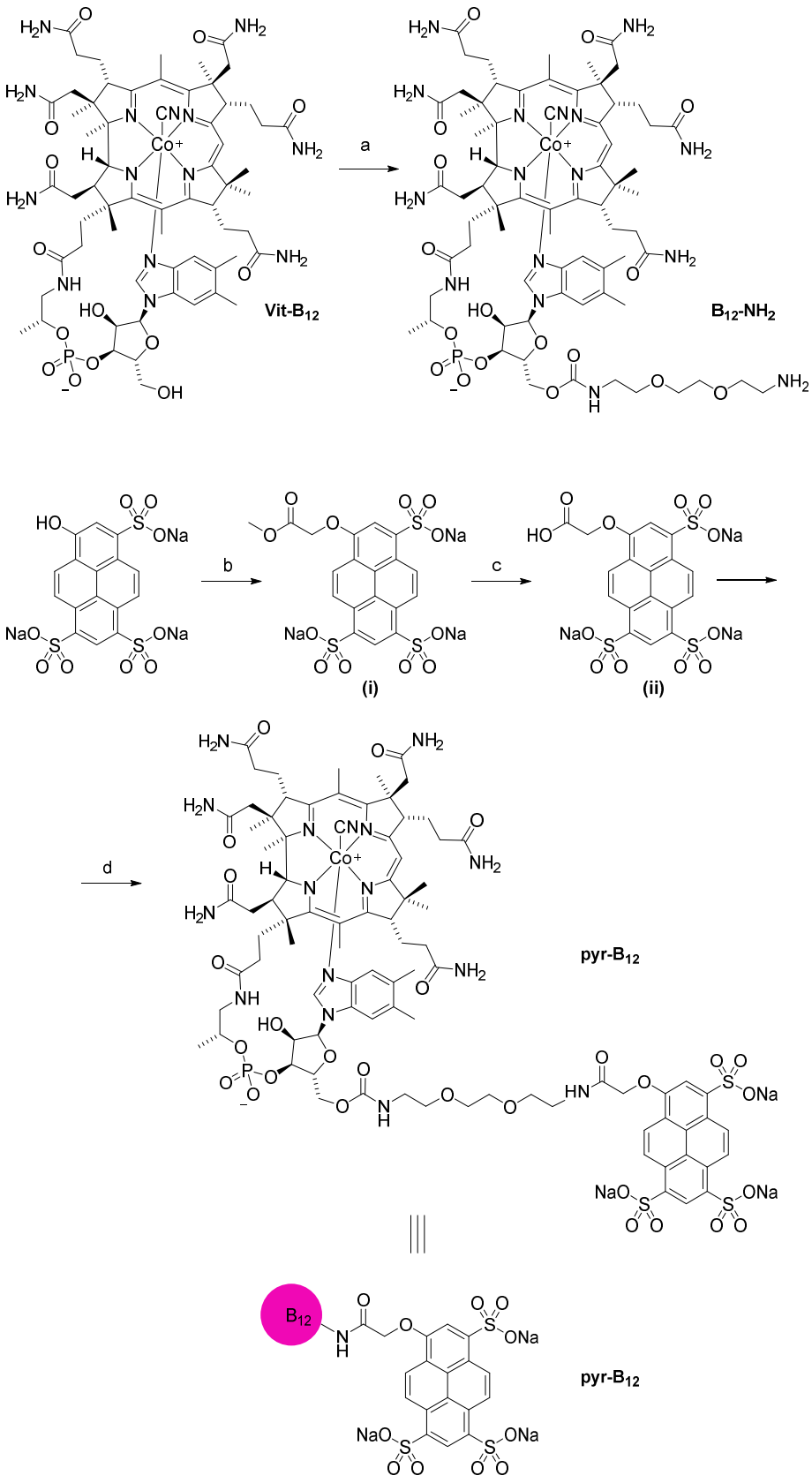


Figure 3.2 *Synthesis of pyranine-tagged vitamin cyanocobalamin (pyr-B_{12}). Reactions and conditions: a. i. 1,1'-carbonyldiimidazole, DMSO ii. 2,2'-(ethylenedioxy)bis(ethylamine); b. methyl bromoacetate, DIPEA, methanol reflux. c. $NaOH_{aq}$;. d. B_{12}-NH_2, DMTMM, methanol.*

3.3.2 Synthesis of mPEG$_{2k}$-*b*-pGA copolymers

Linear copolymers of mPEG-amine and variable number of glutamic acid repeating units were synthesised using method established previously in our group (Nieto-Orellana *et al.* 2017). The amino acid - glutamic acid was chosen as the repeating unit due to its negatively charged carboxyl group side chain, once incorporated into polymeric materials, could be used to complex positively charged proteins through multiple ionic interactions. Ionic interactions can be advantageous compared to covalent attachment in terms of the ease of protein release from the polymer, once the polymer-protein complex reaches the target site (Prompruk *et al.* 2005).

The most common approach to generate polymers for protein conjugation involves the post polymerisation modification of synthetic polymers , e.g. poly(etylene glycol) (PEG) (Liechty *et al.* 2010). PEG, chosen in this study, is an FDA approved polymer for many pharmaceutical formulations, and it is widely used in drug delivery because of its relatively low immunogenicity, antigenicity, and toxicity (Mero *et al.* 2009). In addition, PEG is very hydrophilic and each oxyethylene repeating units can coordinate two or three molecules of water, which helps to protect the polymer-protein complexes from the immune system (Harris and Chess 2003). Furthermore, it is easily chemically modifiable; by introducing a variety of functional groups at the end of the polymer chain ready

for further modifications. In our study, amino-PEG was used as a macroinitiator from which the poly(glutamic acid) block was grown and utilised to confer steric stabilisation to the resulting polymer-protein complexes.

N-Carboxyanhydride ring-opening polymerisation has been widely used to generate homopolypeptides (Habraken *et al.* 2010; Wibowo *et al.* 2014). This method, once appropriate experimental conditions are identified, allow to produce synthetic polypeptides with a predetermined molecular weight and low dispersity, and unfavourable side reactions are minimised (Habraken *et al.* 2012). This reaction requires a nucleophilic initiator, which would attack the NCA ring of the monomer, and result in the insertion of a monomer molecule in growing polymer chain, with concomitant elimination of a molecule of CO_2. In our specific case, the amine group in the $mPEG_{2k}$-NH_2 initiated the polymerisation; then the exposed amine group in the terminal glutamic acid repeating unit acts as the macroinitiator for the subsequent insertion of additional monomer chains. However, loss of control can occur *via* several mechanisms. For example, dry conditions are essential as water can act as an initiator and start the polymerisation process. We carried out the polymerisation at 0°C, as Habraken et al. showed that frequently occurring end-group termination and other side-reactions were absent at 0 °C (Habraken *et al.* 2010).

Linear mPEG$_{2k}$-*b*-pGA A-B copolymers were prepared from mPEG$_{2k}$-NH$_2$ with 10, 30 and 90 glutamic acid (GA) units in the B block by adding different proportion of GA-benzyl ester NCA monomer to the mPEG$_{2k}$-NH$_2$ macroinitiator. An advantage of this strategy is that the polyGA block length can be easily tuned to optimise complexation with different proteins or drugs with varying size and number of positive charges in their structure.

The polymerisations were monitored by ^{1}H NMR by following the disappearance of the α-CH proton signal of the NCA monomer at 5.1 ppm, and stopped at ~70% conversion, which generally occurred within 5 days. Hydrolysis of crude product with NaOH$_{aq}$ afforded the required mPEG$_{2k}$-*b*-pGA copolymers, which were purified by dialysis against deionised water (MWCO 1-3.5 kDa). A typical ^{1}H NMR spectrum of a mPEG$_{2k}$-*b*-GA$_{30}$ copolymer is shown in **Figure 3.4**. $M_{n,NMR}$ were calculated by comparing the integral of the methyl group of the mPEG$_{2k}$ with that of the CHN groups in the glutamic acid repeating units.

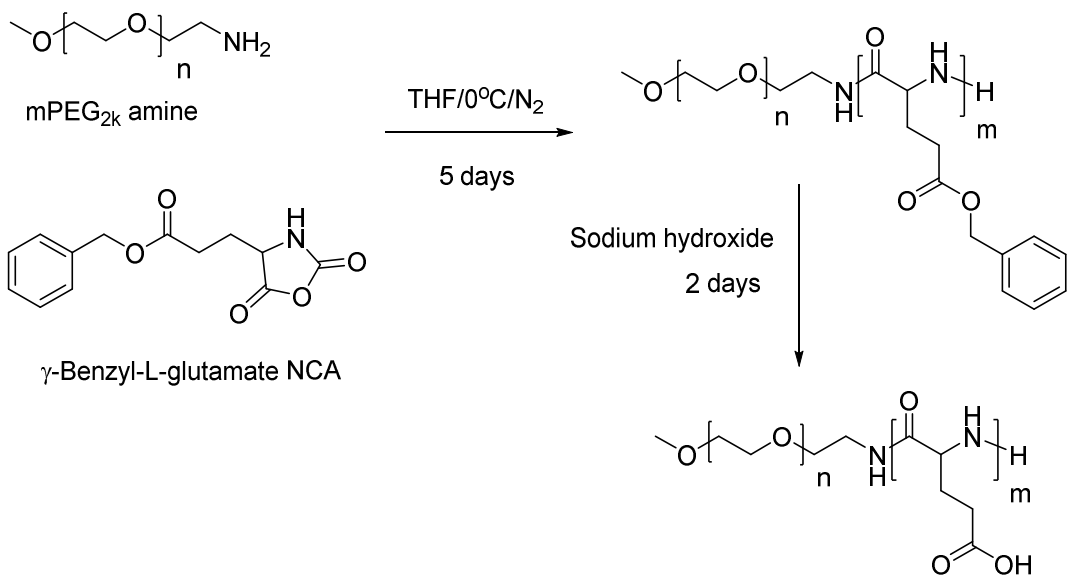


Figure 3.3 *Synthesis of Linear mPEG-b-pGA copolymers.*

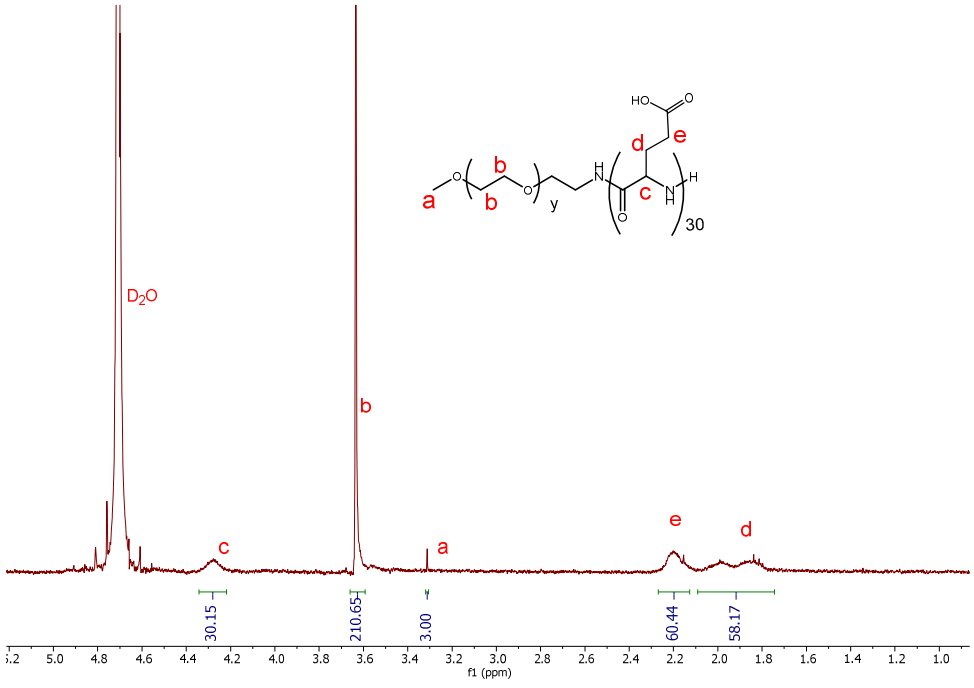


Figure 3.4 *^{1}H NMR of $mPEG_{2k}$-b-GA_{30} copolymer in D_2O.*

3.3.3 Synthesis of targeted B_{12}-$PEG_{3.5k}$-*b*-GA_{30} copolymer

The B_{12}-targeted copolymers, B_{12}-$PEG_{3.5k}$-*b*-GA_{30}, were produced through a modification of an approach developed previously in our group for synthesis of analogous non-targeted counterparts (Nieto-Orellana *et al.* 2019). This original polymerisation method **(Figure 3.5)** required seven steps to achieve the final B_{12} targeted polymer which was complex and time consuming. When considering the potential for scaled up manufacturing production, we aimed to simplify the process.

The second synthetic route we devised for the synthesis of azide-terminated linear PEG-*b*-pGA started from a commercially available key azide-PEG-amine 3500 precursor **(Figure 3.6)**. The latter is available as a trifluoroacetic acid (TFA) salt mixture, and before starting the polymerisation was converted into its free base, suitable to act as a macroinitiator for NCA polymerisation, by treatment with Amberlyst A-21 basic resin. The 3.5 kDa PEG block is longer than the 2 kDa PEG used for the non-targeted analogues, to potentially increase the exposure of B_{12} ligands at the surface of the corresponding protein-polymer complexes. The polymerisation conditions were analogous to those described in section 3.3.2. Polymers with 30 glutamic acid repeating units were synthesised and molecular composition was confirmed by ^{1}H NMR **(Figure 3.7)**. As

the azide group was already present in the PEG chain, no further steps were required in this reaction.

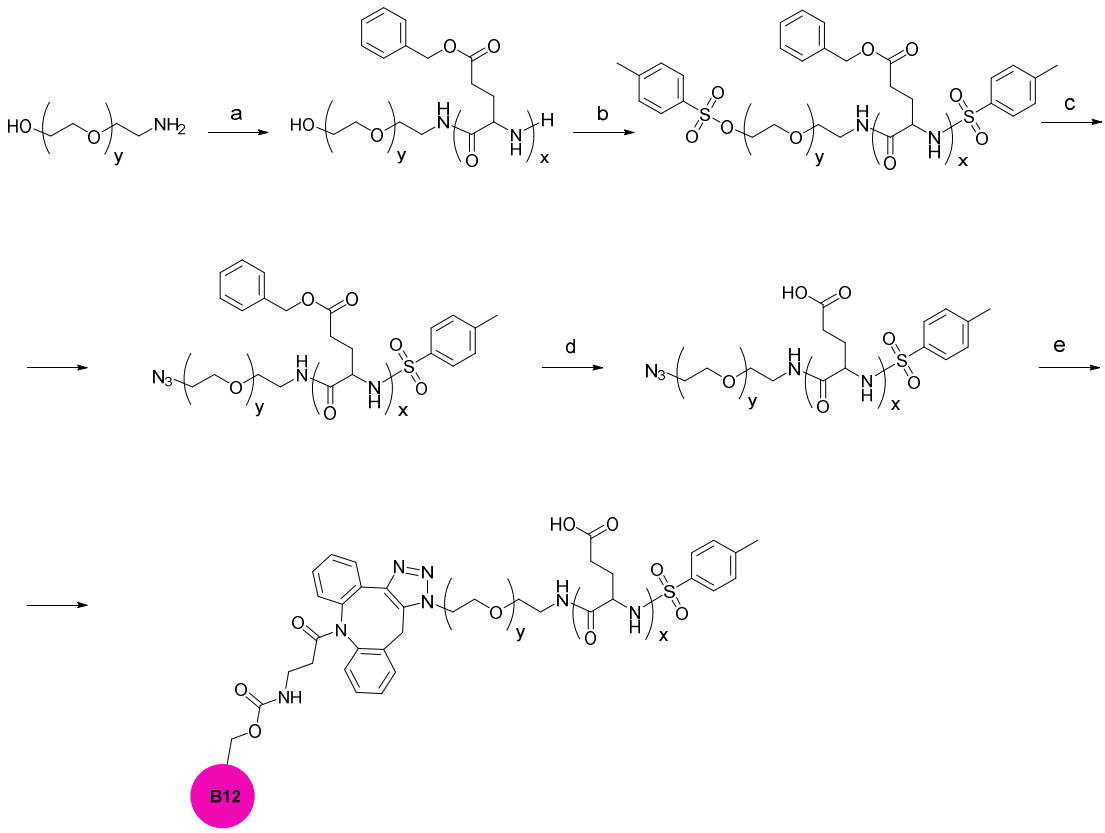


Figure 3.5 *First synthetic route for the preparation of B_{12}-$PEG_{3.5k}$-b-pGA. Reactions and conditions: a. γ-benzyl-L-glutamate NCA, CH_2Cl_2, 5 days; b. p-toluene sulfonyl chloride, triethylamine, CH_2Cl_2, 12 h; c. NaN_3, DMSO, 24 h; d. NaOH, H_2O/THF, 2 days; e. α-dibenzocyclooctyne-vitamin B_{12} (DBCO-B_{12}), DMSO/H_2O, 15 h.*

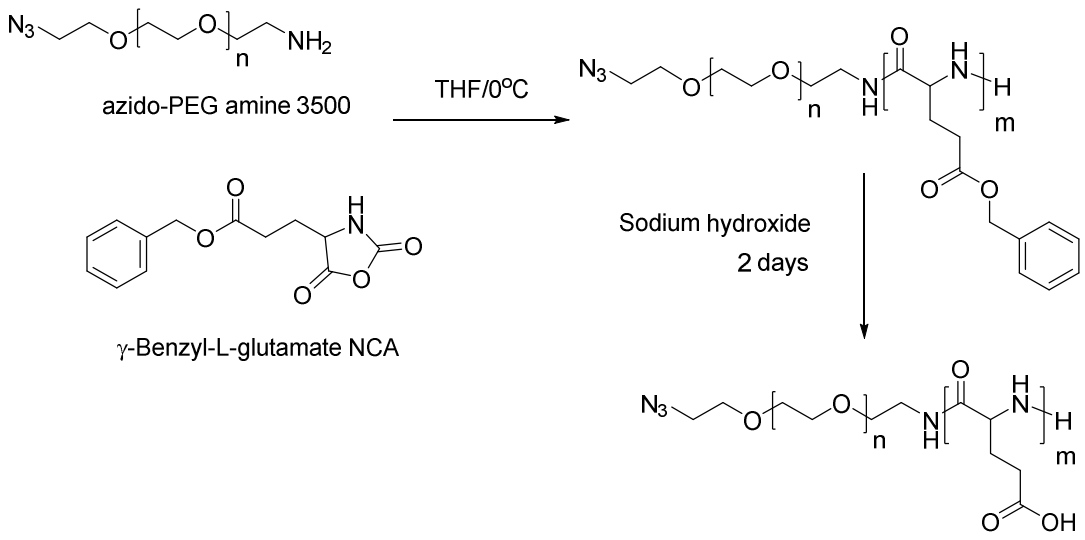


Figure 3.6 *Second and optimised synthetic route for the preparation of azide$PEG_{3.5k}$-b-GA_{30} copolymer, starting from α-amino-ω-azide-PEG.*

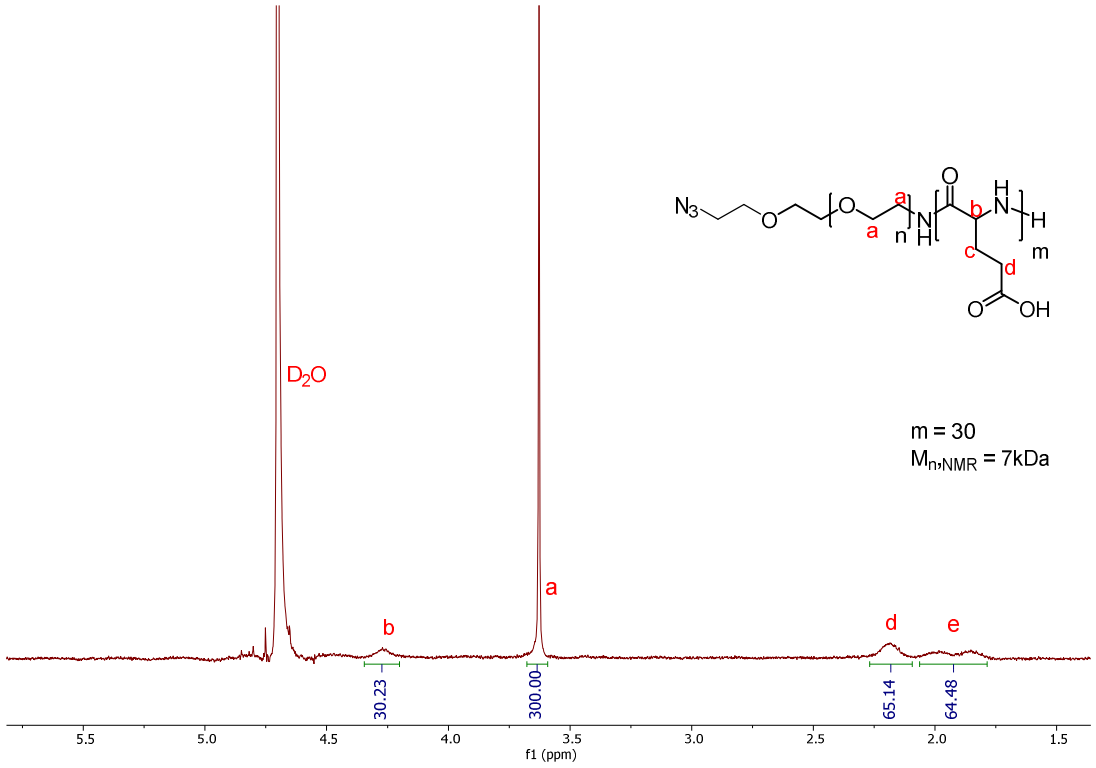


Figure 3.7 *NMR of azide-$PEG_{3.5k}$-b-GA_{30} copolymer.*

In the final step, the required B_{12} ligand was introduced in linear azide-$PEG_{3.5k}$-*b*-GA_{30} intermediate by copper-free strain-promoted Huisgen 1,3-dipolar cycloaddition (Saeed *et al.* 2011; Dix *et al.* 1990). To this aim, α-dibenzocyclooctyne-vitamin B_{12} (DBCO-B_{12}) was synthesised by activating the CH_2OH group at C_5 of cyanocobalamin pentose moiety with carbonyldiimidazole (CDI) for 30 min in DMSO, followed by the addition of commercially available α-dibenzocyclooctyne-amine, to form a stable carbamate linker. Reaction with the azide-containing intermediates in water-DMSO followed by dialysis afforded the final linear B_{12}-$PEG_{3.5k}$-*b*-GA_{30} protein-complexing copolymer **(Figure 3.8)**. Signals from the α-CH_2 of the dibenzocyclooctyne-carbamate at 5.0 ppm shifted to 5.9 ppm in the clicked B_{12} polymer confirming that the dibenzocyclooctyne-B_{12} had been successfully conjugated to the azide-terminated block copolymer. Efficiency of functionalisation was estimated by UV-vis spectrophotometry (λ = 540 nm) at 93.5% for B_{12}-$PEG_{3.5k}$-*b*-GA_{30}. Compared to the previous seven steps method presented in **Figure 3.5**, the current optimised process was simplified down to only three steps.

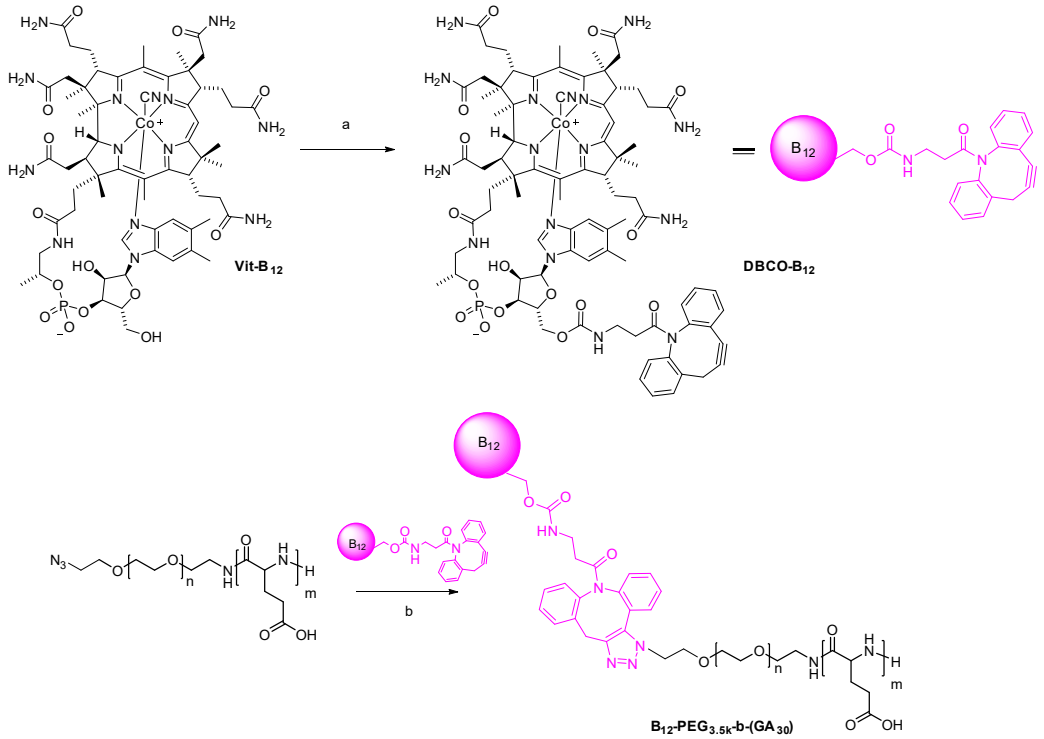


Figure 3.8 *Synthesis of vitamin B_{12}-targeted B_{12}-$PEG_{3.5k}$-b-$(GA)_{30}$ copolymers. Reactions and conditions: a) i. 1,1'-carbonyldiimidazole, ii. dibenzocyclooctyne-amine (DBCO-amine) b) DBCO-B_{12}, DMSO/H_2O, overnight.*

3.3.4 Targeted PEG-*b*-pGA:lysozyme complexes

PEG-*b*-pGA copolymer-protein complexes with lysozyme as a model protein cargo were assembled using a mixture of B_{12}-targeted and non-targeted PEG-*b*-pGA copolymers; in this study a 15:85 molar ratio, respectively was selected. The density of targeting ligands exposed at the surface of nanoparticles can significantly affect their cell internalisation, as illustrated in previous research from our and other groups (Moradi *et al.* 2012; Lee *et al.* 2015; Alkilany *et al.* 2019). Using another nano-sized targeted system with folate ligand we previously achieved significant receptor-mediated cellular internalisation of nanomaterial(Saeed *et al.* 2011), and based on

these previous studies, a 15:85 ratio was considered as a good starting point. A polymer-protein relative molar charge ratio of 2.5 - defined as the molar ratio between glutamic acid polymer repeating units, assumed to be all negatively charged at pH 7.4, and cationic amino acids of lysozyme – was used, as we have previously shown efficient complexation of $mPEG_{2k}$-*b*-pGA copolymers to lysozyme under these conditions (Nieto-Orellana *et al.* 2017). Targeted and non-targeted polymer-protein complexes were measured by DLS, D_H: 137 ± 59 nm and D_H: 143 ± 65 nm (shown in Appendix), respectively - suitable for endocytosis. Gel electrophoresis analysis of complexes incubated in cell culture medium for 3 hours showed that the majority of lysozyme remains complexed under the experimental conditions utilised for our cell uptake studies. However complex dissociation was observed under the same conditions, but at pH 4.5, in simulated lysosomal environment **(Figure 3.9)**. Complex dissociation is likely due to partial or complete protonation of poly(glutamic acid) acid side-chains; pKa of poly-α-glutamic acid is 4.1 (Lu *et al.* 2017) and at pH 4.5 there are equal amounts of protonated and deprotonated forms of the acid, which makes the polymer less able to bind positively charged protein lysozyme.

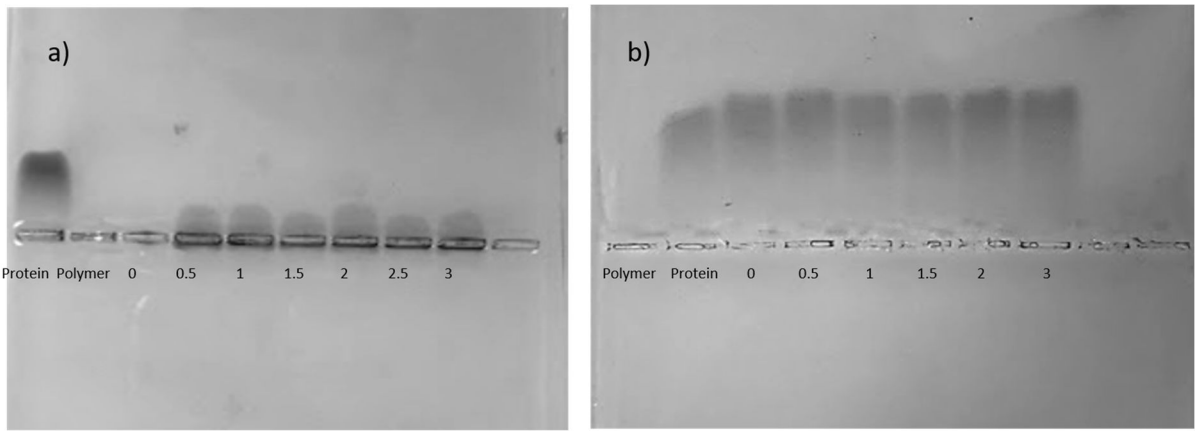


Figure 3.9 *Electrophoretic mobility of protein (lysozyme), polymer ($mPEG_{2k}$-b-GA_{30}), and lysozyme:$mPEG_{2k}$-b-GA_{30} complexes prepared at r: 2.5 following incubation in a) cell culture medium (DMEM, pH 7.4 without phenol red), and b) in simulated lysosomal environment at pH 4.5 (a 50 : 50 mixture of 1 M sodium acetate and 1 M hydrochloric acid). Incubated samples were withdrawn and 50 µl loaded in each well on a 1% agarose gel, run 2 h at 100 mA in trisacetate-EDTA buffer. Numbers in the gel indicated timepoints.*

3.3.5 Cellular internalisation of B_{12}-targeted protein-polymer complexes *in vitro.*

To further confirm that the B_{12}-$PEG_{3.5k}$-*b*-$(GA)_{30}$ polymer synthesised using the new simplified method possessed the same function as the old analogue, cellular internalisation studies were carried out using Calu-3 cells. Data in **Figure 3.10** demonstrate significantly increased cellular internalisation of targeted B_{12}-$PEG_{3.5k}$-*b*-GA_{30}:lysozyme complexes, compared to 'free' Cy5-lysozyme or non-targeted $mPEG_{2k}$-*b*-GA_{30}:lysozyme complexes, mirroring the results obtained with the old B_{12}-PEG_{3k}-*b*-GA_{30} analogue. Cell uptake experiments were also carried out in a more established B_{12} receptor-expressing cell line – Caco-2 intestinal epithelial cells and again the B_{12} targeted complexes were internalised more compared to non-

targeted control complexes. Between the 2 cell-lines, Caco-2 cells expectedly internalised significantly more B_{12} targeted lysozyme-polymer complexes and non-targeted complexes which could be explained by the general nature of intestinal cells to internalise and transport materials in the gastric intestinal system compared to the nature of lung cells. Taken together, these results indicated the newly synthesised B_{12}-$PEG_{3.5k}$-*b*-GA_{30} copolymer retained the functioning of the old analogue while requires less steps during the synthesis process.

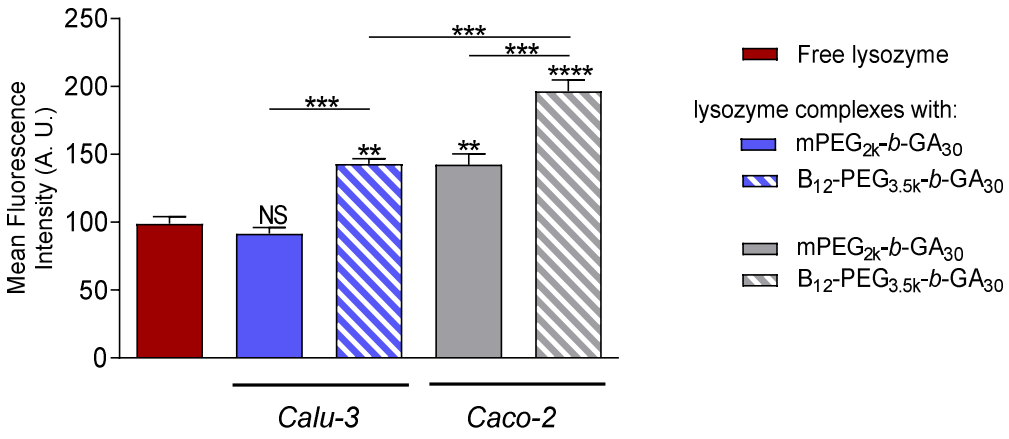


Figure 3.10 *Cellular internalisation of B12-targeted and non-targeted PEG-b-pGA:Cy5-lysozyme complexes by Calu-3 or Caco-2 cells grown as polarised epithelial cell layers. Suspensions of complexes were applied at protein concentration of 10 µg/mL and incubated with cells for 3 h prior to flow cytometry analysis. Cells were grown as polarised layers on Transwell supports under air-liquid (Calu-3) / liquid-liquid (Caco-2) interface conditions. 'free lysozyme' indicates that cells were treated with a solution of Cy5-lysozyme in the absence of PEG-b-pGA complexing copolymers. One-way ANOVA was used for statistical analysis. All column was compared to Free lysozyme and significance indicated above each column., NS not significant, ** $p < 0.01$, *** $p < 0.001$, **** $p < 0.0001$. The error bar shown is the standard deviation of the mean. (N=3, n=3).*

The observed level of cellular internalisation of 'free' Cy5-lysozyme was somewhat unexpected. Data on similar experiments on cellular

uptake of lysozyme are scarce, but recent *in vivo* studies reported on absorption of lysozyme in the intestinal tract (Takano *et al.* 2004), which appears to be occurring by non-saturable and saturable processes, the latter pointing to an involvement of endocytic pathway(s). Furthermore, it has recently been suggested that receptor-mediated endocytosis of lysozyme in renal proximal tubules may be mediated by megalin and cubilin (Seliverstova and Prutskova 2015); the mRNA expression, although at a very low level, of the latter receptor was confirmed in the cell model used in this study. Furthermore it should be noted that complexation of lysozyme with non-targeted copolymers resulted in similar level of internalisation as for 'free' lysozyme **(Figure 3.10)**, a result that would be unexpected if one considers that PEGylation often reduces cellular uptake of colloidal size particulates (Meng *et al.* 2004). As noticed above, the B_{12}-mediated pathway does not appear to be an exclusive transport mechanism for tested systems in the cellular model used, and hence further studies to decipher internalisation pathways would be needed, e.g. (Alshehri *et al.* 2018). These are however beyond the scope of the current work that aims to design targeted excipients for inhalable dry powder formulations. It should be noted that our study used polarised, differentiated epithelial cell layer grown at air-liquid interface, and although a number of previous reports studied intracellular delivery of self-assembled protein carrying systems, these are conducted on a variety of non-polarised cells, such as HeLa

and dendritic cells (Ayame *et al.* 2008; De Koker *et al.* 2007), which makes direct comparisons difficult.

Next, aiming at developing inhalable formulations, we spray-dried PEG-*b*-pGA-protein complexes using a 'standard' process and excipients. These experiments were materially carried out by Drs Alejandro Nieto-Orellana and David Coghlan at Vectura Group Plc (Chippenham, UK) using B_{12}-PEG_{3k}-*b*-GA_{24} copolymer synthesised using the original method described in **Figure 3.5** and discussed here for completeness. In these formulations, trehalose was selected as the matrix excipient due to its well characterised ability to stabilize biologics. When spray dried, trehalose creates an amorphous matrix that forms hydrogen bonds with biologic materials and protects structural integrity following the removal of water. Other excipients that are approved for inhalation formulations, such as mannitol and lactose, are known to crystallize when spray dried, limiting their ability to provide a protective amorphous matrix. The amorphous nature of trehalose renders the particles hygroscopic and highly cohesive. This limits the ability of passive inhalers to efficiently disperse the powder to a respirable size (<5 μm aerodynamic diameter) for lung delivery. Leucine is a surface-active amino acid that accumulates at the surface of the droplet during the spray drying process. This results in high concentrations of leucine localised to the particle surface in comparison to the particle interior. This deposition changes the properties of the spray dried particle, decreasing

cohesion and therefore reducing the energy required to efficiently disperse the powder to a respirable size during inhalation. The addition of leucine dramatically improves the fine particle fraction achievable from the device, directly translating into improved deposition properties of the powder (Nieto-Orellana *et al.* 2018). The resulting formulations possessed aerodynamic properties suitable for inhalable product, with median particle size (D_{50}) < 5 μm which provide the greatest possibility of deposition in the lung, as deposition of large particles with an aerodynamic diameter of >5 μm is held in upper airways by inertial impaction (Rees *et al.* 1982). 10% loading level was selected to ensure stability of the nano-complexes during the spray drying process and to maintain efficient aerosol performance. In this instance, the powders exhibited comparable aerosol performance when formulated as the placebo formulation (trehalose and leucine only, without PEG-*b*-pGA:lysozyme nanocomplexes) and as the nano-complex loaded powder (loaded at 10% level), indicating that inclusion of the nano-complexes did not change the particle properties (Nieto-Orellana *et al.* 2018).

3.3.6 Local pulmonary tolerance of polymer-protein complexes based dry powder formulations in healthy mice.

The safety profile of PEG-*b*-pGA:lysozyme complexes formulated as dry powder inhalable formulations was investigated in healthy mice.

As already noted, all *in vivo* experiments were carried out by our collaborators Drs Remi Rosière and Nathalie Wauthoz at the University of Brussels (Belgium), and these results are briefly discussed here for completeness. Previous reports have shown that administration of polymer-based pulmonary formulations can induce inflammatory responses (Beyerle *et al.* 2011; Patil *et al.* 2018), whilst the presence in dry powder formulations of poorly soluble material has been shown to induce local irritation and pro-inflammatory effect in the respiratory tract (Jones *et al.* 2014; Kumar *et al.* 2014). In addition, the delivery of proteins to the lungs has been shown to induce immunogenicity, local irritation and toxicity (Yamamoto *et al.* 1997; Agu *et al.* 2001; Heinemann *et al.* 2000). In this work, we evaluated the lung tolerance profile of PEG-*b*-pGA:lysozyme dry powders in healthy BALB/c mice, by quantifying cell count and local concentration of IL-1β, IL-6 and TNF-α cytokine in bronchoalveolar lavage fluids after endotracheal administrations of 2 mg of dry powders 3 times *per* week, for 3 weeks period. The dose and the administration schedules were established considering limitations of the preclinical mice model. Aimed, and achieved, administration of 2 mg, corresponds to a dose of ~100 mg/kg of powder mass and ~10 mg/kg protein – within a range potentially expected of a therapeutic protein to be delivered in humans. The administration schedule was devised taking into account limitations associated with general anaesthesia of mice during endotracheal

instillation and their well-being. 48 hours (i.e. three doses per week) was previously assessed as the minimum interval between two such administration procedures (Morello *et al.* 2009; Wauthoz *et al.* 2010). Systems tested included: dry powder formulation of [$mPEG_{2k}$-*b*-GA_{30}/B_{12}-PEG_{3k}-*b*-GA_{24}]-lysozyme targeted complexes (UDP-TC), formulation containing only dry powder excipients (UDP), and system containing 'free' lysozyme formulated with dry powder excipients but with no polymers to complex the protein (UDP-P) (the compositions of these formulations are shown in **Table 3.1**).

Firstly, the potential inflammatory response of these formulations was investigated by quantifying the concentration of IL-1β, IL-6, and TNF-α pro-inflammatory cytokines (Gabay 2006; Ren and Torres 2009), in the epithelial lining fluid of the lungs. Mice treated with lipopolysaccharide (LPS) - outer membrane component of Gram-negative bacteria known as a strong stimulator of innate or natural immunity (Alexander and Rietschel 2001) - were used as a positive control group. As expected, a significant increase in IL-1β, IL-6, and TNF-α level was observed on LPS treatment, compared to untreated mice **(Figure 3.11)**. The levels of measured cytokines did not increase significantly above the negative control level (untreated mice group) following administration of dry powder formulations. The data hence clearly illustrate that on a repeated, prolonged administration the tested PEG-*b*-pGA based formulations are well tolerated .

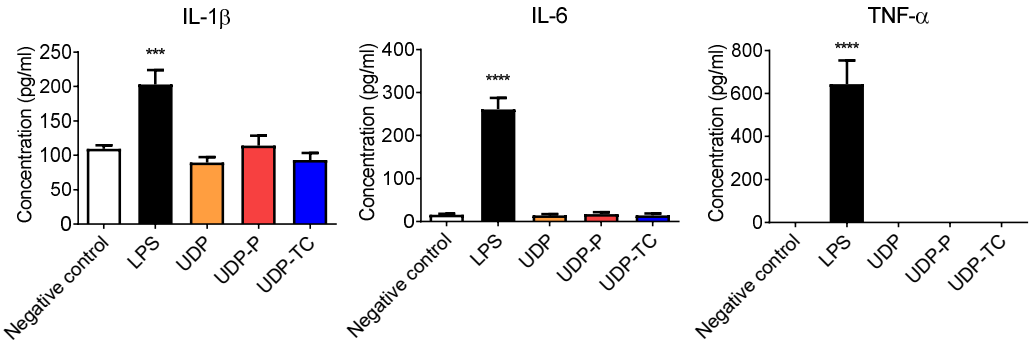


Figure 3.11. *Pro-inflammatory cytokine IL-1β, IL-6, and TNF-α gene expression in lung tissues following administration of 2 mg of dry powder formulations 3 times a week for 3 weeks. Mice groups were untreated (negative control) or treated with LPS (positive control), treated with a formulation containing only dry powder excipients (UDP), free lysozyme formulation containing lysozyme and dry powder excipients (UDP-P), and dry powder formulation containing targeted complexes (UDP-TC) - with 85:15 [mPEG$_{2k}$-b-GA$_{30}$/B$_{12}$-PEG$_{3k}$-b-GA$_{24}$]-lysozyme composition. One-way ANOVA was used for statistical analysis. *** $p < 0.001$, **** $p < 0.0001$. The error bar shown is the standard deviation of the mean. (N=2, n=3).*

To further investigate the tolerability of the designed dry powder formulations upon pulmonary administration, the differential cell count of alveolar macrophages (AM), polymorphonuclear neutrophils (PMN), and lymphocytes (LM) was also performed. Following single administration of 1 µg LPS, the number of AM dramatically decreased to around 50% relative to untreated mice, whereas the percentage of PMN significantly increased, clearly indicating a pro-inflammatory reaction. On the contrary, all the dry powder formulations had values for AM, PMN and LM at the level similar to untreated mice control. This was qualitatively confirmed by optical microscopy observations **(Figure 3.12)**. These experiments thus suggest that, under the conditions investigated, B$_{12}$-PEG-*b*-pGA:lysozyme complexes-based dry powder formulations are well tolerated in the lungs following

endotracheal administration, with no significant toxicity or lung inflammation observed.

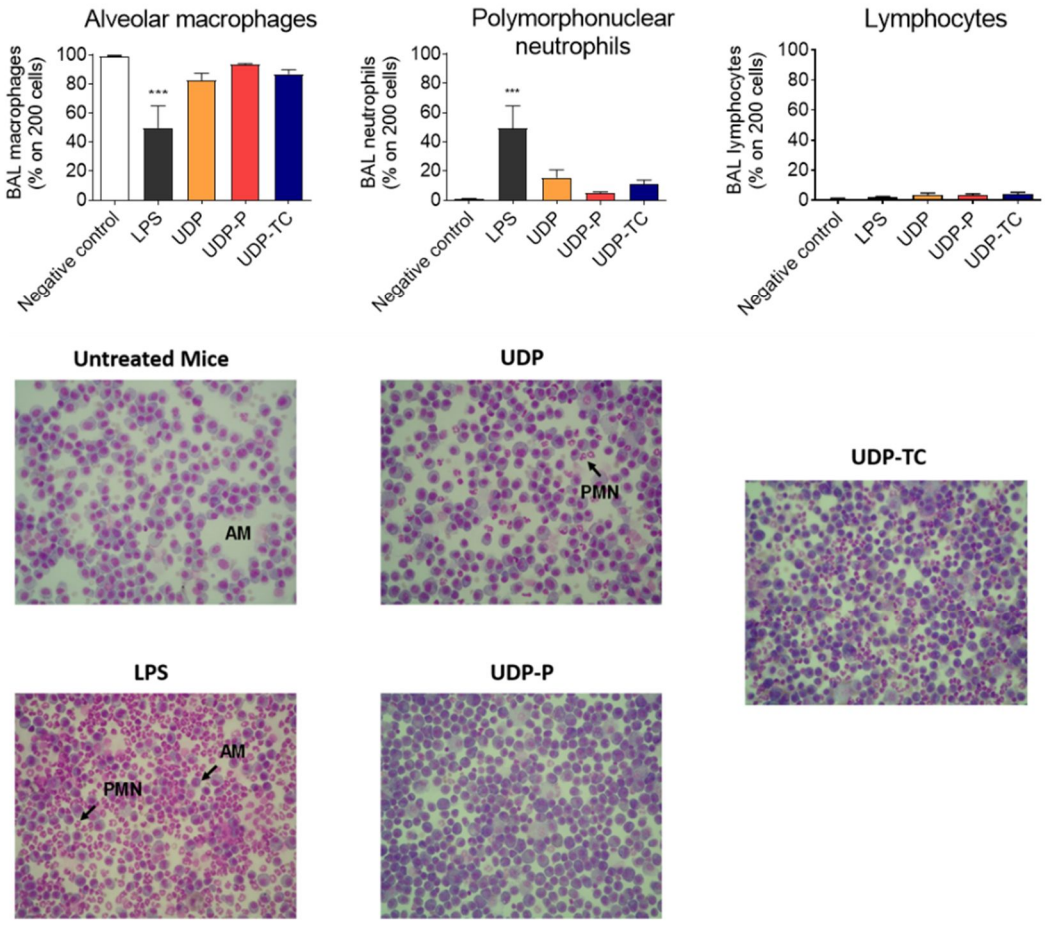


Figure 3.12 *Bronchoalveolar lavage fluid analysis following a single administration of dry powder formulations. Differential cell count and representative images of different cells found in the bronchoalveolar lavage fluid. Mice groups were not treated ((negative control) or treated with single administration of 1 µg LPS (positive control), and 2 mg of dry powder formulation containing formulation excipients (UDP), free lysozyme dry powder formulation (UDP-P), or dry powder formulation containing targeted complexes (UDP-TC) [with composition of 85:15 $mPEG_{2k}$-b-GA_{30}/ B_{12}-PEG_{3k}-b-GA_{24}]-lysozymes] 3 times a week for 3 weeks. One-way ANOVA was used for statistical analysis. *** $p < 0.001$, **** $p < 0.0001$. The error bar shown is the standard deviation of the mean. (N=2, n=3).*

3.3.7 *In vivo* pulmonary deposition and retention of polymer-protein complexes based dry powder formulations in healthy mice

Pulmonary delivery of particle formulations can be challenging, due to different particle clearance mechanisms present at various levels of the airway path in the lungs, such as the mucociliary escalator, proteolytic degradation and macrophage capture (El-Sherbiny *et al.* 2015). However drug delivery system can potentially overcome these removal mechanisms (El-Sherbiny *et al.* 2015) and, by prolonging the time of exposure of lung tissue to relevant protein therapeutics, enhance their therapeutic effects. In this part of our study, the ability of B_{12}-PEG-*b*-pGA:lysozyme complexes to increase the retention of proteins in the lungs was assessed.

Accordingly, a 2 mg dose of dry powder formulation was administered to healthy mice by the endotracheal route, using a Penn-Century insufflator. **Figure 3.13** shows the lung distribution of Cy5-labelled lysozyme following administration of dry powder formulation containing free Cy5-labelled lysozyme (LDP-P), dry powder formulation containing non-targeted $mPEG_{2k}$-*b*-GA_{30}:labelled lysozyme complexes (LDP-NT), and dry powder formulation containing 85:15 [$mPEG_{2k}$-*b*-GA_{30}/B_{12}-PEG_{3k}-*b*-GA_{24}]-lysozyme targeted complexes (LDP-TC). Five non-serial cryo-sections of 7 µm thickness *per* lung were prepared, imaged by fluorescence

microscopy and representative examples are shown in **Figure 3.13**. Images depict that immediately following administration (at t=0 h) Cy5-lysozyme powders were indeed deposited in the lungs, which agrees with the previous studies reporting that dry powders with good dispersion properties can be deposited in the respiratory zone in the mouse lungs (Duret *et al.* 2012). Fluorescent images obtained from different lung tissue sections however indicate that the deposition was not homogeneous throughout the lung, which increases complexity in making comparisons between the systems tested. This non-homogeneous deposition pattern have also been observed in other studies (Capel *et al.* 2018; Wauthoz *et al.* 2010; Li *et al.* 2019). However, analysis of the images **(Figure 3.13, graph)** indicates that in different samples imaged at 14 hours after the administration of dry powders the fluorescence arising from Cy5-lysozyme is higher, relative to nuclear DAPI staining, for targeted complexes formulations (LDP-TC) in comparison to formulations containing 'free' (LDP-P) and non-targeted Cy5-lysozyme complexes (LDP-NT). This would indicate lengthier protein lung retention for the targeted formulation. All data considered; the lung deposition experiment provides an initial evidence of prolonged protein retention following administration of vitamin B_{12}-targeted complexes. Further studies are needed to confirm if this prolonged retention is indeed a consequence of the increased cellular internalisation of targeted complexes seen in the *in vitro* cell culture

experiment, and if this would lead to a potentially improved therapeutic effect of such delivered protein in the lung. Nevertheless, the *in vivo* deposition experiment suggests that targeted polymer-protein complexes can influence and potentially extend retention time of the protein cargo in the lungs.

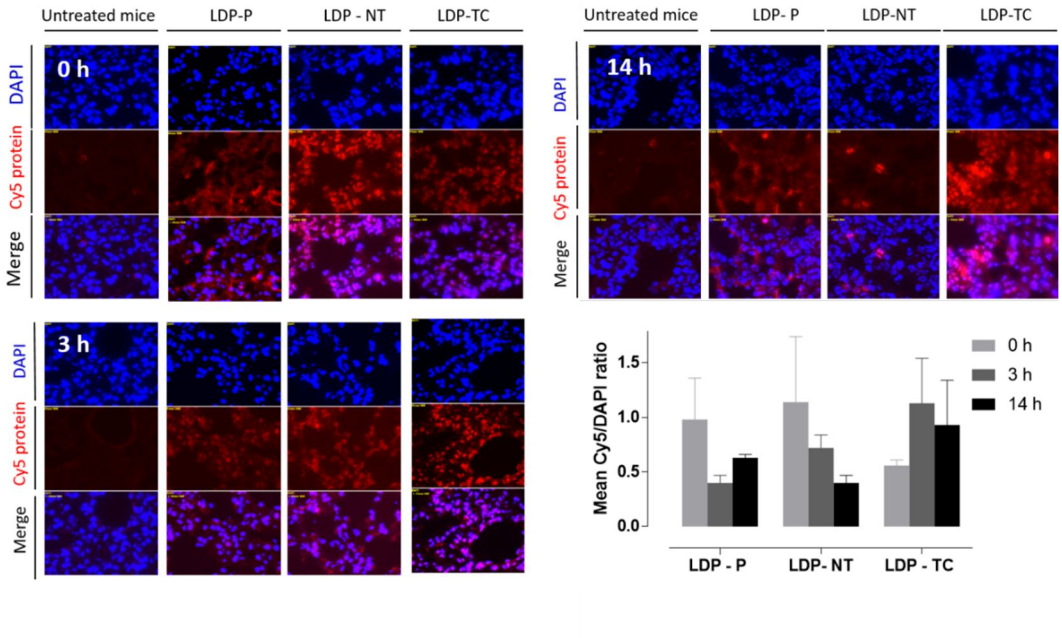


Figure 3.13 *Distribution of fluorescent labelled protein in the lung tissue of healthy mice following endotracheal application using the pulmonary delivery device of 2 mg dry powder formulations at different times after administration (in hours). Examples of a 7-µm longitudinal, non-consecutive lung cryo-sections imaged using a fluorescent microscope at 200 x magnification are. The images show the distribution of red labelled lysozyme-Cy5 ('Cy5 protein'), blue nuclear stain ('DAPI') and merged images ('Merged'); LDP-TC denotes dry powder formulation of [85:15 mPEG$_{2k}$-b-GA$_{30}$/B$_{12}$-PEG$_{3k}$-b-GA$_{24}$]-lysozyme complexes), LDP-NT drug powder formulation of [mPEG$_{2k}$-b-GA$_{30}$]-lysozyme non-targeted complexes, and LDP-P denotes free protein dry powder (without complexing polymers) formulation. Graph shows calculated ratio of Cy5 to DAPI emission intensity, obtained by analysis of images from 5 non-serial, random cryo-sections* per *lung (adopted from Dawson* et al *(Dawson et al. 2009)). Low ratio for LDP-TC at 0 h illustrates the effect of non-homogeneous lung deposition on material present in the cryo-sections prepared for in the analysis.*

3.4 Conclusions

In this study, we assessed the potential of vitamin B_{12} ligand-targeted poly(ethylene glycol)-*block*-poly(glutamic acid) copolymers to self-assemble with a protein cargo into polymer-protein complexes, with the aim to design an inhalation product with prolonged lung retention and intracellular delivery of protein to the lung epithelium. Our study shows that PEG-*b*-pGA:lysozyme complexes did not induce an increased production of pro-inflammatory cytokines in a chronic, repeated administration study in heathy mice. Furthermore, no changes in cell count of alveolar macrophages, polymorphonuclear neutrophils and lymphocytes, relative to untreated control, were observed that would indicate development of an inflammation process in the lung. Hence, toxicity data demonstrate that PEG-*b*-pGA copolymer-based formulations are well tolerated in the lungs following chronic treatment, with no significant toxicity or lung inflammation indications.

The data demonstrate a B_{12}-receptor mediated internalisation of B_{12} ligand-targeted PEG-*b*-pGA:protein complexes *in vitro* in differentiated, polarised Calu-3 cells epithelial model. When fabricated into dry powders for inhalation using a standard spray drying procedure, and applied *in vivo*, the deposition data show prolonged lung retention of the protein cargo at 14 hours after administration for targeted B_{12}-PEG-*b*-pGA:protein complexes, relative to non-targeted or 'free' protein formulations. Taken

together the results presented in this study show that vitamin B_{12}-PEG-*b*-pGA copolymers have a potential as a new class of targeted 'excipients' for inhalation delivery of protein drugs to the lungs.

Chapter 4. Biotin targeted PEG-*b*-poly(glutamic acid) copolymer for delivery of proteins

4.1 Introduction

As discussed in Chapter 1, pulmonary delivery is increasingly seen as an attractive, non-invasive route for the delivery of protein therapeutics (Patil and Sarasija 2012). However, there are significant barriers for macromolecular therapeutics, such as proteins, delivery to, or across lung epithelium (Baker *et al.* 2010; Hussain *et al.* 2004). Research has shown there are a number of natural biological transport pathways present at mucosal surfaces facilitating the internalisation of nutrients and endogenous macromolecules (Tuma and Hubbard 2003; Russell-Jones *et al.* 1995). It has been demonstrated that nanocarriers conjugated with specific ligands can increase the interaction with epithelial cells and potentially adopt these physiological pathways (Russell-Jones *et al.* 1999; Elfinger *et al.* 2007; Bush *et al.* 2018). This knowledge has already been utilised in designing specific B_{12} ligands decorated drug delivery systems and to increase the cellular uptake in the airway mucosa epithelium within our group and discussed in Chapter 3 (Nieto-Orellana *et al.* 2019; Fowler *et al.* 2013). Studies have suggested a potential use of another essential vitamin – biotin – as an endocytosis ligand. Biotin receptor was found overexpressed in

cancer cells, relatively more than folate or vitamin B_{12} receptors (Bhuniya *et al.* 2014; Santra *et al.* 2011). This inspired the current study to assess if biotin could be utilised as targeting ligand of the PEG-*b*-poly(glutamic acid) copolymer-based delivery systems to provide therapeutic benefit to the formulation. In this study, we engineered biotin as targeting ligand for biotin-PEG-*block*-poly(glutamic acid) copolymers, using lysozyme as a model positively charged protein cargo. A mixture of biotin targeted and untargeted PEG-*b*-pGA copolymers were used as a 'complexing excipient' to assemble complexes with the model protein *via* electrostatic interactions at physiological pH, as illustrated in **Figure 4.1**.

After the initial confirmation of the complex formation, cellular internalisation of biotin-targeted protein-polymer complexes were quantitatively assessed by flow cytometry and visualised using confocal microscopy. Colocalization studies were carried out to investigate intracellular localisation of both biotin-PEG-*b*-poly(glutamic acid) and lysozyme.

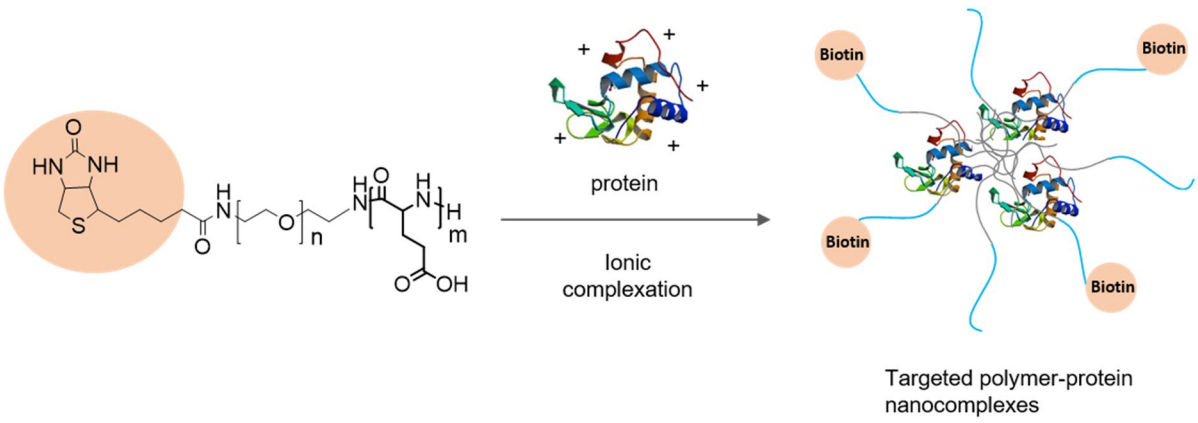


Figure 4.1 *Illustration (drawing not to scale) of polyelectrolyte complexes formed between a model protein and biotin-PEG_{2k}-b-pGA and $mPEG_{2k}$-b-pGA copolymers via electrostatic interaction between the negatively charged carboxylic acid groups on the polyglutamic acid chains and the positively charged groups of the protein.*

4.2 Methods

4.2.1 Biotin-PEG_{2k}-*b*-GA_{10} and biotin-PEG_{2k}-*b*-GA_{60} synthesis

Commercially available biotin-PEG_{2k}-amine (50.0 mg, 0.0217 mmol) (Sigma-Aldrich) was dissolved in toluene (20 mL) and solvent was evaporated under reduced pressure to remove traces of residual water in the polymer starting material. This procedure was repeated three times. The residue was then dissolved in anhydrous tetrahydrofuran (THF) (20 mL) and the resulting solution was either cooled to 0°C (for the synthesis of biotin-PEG_{2k}-*b*-GA_{10}) or kept at room temperature (for biotin-PEG_{2k}-*b*-GA_{60}). γ-Benzyl-L-glutamate NCA (274 mg, 1.04 mmol, 43 eq.) was separately dissolved in THF (20 mL) and cooled to 0°C (for biotin-PEG_{2k}-*b*-GA_{10} only) before being transferred to the flask containing biotin-PEG-NH_2 initiator. The reaction was left to stir in ice bath (for biotin-PEG_{2k}-*b*-GA_{10}) or at room temperature (for biotin-PEG_{2k}-*b*-GA_{60}) under inert atmosphere (N_2) for 5 days, conversion determined by NMR and the resulting polymers were used in the next step without purification.

2.6 mL of 1.0 M sodium hydroxide solution (2.5 equivalent of NaOH per benzyl group) were added slowly to the flask under vigorous stirring on day 5 to hydrolyse the benzyl ester groups in the polymer

repeating units. The reactions were left to stir at room temperature for a further two days, and then the solvent was evaporated under reduced pressure. Deionised water (3mL) was added to dissolve the residue, and the resulting solution was dialysed (SnakeSkin™ 3.5K MWCO) for 2 days (10 L water with 3 changes per day) before being freeze-dried and analysed by ^{1}H NMR.

biotin-PEG$_{2k}$-*b*-GA$_{10}$ yield: 23 mg, 29 %.

biotin-PEG$_{2k}$-*b*-GA$_{60}$ yield: 31 mg, 14 %.

4.2.2 Lysozyme fluorescent labelling

To monitor protein cellular uptake, lysozyme was fluorescently labelled with sulfo-cyanine5 (Cy5) succinimidyl (NHS) ester (Lumiprobe), according to manufacturer protocol (Lumiprobe 2018). Accordingly, 3 equivalents of the fluorescent dye per lysozyme molecule were utilised. Cy5 dye (1 mg, 1.29 μmol 3 eq.) and lysozyme (6 mg, 0.42 μmol 1 eq.) were dissolved in 0.10 M sodium phosphate buffer at pH 8.4, stirred while protected from light for 4 h at room temperature, and extensively dialysed for 24 h at 4°C in 10 mM pH 7.4 phosphate buffer solution, again protected from light. Protein concentration and degree of labelling were determined using Tech Tip #31 Calculate dye:protein (F/P)molar ratio (Scientific 2011) equations after dialysis.

$$\text{Protein concentration (M)} = \frac{A_{280} - (A_{max} \times CF)}{\varepsilon} \times \text{dilution factor}$$

ε = protein molar extinction coefficient (M^{-1} cm^{-1}), ε for lysozyme is 38,940 cm^{-1} M^{-1}

Amax = Absorbance (A) of a dye solution measured at the wavelength maximum (λ_{max}) for the dye molecule, Amax for sulfo-Cy5 is 646 nm

CF = Correction factor; adjusts for the amount of absorbance at 280 nm caused by the dye, CF for sulfo-Cy5 is 0.04

Dilution factor = the extent (if any) to which the protein:dye sample was diluted for absorbance measurement

$$\text{Moles dye per mole protein} = \frac{A_{max} \text{ of the labeled preotin}}{\varepsilon' \times \text{protein concentration (M)}} \times \text{dilution factor}$$

ε’ = molar extinction coefficient of the fluorescent dye

ε' of sulfo-cy5 dye is 271000 $L \cdot mol^{-1} \cdot cm^{-1}$

4.2.3 Complexation of biotin-PEG-*b*-pGA to lysozyme

$mPEG_{2k}$-*b*-GA_{30}:protein nanocomplexes were prepared at relative molar charge ratio of *r* = 2.5 where *r* is the charge ratio between the number of glutamic acid residues present in the copolymer (negatively charged at pH 7.4) and the positively charged residues in the protein at pH 7.4 (surface charges of lysozyme +7.5). Selected copolymer and protein were separately dissolved in phosphate buffer (PB, 10 mM, pH 7.4) and appropriate aliquots were mixed to achieve *r* = 2.5. Example calculation for making 600 µL of 100 µg/mL lysozyme: $mPEG_{2k}$-*b*-GA_{30} suspension; stock (i) of Cy5

labelled lysozyme were prepared at 2.43 mg/mL and stock (ii) of mPEG$_{2k}$-*b*-GA$_{30}$ were prepared at 0.5 mg/mL in 10 mM phosphate buffer. 36.7 µL of stock solution (ii) and 24.7 µL of stock solution (i) were mixed together and diluted with 538.6 µL of phosphate buffer to give the desired suspension.

To prepare biotin targeted biotin-PEG$_{2k}$-*b*-pGA:protein complexes, mPEG$_{2k}$-*b*-GA$_{30}$ and biotin-PEG$_{2k}$-b-GA$_{10}$ (or alternatively biotin-PEG$_{2k}$-*b*-GA$_{60}$) copolymers were mixed at relative charge ratios of 50:50, respectively (e.g 1 *mol of* mPEG$_{2k}$-*b*-GA$_{30}$ */ 3 mol of* biotin-PEG$_{2k}$-*b*-GA$_{10}$). Solutions of polymer mixture and lysozyme were then mixed to achieve relative molar charge ratio of 2.5, as described above. Example calculation for making 600 µL of 100 µg/mL lysozyme: biotin-PEG$_{2k}$-*b*-GA$_{10/30}$ suspension; stock (i) of Cy5 labelled lysozyme were prepared at 2.43 mg/mL; stock (ii) of mPEG$_{2k}$-*b*-GA$_{30}$ were prepared at 0.5 mg/mL and stock (iii) of biotin-PEG$_{2k}$-*b*-GA$_{10}$ were prepared at 0.5 mg/mL in 10 mM phosphate buffer. 28.3 µL of stock solution (ii); 18.3 µL of stock solution (iii) and 24.7 µL of stock solution (i) were mixed together and diluted with 528.7 µL of phosphate buffer to give the desired suspension.

4.2.4 Agarose gel electrophoresis

Biotin-PEG$_{2k}$-*b*-pGA:lysozyme complexes were prepared as described above. Protein concentration was kept constant at 300 µg/ml. 25 µL of complexes suspension was loaded onto 1% (w/v)

agarose gel and the electrophoresis was run with 1% w/v TRIS-acetate-EDTA (TAE) buffer at 100 mA for 1 h. The resulting gel was stained with Coomassie blue. Solutions of protein (lysozyme) at 300 µg/ml, and copolymers were used as 'free' controls.

4.2.5 Cell culture

Human epithelial lung carcinoma cells A549 were obtained from the American Type Culture Collection (ATCC) and used between passages 20-40. Cells were grown to confluence in 75 cm^2 flasks (canted neck and vented caps, Corning) in Dulbecco's Modified Eagle's (DMEM) with addition of Foetal Bovine Serum (FBS, 10% v/v), L-glutamine (1% v/v), penicillin (100 units/mL), and streptomycin (100 µg/mL). Upon confluence, Dulbecco's Phosphate-Buffered Saline (DPBS) and trypsin/EDTA were used to wash and detach adherent cells in the process of cell splitting.

4.2.6 Determination of cells metabolic activity by MTS assay

Biotin-PEG_{2k}-*b*-GA_{10}:lysozyme nanocomplexes were prepared in 10 mM PB at relative molar charge ratio 2.5 with different protein concentrations and diluted in non-supplemented medium (dilution factor 10x) to reach final protein concentrations of 25, 50, 100 and 200 µg/mL in culture wells on 96 well plate.

Once cells reached 90% confluency in the culture flask, A549 cells were detached and seeded on to 96-well plates at 8×10^3 cells *per* well and grown for 24 h. Medium were then removed, cells washed

with DPBS, test samples added to the cells (200 µL per well), and incubated for 4 hours. Subsequently medium were removed, cells washed with DPBS, and 120 µL of MTS solution (20 µL MTS + 100 µL medium) were added. After 3 h incubation, the absorbance of the solution was read at λ = 490 nm (Beckman Coulter Platereader). Experiments were carried out in triplicates.

4% (*v/v*) Triton X-100 solution and untreated cells were employed as controls indicating 0% metabolic activity (positive control) and 100% metabolic activity (negative control), respectively. The metabolic activity was calculated using the following formula:

$$\%Metabolic\ activity = \frac{S - P}{N - P} \times 100$$

where S, N and P are the absorbance values of cells treated with test sample, negative control and positive control, respectively.

4.2.7 Cellular uptake biotin-PEG$_{2k}$-*b*-pGA:lysozyme nanocomplexes

A549 cells were seeded at 100,000 *per* well and cultured on 12 well plates for 48 h. DMEM culture medium was then aspired from wells and replaced with phenol red free DMEM medium without additional supplements. Biotin-PEG$_{2k}$-*b*-pGA:lysozyme complexes were prepared as described in section 4.2.3 and diluted to suspend in medium at protein concentration of 10 µg/mL; 0.5 mL of the suspension were added to each well. Cells were incubated at 37°C

for 3 h, detached as described above in section 4.2.5 and fixed using 0.4% v/v formaldehyde solution. Cell suspension was analysed by flow cytometry (Beckman MoFlo Astrios EQ, λ_{ex} = 649 nm and λ_{em} = 666 nm) in at least triplicate experiments, with more than 5000 cells measured in each analysed sample.

The effect of a competitive ligand on receptor-mediated uptake of biotin targeted complexes was studied in the presence of an excess of either biotin or pantothenic acid. Firstly, 500 µL of a 0.5 mg/mL solution of either biotin or pantothenic acid in culture medium were added to the wells containing A549 cells grown overnight, after removal of growth medium. Cells were then incubated at 37 °C for 30 min following addition of targeted biotin-PEG_{2k}-*b*-pGA:lysozyme nanocomplexes in the presence of excess biotin or pantothenic acid (500 µL, final protein concentration 10 µg/mL). Cells were incubated again at 37 °C for 3 h, washed with DPBS and fixed with 4% v/v% formaldehyde before being analysed by flow cytometry as described above in this section. Experiments were repeated at least three times, with more than 5,000 cells measured in each sample.

4.2.8 Confocal Microscopy

Live cell imaging. For live cell confocal imaging, A549 were cultured overnight in a glass bottom Petri dish (Thermo Fisher, 35 mm) at a density of 75,000 cells per dish. 1.0 mL of 10 µg/mL of suspension of biotin-PEG_{2k}-*b*-$GA_{10/30}$:lysozyme complexes in DMEM medium

without phenol red was applied to each dish after washing with DPBS. After the 1 h treatment, cells were washed with DPBS and phenol red free DMEM medium without additional supplements added for immediate live cell imaging. Zeiss LSM880 confocal laser scanning microscope with Cy5 filter, laser line 633/647 was used to obtain the images.

Imaging of fixed cell. For fixed cell confocal imaging, A549 cells were seeded at the density of 3×10^5 *per* well onto the glass coverslips with 12 mm diameter which were placed in each well of a 6-well plate and cultured overnight in DMEM medium with supplements described in section 4.2.5. After washing with DPBS, 2 mL of 10 μg/mL free lysozyme, biotin-PEG_{2k}-*b*-$GA_{10/30}$:lysozyme nanocomplexes, or non-targeted nanocomplexes in suspensions in what DMEM medium without phenol red were applied to each well. After 1 h of incubation, the medium was removed and coverslips containing cells were washed three times by DPBS. The cells were then fixed by immersing the coverslips into the 4% v/v paraformaldehyde solution for 20 min in the dark, at room temperature, and then washed twice with DPBS. Next, the cells were permeabilised using 1x Intracellular Staining Permeabilization Wash Buffer (BioLegend®) for 10 min before being washed twice with DPBS. Either 1 mL of 5 μg/mL Streptavidin-Alexa Fluor™ 488 conjugate (Invitrogen), or 1 mL of 1X Phalloidin FITC Reagent (Invitrogen) were applied for 1 h. Cells were then washed with DPBS

and stained with Hoechst 33342 (Invitrogen) for 5 min at working concentration of 5 µg/mL. After staining, each coverslip with cells was washed by the DPBS three times and transferred onto a glass slide with a drop of Fluoromount mounting medium (Sigma). The glass slides were then imaged using a Zeiss PS1 Super Resolution Microscope with Cy5 filter, laser line 633/647.

4.3 Results and discussion

Vitamin-mediated drug targeting is a valuable strategy for targeted drug delivery (Tripodo *et al.* 2014). Living cells utilise vitamins during their life cycle for cellular development, whereby rapidly dividing, such as cancer, cells often show an increased demand for vitamins to sustain their fast growth. Consequently, receptors for vitamin internalisation are often overexpressed on fast dividing and cancer cells (Reddy and Low 1998; Seubwai *et al.* 2007). Among the specific cancer targeting ligands, biotin (vitamin B7) gained attention in the years due to its relatively simple chemical structure, low molecular weight, and high tumour specificity (Ren *et al.* 2015). Recent reports indicate that biotin receptors are overexpressed in many types of cancer cells, including leukaemia (L1210FR), ovarian (Ov2008, ID8), colon (Colo-26), mastocytoma (P815), lung (M109 and A549), renal (RENCA, RD0995), and breast (MCF-7) cancer cell lines (Russell-Jones *et al.* 2004; Ren *et al.* 2015; Bui *et al.* 2014). The employment

of biotin targeted systems in delivering nano-sized particles have already been explored by several studies (Aleandri *et al.* 2015; Tripodo *et al.* 2014; Jung *et al.* 2014).

However, biotin is a promoter of cell growth in many cell types which does not limit this delivery system to solely targeting cancer cells (Yang *et al.* 2009). In this study we synthesised two biotin conjugated PEG_{2k}-*b*-poly(glutamic acid) linear copolymers, with either 10 or 60 glutamic acid repeating units. The aim was to test the ability of both polymers in aiding cellular uptake of model protein lysozyme, exploiting the potential impact of different surface ligand densities on protein cell internalisation. The difference between surface density was previously proven to effect cell receptor interaction with nanoparticles and its internalisation (Moradi *et al.* 2012).

4.3.1 biotin-PEG_{2k}-*b*-GA_{10} and biotin-PEG_{2k}-*b*-GA_{60} synthesis

In the present study, biotin-PEG_{2k}-*b*-pGA block copolymers with linear structure were prepared. Commercially available biotin-PEG_{2k}-amine was used which acted as a macroinitiator for *N*-Carboxyanhydrides (NCA) ring opening polymerisation **(Figure 4.2)**. The number of glutamic acid (GA) repeating units in the pGA block were either 10 or 60 (Đ = 1.04 and 1.12 respectively). All polymerisation reactions were monitored by ^{1}H NMR, by following the disappearance of the α-CH proton signal of the NCA monomer at

4.4 ppm. Biotin-PEG_{2k}-*b*-GA_{10} polymerisation were carried out at 0°C while biotin-PEG_{2k}-*b*-GA_{60} were at room temperature to promote rate of reaction, affording polymer with higher number of repeating units in the latter condition in the same period of time (5 days). Reaction were stopped when the conversion reached about 70 % monitored by NMR. Treatment of the reaction crude product with $NaOH_{aq}$ hydrolysed the ester bond of the glutamate repeating units gave the required biotin-PEG_{2k}-*b*-pGA copolymers, which were purified by dialysis against deionised water (MWCO 1–3 kDa). ^{1}H NMR spectra of biotin-PEG_{2k}-*b*-GA_{10} and biotin-PEG_{2k}-*b*-GA_{60} copolymers are shown in **Figure 4.3** and **Figure 4.4**, respectively. The number of GA repeating units in each copolymer was calculated by comparing the integral of biotin in Biotin-PEG_{2k}-amine with that of the CHN groups in the GA repeating units. Further *in vitro* experiments were carried out to test the ability of both copolymers in aiding cellular uptake utilising the effect of different surface ligand density.

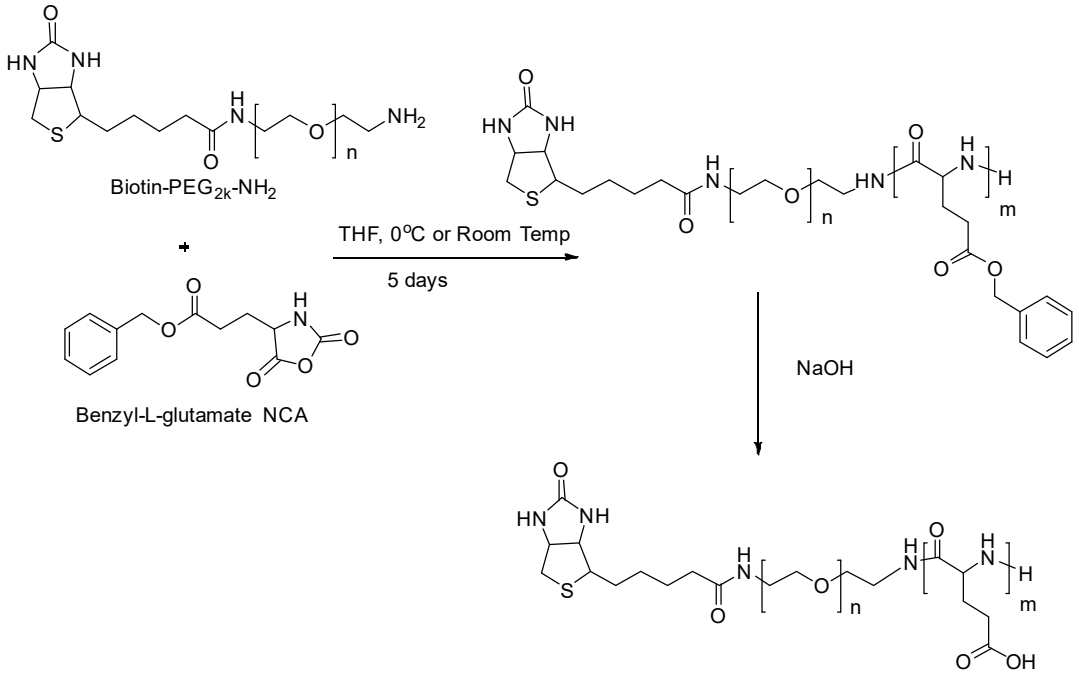


Figure 4.2 *Synthesis of biotin-PEG$_{2k}$-b-pGA copolymers. Reaction conditions: benzyl-L-glutamate NCA reacting with biotin-PEG$_{2k}$-NH$_2$ in THF for 5 days, 0 °C for biotin-PEG$_{2k}$-b-GA$_{10}$ and room temperature for biotin-PEG$_{2k}$-b-GA$_{60}$; solutions were then dialysed in NaOH, H$_2$O/THF for 2 days.*

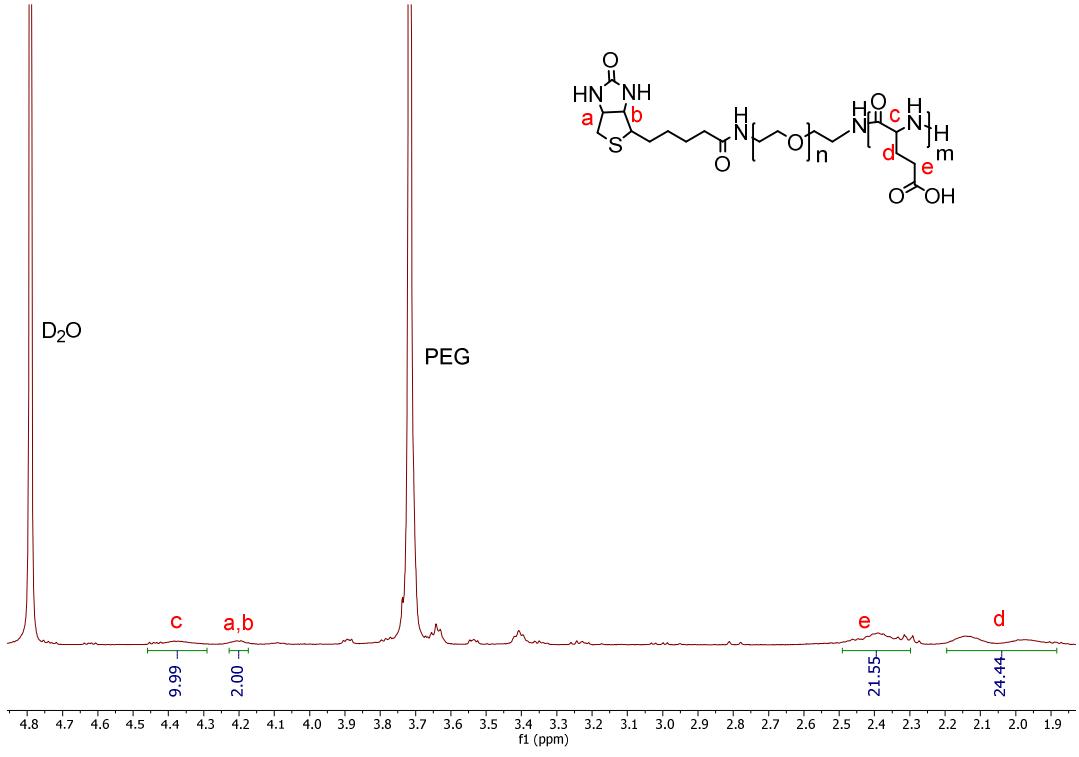


Figure 4.3 *^{1}H-NMR of biotin-PEG$_{2k}$-b-GA$_{10}$ in D$_2$O.*

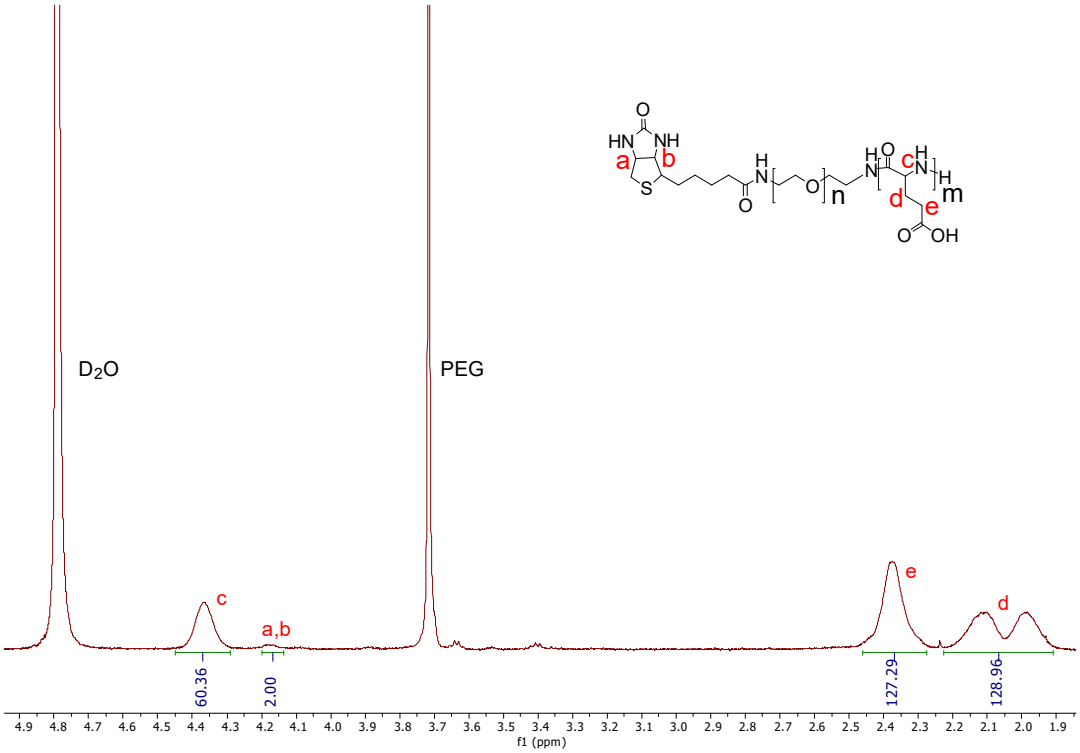


Figure 4.4 *^{1}H-NMR of biotin-PEG$_{2k}$-b-GA$_{60}$ in D$_2$O.*

4.3.2 Biotin-PEG$_{2k}$-*b*-pGA:lysozyme complexation

Biotin-PEG$_{2k}$-*b*-pGA:protein complexes with lysozyme as a model protein cargo were assembled using a mixture of biotin-conjugated and non-conjugated PEG$_{2k}$-*b*-pGA copolymers. Our studies with analogue targeted systems using vitamin B$_{12}$ as the ligand showed efficient cellular internalisation using a 15:85 molar charge ratio of B$_{12}$-PEG$_{2k}$-*b*-GA$_{30}$ to mPEG$_{2k}$-*b*-GA$_{30}$ was previously achieved in our group and described in Chapter 3 (Nieto-Orellana *et al.* 2019). Reasoning that biotin is a smaller molecule compared to vitamin B$_{12}$, a higher proportion of the biotin targeted polymer may be needed to increase surface 'exposure' to compensate for its smaller size. In

this study a 50:50 molar charge ratio of biotin-conjugated and non-conjugated copolymers was selected. mPEG$_{2k}$-*b*-GA$_{30}$ copolymer with 30 repeating units of glutamic acid units was used here as a non-targeted copolymer for the formulation of polyelectrolyte complexes with both biotin-PEG$_{2k}$-*b*-GA$_{10}$ and biotin-PEG$_{2k}$-*b*-GA$_{60}$ copolymers.

Figure 4.5 shows the gel electrophoresis analysis of free lysozyme, free biotin, biotin-PEG$_{2k}$-*b*-GA$_{10}$ and biotin-PEG$_{2k}$-*b*-GA$_{60}$ copolymers on their own and as nanocomplexes with lysozyme. Non-targeted mPEG$_{2k}$-*b*-GA$_{30}$: lysozyme nanocomplexes were also analysed for comparative purposes. Staining with Coomassie blue dye was effective at displaying lysozyme, whilst under these conditions polymers could not be visualised on the gel. Wells 5 – 7 indicate formation of complexes between polymers and lysozyme preventing migration of lysozyme (which was shown to migrate towards the negative electrode in well 1) through either modification of surface charge or increase in spatial size. Although the smear in lane 1 for lysozyme is rather unexpected, research have suggested the buffer concentration could greatly affect smearing of lysozyme in agarose gel - lower concentrations increase smearing - possibly due to uneven pH during migration of lysozyme: namely, lysozyme may have caused pH gradient as it moved in the gel (Li and Arakawa 2019).

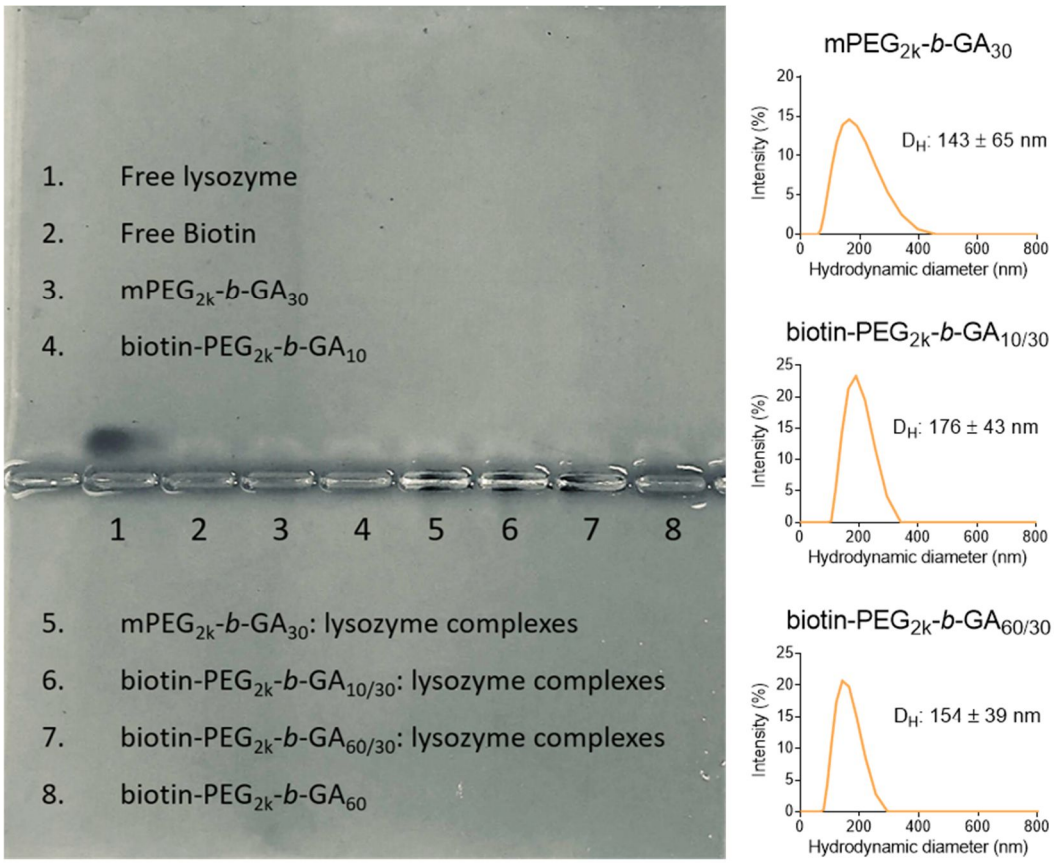


Figure 4.5 Left *Gel electrophoresis analysis of lysozyme, biotin, mPEG$_{2k}$-b-GA$_{30}$, biotin-PEG$_{2k}$-b-GA$_{10}$ and biotin-PEG$_{2k}$-b-GA$_{60}$ copolymers and lysozyme complexes with mPEG$_{2k}$-b-GA$_{30}$, biotin-PEG$_{2k}$-b-GA$_{10}$ and biotin-PEG$_{2k}$-b-GA$_{60}$ copolymers at polymer to protein charge ratio 2.5. Concentration of lysozyme used was 300 µg/mL in all samples; pH 7.4, 1.0 % agarose gel, ran 1 h at 100 mA in Tris-Acetate-EDTA (TAE) buffer.* ***Right*** *Particle size distribution of lysozyme complexes assembled from non-targeted mPEG$_{2k}$-lin-GA$_{30}$ and biotin-PEG$_{2k}$-b-GA$_{10/30}$ as assessed by dynamic light scattering (DLS). biotin-PEG$_{2k}$-b-GA$_{10/30}$ refer to complexes assembled with 50:50 molar charge ratio of biotin-PEG$_{2k}$-b-GA$_{10}$ and mPEG$_{2k}$-b-GA$_{30}$ complexing copolymers. biotin-PEG$_{2k}$-b-GA$_{60/30}$ refer to complexes assembled with 50:50 molar charge ratio of biotin-PEG$_{2k}$-b-GA$_{60}$ and mPEG$_{2k}$-b-GA$_{30}$ complexing copolymers. D$_H$ is the average hydrodynamic diameter (± SD) of polymer-protein complexes.*

4.3.3 Cellular internalisation of biotin-PEG$_{2k}$-*b*-pGA:lysozyme nanocomplexes *in vitro*

It has been demonstrated that cellular internalisation of biotin by human small intestinal epithelial cells occurs *via* a carrier-mediated mechanism which is Na^+ dependent(Mcmahon 2002; Quick and Shi

2015). The transport system is referred to as the sodium-dependent multi-vitamin transport system (SMVT) (De Carvalho and Quick 2011). The presence of biotin receptor on other cells, apart from human intestinal cells, was previously established on A549 lung epithelial cell line (Jung *et al.* 2014; Shin *et al.* 2016). For instance, Maiti *et al* proposed that gemcitabine–coumarin–biotin conjugate was internalised by A549 cells via biotin receptor-mediated endocytosis (Maiti *et al.* 2013). Therefore, A549 cells were chosen in this work as the *in vitro* model to test interactions with, and potential cellular internalisation of biotin-targeted protein-polymer complexes following pulmonary application.

Data in **Figure 4.6** demonstrate statistically significantly increased cellular internalisation of biotin-PEG_{2k}-*b*-$GA_{10/30}$:lysozyme nanocomplexes (~173 nm), relative to non-biotin targeted mPEG_{2k}-*b*-GA_{30}:lysozyme complexes (~143 nm) or 'free' Cy5-lysozyme (~6 nm) in A549 cells, measured by flow cytometry. Interestingly, the increased cellular internalisation is not seen for the biotin-PEG_{2k}-*b*-$GA_{60/30}$:lysozyme nanocomplexes (~154 nm).

Both formulations were prepared in 50:50 % molar charge ratio of mPEG_{2k}-*b*-GA_{30} copolymer and biotin-PEG_{2k}-*b*-GA_{10} or biotin-PEG_{2k}-*b*-GA_{60} with lysozyme at *r* charge ratio of 2.5. As the concentration of lysozyme was the same for both samples (10 μg/mL), given that the 'input' ratio of copolymers was maintained in the final

complexes, this would result in a different biotin ligand density at the surface of the complexes. Potentially result in higher interaction probability between biotin-targeted nanocomplex with cellular receptors and a consequent higher cellular internalisation as shown in **Figure 4.6**. This study here indicates different surface ligand density might play a role in the extent of ligand receptor recognition hence effecting rate of cellular uptake. Further studies would be required, which were not carried out due to prioritisation of other experiments, to generate a series of biotin-conjugated and non-conjugated PEG_{2k}-*b*-pGA copolymers in order to define what may be the optimised formulation in respect to cellular internalisation, such as previous study on folate targeted nanoparticles (Moradi *et al.* 2012). Based on these initial findings, subsequent experiments were performed using the biotin-PEG_{2k}-*b*-GA_{10} copolymer.

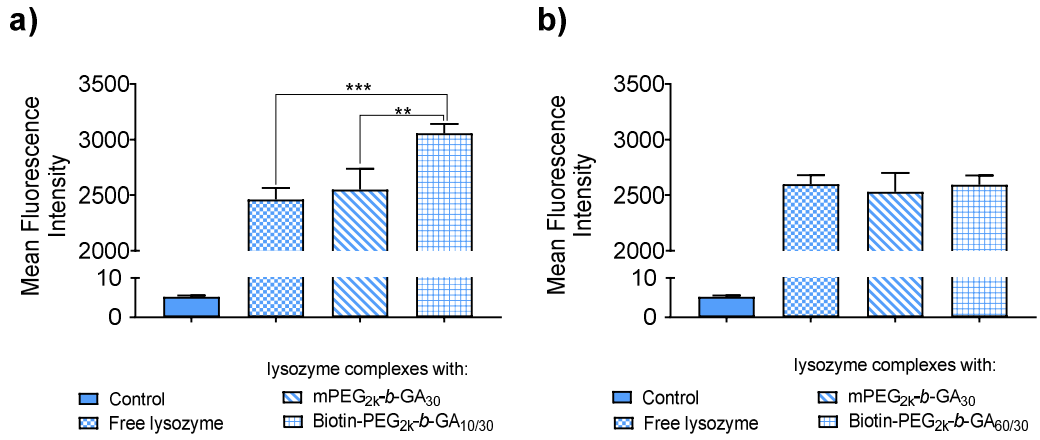


Figure 4.6 *Cellular internalisation by A549 cells of lysozyme complexes with $mPEG_{2k}$-b-pGA copolymers; a) biotin-PEG_{2k}-b-$GA_{10/30}$:lysozyme and b) biotin-PEG_{2k}-b-$GA_{60/10}$: lysozyme where lysozymes were fluorescently labelled by Cy5.*

*Suspensions of complexes were applied at protein concentration of 10 µg/mL and incubated with cells for 3 h prior to flow cytometry analysis. Complexes were prepared at r charge ratio of 2.5 'Control' denotes untreated cells. 'Free lysozyme' indicates that cells were treated with a solution of Cy5-lysozyme in the absence of complexing copolymers. One-way ANOVA was used for statistical analysis. ** $p < 0.01$, *** $p < 0.001$. The error bar shown is the standard deviation of the mean. (N=3, n=3)*

The biotin transport system is considered to be the sodium-dependent multi-vitamin transporter, and has been suggested that it is utilised by two other nutrients: pantothenic acid and lipoic acid (Prasad *et al.* 1998). These nutrients have been demonstrated to exhibit competitive, reversible inhibition relationship with biotin (Uchida *et al.* 2015). In this study, an excess of either biotin or pantothenic acid was employed in competitive experiments with biotin-PEG_{2k}-*b*-$GA_{10/30}$:lysozyme complexes. Data in **Figure 4.7** demonstrate significantly increased cellular internalisation of biotin-PEG_{2k}-*b* $GA_{10/30}$:lysozyme nanocomplexes, compared to non-biotin targeted $mPEG_{2k}$-*b*-GA_{30}:lysozyme counterparts or 'free' lysozyme. Notably, cellular internalisation of biotin targeted complexes decreased significantly ($p < 0.0001$ or $p < 0.01$) in the presence of excess of 'free' biotin or 'free' pantothenic acid competitive ligands, respectively. The data would hence indicate to a prominent role that biotin transport mechanism has in internalisation of biotin-PEG_{2k}-*b*-$GA_{30/10}$:lysozyme complexes by A459 cells. In this study, the use of excess pantothenic acid was not as efficient as the excess biotin; although pantothenic acid have

been proposed to utilise the sodium-dependent multivitamin transporter, relative little is known about regulation of the pantothenic acid uptake process (Said and Nexo 2018). Studies investigating the effect of pantothenic acid regarding biotin transport have demonstrated strikingly different results; one study using cloned rat placenta cells showed pantothenic acid reduced biotin transport by greater than 90% compared with control values (Prasad *et al.* 1998). A similar study carried out in peripheral blood mononuclear cells showed minor effect of pantothenic acid on the uptake of biotin, for which the authors suggested 3 possible explanations: i) difference in cell line, ii) existence of a transporter that recognises biotin but not pantothenic acid and iii) low pantothenic acid concentrations (Zempleni and Mock 1999). Solubility of biotin and pantothenic acid in water are 220 mg/L and 1.46 g/mL respectively (Pubchem ; Pubchem), the high water solubility of pantothenic acid could mean the 'excess' of pantothenic acid used in the experiment might not be sufficient high enough in concentration to present maximum efficiency as competition for the ligand receptor. Normal blood concentrations of pantothenic acid range from 1.6 to 2.7 µmol/L (0.35 - 0.59 mg/L), 0.5 mg/mL was used in this study which is about 1000 times excess. Therefore, the use of even higher concentration of pantothenic acid could not be justified in this study.

A number of previous reports studied intracellular delivery of self-assembled protein or drug-carrying systems, some of which incorporated targeted ligands and successfully achieved higher cellular uptake, as observed in our study (Habibi *et al.* 2016; Garg *et al.* 2009; Ayame *et al.* 2008). The current result parallels previous findings on the increase in uptake of vitamin B_{12}-targeted protein complexes based on linear B_{12}-PEG_{2k}-*b*-pGA copolymers compared to non-targeted complexes and non-complexed proteins (Nieto-Orellana *et al.* 2019) and further consolidates the utility of the PEG-*b*-poly(glutamic acid) copolymers as a potential delivery system. As literature suggests that biotin receptors are overexpressed at higher levels compared to the folate and/or vitamin B_{12} receptors in many cancer cells (Santra *et al.* 2011; Bhuniya *et al.* 2014) this also widens the potential application of the current delivery system.

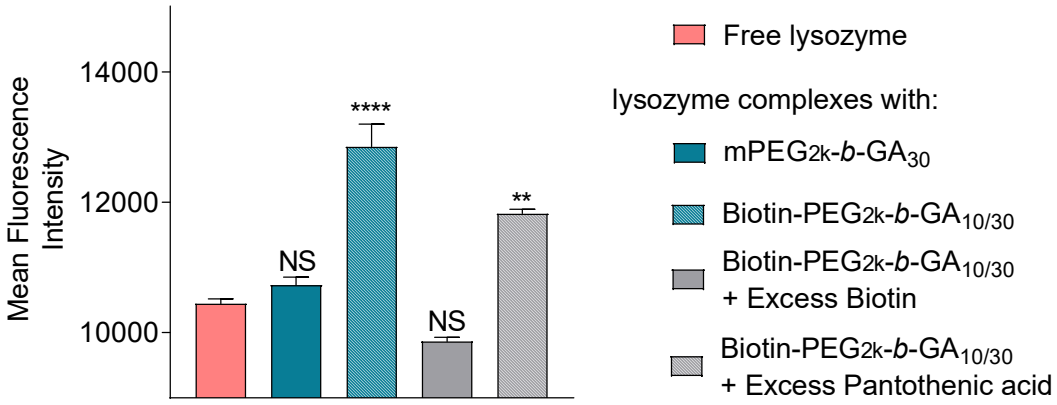


Figure 4.7. *Cellular internalisation of biotin-conjugated and non-conjugated PEG-p(GA)$_{10/30}$ copolymers complexes with Cy5-lysozyme protein by A549 cells. Suspensions of complexes were applied at protein concentration of 10 µg/mL and incubated with cells for 3 h prior to flow cytometry analysis. '+ Excess Biotin at*

*0.5 mg/mL' and '+ Excess Pantothenic acid at 0.5 mg/mL' denotes presence of excess of soluble biotin and pantothenic acid, respectively as competitive ligands in the medium, 'free lysozyme' indicates a treatment with a solution of Cy5-lysozyme in the absence of PEG-poly(GA) complexing copolymers. Each category was compared to uptake of 'Free lysozyme'. One-way ANOVA was used for statistical analysis. NS Not Significant, ** $p < 0.01$, **** $p < 0.0001$. The error bar shown is the standard deviation of the mean. (N=3, n=3).*

4.3.4 Live confocal microscope imaging of biotin-PEG$_{2k}$-*b*-GA$_{10/30}$: lysozyme complexes cellular internalisation

In addition to flow cytometry, cellular internalisation of biotin-PEG$_{2k}$-*b*-GA$_{10/30}$:lysozyme complexes was investigated by confocal microscopy. **Figure 4.8** shows a series of z-stack images taken from the top to bottom of the cells. These indicate the presence of red fluorescently labelled Cy5-lysozyme, applied to cells complexed with biotin-PEG$_{2k}$-*b*-GA$_{10/30}$ copolymers, within cell cytosol as individual 'puncta'. The complexes are not seen present at the cellular surface (i.e. in first two images), and the most fluorescent 'puncta' can be observed in the images from the middle of cells. Higher magnification image of a selected 'slice' in **Figure 4.9** illustrates that the 'puncta' of Cy5-lysozyme red fluorescence follow a circular distribution pattern which, comparing with relevant bright field image, would indicate their position in cell cytoplasm, around the nucleus. These results confirmed that the observed fluorescence within A549 cells detected by flow cytometry was due to cellular uptake and not by simple association of Cy5-lysozyme complexes with the cell membrane.

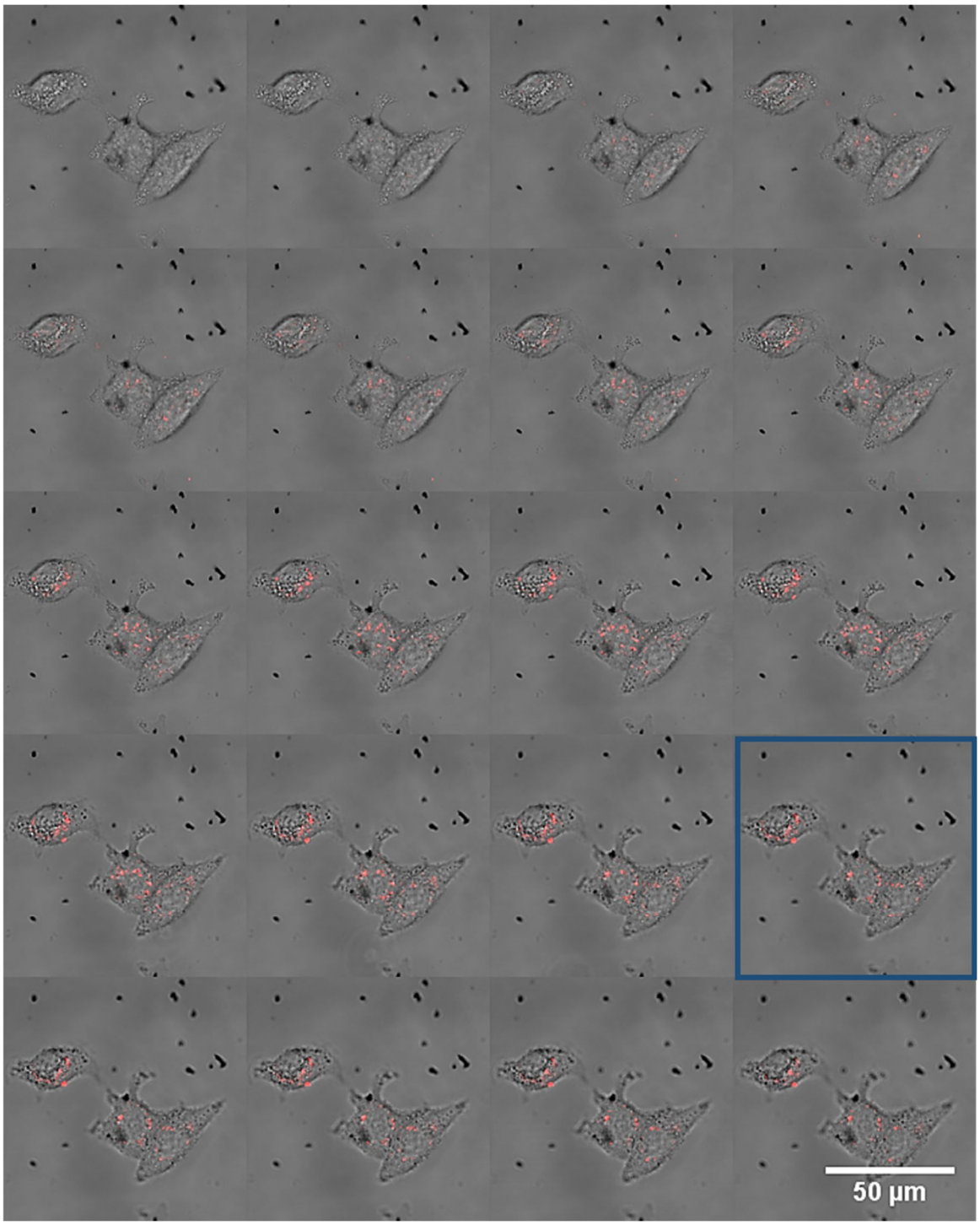


Figure 4.8. *Confocal microscopy panel of z-stack micrographs (0.4 µm per slice) of biotin-PEG$_{2k}$-b-GA$_{10/30}$: lysozyme nanocomplexes cellular uptake in A549 cells. Cells were incubated with biotin-PEG$_{2k}$-b-GA$_{10/30}$: lysozyme noncomplexed for 3 h and then assessed using confocal microscopy. Z-stack sections images from the top to the bottom of the cells are presented in individual panels. Scale bars correspond to 50 µm.* ***Figure 4.9*** *shows detailed orthogonal view of the selected slice (in blue rectangle).*

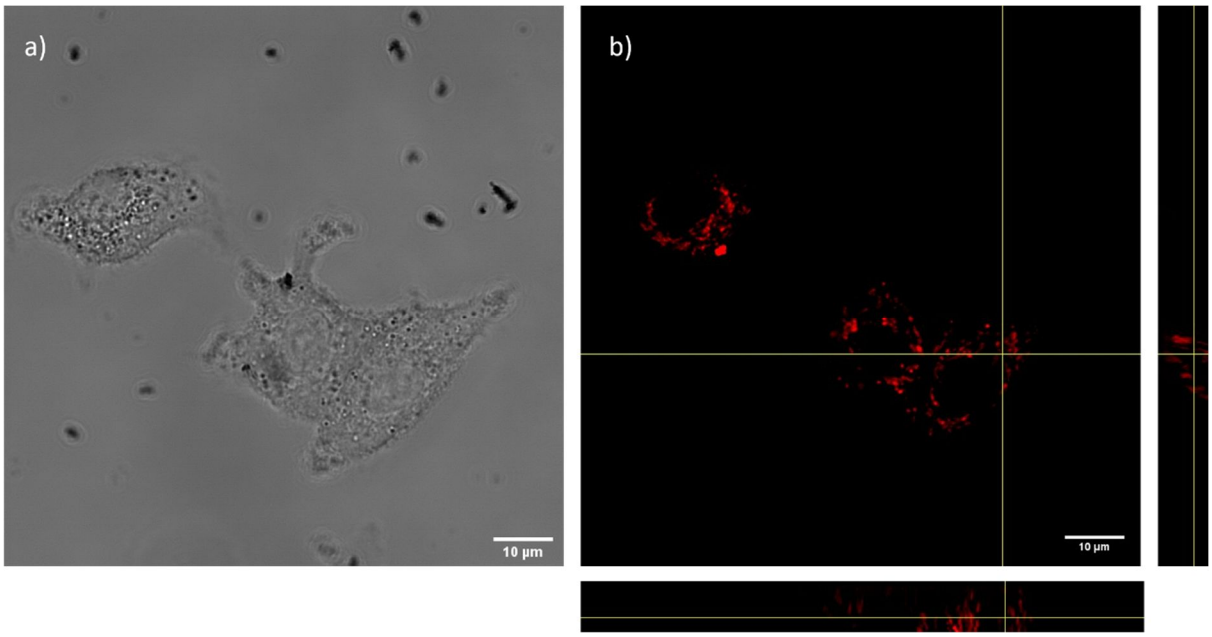


Figure 4.9. *Confocal microscopy of biotin-PEG$_{2k}$-b-GA$_{10/30}$: lysozyme nanocomplexes cellular uptake in A549 cells (live cell imaging). a) Brightfield image of b. b) Orthogonal view from different planes (x/y, x/z or y/z) of the confocal microscope images used to analyse biotin-PEG$_{2k}$-b-GA$_{10/30}$: lysozyme nanocomplexes uptake in A549 cells, localisation of fluorescently labelled lysozyme (with Cy5, in red). Scale bars correspond to 10 µm.*

4.3.5 Confocal microscope imaging of biotin-PEG$_{2k}$-*b*-GA$_{10/30}$: lysozyme complexes in fixed cells

The aim of this part of the thesis work was to assess if biotin-PEG$_{2k}$-*b*-GA$_{10}$ complexes with lysozyme stay together once internalised by the cells. To this end, streptavidin-biotin interaction was utilised; Alexa 488 labelled streptavidin was expected to bind to the exposed biotin from biotin-PEG$_{2k}$-*b*-GA$_{10}$ copolymer used to complex lysozyme, hence provide information on the copolymer intracellular localisation. Confocal fluorescence microscopy imaged for lysozyme (Cy5, red), streptavidin (Alexa 488, green) and nucleus (DAPI, blue) **(Figure 4.10)**.

In the current polymer–protein nanocomplex system, only the protein lysozyme was fluorescently labelled; thus, to locate the polymer intracellularly one has to fluorescently tag the polymer. The presence of targeting ligand biotin on the biotin-PEG_{2k}-*b*-GA_{10} polymer are available to be recognised by the fluorescently labelled streptavidin even when biotin-PEG_{2k}-*b*-GA_{10} are in the complexed form with the protein lysozyme; such makes an excellent marker for the position of the polymer. The non-covalent interaction of biotin and avidin or streptavidin has been exploited for use in many protein and nucleic acid detection and purification methods (Bayer and Wilchek 1980; Chivers *et al.* 2011).

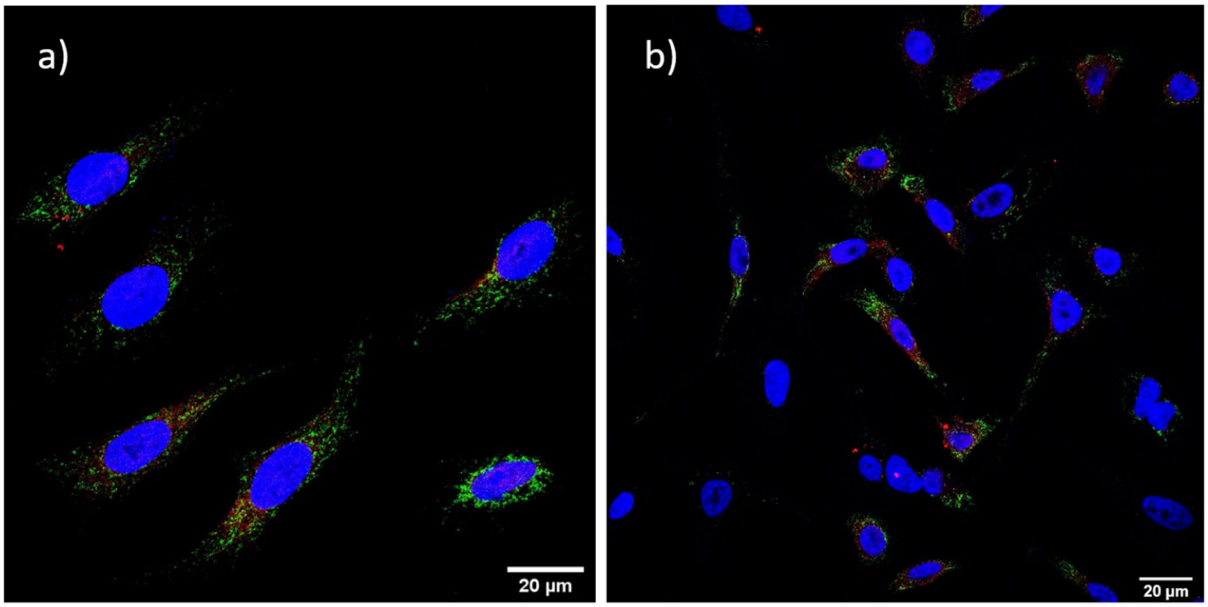


Figure 4.10. *Representative confocal microscopy images of A549 lung epithelial cells incubated with biotin-PEG_{2k}-b-$GA_{30/10}$:lysozyme complexes, followed by a subsequent application of Alexa 488-conjugated streptavidin in fixed and permeabilized cells. Pearson's Correlation Coefficient analysis was used for intracellular colocalization studies of labelled protein (Cy5-lysozyme, red) and Alexa 488 (green) conjugated streptavidin; nuclear stain (DAPI, blue). Pearson's coefficients for images: a) r = 0.57 and b) r =0.50.*

Avidin is a highly cationic 6.6 kDa glycoprotein with an isoelectric point of about 10.5 (Green 1975). It is thought that a positively charged residues on the avidin and its oligosaccharide component (heterogeneous structures composed main of mannose and *N*-acetylglucosamine) can interact non-specifically with negatively charged cell surfaces and nucleic acids and give arise to non-specific binding (Livnah *et al.* 1993). Streptavidin with a near-neutral isoelectric point was reported to exhibit lower levels of non-specific binding compared to avidin and was chosen in this study. Streptavidin is an ~56 kDa homotetramer that binds up to four biotin molecules with K_d ~ 10−14 M (Wilchek *et al.* 2006). Binding of biotin to streptavidin involves a highly stabilised network of polar and hydrophobic interactions. One type of such bonds is the hydrogen bonding with the ring structure on biotin, namely the ureido oxygen group of biotin (Livnah *et al.* 1993). An Alexa Fluor™ 488-conjugated streptavidin was selected to bind biotin-PEG_{2k}-*b*-GA_{10} polymer in cells and was visualised using confocal microscopy. Alexa Flour 488 dye has λ_{ex} 490 nm and λ_{em} 525 nm which does not interfere with the Cy5 absorbance that tags the protein. Due to the large size of streptavidin protein, for it to enter the cells in order to bind internal biotin polymers, the cells would need to be fixed and permeabilised. Paraformaldehyde was chosen as the fixation agent due to significant better performance compared to organic solvents with

less severe loss of biochemical information by crosslinking proteins and nucleic acid (Hobro and Smith 2017).

Prior to further discussion it should be noted that streptavidin exhibits lower non-specific binding compared to avidin, but it has been shown to bind integrins on cells (Alon *et al.* 1993). Binding of streptavidin to intracellular structures, e.g mitochondria has also been shown (Hollinshead *et al.* 1997). To assess the influence of potential 'background' streptavidin binding on the microscopy analysis, control confocal images of i) cells without treatment with lysozyme complexes, or ii) cells treated with control non-targeted lysozyme complexes with PEG_{2k}-*b*-GA_{30} were performed. Upon fixation, permeabilization with Triton-X and treatment with Alexa 488-labelled streptavidin, both control samples show negligible level of green fluorescence **(Figure 4.11 a** and **b),** respectively.

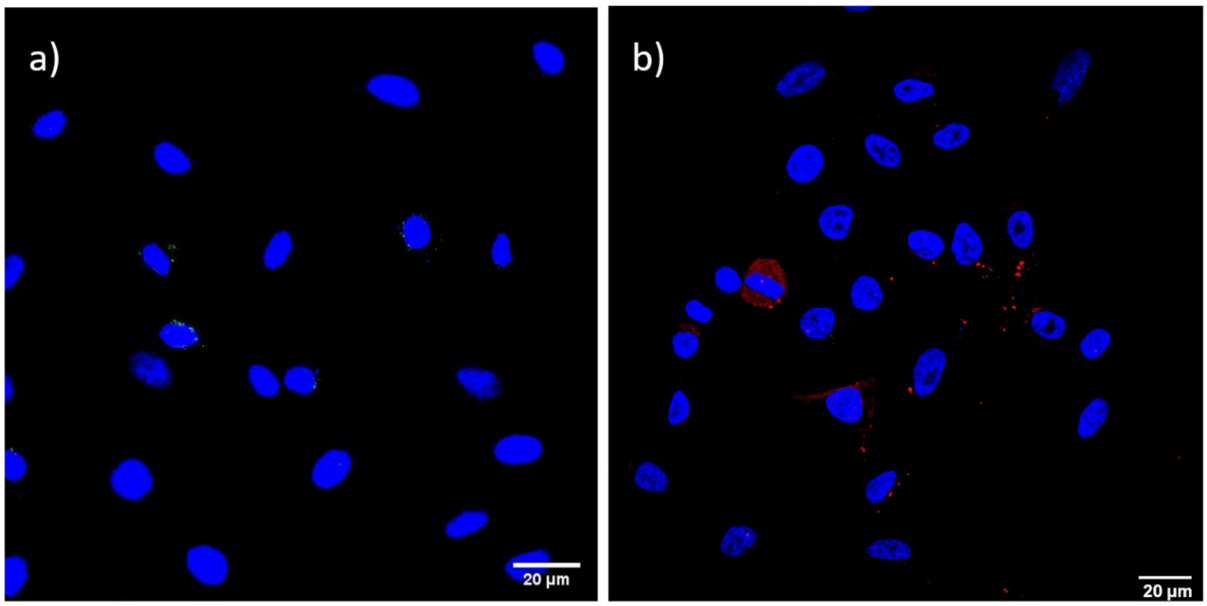
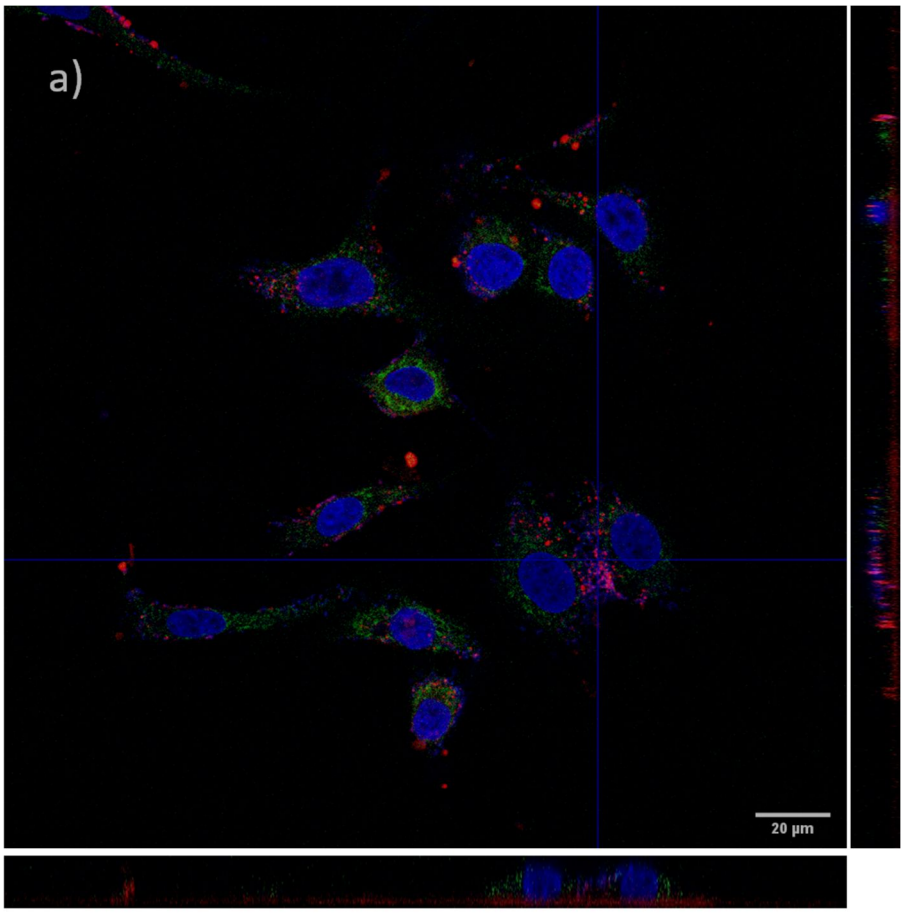


Figure 4.11. *Representative confocal microscopy images of A549 lung epithelial cells showing application of Alexa 488 labelled streptavidin (green) to cells a) untreated cells (absent of biotin-PEG$_{2k}$-b-GA$_{30/10}$:lysozyme complexes) and b) cells treated with mPEG$_{2k}$-b-GA$_{30}$:lysozyme complexes (no biotin conjugation). Fluorescently labelled lysozyme (Cy5, in red), Alexa 488 conjugated streptavidin (green), nuclear stain (DAPI, blue). Scale bars correspond to 20 μm.*

The analysis of images in **Figure 4.10** confirms the intracellular presence of both labelled species; Cy5 lysozyme and Alexa 488 labelled streptavidin - the latter pointing to the intracellular localisation of biotin-PEG$_{2k}$-*b*-GA$_{10}$ copolymer. Co-localisation analysis of the two fluorescently labelled species was performed on several confocal images, and resulted in using Pearson's correlation coefficient *r* value of ~ 0.5 **(Figure 4.10** and **Figure 4.12)**. The Pearson coefficient value of 0.5 indicates a positive trend relating to the intracellular location of the labelled lysozyme and 'streptavidin detected' biotin-PEG$_{2k}$-*b*-GA$_{10}$. This finding indicates that at 1 h after the complexes were applied to, and internalised by the cells, the protein and biotin-PEG$_{2k}$-*b*-GA$_{10}$ copolymers were still largely co-localised. The resolution of confocal microscopy used does not allow assessment of the location of individual protein or copolymer molecules, to be able to clearly ascertain if the complexes' integrity is maintained, or if the protein and copolymer molecules are present in the same sub-cellular region, but dissociated.

Taken together the data would indicate that biotin-PEG$_{2k}$-*b*-GA$_{10/30}$ complexes with lysozyme enter A549 cells as integral species, with a prominent role of receptor mediated endocytosis in the process

(Figure 4.7). It should be noted that experiments in our previous work (Nieto-Orellana *et al.* 2019) showed that a proportion of PEG_{2k}-*b*-$GA_{:}$lysozyme complexes may dissociate into constitutive species when in high ionic strength environments, e.g. cell culture medium. There may be possibilities that some intracellularly present lysozyme was internalised as 'free' lysozyme. From results observed in flow cytometry cell culture study in **Figure 4.7** and confocal image shown in appendix, we established that 'free' lysozyme can be internalised by the cells in uncomplexed form; therefore, the free lysozyme population would not be expected to co-localise with biotin-PEG_{2k}-*b*-GA_{10} copolymer. This would in turn reduce the expected value of Pearson's coefficient.


a)
20 µm

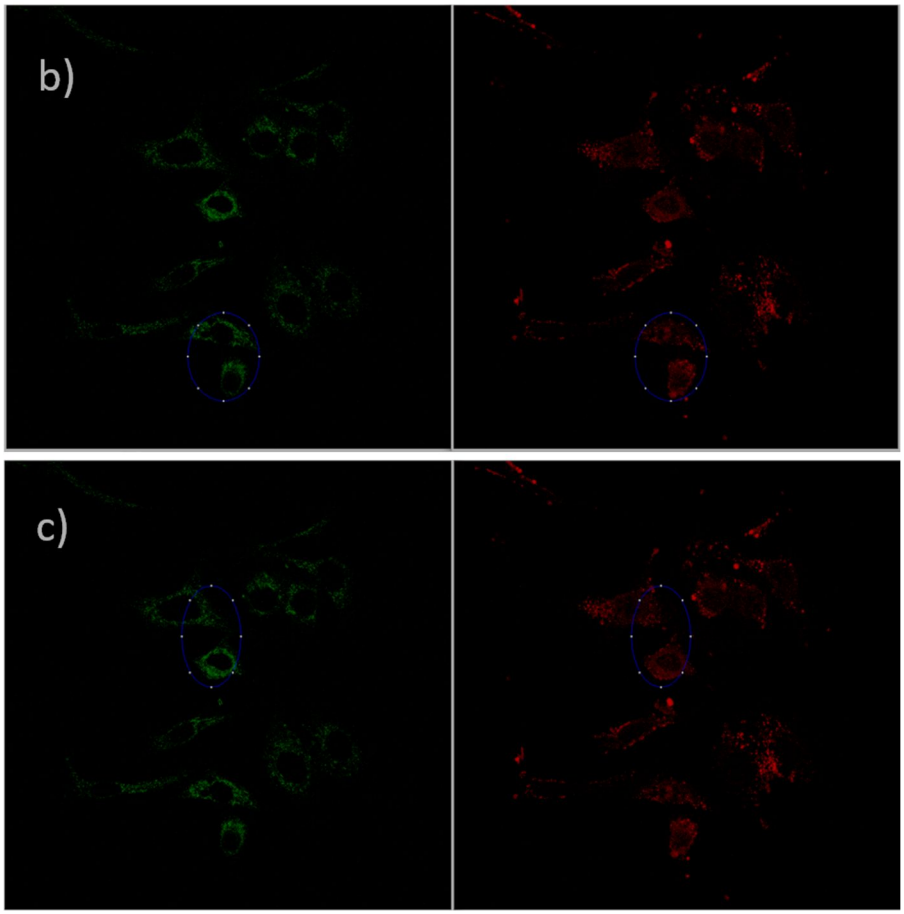

b)
c)

Figure 4.12. *Representative confocal microscopy images of A549 lung epithelial cells incubated with biotin-PEG$_{2k}$-b-GA$_{10/30}$:lysozyme nanocomplexes containing fluorescently labelled lysozyme (Cy5, red), followed by a subsequent application of Alexa 488 labelled streptavidin (green) for detection of biotin moiety in biotin-PEG$_{2k}$-b-GA$_{10/30}$ copolymer; nuclear stain (DAPI, blue). a) Orthogonal view from different planes (x/y, x/z or y/z) of the confocal microscope images used to analyse biotin-PEG$_{2k}$-b-GA$_{10/30}$:lysozyme complexes. Scale bars correspond to 20 µm. Region of interest were selected in images b and c for focused analysis, Pearson's Correlation Coefficient analysis was used for intracellular colocalization studies of (red) labelled protein (Cy5-lysozyme) and (green) Alexa 488 conjugated streptavidin tagged biotin-PEG$_{2k}$-b-GA$_{10/30}$ in A549 cells. b) r = 0.36, c) r =0.40*

To the best of our knowledge this is the first study attempting to assess the intracellular location of polymers used in formulation of targeted nanocomplexes, and their co-localization with delivered cargo. The study shows that biotin-PEG$_{2k}$-*b*-GA$_{30/10}$:lysozyme nanocomplexes were both internalised by A549 cells, driven by biotin receptor recognition and internalised as intact entities *via* endocytosis mechanism. Comparing to other studies that observed uptake of fluorescently labelled drugs or molecules in cells, the target agents were commonly chemically linked (*via* covalent linker) to the drug or molecule (Chen *et al.* 2010; Jung *et al.* 2014; Santra *et al.* 2011).

4.4 Conclusions

In this study, biotin-conjugated poly(ethylene glycol)-*block*-poly(glutamic acid) copolymers were synthesised, and the potential of these copolymers to self-assemble with a protein cargo into targeted polymer-protein complexes assessed. The data obtained

suggest a biotin-receptor mediated internalisation of biotin-PEG_{2k}-*b*-$GA_{10/30}$:lysozyme complexes *in vitro* in A549 lung epithelial cell. The role of biotin-receptor mediated internalisation is demonstrated in a competition study with excess of biotin or pantothenic acid, and is also evident from a lack of improvement in cellular internalisation of biotin-PEG_{2k}-*b*-$GA_{10/60}$:lysozyme complexes; the later were prepared at the same polymer to protein charge ratio and hence have a 6-fold reduced content of biotin targeting moiety. In addition, biotin-PEG_{2k}-*b*-$GA_{10/30}$:lysozyme nanocomplexes did not negatively impact on lung epithelial A549 cells' viability, up to the 200 µg/mL.

Confocal microscopy study, utilising biotin recognition by Alexa 488 labelled streptavidin, indicates a colocalization of biotin-PEG_{2k}-*b*-GA_{10} copolymers with lysozyme protein in the cell cytosol; with a Pearson's coefficient value of $r \sim 0.5$ evidencing a positive relationship between location of the protein and biotin-PEG_{2k}-*b*-GA_{10} polymer.

Taken together the results presented in this chapter show that biotin targeted complexes of biotin-PEG_{2k}-*b*-GA_{10} and lysozyme achieve biotin receptor targeted cellular internalisation of the protein cargo, whereby the intracellular analysis of biotin-conjugated copolymer provided evidence that the complexes enter the cell as intact species and that constitutive polymers and protein cargo are colocalized in cell cytosol following the internalisation. The study outcome provides

an extension of the applicability of the PEG-b-poly(glutamic acid) group of copolymers at delivering protein cargo to different cell types exploring targeting ligand approach utilising different receptor targets.

Chapter 5. Endocytosis Mechanism of Biotin-PEG-*block*-poly(glutamic acid) protein nanocomplexes

5.1 Introduction

Particles up to 1 μm in size can be internalised by non-phagocytic eukaryotic cells through different endocytic pathways (Rejman *et al.* 2004), such as clathrin-mediated endocytosis, caveolae-mediated endocytosis and macropinocytosis. In addition to these, other clathrin- and caveolin-independent pathways have also been suggested to play a role in cellular uptake of material (Mayor and Pagano 2007). The discussed uptake pathways are presented schematically in **Figure 5.1**. In the previous chapter, we engineered biotin-PEG-poly(glutamic acid) polymers with biotin as targeting ligand and used as a 'complexing excipient' to assemble complexes with the model protein for targeted cellular delivery. The ligand acted as a targeting agent guiding the carrier towards intracellular pathway(s), enabling the delivery of protein intracellularly *via* the ligand internalisation pathway. However, studies have demonstrated targeted formulations may not always utilise the designated ligand-directed pathway, which means that some trafficking pathways can be pursued by synthetic nanoparticles in ways that differ from the transport activated by the ligand functionality alone (Tekle *et al.* 2008; Sayers *et al.*

2018). It is important to understand the cellular internalisation and the processing mechanisms of the delivery system, to improve cellular uptake and to avoid the potentially destructive cellular pathways (Vranic *et al.* 2013). The principal aim of this work, therefore, was to probe the mechanisms of entry into the cells of targeted biotin-PEG_{2k}-*b*-$GA_{10/30}$:lysozyme nanocomplexes, and whether it significantly differs to free lysozyme or non-targeted $mPEG_{2k}$-*b*-GA_{30}:lysozyme nanocomplexes. In this respect, a panel of pharmacological inhibitors **(Table 5.1)** was used here to investigate which endocytic mechanisms are responsible for cellular uptake of these nanoparticles.

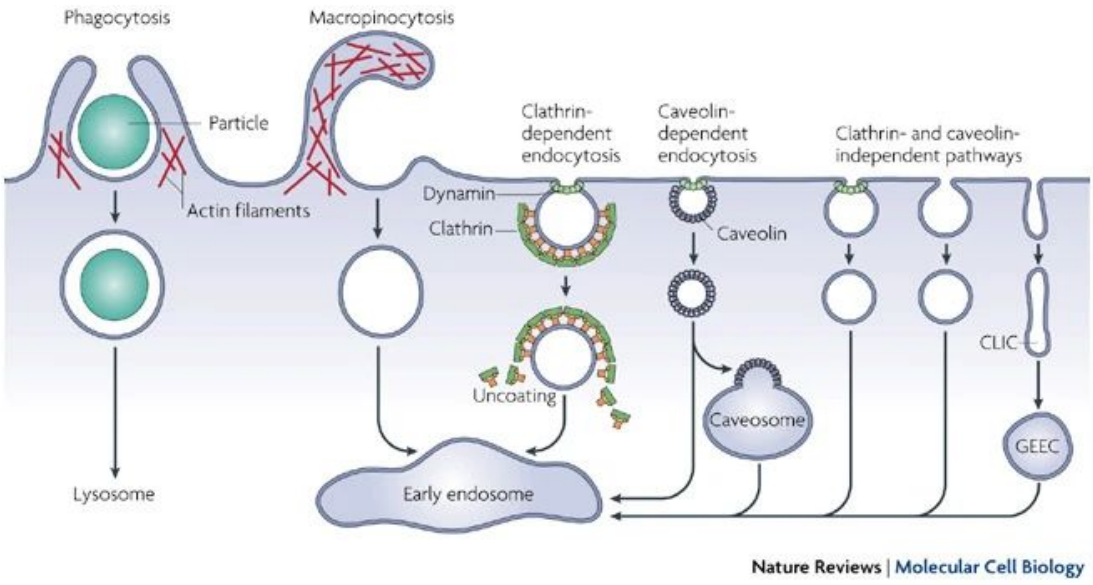


Figure 5.1 *Cell entry pathways. Large particles can be taken up by phagocytosis, whereas fluid uptake occurs by macropinocytosis. Compared with other endocytic pathways, the size of the vesicles formed by phagocytosis and macropinocytosis is much larger. Cargoes can also be endocytosed by mechanisms that are independent of the coat protein clathrin and the fission GTPase, dynamin. Most internalised cargoes are delivered to the early endosome via vesicular (clathrin- or caveolin-coated vesicles) or tubular intermediates (known as clathrin- and dynamin- independent carriers (CLICs) that are derived from the plasma membrane. Some pathways may first traffic to intermediate compartments, such as the caveosome or glycosyl phosphatidylinositol-*

anchored protein enriched early endosomal compartments (GEEC), before reaching the early endosome. Adopted from (Mayor and Pagano 2007).

For the inhibition of clathrin-mediated pathways, chlorpromazine, concanavalin A and dynasore were used. Chlorpromazine is an amphiphilic drug which reversibly translocate clathrin and its adapter protein to intracellular vesicles from the plasma membrane, leading to inhibition of clathrin-coated pit formation (Wang *et al.* 1993; Hussain *et al.* 2011). Concanavalin A, another inhibitor that prevents the assembly of clathrin coated pits by interfering with the signalling of transmembrane G protein-coupled receptors located on the surface of cells (Guo *et al.* 2015). The third inhibitor, dynasore, inhibits dynamin by blocking the GTPase activity of dynamin and hence vesicle detachment from the cell plasma membrane in dynamin-dependent endocytosis in cells (Macia *et al.* 2006). However, dynasore can also exert inhibition effect in the caveolae-mediated pathway by preventing caveolar budding or fission from the plasma membrane to form free vesicles (Oh *et al.* 2012), thus it is not a fully selective inhibitor clathrin-mediated pathways.

Four more inhibitors were used to prob the caveolae-mediated pathway, genistein, filipin, nystatin and MßCD. Genistein inhibits the caveolae/raft-mediated endocytosis through inhibition of tyrosine kinases, preventing phosphorylation of proteins in

caveolae (Le and Nabi 2003; Pelkmans *et al.* 2002). Filipin binds to and eliminate cholesterol from plasma membrane, causing disassembly of vesicles and selectively inhibits caveolae-mediated intracellular transport of macromolecules (Schnitzer *et al.* 1994). Nystatin works in a similar way as a cholesterol sequestering agent that interferes with caveolae/lipid raft-dependent endocytosis without affecting the clathrin-mediated pathway (Simons and Toomre 2000; Yumoto *et al.* 2012). MßCD, a cholesterol-depleting agent, extracts cholesterol from the cell membrane, consequently inhibiting caveolae/raft-mediated endocytosis (Rodal *et al.* 1999). MßCD was also reported having an impact on the micropinocytosis pathway (Saeed *et al.* 2010).

EIPA and cytochalasin D were used to inhibit the macropinocytosis pathway. The former is a selective inhibitor that lowers the sub-membranous pH by inhibiting Na^+/H^+ exchange within membranes (Ivanov 2008; Commisso *et al.* 2013). Cytochalasin D disassemble the actin cytoskeleton in living cells by blocking actin polymerisation and inhibit macropinocytosis (Dharmawardhane *et al.* 2000; Montaner *et al.* 1999).

To the best of our knowledge this is the first study attempting to investigate the effect of pharmacological endocytosis inhibitors on the internalisation mechanism of self-assembled targeted polymer protein nanocomplexes in epithelial cells. Overall, this study aims

to assess whether the presence of natural ligand biotin on the surface of the polymer protein nanocomplex can alter cellular trafficking behaviour in a way that can be exploited for the delivery of biotherapeutics.

Table 5.1. *Pharmacological endocytosis inhibitors used in this work to investigate endocytosis mechanisms used by biotin-PEG$_{2k}$-b-GA$_{10/30}$:lysozyme nanocomplexes.*

Inhibitors	**Mechanism**
Chlorpromazine	Clathrin-mediated inhibitor, inhibits clathrin-coated pit formation
Concanavalin A	Clathrin-mediated inhibitor, prevents the assembly of clathrin coated pits
Dynasore	Dynamin inhibitor, blocking the GTPase activity of dynamin
Genistein	Caveolae-mediated inhibitor, inhibits tyrosine kinase and the caveolae pathway
Filipin	Caveolae-mediated inhibitor, eliminates cholesterol from plasma membrane
Nystatin	Caveolae-mediated inhibitor, as cholesterol sequestration agent that interferes with caveolae/lipid raft-dependent endocytosis
MßCD	Caveolae/raft-mediated inhibitor, extracts cholesterol from cell membrane
EIPA	Macropinocytosis inhibitor, inhibits Na+/H+ exchange of cells
Cytochalasin D	Macropinocytosis inhibitor, blocks actin polymerisation

5.2 Methods

5.2.1 Complexation of biotin-PEG-*b*-p(GA) to lysozyme

biotin-PEG_{2k}-*b*-$GA_{10/30}$:lysozyme nanocomplexes were prepared at relative molar charge ratios r = 2.5 where r is the charge ratio between the number of glutamic acid residues present in the copolymer (negatively charged at physiological pH) and the positively charged residues in the protein at physiological pH (surface charges: lysozyme +7.5). Polymer and protein were separately dissolved in phosphate buffer (PB, 10 mM, pH 7.4) and appropriate aliquots were mixed to achieve r = 2.5.

To prepare biotin targeted polymer-protein complexes, mPEG_{2k}-*b*-GA_{30} and biotin-PEG_{2k}-*b*-GA_{10} copolymers were mixed at relative molar ratios 50/50 (% *mol/mol*), respectively. Polymer mixture and lysozyme were then mixed at relative molar charge ratio of 2.5 as described in chapter 4.

5.2.2 Cell culture

Human epithelial lung carcinoma cells A549 were obtained from the American Type Culture Collection (ATCC) and used between passages 20-40. Cells were grown to confluence in 75 cm^2 flasks (canted neck and vented caps, Corning) in Dulbecco's Modified Eagle's (DMEM) plus Foetal Bovine Serum (FBS, 10% v/v), L-glutamine (1% v/v), penicillin (100 units/mL) and streptomycin

(100 µg/mL). Upon confluence, Dulbecco's Phosphate-Buffered Saline (DPBS) and trypsin/EDTA were used to wash and detach adherent cells in the process of cell splitting detailed in chapter 2.

5.2.3 Cytotoxicity of endocytosis inhibitors (MTS assay)

The cytotoxicity of endocytosis inhibitors was assessed in A549 cells using MTS assays to confirm cell metabolic rate during uptake studies. A range of inhibitor concentrations were applied to A549 cells to determine optimal non-toxic doses: chlorpromazine (2.5 – 40.0 µg/mL), concanavalin A (12.5 – 200.0 µg/mL), dynasore (10.0 – 160.0 µg/mL), genistein (1.9 – 30.0 µg/mL), filipin (2.5 – 40.0 µg/mL), nystatin (2.5 – 40.0 µg/mL), MβCD (37.5 – 600.0 µg/mL), EIPA (1.9 – 30.0 µg/mL) or cytochalasin D (0.3 – 4.0 µg/mL).

Once cells reach 90% confluency in the T75 culture flask, A549 cells were detached and seeded on to 96-well plates at 8×10^3 cells per well and grown for 24 h. Medium were then removed, cells washed with DPBS and inhibitor solutions were added to the cells (200 µl per well) for 4 h. Subsequently medium were removed, cells washed with DPBS and 120 µL of MTS solution (20 µL MTS + 100 µL medium) were added. After 3 h incubation, the absorbance of the solution was read at 490 nm.

4% (*v/v*) Triton X-100 and untreated cells were employed as controls indicating 0% metabolic activity (positive control) and

100% metabolic activity (negative control), respectively. The metabolic activity was calculated using the following formula:

$$\%Metabolic\ activity = \frac{S - P}{N - P} \times 100$$

where S, N and P are the absorbance of cells treated with samples, negative control and positive control, respectively.

5.2.4 Assessment of transferrin and cholera toxin subunit B cellular uptake by A549 cells.

A549 cells were seeded at 300,000 per well and cultured on 12 well plates for 24 h. Culture medium were then removed from wells and replaced with 500 µL inhibitors solution in phenol red free DMEM medium; A549 cells were incubated with inhibitors chlorpromazine (5.0 – 20.0 µg/mL), concanavalin A (50.0 – 150.0 µg/mL), dynasore (5.0 – 20.0 µg/mL), genistein (3.8 – 15.0 µg/mL), filipin (21.0 – 4.0 µg/mL), nystatin (5.0 –20.0 µg/mL) or MβCD (75.0–300.0 µg/mL). After 30 min incubation, the inhibitor solutions were then removed and the cells were washed with DPBS after which, either i) Transferrin, Alexa Fluor™ 488 Conjugate at 100.0 µg/ml; or ii) Cholera Toxin Subunit B (Recombinant), Alexa Fluor™ 488 Conjugate at 5.0 µg/ml, suspended in inhibitor solution were added to the wells. In the control experiments, the medium did not contain inhibitors, before or during application of transferrin or cholera toxin subunit b. Cells were incubated again at 37 °C for

3 h, washed and fixed before being analysed by flow cytometry. Experiments were made in at least triplicates, with more than 5,000 cells measured in each sample.

5.2.5 Investigate mechanism of endocytosis of lysozyme and biotin-PEG$_{2k}$-*b*-GA$_{10/30}$:lysozyme nanocomplexes

A549 cells were seeded at 300,000 per well and cultured on 12 well plates for 24 h. Culture medium were then removed from wells and replaced with 500 µL inhibitors solution in phenol red free DMEM medium: A549 cells were incubated with previously optimised (in terms of toxicity) doses of chlorpromazine (5 µg/mL), concanavalin A (100 µg/mL), dynasore (20 µg/mL), genistein (15 µg/mL), filipin (3 µg/mL), nystatin (20 µg/mL), MßCD (300 µg/mL), cytochalasin D (1 µg/mL) and EIPA (15 µg/mL). These were applied individually to the wells. After 30 min incubation, the inhibitor solutions were removed and the cells were washed with DPBS after which, i) cy5 labelled lysozyme; ii) non-targeted mPEG$_{2k}$-*b*-GA$_{30}$:lysozyme; or iii) targeted biotin-PEG$_{2k}$-*b*-GA$_{10/30}$:lysozyme nanocomplexes suspension at 10 µg/mL protein concentration suspended in inhibitor solution were added to the wells. Cells were incubated again at 37 °C for 3 h, washed and fixed before analysed by flow cytometry. Experiments were made in at least triplicate, with more than 5,000 cells measured in each sample.

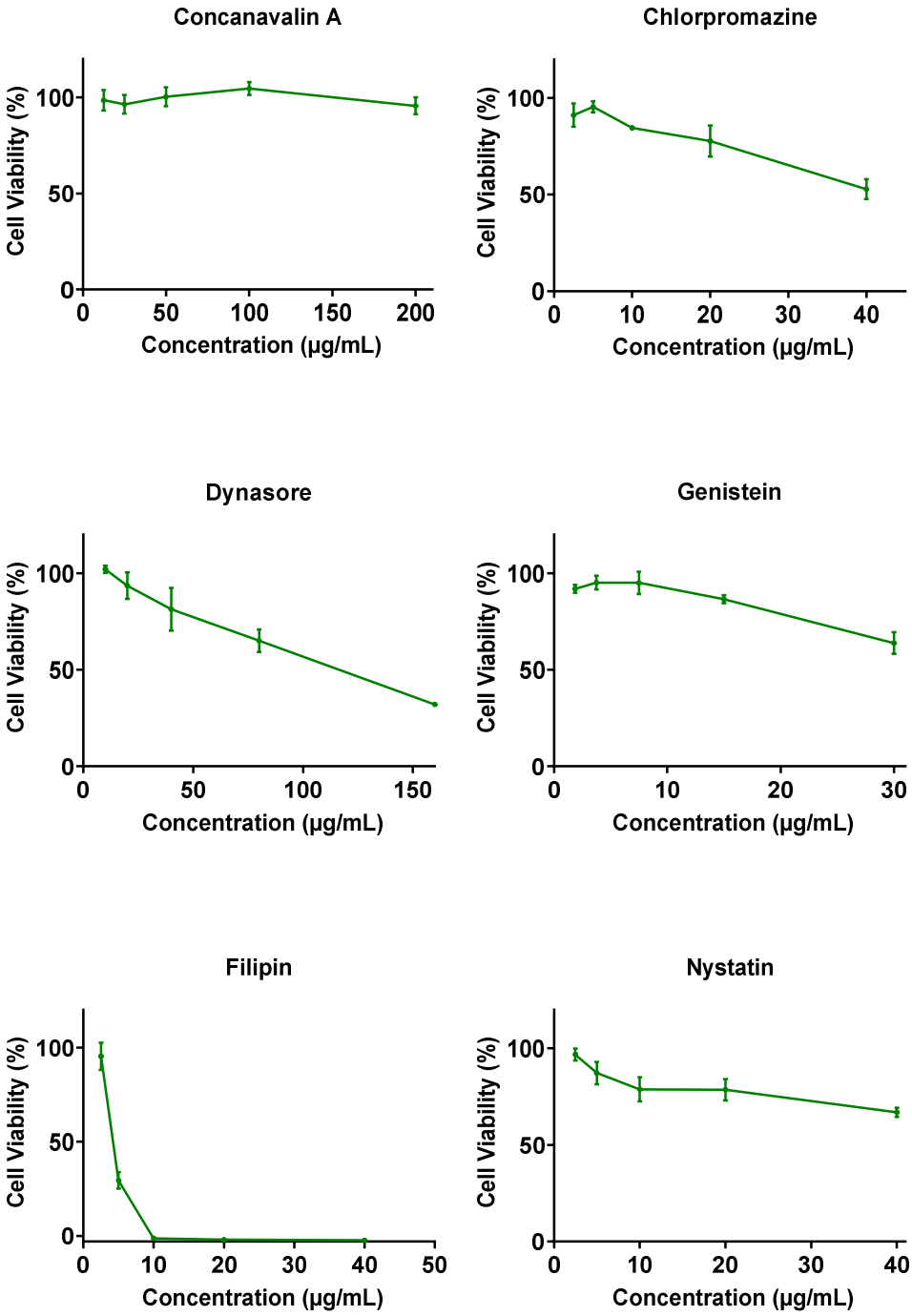
5.3 Results

5.3.1 Effect of inhibitor on A549 metabolic activity *via* MTS assays

A panel of 9 pharmacological inhibitors of endocytosis spanning effects across the clathrin-mediated, caveolae-mediated and macropinocytosis uptake pathways were selected to study the pathways of cellular uptake of: free lysozyme; non-targeted $mPEG_{2k}$-*b*-GA_{30}: lysozyme nanocomplexes; and targeted biotin-PEG_{2k}-*b*-$GA_{10/30}$: lysozyme nanocomplexes. Prior to conducting experiments assessing the inhibitor effect on cellular uptake of nanoparticles, MTS toxicity assays were performed to determining optimal inhibitor concentrations that preserved at least 75 % metabolic rate of the A549 lung epithelial cells for the duration of 4 h.

Figure 5.2 demonstrates that concanavalin A and MβCD exhibited no cytotoxicity for A549 cells in the concentration range tested. Chlorpromazine had a 25% effective concentration (EC25) of ~22 µg/mL - the concentration that cells retained 75% metabolic rate. EC25 of dynasore, the dynamin inhibitor was ~59 µg/mL. Incubation of A549 cells for 4 h with tyrosine kinase inhibitor, genistein, showed an EC25 of ~23 µg/ml. Inhibitors of caveolae-mediated pathway, filipin and cholesterol sequestering agent

nystatin, demonstrated EC25 of ~3 and ~25 µg/mL, respectively. The MTS data for macropinocytosis inhibitors, EIPA and cytochalasin D, had EC25 at of ~23 and ~1.5 µg/ml, respectively. Inhibitor concentrations below EC_{25} values were deemed as suitable for further study, and **Table 5.2** summarises the inhibitor concentrations that were selected based on A549 cell metabolic rate for the subsequent work.



Continues on next page

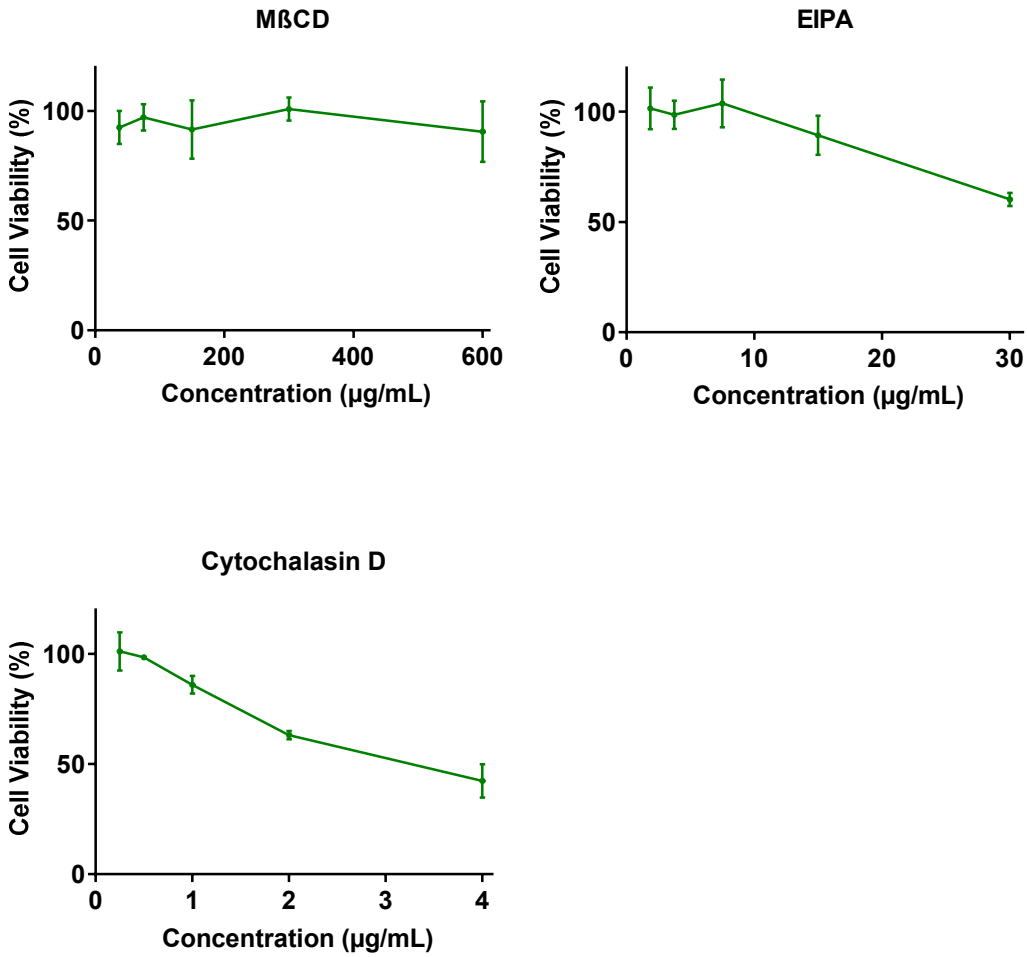


Figure 5.2. *Relative cell metabolic rate (%) after incubating A549 cells with different endocytosis inhibitors for 4 hours. Data are the results of MTS assays and expressed as relative cell metabolic activity and presented as the mean ± SD. (N=3, n=3).*

Table 5.2. *Selected concentrations of inhibitors and A549 cell metabolic rate at chosen concentrations.*

Inhibitors	Concentrations	Cell metabolic rate (%)
Chlorpromazine	5 µg/mL	91
Concanavalin A	100 µg/mL	98
Dynasore	20 µg/mL	94
Genistein	15 µg/mL	82
Filipin	3 µg/mL	83
Nystatin	20 µg/mL	79
MβCD	300 µg/mL	94
EIPA	15 µg/mL	85
Cytochalasin D	1 µg/mL	87

5.3.2 Effect of inhibitors on cholera toxin β and transferrin uptake into A549 cells

After adjusting the concentrations of the pharmacological inhibitors in terms of their cellular metabolic rate in A549 epithelial cells, the next step was to confirm their effectiveness at inhibiting the endocytosis pathways at the selected concentrations. Transferrin and cholera toxin β, have been reported to selectively enter cells

via the clathrin (Motley *et al.* 2003; Delos Santos *et al.* 2017; He *et al.* 2020) and caveolae (Schnitzer *et al.* 1994; Sandvig *et al.* 2018; Alshehri *et al.* 2018) pathways, respectively.

Transferrin (100 µg/mL) internalisation **(Figure 5.3)** was explored in the presence of chlorpromazine (5.0 – 20.0 µg/mL), concanavalin A (50.0 – 150.0 µg/mL), and dynasore (5.0 – 20.0 µg/mL); while cholera toxin β (5 µg/mL) uptake **(Figure 5.4)** was studied in the presence of dynasore (5.0 – 20.0 µg/mL), genistein (3.8 -15.0 µg/mL), filipin (1.0 - 4.0 µg/mL), nystatin (5.0 -20.0 µg/mL) and MßCD (75.0 – 300.0 µg/mL).

Figure 5.3 indicates the uptake of transferrin by A549 cells was significantly reduced by ≥ 5.0 µg/mL chlorpromazine, ≥ 150.0 µg/mL of concanavalin A and ≥ 5.0 µg/mL of dynasore. At the chosen concentrations in **Table 5.2**, the use of these inhibitors correspond to 40% (***P ≤ 0.001), 10% (*P ≤ 0.05) and 60% (****P ≤ 0.0001) reduction in uptake of transferrin by A549 cells respectively.

Cholera toxin β uptake by A549 cells in the presence of inhibitors are shown in **Figure 5.4**. At the previously determined inhibitor concentrations, the use of dynasore (20.0 µg/mL), genistein (15.0 µg/mL) and filipin (4.0 µg/mL) correspond to 16% (***P ≤ 0.001), 24% (**P ≤ 0.01) and 26% (****P ≤ 0.0001) reduction in uptake of cholera toxin β by A549 cells, respectively. The use of nystatin

appeared to increase cholera toxin β by 8% at 10.0 µg/mL. However significant decrease (***P ≤ 0.001) in cellular internalisation of cholera toxin β was observed at 20.0 µg/mL nystatin concentration. Filipin at 4 µg/mL had 26% reduction in cellular uptake of cholera toxin β.

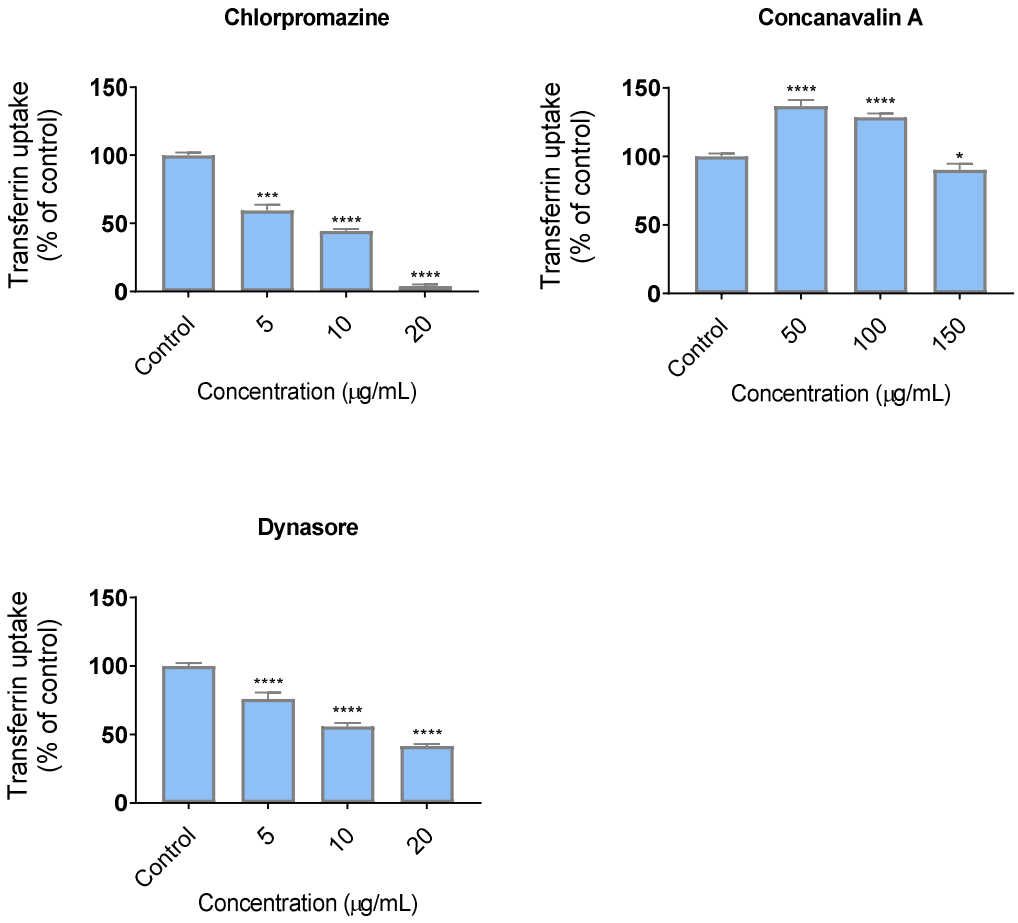


Figure 5.3. *The effect of inhibitors, at different concentrations, on internalisation of transferrin in A549 cells. Cells were pre-treated with various concentrations of chlorpromazine, concanavalin A, and dynasore solutions for 30 min, followed by 180 min of exposure to Transferrin, Alexa Fluor™ 488 Conjugate in the presence of the inhibitors. One-way ANOVA was used for statistical analysis. *P ≤ 0.05, **P ≤ 0.01, ***P ≤ 0.001, **** P ≤ 0.0001, NS not significant. The error bar represents their standard deviation of the mean. (N=3, n=3).*

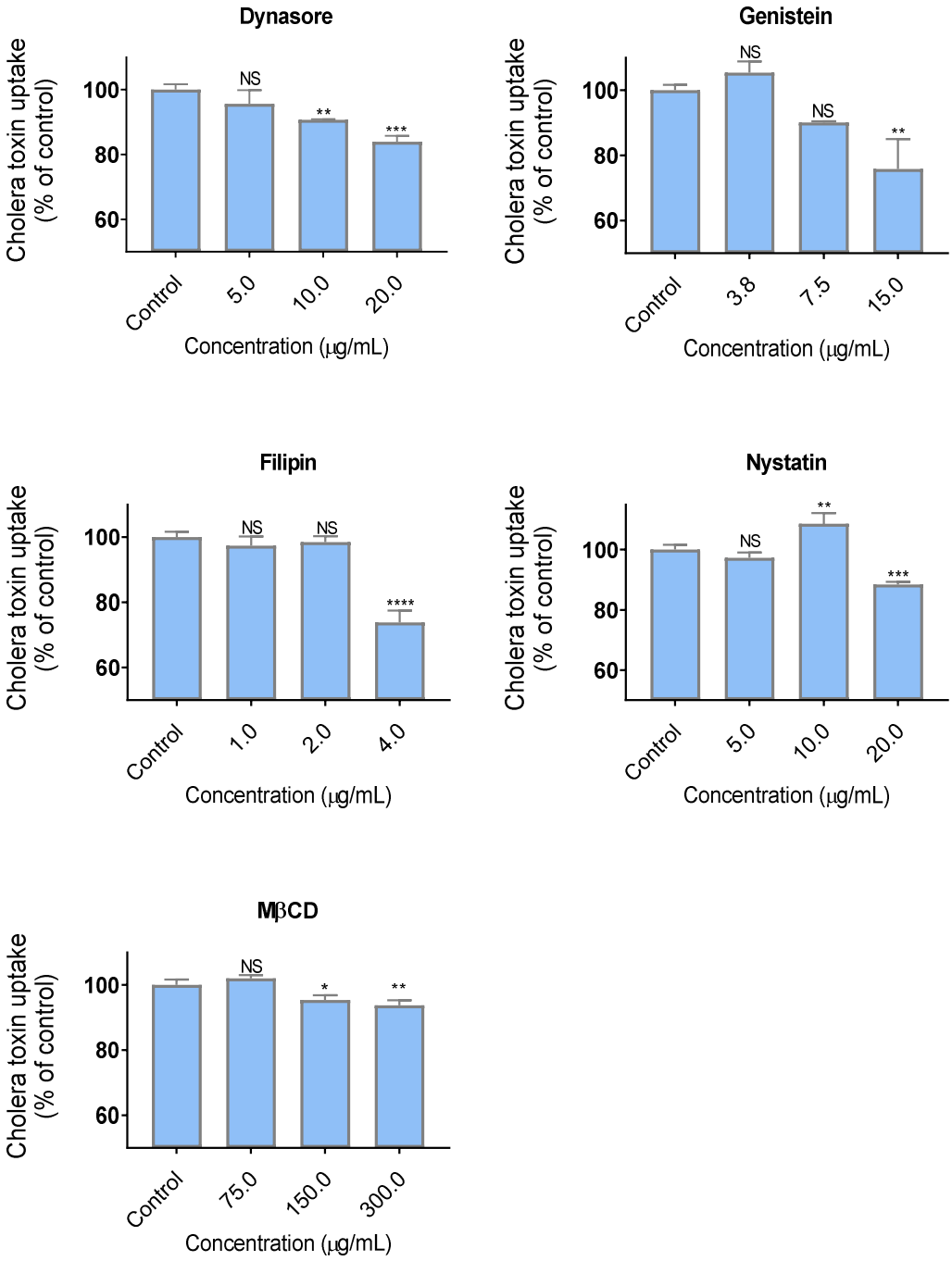


Figure 5.4. *The effect of inhibitors, at different concentrations, on internalisation of cholera toxin ϐ in A549 cells. The cells were pre-treated with various concentrations of dynasore, genistein, MβCD, nystatin and filipin solution for 30 min, followed by 180 min of exposure to Cholera Toxin Subunit B (Recombinant), Alexa Fluor™ 488 Conjugate in the presence of the inhibitors. One-way ANOVA was used for statistical analysis. *P ≤ 0.05, **P ≤ 0.01, ***P ≤ 0.001, **** P ≤ 0.0001, NS not significant. The error bar represents their standard deviation of the mean. (N=3, n=3).*

5.3.3 The effect of endocytosis inhibitors on the uptake of biotin-PEG$_{2k}$-*b*-GA$_{10/30}$:lysozyme nanocomplexes into A549 cells

5.3.3.1. Role of clathrin-mediated endocytosis (chlorpromazine and concanavalin A)

To determine the influence of clathrin-dependent endocytosis on lysozyme, mPEG$_{2k}$-*b*-GA$_{30}$:lysozyme, biotin-PEG$_{2k}$-*b*-GA$_{10/30}$:lysozyme nanocomplexes uptake, two inhibitors chlorpromazine and concanavalin A were applied to A549 epithelial cells. Chlorpromazine significantly reduced the uptake of lysozyme and mPEG$_{2k}$-*b*-GA$_{30}$:lysozyme by 50% and 23% respectively **(Figure 5.5)**. It had the most impact on uptake of 'free' lysozyme, which is just lysozyme labelled with cy5 dye for quantitative flow cytometry analysis of cellular uptake while not effecting the uptake of biotin-PEG$_{2k}$-*b*-GA$_{10/30}$:lysozyme nanocomplexes. The difference between uptake of free lysozyme and nanocomplexes were significant ($P \leq 0.001$).

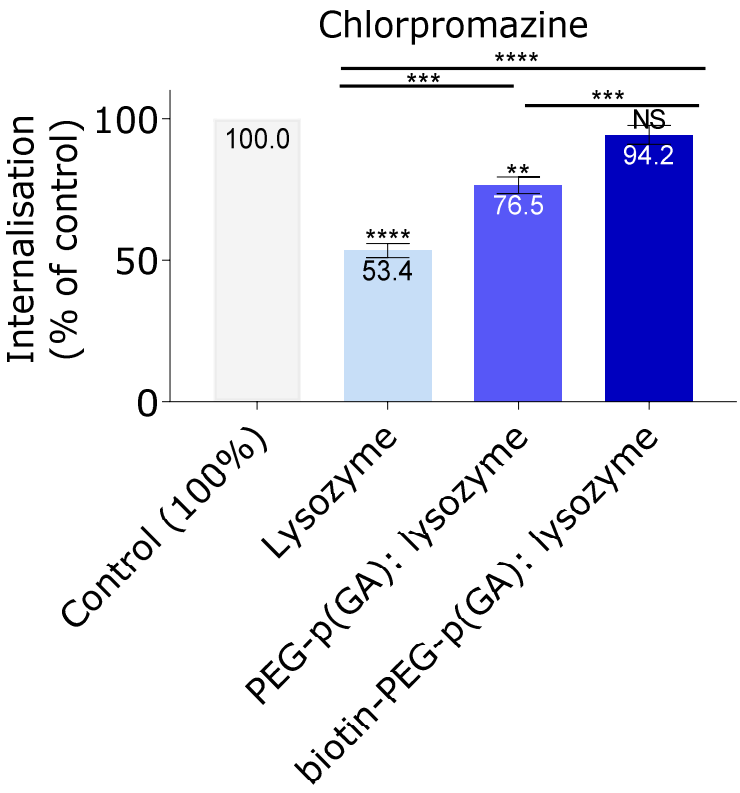


Figure 5.5. *Effect of chlorpromazine on the internalisation of lysozyme; mPEG$_{2k}$-b-GA$_{30}$:lysozyme; and biotin-PEG$_{2k}$-b-GA$_{10/30}$:lysozyme by A549. Cells were pre-incubated with chlorpromazine at 5 µg/mL for 30 minutes, followed by exposure to nanocomplexes (at protein concentration of 10 µg/mL) in the presence of chlorpromazine for 3 h prior to flow cytometry analysis. Results are reported as the amount of internalised of nanocomplexes relative to the control, expressed as a percentage of the quantity found in the uninhibited control cells. Data represent the mean ± SD (n=3, N=3). One-way ANOVA was used for statistical analysis. ***P ≤ 0.001.*

Concanavalin A is a clathrin-mediated endocytosis inhibitor which prevents the formation of clathrin coated pits (Guo *et al.* 2015). Although concanavalin A universally significantly reduced the uptake of all nanoparticles tested, but its order of effect is in contrast to the chlorpromazine data. Concanavalin A data in **Figure 5.6** show that concanavalin A had the most effect on the uptake of biotin-PEG$_{2k}$-b-GA$_{10/30}$:lysozyme nanocomplex (70%

reduction) while least impacted free lysozyme uptake (45% reduction); the difference in between the two was significant at P ≤ 0.0001.

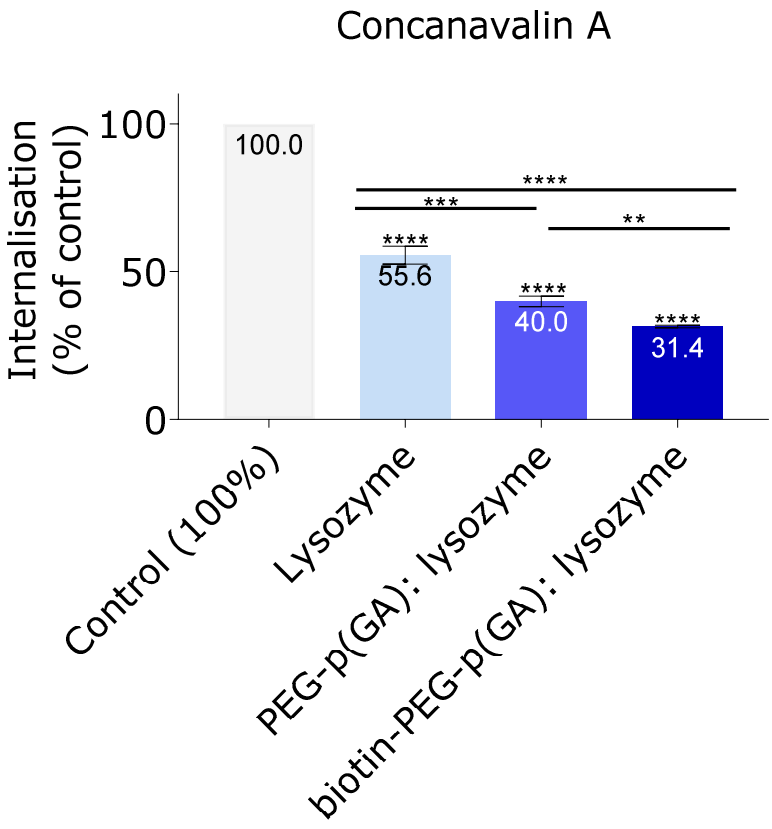


Figure 5.6. *Effect of concanavalin A on the internalisation of lysozyme; mPEG$_{2k}$-b-GA$_{30}$:lysozyme; and biotin-PEG$_{2k}$-b-GA$_{10/30}$:lysozyme by A549. The cells were pre-incubated with concanavalin A at 100 µg/mL for 30 minutes, followed by exposure to nanocomplexes (at protein concentration of 10 µg/mL) in the presence of concanavalin A for 3 h prior to flow cytometry analysis. Results are reported as the amount of internalised of nanocomplexes relative to the control, expressed as a percentage of the quantity found in the uninhibited control cells. Data represent the mean ± SD (n=3, N=3). One-way ANOVA was used for statistical analysis. **P ≤ 0.01, ***P ≤ 0.001.*

5.3.3.2. Role of endocytosis pathway involving dynamin (dynasore)

To investigate the pathway influenced by dynamin inhibition, dynasore, a dynamin inhibitor, was used. Dynasore is reported to block the GTPase activity of dynamin, it can effect both the clathrin and caveolae – dependent pathways (Doherty and Mcmahon 2009). **Figure 5.7** illustrates dynasore (20 µg/mL) inhibition effect on the cellular uptake of tested nanomaterial. Data showed that dynasore had significant effect ($P \leq 0.0001$) on the internalisation of lysozyme, mPEG$_{2k}$-*b*-GA$_{30}$:lysozyme nanocomplexes and biotin-PEG$_{2k}$-*b*-GA$_{10/30}$:lysozyme nanocomplexes. Dynasore had the biggest impact on the uptake of mPEG$_{2k}$-*b*-GA$_{30}$:lysozyme with reduction of 58%, followed by biotin-PEG$_{2k}$-b-GA$_{10/30}$:lysozyme (53%) and free lysozyme (45%) compared to control at 100%. The difference between the formulations were also significant $P \leq 0.0001$.

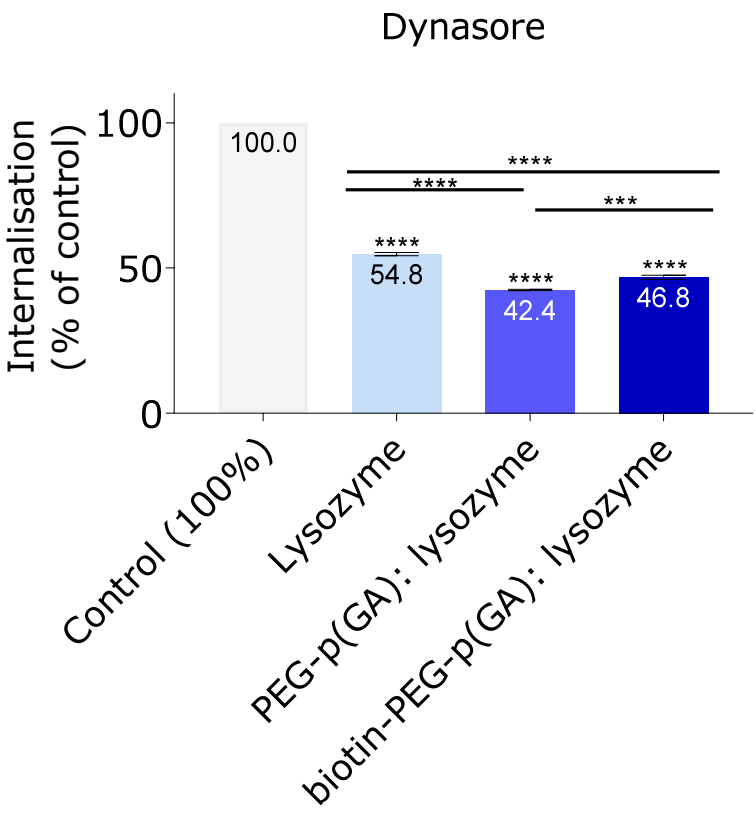


Figure 5.7. *Effect of dynasore on the internalisation of lysozyme; mPEG$_{2k}$-b-GA$_{30}$:lysozyme; and biotin-PEG$_{2k}$-b-GA$_{10/30}$:lysozyme by A549. The cells were pre-incubated with dynasore at 20 µg/mL for 30 minutes, followed by exposure to nanocomplexes (at protein concentration of 10 µg/mL) in the presence of dynasore for 3 h prior to flow cytometry analysis. Results are reported as the amount of internalised of nanocomplexes relative to the control, expressed as a percentage of the quantity found in the uninhibited control cells. Data represent the mean ± SD (n=3, N=3). One-way ANOVA was used for statistical analysis. ***P ≤ 0.001, **** P ≤ 0.0001.*

5.3.3.3. Tyrosine kinase and caveolae dependent pathway (genistein)

Figure 5.8 shows the effect of genistein on the caveolae pathway through inhibition of tyrosine kinase (Iversen *et al.* 2011) in A549. All materials showed reduced cell internalisation upon application of genistein (15 µg/mL) with the most pronounced effect shown for

biotin-PEG$_{2k}$-*b*-GA$_{10/30}$:lysozyme nanocomplex with 24% reduction compared to untreated cells. This reduction was significantly ($P \leq 0.01$) lower compared to the impact on uptake of free lysozyme (14% reduction).

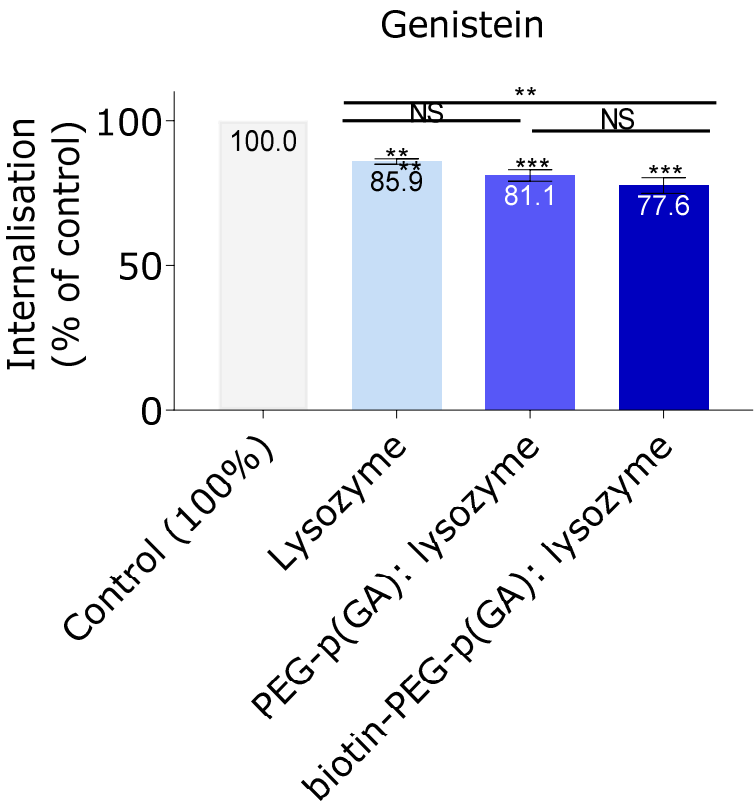


Figure 5.8. *Effect of genistein on the internalisation of lysozyme; mPEG$_{2k}$-b-GA$_{30}$:lysozyme; and biotin-PEG$_{2k}$-b-GA$_{10/30}$:lysozyme by A549. The cells were pre-incubated with genistein at 15 µg/mL for 30 minutes, followed by exposure to nanocomplexes (at protein concentration of 10 µg/mL) in the presence of genistein for 3 h prior to flow cytometry analysis. Results are reported as the amount of internalised of nanocomplexes relative to the control, expressed as a percentage of the quantity found in the uninhibited control cells. Data represent the mean ± SD (n=3, N=3). One-way ANOVA was used for statistical analysis. **P ≤ 0.01, NS not significant.*

5.3.3.4. Caveolae-mediated endocytosis (filipin)

Filipin, a cholesterol sequestering agent, was used to examine the involvement of caveolae-mediated endocytosis in the uptake of testing nanomaterials. Filipin significantly ($P \leq 0.0001$) reduced the uptake of 3 formulations compared to untreated control A549 cells **(Figure 5.9)**. The impact of filipin on the uptake in ascending order are lysozyme (40% reduction), $mPEG_{2k}$-b-GA_{30}:lysozyme (47%) and biotin-PEG_{2k}-b-$GA_{10/30}$:lysozyme (58%). The difference of uptake expressed as percentage of control between different formulations was also statistically significant.

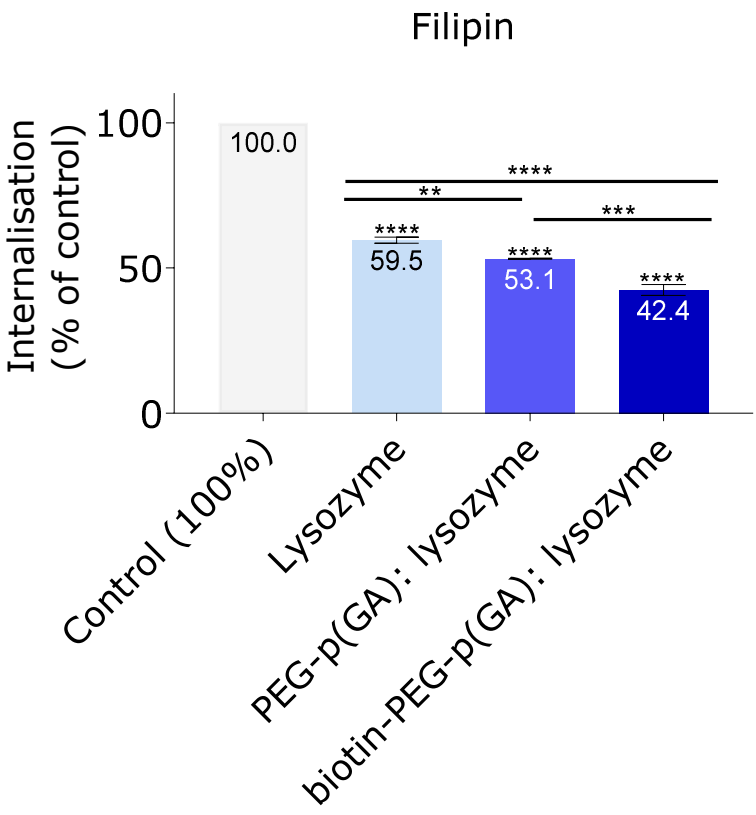


Figure 5.9. *Effect of filipin on the internalisation of lysozyme; mPEG$_{2k}$-b-GA$_{30}$:lysozyme; and biotin-PEG$_{2k}$-b-GA$_{10/30}$:lysozyme by A549. The cells were pre-incubated with filipin at 3 µg/mL for 30 minutes, followed by exposure to nanocomplexes (at protein concentration of 10 µg/mL) in the presence of filipin for 3 h prior to flow cytometry analysis. Results are reported as the amount of internalised of nanocomplexes relative to the control, expressed as a percentage of the quantity found in the uninhibited control cells. Data represent the mean ± SD (n=3, N=3). One-way ANOVA was used for statistical analysis. **P ≤ 0.01, ***P ≤ 0.001, **** P ≤ 0.0001.*

5.3.3.5. Role of cholesterol (nystatin and MβCD)

Figure 5.10 shows the effect of inhibition of caveolae by sequestration of cholesterol using nystatin inhibitor (20 µg/mL) in A549 cells. Nystatin significantly reduced the uptake of all three formulations and had the highest impact on the uptake of non-targeted mPEG$_{2k}$-*b*-GA$_{30}$:lysozyme nanocomplexes with up to 23%

reduction compared to cells not treated with nystatin inhibitor. The difference in respect of percentage of uptake compared to control cells between the non-targeted and biotin targeted nanocomplexes was also significant (P ≤ 0.001).

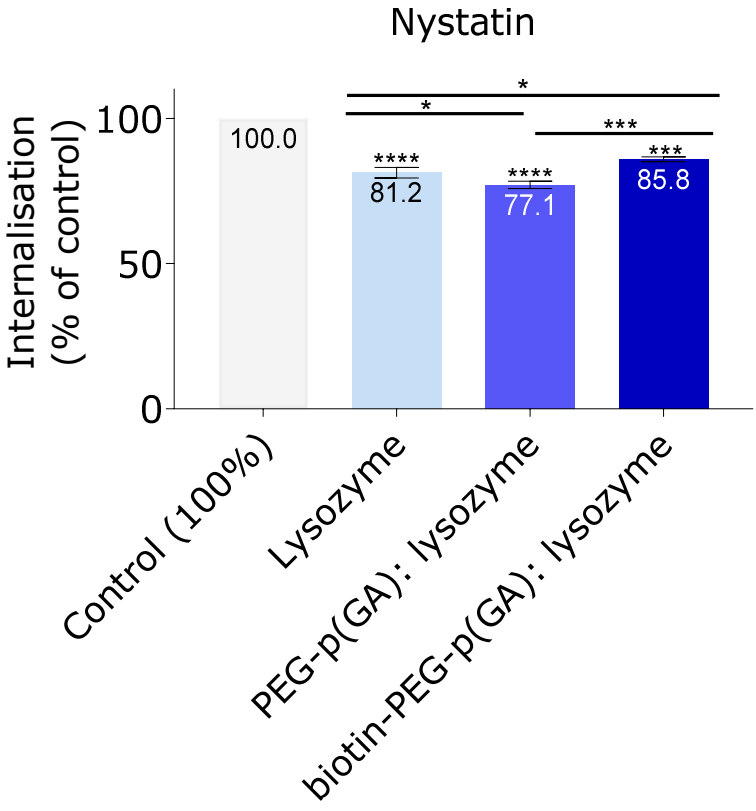


Figure 5.10. *Effect of nystatin on the internalisation of lysozyme; mPEG$_{2k}$-b-GA$_{30}$:lysozyme; and biotin-PEG$_{2k}$-b-GA$_{10/30}$:lysozyme by A549. The cells were pre-incubated with nystatin at 20 µg/mL for 30 minutes, followed by exposure to nanocomplexes (at protein concentration of 10 µg/mL) in the presence of nystatin for 3 h prior to flow cytometry analysis. Results are reported as the amount of internalised of nanocomplexes relative to the control, expressed as a percentage of the quantity found in the uninhibited control cells. Data represent the mean ± SD (n=3, N=3). One-way ANOVA was used for statistical analysis. *P ≤ 0.05, ***P ≤ 0.001.*

The effect of methyl-β-cyclodextrin (MβCD) (300 µg/mL) , which depletes cell membrane-associated cholesterol (Smart and Anderson 2002) were evident in the uptake of both the biotin-

PEG_{2k}-*b*-$GA_{10/30}$:lysozyme and $mPEG_{2k}$-*b*-GA_{30}:lysozyme nanocomplexes, but not significantly impacting the uptake of free lysozyme **(Figure 5.11)**. MβCD reduced the uptake of the polymer – protein nanocomplexes by about 10 % relative to control of untreated cells, no significant differences were observed for both biotin targeted and non-targeted polymer-protein nanocomplexes.

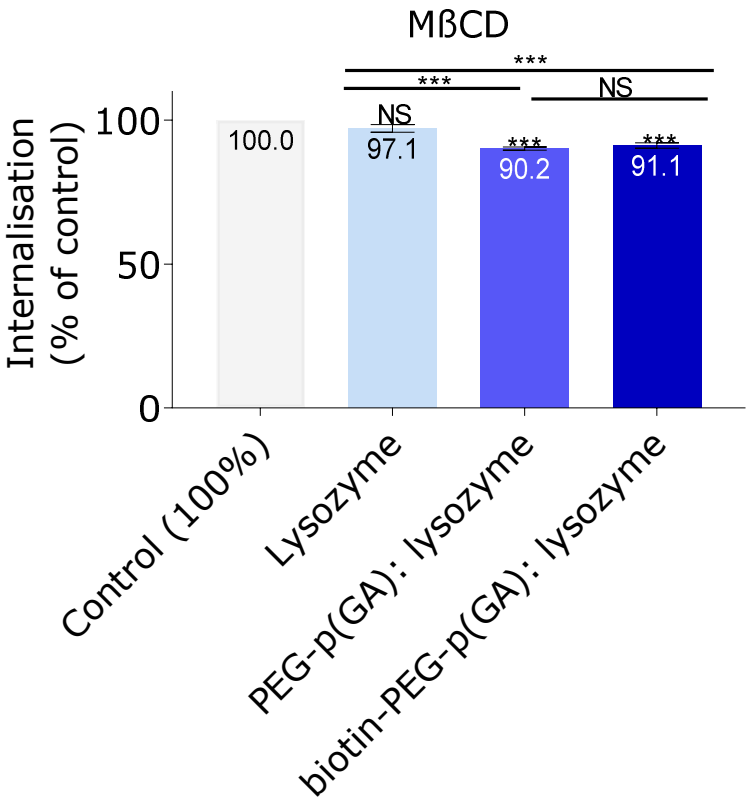


Figure 5.11. *Effect of MβCD, on the internalisation of lysozyme; $mPEG_{2k}$-b-GA_{30}:lysozyme; and biotin-PEG_{2k}-b-$GA_{10/30}$:lysozyme by A549. The cells were pre-incubated with MβCD at 300 µg/mL for 30 minutes, followed by exposure to nanocomplexes (at protein concentration of 10 µg/mL) in the presence of MβCD for 3 h prior to flow cytometry analysis. Results are reported as the amount of internalised of nanocomplexes relative to the control, expressed as a percentage of the quantity found in the uninhibited control cells. Data represent the mean ± SD (n=3, N=3). One-way ANOVA was used for statistical analysis. ***P ≤ 0.001, NS not significant.*

5.3.3.6. Macropinocytosis (EIPA and cytochalasin)

Ethyl-isopropyl amiloride (EIPA) have been reported to inhibit the macropinocytosis process by inhibition of Na^+/H^+ exchange, consequently, lowers the sub-membranous pH of the cells (Gekle *et al.* 1999). Together with cytochalasin D, which is an actin filament depolymerising agent (Lam *et al.* 2011; Huth *et al.* 2006) are used in the literature to investigate the role of micropinocytosis pathway in cells.

The effect of EIPA (15 µg/mL) on reducing cellular internalisation of tested nanomaterials: lysozyme, mPEG$_{2k}$-b-GA$_{30}$:lysozyme and biotin-PEG$_{2k}$-*b*-GA$_{10/30}$:lysozyme nanocomplexes were significant ($P \leq 0.0001$) relative to control cells without presence of inhibitor, reducing ~ 30% of control uptake. The difference between tested formulations were minimal, minor significant ($P \leq 0.05$) difference was only observed between the mPEG$_{2k}$-*b*-GA$_{30}$:lysozyme (27%) and biotin-PEG$_{2k}$-*b*-GA$_{10/30}$:lysozyme nanocomplexes (32%).

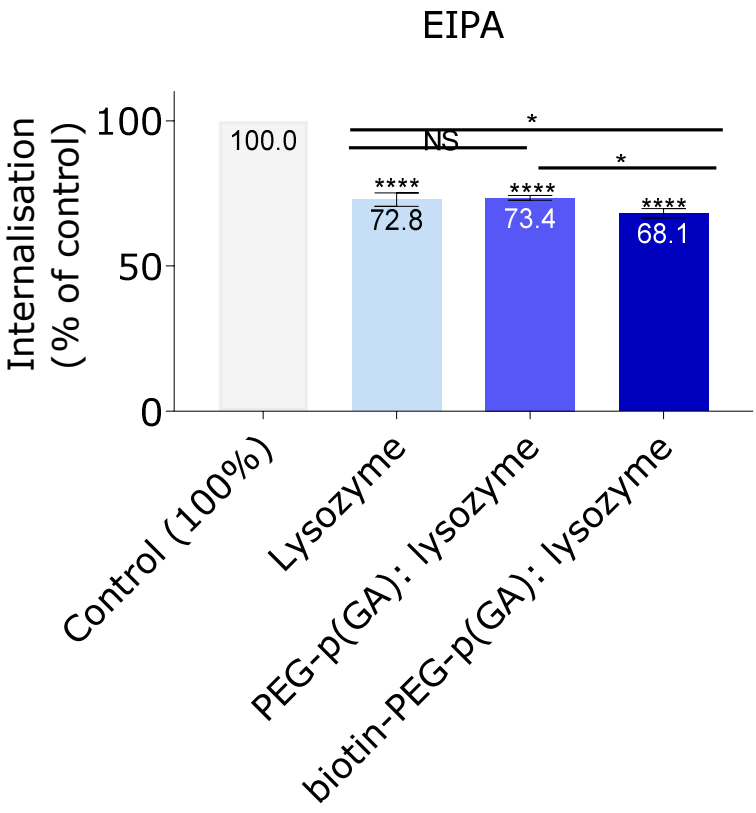


Figure 5.12. *Effect of EIPA on the internalisation of lysozyme; mPEG$_{2k}$-b-GA$_{30}$:lysozyme; and biotin-PEG$_{2k}$-b-GA$_{10/30}$:lysozyme by A549. The cells were pre-incubated with EIPA at 15 µg/mL for 30 minutes, followed by exposure to nanocomplexes (at protein concentration of 10 µg/mL) in the presence of EIPA for 3 h prior to flow cytometry analysis. Results are reported as the amount of internalised of nanocomplexes relative to the control, expressed as a percentage of the quantity found in the uninhibited control cells. Data represent the mean ± SD (n=3, N=3). One-way ANOVA was used for statistical analysis. *P ≤ 0.05, NS not significant.*

Figure 5.13 shows the effect of inhibition of macropinocytosis by cytochalasin D (1 μg/mL). The graph shows only the uptake of biotin-PEG$_{2k}$-*b*-GA$_{10/30}$:lysozyme nanocomplex by A549 cells was significantly reduced in the presence of cytochalasin D to about 64% compared to control cells without inhibitor treatments.

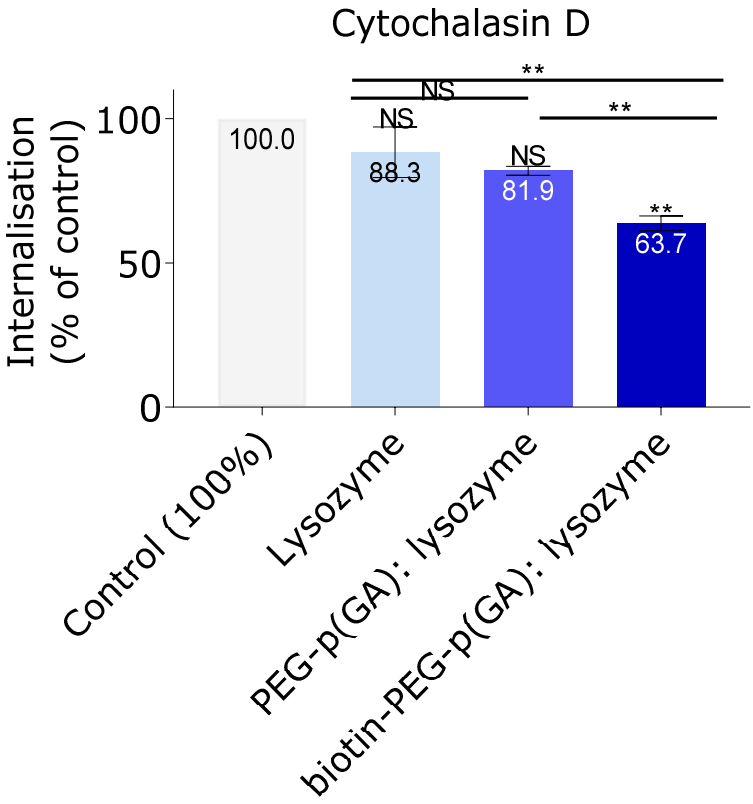


Figure 5.13. *Effect of cytochalasin D on the internalisation of lysozyme; mPEG$_{2k}$-b-GA$_{30}$:lysozyme; and biotin-PEG$_{2k}$-b-GA$_{10/30}$:lysozyme by A549. The cells were pre-incubated with cytochalasin D at 1 μg/mL for 30 minutes, followed by exposure to nanocomplexes (at protein concentration of 10 μg/mL) in the presence of cytochalasin D for 3 h prior to flow cytometry analysis. Results are reported as the amount of internalised of nanocomplexes relative to the control, expressed as a percentage of the quantity found in the uninhibited control cells. Data represent the mean ± SD (n=3, N=3). One-way ANOVA was used for statistical analysis. **P ≤ 0.01, NS not significant.*

5.4 Discussion

5.4.1 Mechanisms of Cellular Internalisation of lysozyme and polymer-lysozyme complexes

As briefly discussed in Chapter 4, there have not been extensive studies to provide a mechanistic insight on cellular processing of model proteins such as lysozyme nor polymer-protein complexes; hence, in this chapter experiments were carried out to investigate the potential endocytosis pathways of biotin-PEG_{2k}-*b*-$GA_{10/30}$:lysozyme complexes and whether it differs to the cellular internalisation of free lysozyme or non-targeted mPEG_{2k}-*b*-GA_{30}:lysozyme nanocomplexes.

Pharmacological inhibitors are commonly utilised for investigating mechanisms of endocytosis responsible for the internalisation and trafficking of nano sized particles (Iversen *et al.* 2011). A number of advantages are presented by this method; the inhibitors have shown activity towards multiple cell types and results are quantifiable (Ivanov 2008). However, the cytotoxic effect of inhibitors can be a drawback; this is mainly cell-type and concentration dependent, but it can be avoided by decreasing the incubation time with the tested cells (Vercauteren *et al.* 2010). One other point that is worth noting is that some pharmacological inhibitors of endocytosis could have poor specificity, by inhibiting one pathway whilst simultaneously affecting other mechanisms and

cell processes (Francia *et al.* 2019). Therefore, several inhibitors were used in this work to probe each pathway in order to be able to provide more comprehensive analysis and aiming to overcome problems potentially associated with some inhibitors on the endocytosis pathway.

As mentioned above, the cytotoxic effect of inhibitors is cell type and concentration dependent. MTS cell metabolic rate assays were therefore carried out by incubating A549 cells for 4 h with chlorpromazine, concanavalin A, dynasore, genistein, filipin, nystatin, MβCD, EIPA and cytochalasin D inhibitors, over a range of concentrations. It is noted that MST assay alone cannot confirm cell viability as cell metabolism rate might not always directly relate to cell viability. It could be highly dependent on cell type; the particular cell viability and proliferation assays utilised may also significantly influence quantitative results (Wang *et al.* 2010). This test does not allow evaluation of the possibility of certain inhibitors having direct impact on mitochondria activity. However the MTS assay is sufficient for this part of the investigation as an indicator of general cell health within the experiment period.

Inhibitor concentration ranges used in the study were analogous to those reported in other endocytosis studies (Dos Santos *et al.* 2011; Patlolla *et al.* 2004; Manzanares and Ceña 2020). From the MTS results shown in **section 5.3.1**, cellular metabolic rate upon 4

h inhibitor treatments showed concentration dependent pattern in all inhibitors other than concanavalin A and MβCD, non-toxic doses were determined in this study that preserved at least 75 % metabolic rate of the A549 lung epithelial cells, these are listed in **Table 5.2**.

While it is important to confirm cell metabolic rate at specific concentration of inhibitors used, the ability of the inhibitors to have an effect on the endocytosis pathway of a particular cell line is also important to establish before studying the uptake and trafficking pathways of nanoparticles.

A549 cells express both clathrin and caveolin-1 protein on the cell membrane, which implies clathrin and caveolae-mediated endocytosis capability of A549 cells (Kuhn *et al.* 2014). Hence, studies were performed using two classical ligands: transferrin and cholera-ß-toxin, which are known to be preferentially internalised by caveolae- and clathrin-mediated endocytosis, respectively (Yumoto *et al.* 2012). These 2 ligands were used to investigate the pathway specificity of the chosen inhibitors as well as the concentrations at which they affect the uptake of these ligands.

Results in **section 5.3.2** shows that chlorpromazine at 5 µg/mL and concanavalin A at 150 µg/mL were able to significantly reduce uptake of transferrin by A549 cells **(Figure 5.3)**. Similar results were observed in other studies showing inhibition of transferrin

uptake in the presence of chlorpromazine and concanavalin A (Lorén *et al.* 2015; Dos Santos *et al.* 2011; Fazlollahi *et al.* 2013; Rodal *et al.* 1999). However, concanavalin A at concentration 50 and 100 µg/mL significantly increased the uptake of transferrin, the cause of this observation is not clear at this stage and might need further investigation in the future.

Dynasore were used to inhibit both transferrin and cholera toxin β as it inhibits dynamin which is involved in the 'pinch off' process of clathrin and caveolin coated pits from cell membrane. 5 µg/mL was effective in producing significant inhibition of transferrin uptake, but 10 µg/mL was needed to significantly reduce cholera toxin β internalisation by A549. This effect was also observed in other epithelial cell lines namely human breast cancer cell line MDA-MB-231 and cervical HeLa cells (Mutch *et al.* 2014; Macia *et al.* 2006).

The lowest concentrations of the tested caveolae-mediated endocytosis inhibitors which significantly reduced internalisation of cholera toxin β in A549 cells are listed as the following: genistein (15 µg/mL), filipin (4.0 µg/mL), nystatin (20 µg/mL) and MßCD (150 µg/mL) **(Figure 5.4)**. Date obtained from this study predominantly proved that the inhibitory effect increases with a corresponding increase in inhibitor concentration, agreeing with published studies apart from nystatin (Orlandi and Fishman 1998; Walker *et al.* 2016). In the presence of nystatin at 10 µg/mL,

uptake of cholera toxin β was increased by 10% ($P \leq 0.01$). This is somewhat unexpected; but the literature suggests that the effect nystatin on ligand uptake is highly dependent on cell type. Chen Y. *et al* observed increased cellular of endostatin in the presence of nystatin. They proposed that this may be a consequence of nystatin 'switching' the endostatin internalisation predominantly to the clathrin-mediated pathway which enhances endostatin uptake and biodistribution in tumour blood vessels and tumour tissues (Chen *et al.* 2011). Another study reported nystatin at 25 μg/mL had no effect on the uptake of cholera toxin β in Caco-2 and HeLa cells (Torgersen *et al.* 2001). One interpretation of nystatin result shown in **Figure 5.4** could be that at low concentrations nystatin predominantly switch the uptake to clathrin pathway, whilst only at higher concentrations the effect of inhibiting caveolae pathway becomes apparent, reducing the overall cell uptake of cholera toxin β.

Concentration of inhibitors used to perform subsequent uptake studies were chosen based on the MTS results and inhibitor uptake experiments and are summarised in **Table 5.2**. Inhibitors at the selected concentration showed low cytotoxicity and had significant inhibition effect on ligand uptake.

Chlorpromazine and concanavalin A were used to explore the clathrin-mediated pathway, however these two inhibitors showed

contradictory results regarding their impacts on the uptake of lysozyme, mPEG$_{2k}$-*b*-GA$_{30}$:lysozyme and biotin-PEG$_{2k}$-*b*-GA$_{10/30}$:lysozyme. While chlorpromazine had greatest effect in free lysozyme internalisation followed by mPEG$_{2k}$-*b*-GA$_{30}$:lysozyme and biotin-PEG$_{2k}$-*b*-GA$_{10/30}$:lysozyme nanocomplexes, concanavalin A showed complete reverse order with the lowest impact being free lysozyme uptake. Reduction in uptake of lysozyme were consistently at 45% with both inhibitors. It is important to note, although the effect of clathrin-mediated inhibitors on the internalisation of nanoparticles has been reported widely (Ng *et al.* 2015; Mettlen *et al.* 2018; Kaksonen and Roux 2018), studies rarely use both inhibitors in conjunction. One study in our group observed similar phenomenon with the uptake of cy3-siRNA in A549 cells, where chlorpromazine showed significant inhibition when concanavalin A had no effect on cy3-siRNA uptake (Alshehri *et al.* 2018). It was proposed the difference in effect of the 2 inhibitors could be due to the various mechanisms they use to inhibit the clathrin-mediated pathway. Chlorpromazine is a cationic amphipathic drug that causes the assembly of adaptor proteins and clathrin on endosomal membranes thus depleting it from the plasma membrane, leading to a block in clathrin-mediated endocytosis; concanavalin A is a lectin that non-specifically interferes with the signalling of several G protein–coupled receptors, and also has an effect on the caveolar pathway (Guo *et*

al. 2015; Dutta and Donaldson 2012). Out of the 2 inhibitors, chlorpromazine is more specific towards the clathrin pathway, results at this stage indicate clathrin-mediated pathway plays a major role in the uptake of lysozyme into the A549 cells. The formation of lysozyme-polymer complexes shifts the endocytosis mechanism away from the clathrin dependent endocytosis pathway. The current hypothesis agrees with a previous study in the uptake of FITC-lysozyme in rat intestine, which proposed that lysozyme was absorbed by clathrin-mediated endocytosis and the cationic charge of lysozyme may be important for its absorption (Takano *et al.* 2004). This shielding of the charges on the lysozyme surface by the PEG-glutamic acid polymers could also explain the difference observed in the uptake studies.

The inhibition of dynamin by dynasore, an inhibitor which blocks the GTPase activity of dynamin and hence detachment of vesicle from the cell plasma membrane in dynamin-dependent endocytosis in cells (Macia *et al.* 2006), exhibited highly significant reduction ($p < 0.0001$) in the internalisation of all three lysozyme formulations tested by about 50%. Uptake of siRNA-polyplexes with an average diameter of ~150 nm in A549 cells was previously investigated in our group (Capel *et al.* 2016), and dynasore appeared to have the same effect as observed in the current study. Considering dynasore plays an essential role in both caveolin and clathrin-coated pathways and some lipid raft-mediated processes, this

reduction in the uptake of all three lysozyme formulations was to be expected.

Genistein was used to investigate the role of the caveolae pathway in cellular uptake of the nanomaterials. A tyrosine kinase inhibitor, genistein produced highest reduction in internalisation of biotin-PEG_{2k}-*b*-$GA_{10/30}$:lysozyme nanocomplex. Genistein causes local disruption of the actin network at the site of endocytosis and inhibits the recruitment of dynamin II (Parton *et al.* 1994), this can be linked to the action of dynasore in inhibiting cellular uptake of materials. Results shown in **Figure 5.7** for dynasore and **Figure 5.8** for genistein indicate a prominent effect of dynamin involvement in the uptake of all three tested substances in A549 cells.

The genistein effect of reduced cellular uptake of lysozyme formulations was also mirrored by the use of filipin, a macrolide pentene polyene antibiotic that binds sterols such as cholesterol (Schnitzer *et al.* 1994). However, another inhibitor used in the study which also interact with membrane cholesterol, nystatin did not elicit an the effect on ligand uptake seen with genistein and filipin. Nystatin produced the most reduction in the uptake of $mPEG_{2k}$-*b*-GA_{30}:lysozyme followed by free lysozyme and biotin-PEG_{2k}-*b*-$GA_{10/30}$:lysozyme uptake was least effected. It is important to emphasise that caveolae are cholesterol-rich and clathrin-free

invaginated microdomains at the cell surface (Fielding and Fielding 2000); although cholesterol depletion approach is often used to investigate the caveolae-mediated pathways, care and attention should also be directed to consider the other effects that may be elicited on the cells. Both filipin and nystatin are polyene macrolide antibiotics that exhibit potent antifungal effects. Study have shown that filipin shows higher toxicity to mammalian cells as it targets cholesterol more specifically compared to nystatin, which has relatively high affinity for ergosterol than for cholesterol, and enables the preferential interaction of nystatin with fungus (Behnke *et al.* 1984; Baek *et al.* 2013). This could explain the overall higher impact on the uptake pathway achieved using filipin than nystatin.

Data in **Figure 5.11** however show that, unlike other caveolae inhibitors effecting cell membrane cholesterol (filipin and nystatin), MßCD, an inhibitor that also affects cell membrane associated cholesterol, had no effect on lysozyme internalisation by the cells while equally reduced the uptake of both nanocomplex formulations. It should be however noticed that filipin and nystatin are cholesterol-binding compound which sequester cholesterol in the cell membrane (Baek *et al.* 2013), whilst MßCD depletes cholesterol from the cell membrane to form cholesterol–MBCD dimer complex (Mahammad and Parmryd 2015). This may be a possible reason for the observed difference.

Taken together, although all 3 nanomaterials rely on various dynamin dependent endocytosis pathways **(Figure 5.7)**, results indicate lysozyme in the complexed form with polymers tend to have higher utilisation of the caveolae pathway **(Figure 5.9**, **Figure 5.10** and **Figure 5.11)**, biotin-PEG_{2k}-*b*-$GA_{10/30}$:lysozymemore than $mPEG_{2k}$-b-GA_{30}:lysozyme, with membrane cholesterol playing a major role. The caveolar pathway has been proposed to be advantageous over the clathrin-mediated pathway due to the avoidance of the acidic environment of endosomal vesicles and lysosomes which drugs will encounter following clathrin uptake (Wong *et al.* 2007). A previous study has shown that the uptake of biotin in Caco-2 cells was under cellular regulation of protein kinase C (Said 1999). In **Figure 5.8** genistein, a tyrosine kinase inhibitor, had the highest effect on the uptake of biotin-PEG_{2k}-*b*-$GA_{10/30}$:lysozyme, suggesting the role of biotin receptor at play. Adding to the difficulties in determining the exact endocytosis pathway of biotin-PEG_{2k}-*b*-$GA_{10/30}$:lysozyme, Zempleni and Mock hypothesized that the density of biotin receptor on the cell surface is transiently reduced by endocytosis (Zempleni and Mock 1998), so the reduced cellular uptake of biotin-PEG_{2k}-*b*-$GA_{10/30}$:lysozyme *via* biotin receptor mediated endocytosis in the presence of inhibitors might not be solely attributed to the inhibition of the endocytosis pathway.

The macropinocytosis mechanism of endocytosis was investigated using EIPA and cytochalasin D in this work. EIPA significantly decreased the uptake of both lysozyme and mPEG$_{2k}$-*b*-GA$_{30}$:lysozyme equally but has slightly higher impact ($P \leq 0.05$) on the uptake of biotin-PEG$_{2k}$-*b*-GA$_{10/30}$:lysozyme. EIPA mechanism of macropinocytosis inhibition is based on Na^+/H^+ exchange, by inducing acidification of the cytosol and an alkalinisation of endosomes (Koivusalo *et al.* 2010; Gekle *et al.* 1999). EIPA was shown as a powerful inhibitor for the uptake positively charged nanoparticles in a previous study (Dausend *et al.* 2008). In our group the uptake of positively charged polystyrene nanoparticles in Caco-2 cells was also investigated in the presence of 10 µg/mL EIPA and were shown to significantly reduce internalisation of the nanoparticles (Bannunah *et al.* 2014). The finding in this study together with previous studies suggest that micropinocytosis could have a significant involvement in the endocytosis pathway of the nanocomplexes used in this work.

Lastly, cytochalasin D did not produce significant effect on the internalisation of lysozyme or mPEG$_{2k}$-*b*-GA$_{30}$:lysozyme; like EIPA, significant effect was seen with the uptake of biotin-PEG$_{2k}$-*b*-GA$_{10/30}$:lysozyme. Cytochalasin D is an actin filament depolymerising agent that inhibits macropinocytosis by binding to the positive termini of actin filaments and preventing the elongation of microfilament (Sampath and Pollard 1991). The exact

reason why cytochalasin D only had significant effect on the uptake of the targeted complex is unknown at this stage. Literature has reported contrasting results regarding the use of this inhibitor. Huth *et al.* reported that the internalisation of pH-sensitive liposomes was significantly inhibited by cytochalasin D in HUVEC cells (human endothelial cells from umbilical cords), whereas uptake in COS-7 cells (monkey kidney carcinoma cells, SV 40 transformed) were not affected by cytochalasin D (Huth *et al.* 2006). Indirectly, without the use of inhibitor, another study looked into the siRNA-loaded cationic lipid nanoparticles uptake in HeLa cells by down-regulating macropinocytosis components (Cdc42 and Rac1) and found ~ 80% lower uptake of the nanoparticles (Sahay *et al.* 2013). Studies carried out in our group have also observed different effects of cytochalasin D in A549 cell line. Result in one study showed small but significant internalisation reduction of siRNA-polyplexes uptake in A549 cells, while another study reported no significant effect on the cellular uptake of cy3-siRNA-liposomes in A549 cells (Capel *et al.* 2016; Alshehri *et al.* 2018). In addition, transfection efficiency of 2-(dimethylamino)ethyl methacrylate (DMAEMA)-DNA polyplexes was significantly reduced by cytochalasin D, which was considered to primarily affects invagination of vesicles at the early stage of endocytosis by inhibiting actin polymerisation (Lam *et al.* 2011). As mentioned above, biotin receptor on the cell surface is likely

involved in the uptake of biotin-PEG_{2k}-*b*-$GA_{10/30}$:lysozyme, the density of biotin receptor on the cell surface can be transiently reduced as endocytosis progresses (Zempleni and Mock 1998). The proportion of interiorised membrane can be large; for example, 50% of the cell surface area can be interiorised during each hour of endocytic activity in fibroblasts; under normal conditions, the endocytosed membrane receptors can be recycled to the cell membrane within minutes (Steinman *et al.* 1983; Grant and Donaldson 2009). Study have suggested rapid recycling of receptors is dependent on the actin cytoskeleton, the effect of cytochalasin D on the actin filament might explain the reduction in biotin-PEG_{2k}-*b*-$GA_{10/30}$:lysozyme uptake by A549 cells.

To the best of our knowledge, no known studies have investigated the endocytosis mechanisms of dynamic nanocomplex formed *via* self-assemble system or exploring the difference regarding cellular internalisation of ligand targeted nanocomplex to non-targeted nanocomplex. This emphasises the importance of the present study and the need for further examinations in the future.

5.5 Conclusions

In this study, pharmacological inhibitors were used to investigate the endocytosis mechanisms involved in the uptake of lysozyme, mPEG_{2k}-*b*-GA_{30}:lysozyme and biotin-PEG_{2k}-*b*-$GA_{10/30}$:lysozyme

nanocomplex in A549 cells. Dynamin was found to play a major role in the uptake of all 3 nanomaterials, with lysozyme predominantly taken up via the clathrin-mediated pathway while mPEG$_{2k}$-*b*-GA$_{30}$:lysozyme and biotin-PEG$_{2k}$-*b*-GA$_{10/30}$:lysozyme preferred the caveolae-mediated pathway; inhibiting the caveolae pathway had higher impact on the uptake of the latter out of the 2 polymer-protein complex formulations. Further work can be carried out in the future to consolidate current findings, such as the use of molecular biological approaches include the use of dominant-negative mutants and RNA interference technology to compete with and downregulate the expression of endogenous proteins involved in specific endocytosis pathways.

Overall, this work revealed a relatively unexplored route of polymer-protein complex cell internalisation and improved understanding of switching of cellular endocytosis mechanism due to cellular receptor involvement, with a potentially important impact in the area of mucosal delivery of nanocomplexes.

Chapter 6. Complexations and antibacterial effects of colistin:mPEG$_{2k}$-*b*-GA$_{30}$ polymer nanocomplex

6.1 Introduction

Polymyxins are a group of lipopeptide antibiotics discovered more than 50 years ago which are active against many Gram-negative bacteria (Li *et al.* 2006; Ainsworth *et al.* 1947). Owing to concerns over their potential to cause nephrotoxicity and neurotoxicity, the use of polymyxins fell out of favour in the mid-1970s (Koch-Weser *et al.* 1970). However, clinical interest in polymyxins has been growing over the last two decades due to the emergence of drug-resistant Gram-negative bacteria coupled with scarce new antibiotics development (Nation *et al.* 2015).

Currently, two closely related polymyxin antibiotics are used clinically: colistin (polymyxin E) and polymyxin B. These drugs possess very similar chemical structures, consisting of a hydrophobic acyl tail linked to a 7 amino acids-cationic cyclic peptide ring of through a linear chain of 3 amino acids. The only difference in chemical structure between colistin and polymyxin B is a d-leucine instead of d-phenylalanine at position 6 in the peptide ring **(Figure 6.1)** (Biswas *et al.* 2012; Velkov *et al.* 2010). Colistin is commonly administered in the form of an inactive prodrug as colistimethate

sodium (CMS) (a polyanion at physiological pH), while polymyxin B (a polycation at physiological pH) is administered in the active form (Nation *et al.* 2015).

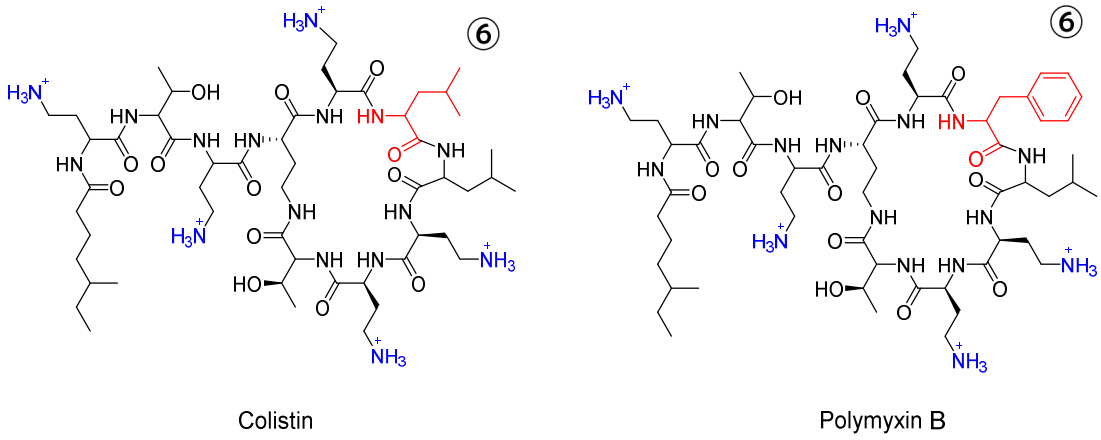


***Figure 6.1**. Chemical Structures of Colistin (Polymyxin E) and Polymyxin B. Red colour highlight the amino acid difference at position 6 in the peptide ring between the 2 polymyxins, D-Leucine at position 6 of colistin and D-Phenylalanine at position 6 of polymyxin B.*

Polymyxins are only active towards Gram-negative bacteria and are believed to interact with bacterial lipopolysaccharide (LPS) in their outer membrane. LPS consists of three distinctly structural domains: i) lipid A domain, the endotoxic portion of LPS acting as an anchor in the bacterial membrane containing anionic phosphate groups; ii) core domain, consisting of a branched saccharide chain of hexose and heptose sugars; and iii) the *O*-antigen side chain, a polysaccharide block that extends into the extracellular milieu. (Russo *et al.* 2003; Murray *et al.* 2003). LPS has been classified as rough or smooth depending on the nature of *O*-antigen side chains. The absence, or small size of *O*-antigen side chains render the LPS

rough, whereas fully expressed O-chains make the LPS smooth (Rittig *et al.* 2003). Since a rough LPS is more hydrophobic, bacteria with rough LPS are usually more susceptible to hydrophobic antibiotics compared to bacteria with smooth LPS (Tsujimoto *et al.* 1999; Delcour 2009).

A body of literature suggests that the mechanism of action of the polymyxins is the targeting of LPS in the outer membrane of Gram-negative bacteria *via* a two-step process. First, the positively charged peptide ring of polymyxin binds to the anionic phosphate groups on the lipid A moiety of LPS, causing the displacement of divalent cations such as magnesium and calcium ions that form bridges between LPS molecules, thus destabilising the outer leaflet of the outer membrane and leading to membrane disruption. Further outer membrane disruption occurs *via* the association of the acyl tail of polymyxin molecules with the fatty acid tails of lipid A (Velkov *et al.* 2010; Biswas *et al.* 2012; Nikaido 2003).

Although it is established that the binding of polymyxins to LPS on the surface of Gram-negative bacteria leads to disruption of the outer membrane, it is not clear how this results in cell lysis and bacterial death. Sabnis *et al*, recently proposed a mechanism of action for colistin (Sabnis *et al.* 2020) where the drug first binds to LPS, leading to destabilisation of the outer membrane, as described previously **(Figure 6.2)**. Consequently, the intermolecular bonds in

the outer membrane are weakened, resulting in the release of LPS from the outer membrane, allowing colistin to further damage the outer membrane *via* the action of the polymyxin lipid tail. Consequently, colistin molecules gain access to the periplasm space between the inner cytoplasmic membrane and the bacterial outer membrane, where colistin interacts with LPS on the cytoplasmic membrane (CM) resulting in disruption of the CM; ultimately resulting in permeabilization and culminating in the loss of cytoplasmic contents, cell lysis and eventually bacterial death.

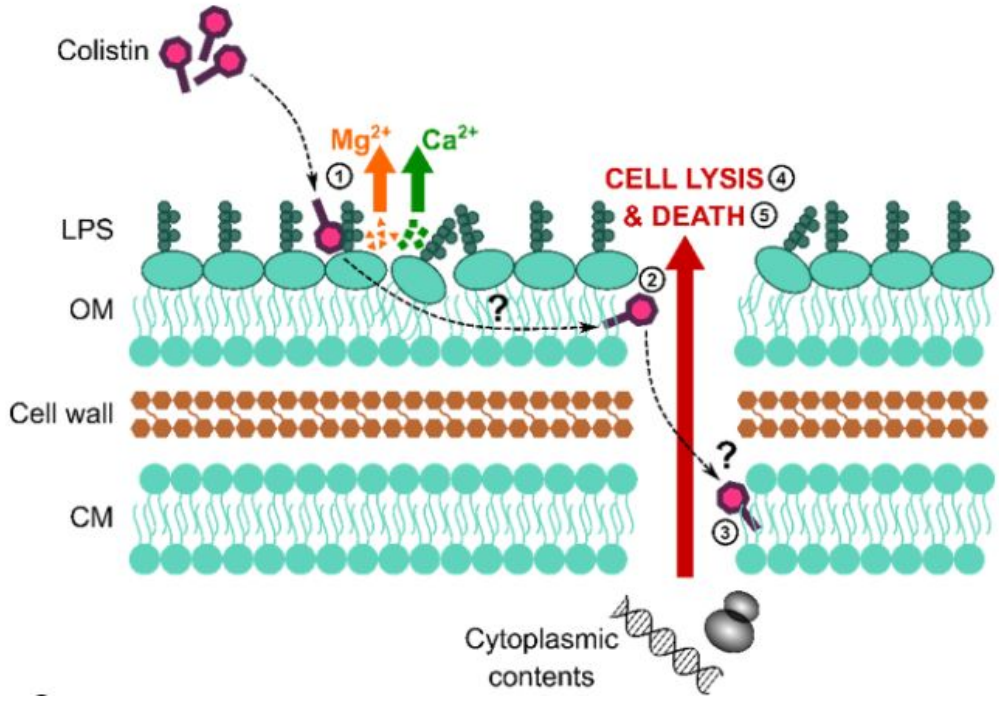


Figure 6.2. *Diagrammatic representation of a proposed mechanism of action of colistin: (1) Colistin binds to lipopolysaccharide (LPS) in the outer membrane (OM), causing displacement of cations that form bridges between LPS molecules and leading to membrane disruption. (2) The antibiotic then crosses the OM via a process termed 'self-directed uptake'. (3) Colistin subsequently disrupts the CM through a mechanism that remains unclear. (4, 5) Once the cell envelope is permeabilised, the bacteria lyse and are killed. Adapted from (Sabnis et al. 2020).*

In clinical setting, colistin is commonly administered as CMS prodrug due to its lower toxicity, however CMS has reduced antibacterial activity compared to native colistin at the same concentration (Li *et al.* 2001; Bergen *et al.* 2006). Whilst polymyxins have a clinical breakpoint of 2 μg/mL, the peak serum concentration of these drugs is typically only 1-4 μg/mL, which means that even small changes in a pathogen's susceptibility would render the drug ineffective and lead to antibiotic resistance (Tran *et al.* 2016).

The aim of the current work is to design a polymeric delivery system for colistin with similar, or ideally improved, antibacterial properties and better safety profile compared to current therapies. In this chapter, linear mPEG$_{2k}$-*b*-GA$_{30}$ copolymer was employed to form electrostatic complexes with positively charged colistin in sub-micron size range (nanocomplexes) **(Figure 6.3)**. The use of mPEG$_{2k}$-*b*-GA$_{30}$ based materials to complex positively charged proteins and formulate delivery systems for pulmonary application was previously demonstrated by our group (Nieto-Orellana *et al.* 2019).

mPEG$_{2k}$-*b*-GA$_{30}$ copolymer was employed in this study to test the ability of the mPEG$_{2k}$-*b*-GA$_{30}$ copolymers to form nanocomplexes with colistin. Formation of colistin:mPEG$_{2k}$-*b*-GA$_{30}$ nanocomplexes was investigated at different colistin to polymer charge ratios, in

different ionic strength buffers and formed complexes tested for their antibacterial effect on bacteria-infected cells *in vitro*.

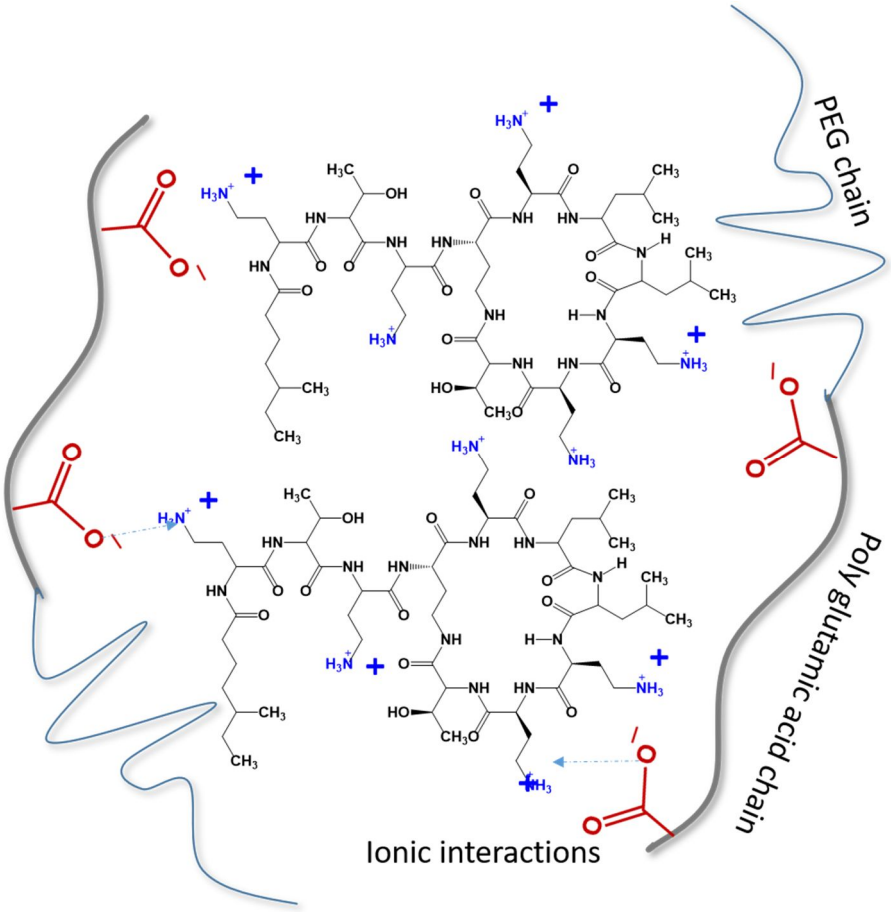


Figure 6.3. *Illustration (drawing not to scale) of nanocomplex formed between colistin and mPEG$_{2k}$-b-GA$_{30}$ copolymer via ionic interaction between the negatively charged carboxylic acid groups on the poly glutamic acid chain and the positively charged amine groups on colistin.*

6.2 Methods

6.2.1 Preparation of colistin-polymer nanocomplexes

Nanocomplexes were formulated at different colistin:mPEG$_{2k}$-*b*-GA$_{30}$ charge ratios (r = 1.0, 2.0, 3.0, 4.0, 5.0 and 6.0) where r is the ratio

between the number of amine groups present in colistin (pK_a 10.2), and the number of glutamic acid residues present in $mPEG_{2k}$-*b*-GA_{30} chain at pH 7.4. Colistin and polymer solutions were prepared by separately dissolving them in phosphate buffer (PB, 10 mM, pH 7.4; Na_2HPO_4 8.1 mM, $NaH_2PO_4 \cdot 2H_2O$ 1.47 mM) at various concentrations to achieve final colistin concentrations between 15 – 1000 µg/mL. For example, 3 mg and 7 mg of colistin and $mPEG_{2k}$-*b*-GA_{30}, respectively, were dissolved in 10 mM PB and used as stock solution. 384.6 µL of colistin stock solution was mixed with 416.7 µL of polymer solution and up to 1mL of 10 mM PB to achieve 1.0 mL of 1.0 mg/mL colistin–polymer nanocomplex suspension.

6.2.2 Agarose gel electrophoresis

Colistin:$mPEG_{2k}$-*b*-GA_{30} nanocomplexes at different *r* ratios were prepared as described above. Colistin concentration was kept constant at 230 µg/mL and the required amount of $mPEG_{2k}$-*b*-GA_{30} in solution was added to achieve desired charge ratio *r.* 25 µL of nanocomplex suspensions was loaded onto 1.5% (*w/v*) agarose gel and the electrophoresis was performed with 1x TRIS-acetate-EDTA (TAE, pH 7.4) buffer at 100 mA for 1 h using PowerPac™ Basic Power Supply (BioRad). The resulting gel was stained with Coomassie blue. 230 µg/mL free colistin and free $mPEG_{2k}$-*b*-GA_{30} copolymer was used as controls.

6.2.3 Assessing complex dissociation

Sample preparations. Colistin and mPEG$_{2k}$-*b*-GA$_{30}$ stock solutions were prepared by dissolving them separately in 10 mM pH7.4 phosphate buffer (PB) or phosphate buffer saline (1x PBS pH 7.4) before mixing to achieve 1 mL of final colistin concentration of 1 mg/mL suspensions in the respective buffers. For example, 3 mg and 7 mg of colistin and mPEG$_{2k}$-*b*-GA$_{30}$, respectively, were dissolved in 1 mL of 10 mM PB and used as stock solution. 384.6 µL of colistin stock solution was mixed with 416.7 µL of mPEG$_{2k}$-*b*-GA$_{30}$ solution and topped up with 10 mM PB to achieve 1 mL of 1 mg/mL colistin:mPEG$_{2k}$-*b*-GA$_{30}$ nanocomplex suspension.

Size exclusion (SEC) column separation of colistin:mPEG$_{2k}$-b-GA$_{30}$ nanocomplexes. PD 10 columns (Cytiva) were first equilibrated with elution buffer (10-20 mL of either 10 mM PB or PBS, pH 7.4) to remove the storage solution, before 1.0 mL of the 1 mg/mL colistin:mPEG$_{2k}$-*b*-GA$_{30}$ complex suspension was loaded to the column.

As SEC separation of the nanocomplexes using PD 10 column was expected to dilute the suspension according to manufacture protocol (1.4 times dilution if 2.5 mL sample volume is used). Therefore, a high colistin concentration of 1.0 mg/mL in the initial nanocomplex suspension was chosen as only 1 mL of the sample was used. 5 mL of the corresponding buffers were used to elute the suspension

according to the manufacturer's 'gravity' protocol with 5 mL of the relevant buffer and 300 µL fractions were collected (Healthcare 2007). Molecules were separated based on differences in size (Stellwagen 2009). The exclusion limit of the PD 10 SEC column is 5 kDa, thus free colistin (1155 Da) would travel through the pores within the beads and be retained for longer during elution, whilst colistin:mPEG$_{2k}$-*b*-GA$_{30}$ nanocomplexes would be too large to enter the pores and therefore travel in between the beads and be eluted out faster.

25 µL of each collected fraction was loaded on the agarose gel and ran as described above. Unused samples from each fraction were stored at 4 °C for 1 week and run on agarose gel electrophoresis.

6.2.4 Cell culture conditions and sample preparations

Human epithelial lung carcinoma cells A549 (ATCC® CCL185™) were routinely cultured in Dulbecco's Modified Eagle's Medium (DMEM) with addition of Foetal Bovine Serum (FBS, 10% *v/v*), non-essential amino acids (1% *v/v*), L-glutamine (1% *v/v*), penicillin (100 units/mL) and streptomycin (100 µg/mL). Dulbecco's Phosphate-Buffered Saline (DPBS) and trypsin/EDTA were used to wash and detach adherent cells in the process of cell splitting. Cells were always incubated in T75 flasks at 37°C and 5% CO_2.

HeLa-Mitotrap (Sigma) cells were routinely cultured in tissue culture flasks at 37°C and 5% CO_2. Cells were grown in Dulbecco's minimal

Eagles Medium (DMEM) GlutaMAX supplemented with FBS (10% *v/v*) and 100 µg/mL of Hygromycin B (Sigma-Aldrich). Every two days, the culture medium was replaced with 15 mL of fresh medium, pre-warmed to 37°C. Before 100% confluence, cells were trypsinised for 5 min at 37°C and the resulting cell suspension centrifuged (250 x *g*, 5 min, Thermo Scientific Megafuge), resuspended and diluted in fresh culture medium. For seeding density, cells were counted using a haemocytometer (Laboratory Supplies).

6.2.5 Determination of the metabolic activity by MTS assay

Samples preparation. Colistin and colistin:mPEG$_{2k}$-*b*-GA$_{30}$ nanocomplex suspensions were prepared in 10 mM PB at molar charge ratio of 2.5, and diluted in DMEM (dilution factor 10x) to reach final colistin concentrations of 0.25, 0.50, 1.0, 2.0 and 4.0 µg/mL in culture wells.

Once A549 cells reached approximately 90% confluency in the culture flask they were detached, as described above, and seeded on to 96-well plates at 8×10^3 cells *per* well and grown for 24 h. Medium was then removed, cells washed with DPBS and tested samples added to the cells (200 µl per well) for 4 hours. Subsequently medium was removed, cells washed with DPBS and 120 µL of MTS solution (20 µL MTS + 100 µL medium) were added. After 3 h incubation, the absorbance of the solution was read at λ =

490 nm (Beckman Coulter platereader). Experiments were carried out in triplicates. 4% (*v/v*) Triton X-100 solution and untreated cells were employed as controls indicating 0% metabolic activity (positive control) and 100% metabolic activity (negative control), respectively. The metabolic activity was calculated using the following formula:

$$\%\ Metabolic\ activity = \frac{S - P}{N - P} \times 100$$

where S, N and P are the absorbance of cells treated with samples (cells treated with colistin:mPEG$_{2k}$-*b*-GA$_{30}$ nanocomplexes), negative control and positive control, respectively.

6.2.6 Antibacterial activity of colistin:mPEG$_{2k}$-*b*-GA$_{30}$ nanocomplexes

Samples preparation. Colistin and colistin:mPEG$_{2k}$-*b*-GA$_{30}$ nanocomplex suspensions were prepared in 10 mM PB pH 7.4 at molar charge ratio 2.0, 2.5 and 3.0 with final colistin concentration of 1 μg/mL. A free mPEG$_{2k}$-*b*-GA$_{30}$ copolymer solution was also tested at a concentration corresponding to the polymer concentration in the nanocomplexes suspension with charge ratio of 3.0 (containing the highest polymer concentration).

Bacteria work in this chapter were assisted by Dr Rosa Catania. Broth microdilution assays were performed according to the guidelines of the National Committee for Clinical Laboratory

Standards (NCCLS), except that the nanocomplexes stock solutions (20 µg/mL) were prepared in 10 mM phosphate buffer (pH 7.4) instead of in Mueller-Hinton (MH) broth.

Initially, the preinoculum of *E. coli* XL-1 blue bacteria in MH broth (containing 12.5 µg/mL of tetracycline for *E. coli* XL-1) was grown at 37°C, shaken at 245 rpm for 16 h. Then the culture was adjusted using spectrophotometry measurements (OD_{600nm} = 0.025) to provide appropriately 10^5 CFU/mL in fresh double concentrated MH broth. 100 µL aliquots of these bacterial cell suspension were mixed with 100 µL of free colistin or equivalent amount of colistin in nanocomplexes solution in 10 mM phosphate buffer at different concentrations (to achieve final concentrations of 1.0 µg/mL, 0.75 µg/mL, 0.50 µg/mL, 0.25 µg/mL of colistin in 200 µL) in a 96 well plate covered with Breathe-Easy® sealing membrane and incubated at 37°C and 245 rpm in an Epoch 2 microplate reader (BioTek). The growth kinetic curves were determined by measuring OD at λ = 600 nm at 15 min intervals over 20 hours. Data are reported as the mean ± standard deviation of measurements.

For ease of direct comparison, Widdel have proposed an equation for the calculation of bacteria growth rate (Widdel 2007) shown below:

$$\mu = \frac{2.303(\log OD_2 - \log OD_1)}{(t_2 - t_1)}$$

Where μ, is the growth rate, OD 2 and 1 are OD readings at time point 2 and 1, t 2 and 1 are time (h) at point 2 and 1. Growth rate μ are calculated and incorporated in the analysis sections.

6.2.7 Time-kill bactericidal activity assay

An overnight broth culture of Enteropathogenic *Escherichia coli* (EPEC) E2348/69 in MH broth was diluted in fresh 2x MH broth to achieve approximately $1x10^9$ CFU/mL of bacteria. 100 µL of this EPEC suspension was incubated with 100 µL of i) 10 mM phosphate buffer, ii) colistin or equivalent amount of colistin in nanocomplex (to achieve final concentration of 1 µg/mL), and iii) $mPEG_{2k}$-*b*-GA_{30}, in a 96-well plate at 37°C using an orbital shaker for 2 h. Every 20 min during this incubation period, ten-fold serial dilutions were prepared with PBS and 10 µL samples were plated onto Mueller–Hinton agar plates. Possible effect of antibiotic carryover of either free or nanocomplex colistin was minimised by the PBS dilution of the samples. The CFU for each sample at different time points were counted after 16 h.

Equation $N = N_0\ e^{\mu\ t}$ was employed (Widdel 2007) to calculate bacteria growth rate, where N = number of cells at current time, N_0 = number of cells at the beginning, µ is the growth rate and t is the difference in time between N and N_0. µ are calculated to assess bacteria growth rate, a negative number indicate bacteria dying rate.

6.2.8 Enteropathogenic Escherichia coli infection treatment

HeLa-Mitotrap cells were seeded at $1x10^5$ *per* mL into a 12 well plate (1.0 mL *per* well) and cultured in growth medium (DMEM, 10% FBS, 100 µg/mL of Hygromycin B) for 48 hours at 37°C. (Hela-Mitotrap cells were readily available in our lab, which are cervical epithelial HeLa cells transfected and expressing a mitochondrial trapping protein containing FKBP12 and Rapamycin Binding (FRB) domains.)

The day before the infection assay, a colony of EPEC from a fresh cultured Luria-Bertani (LB) agar plate was inoculated in 1.5 mL of LB medium and incubated at 37°C and 245 rpm for 8 hours in an orbital shaker. this was diluted 1:500 in 5 mL LB medium and incubated at 37°C and 245 rpm for 16 hours in an orbital shaker. After 16 h, the bacterial suspension was diluted (1:1000) in FAS medium (DMEM supplemented with FBS 3% *v/v* and 1M HEPES 2.5 *v/v*). For the infection of HeLa-Mitotrap cells, the growth medium was removed, cells were washed twice with PBS (1 mL per well) and 0.5 mL of FAS medium containing bacteria were added to wells. The plate was centrifuged (700 x *g* for 10 min, Thermo Scientific Megafuge) and incubated for 3.5 h at 37°C. Then medium was aspirated, each well was rinsed twice with PBS (0.5 mL) and incubated with 0.5 mL of i) FAS medium (without bacteria) ii) 1 µg/mL free colistin in FAS medium, iii) 1 µg/mL of colistin in nanocomplex 1:2 in FAS medium, and iv) equivalent of $mPEG_{2k}$-*b*-GA_{30} in FAS medium, and incubated for 2 hours. After this time, the

cells were washed three times with PBS, and the surviving bacteria were harvested by lysing the cells with 0.2% Triton X-100 in PBS for 10 min at 37°C. The supernatants were immediately serially diluted with PBS and spotted onto LB agar plates. After incubation for 16 h at 37°C, the numbers of bacterial colonies for each sample were counted and expressed as colony-forming units (CFU) *per* mL.

6.3 Results and discussion

6.3.1 Colistin:mPEG$_{2k}$-*b*-GA$_{30}$ polymer complexation

In this study colistin:mPEG$_{2k}$-*b*-GA$_{30}$ complexes were prepared by mixing colistin and mPEG$_{2k}$-*b*-GA$_{30}$ in 10 mM phosphate buffer pH 7.4 at mixing ratios *r* in the 1-6 range.

Native agarose gel electrophoresis, applied to characterise protein - polymer nanocomplexes in previous chapters 3 & 4, was also utilised in this part of the study. To visualize colistin within the gel, Coomassie blue, dye routinely used to visualise proteins by interacting with basic amino acids (Simpson 2010), was initially tested with the view that it would interact with the amine groups on colistin. Gel analysis was first conducted applying colistin solutions of various concentrations to determine the sensitivity of the analysis.

Image in **Figure 6.4a** illustrates that bands of colistin staining were visible from colistin concentration of 62.5 μg/mL. Colistin concentration of 230 μg/mL (0.4 mM) was selected for all further

agarose gel analyses of colistin; with the presence of mPEG$_{2k}$-*b*-GA$_{30}$ required to achieve specified *r* value.

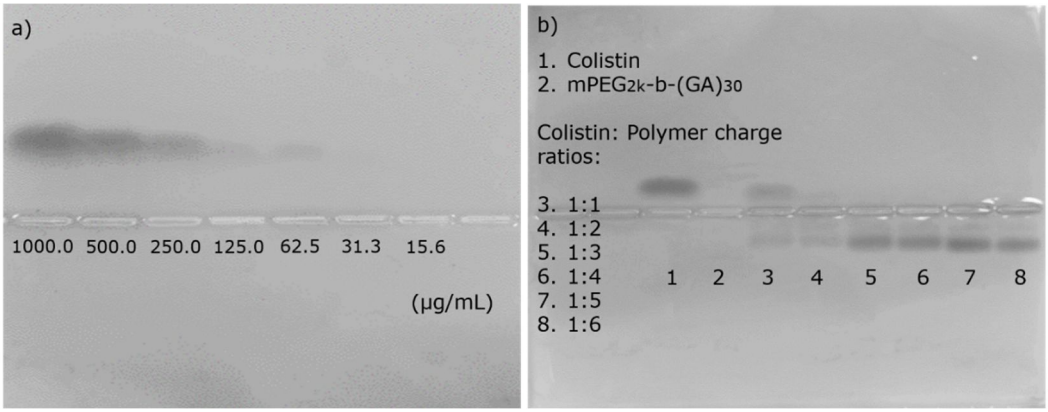


***Figure 6.4**. Electrophoretic gel analysis at pH 7.4 of colistin and colistin:mPEG$_{2k}$-b-GA$_{30}$ complexes. a) free colistin solution in what at pH 7.4 in the 15.6 - 1000 µg/mL concentration range; 1 % agarose gel, ran 1 h at 50 mA in Tris-Acetate-EDTA (TAE) buffer pH 7.4. Agarose concentration was subsequently increased to 1.5 % and electrophoretic separation performed for longer mPEG$_{2k}$-b-GA$_{30}$ to improve band definition. b) colistin:mPEG$_{2k}$-b-GA$_{30}$ complexes at varying molar charge ratios r of 1:1 to 1:6; 1.5% agarose gel, ran 1 h at 100 mA in Tris-Acetate-EDTA (TAE) buffer.*

Gel electrophoresis image in **Figure 6.4b** illustrates colistin complexation with mPEG$_{2k}$-*b*-GA$_{30}$ copolymer at different mPEG$_{2k}$-*b*-GA$_{30}$ molar charge ratio *r.* The gel depicts that, as *r* decreases from 1:1 to 1:8, few features can be observed. At ratios 1:1 and 1:2 there is a clear presence of free colistin, although the fainter band would indicate a reduction in the colistin centration relative to 'free' colistin (230 µg/mL). In the same time there is a presence of species with negative charges, attributable to overall negatively charged colistin:mPEG$_{2k}$-*b*-GA$_{30}$ complexes. At lower ratios, *r* above 1:5, a free colistin band cannot be observed, indicating concertation of free

colistin is lower than 62.5 μg/mL – the determined minimum detectable colistin concentration in the gel **(Figure 6.4a)**.

Interestingly with an increase in mPEG$_{2k}$-*b*-GA$_{30}$ content, i.e *r* ratio, the presence of negatively charged species in the gel containing colistin indicates formation of overall negatively charged complexes containing colistin, but sufficiently small in size to move within the gel. The visualisation of free mPEG$_{2k}$-*b*-GA$_{30}$ in the gel analysis was not practically feasible, as appropriate staining could not be identified, so it is not possible to ascertain if, and at which ratio, free copolymer may be present.

It has been estimated that the pore size of a 2% agarose gel casted in a 0.1 M PBS solution is around 470 ± 18 nm, while for the same concentration of agarose gel but casted in water the pore size was estimated to around 364 ± 8 nm (Pluen *et al.* 1999; Pernodet *et al.* 1997). The pore size was determined to be agarose concentration dependant; generally, the higher the concentration the smaller the pore size. The positive colistin in complexes that are overall negative showed migration toward the positive electrode on the gel, which implies the complexes were of sufficient small size to travel through the pores in the gel.

From the gel electrophoresis data, colistin:mPEG$_{2k}$-*b*-GA$_{30}$ *r* ratio of 1:2.5 was selected for further studies. This selection was made with the view to prepare complexes close to stoichiometric ratio, i.e.

minimum presence of free interacting species, colistin and mPEG$_{2k}$-*b*-GA$_{30}$ copolymer. At *r* ratio of 1:2 (for nanocomplexes prepared using 230 μg/mL of colistin) free colistin band is visible, indicating concentration above the detection limit (62.5 μg/mL); this is absent at ratio 1:3, indicting presence of a low concertation of free colistin, in the presence of nanocomplexes with negative overall charge. This does not appreciably change at lower ratios, i.e. increased concentrations of the copolymer.

Colistin:mPEG$_{2k}$-*b*-GA$_{30}$ nanocomplexes with *r* ratio of 1:2.5 were visualised by transmission electron microscopy (TEM) **(Figure 6.5)**. Images indicate the presence of species with diameter in approximately the 90 – 100 nm range.

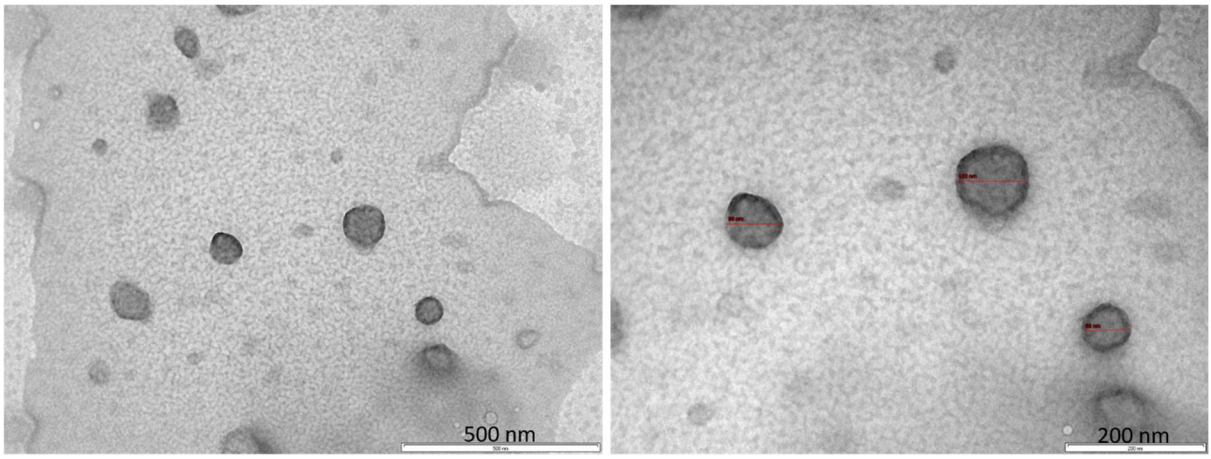


Figure 6.5. *Transmission electron microscopy images of colistin:mPEG$_{2k}$-b-GA$_{30}$ complexes prepared at ratio 1:2.5. Scale bar 500 nm (left) and 200 nm (right).*

The TEM measurements, taken together with the electrophoresis gels, suggest that binding of the mPEG$_{2k}$-*b*-GA$_{30}$ to colistin give arise

to complexes, in which the mPEG$_{2k}$-*b*-GA$_{30}$ chains and colistin molecules interact *via* ionic interaction.

6.3.2 Assessing complex dissociation

Polyelectrolyte complexes are held together by ionic interaction of the complexing species and are hence potentially reversible; this part of the study hence assessed potential dissociation of colistin:mPEG$_{2k}$-*b*-GA$_{30}$ nanocomplexes in buffers with different ionic strengths.

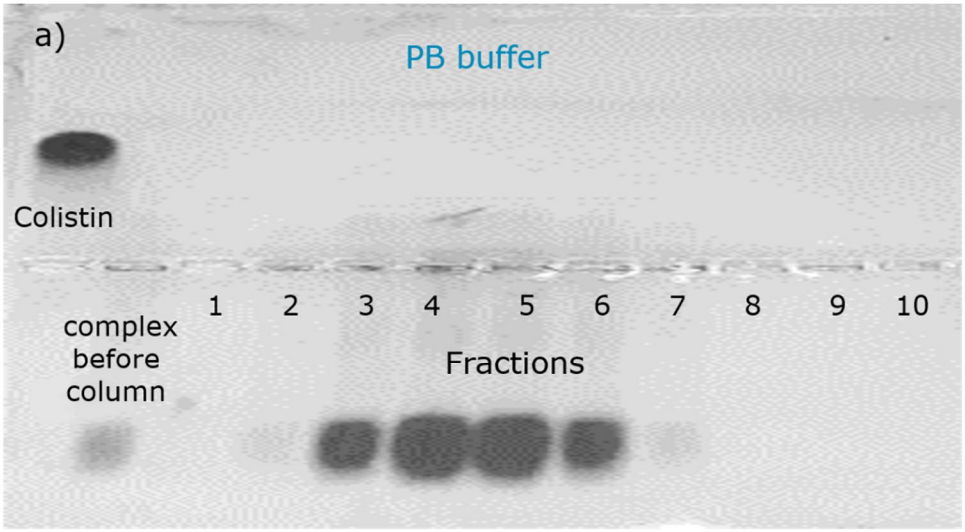
Colistin:mPEG$_{2k}$-*b*-GA$_{30}$ nanocomplexes were assembled in 10 mM phosphate buffer (PB) or phosphate buffer saline (PBS) , at pH 7.4, and eluted with the respective buffers. Gel electrophoresis data for collected eluted samples are shown in **Figure 6.6**. For complexes prepared and eluted in 10 mM PB buffer pH7.4 (ionic strength 60 mM), gel illustrates the presence of overall negative species stained for colistin in fractions 3-6; they travelled the same distance from the wells as the nanocomplexes in the reaction mixture before elution. It is important to notice that no free colistin (above detection limit of 62.5 µg/mL) was detected in the fractions collected **(Figure 6.6a)**. Furthermore, there is no presence of detectable colistin concentration in the later fractions, indicating that colistin present is generally associated with the copolymer in the complexes (fractions 3-6).

For the complexes made in PBS and eluted with PBS, gel analysis of elution fractions **(Figure 6.6b)** shows the presence of bands of colistin containing negative species in fractions 2-5, accompanied by the appearance of free colistin 'smear'. Free colistin bands appear in the later fractions, indicating the presence of uncomplexed colistin; this was not observed in lower ionic strength PB buffer. These results suggest that the complexation / complexes integrity are affected by the ionic strength of the buffer, conforming the role of electrostatic interaction in their formation and stability.

Both PB and PBS buffers used are 10 mM potassium or sodium phosphate concentration, respectively, but the ionic strength of these buffers differ; for PBS is 162.7 mM and for PB is 60 mM. PBS as a high ionic strength buffer causes a reduction in the Debye length; in physiological salt environment of PBS it is near 0.7 nm, and increases with the buffer dilution to 2.4 nm for 10-times diluted PBS and 7.4 nm for 100-times diluted PBS. The decrease in Debye length in high ionic strength buffer reduces net electrostatic effect of charge carriers, thus affecting the ability of colistin to interact with $mPEG_{2k}$-*b*-GA_{30} to form, or maintain integrity of nanocomplexes.

These results also suggest that colistin:$mPEG_{2k}$-*b*-GA_{30} nanocomplexes are stable when in 10 mM PB in the conditions utilised for their separation by SEC, as no free colistin was observed by agarose electrophoretic analysis of the collected fractions

(Figure 6.6a). When complexed in and eluted using PBS buffer, simulating physiological conditions of ionic strength, majority of colistin is present in the complexes with $mPEG_{2k}$-*b*-GA_{30} copolymer, with some colistin existing in the non-complexed form.



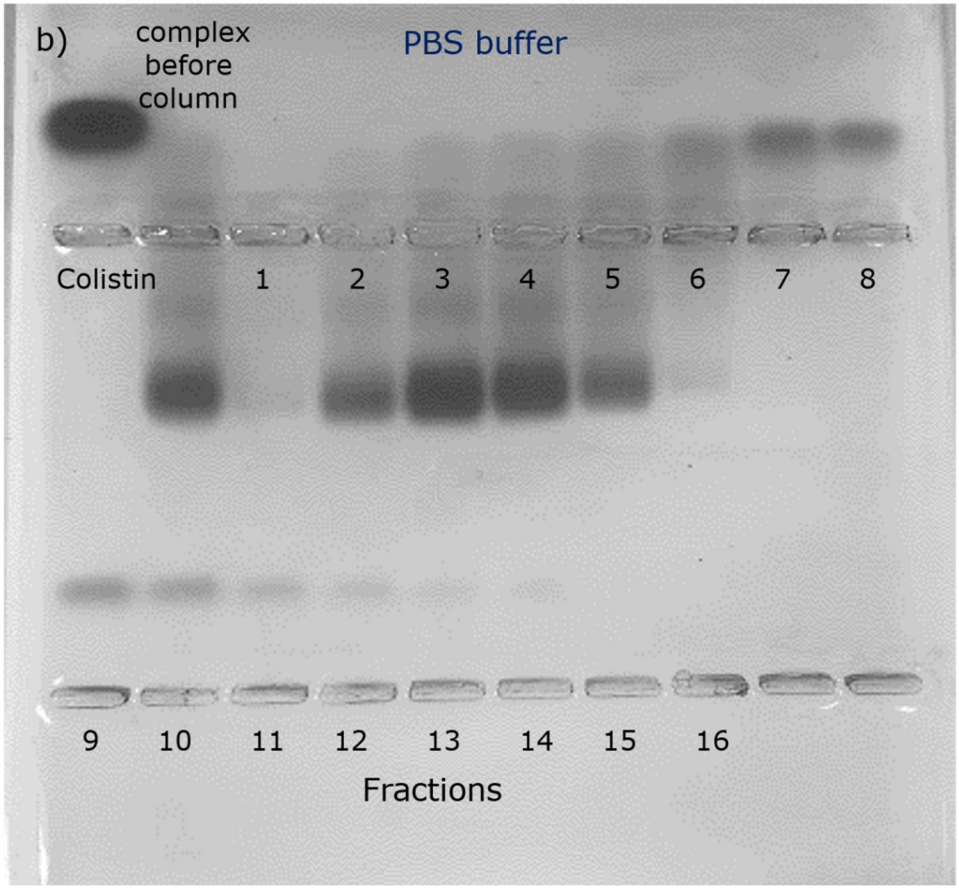


***Figure 6.6**. Electrophoretic gel analysis of colistin:mPEG$_{2k}$-b-GA$_{30}$ complexes prepared at r ratio of 2.5. a) complexes made and eluted in 10 mM PB, pH 7.4 using PD10 column and b) complexes made and eluted in 10 mM PBS using PD 10 column. Samples from collected fractions ran in 1.5 % agarose gel for 1 h at 100 mA in Tris-Acetate-EDTA (TAE) buffer. Colistin concentrations in each fraction can vary and data are not used for quantitative comparison purposes.*

In the next step, the stability of colistin:mPEG$_{2k}$-*b*-GA$_{30}$ complexes was assessed in increasing ionic strength of the suspension medium. The nanocomplexes were made in 10 mM PB (ionic strength 60 mM) and eluted by SEC using PBS (ionic strength 162.7 mM) as the mobile phase. **Figure 6.7a** shows the gel carried out immediately after collections of column fractions. Compared to **Figure 6.6a** and **b**, the bands for fractions 4-7 appear to be less defined than for nanocomplexes made and eluted with PB, with the presence of some free colistin in the later fractions. Comparing to the complexes made and ran with PBS, the bands are not as smeary and the presence of free colistin is less pronounced.

Fractions collected from column were kept in the fridge at 4 °C for 1 week and assessed by agarose gel electrophoresis in the same manner as previously employed. **Figure 6.7b** shows no noticeable differences in bands appearance, relative to **Figure 6.6a**.

Overall, these results indicate that electrostatic interactions of colistin and mPEG$_{2k}$-*b*-GA$_{30}$ complexes at molar charge ratio of 2.5 in low ionic strength buffer (PB) results in formation of complexes; presence of free, uncomplexed colistin is below detection level of

62.5 µg/mL. The uncomplexed colistin is clearly observed when these complexes were exposed to a high ionic strength buffer (PBS), more representative of physiological ionic strength conditions, however the data illustrate that even under these conditions the majority of colistin is still complexed with mPEG$_{2k}$-*b*-GA$_{30}$ in overall negatively charged complexes.

Furthermore, the complexes are stable towards dissociation over a period of 7 days. The results hence provide confidence over the stability of colistin:mPEG$_{2k}$-*b*-GA$_{30}$ complexes towards dissociation in ionic strength of biological medium, and on their storage in suspension.

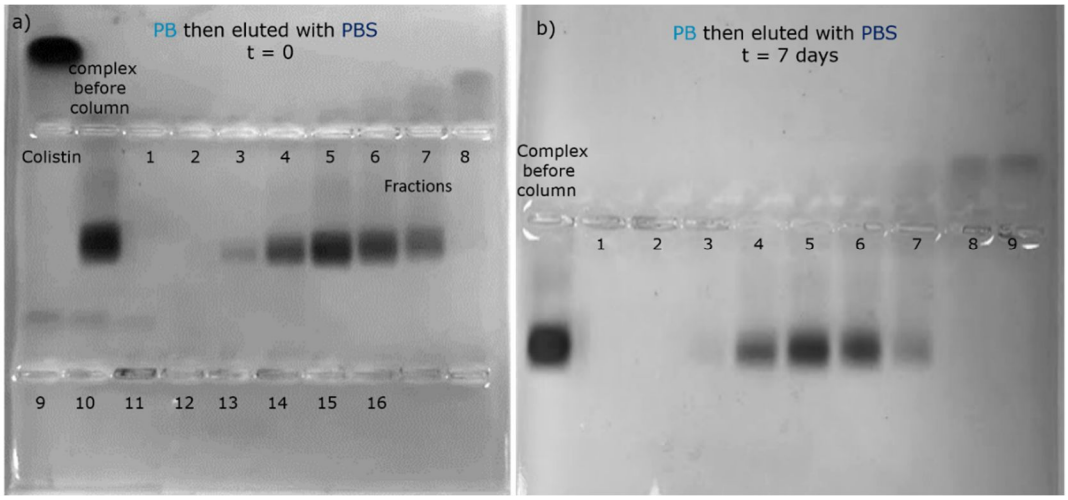


***Figure 6.7**. Electrophoretic mobility of colistin:mPEG$_{2k}$-b-GA$_{30}$ complexes prepared at ratio 1:2.5. a) complexes prepared and eluted in 10 mM PB using PD 10 column; b) complexes prepared and eluted in 10 mM PBS using PD 10 column. Fractions collected ran in 1.5 % agarose gel for 1 h at 100 mA in Tris-Acetate-EDTA (TAE) buffer.*

6.3.3 MTS toxicity assay of complexes on A549 cells

MTS toxicity assays **(Figure 6.8)** showed that colistin:mPEG$_{2k}$-*b*-GA$_{30}$ nanocomplexes at concentrations up to 4 µg/mL presented no significant toxicity towards A549 cells after 4 h exposure.

Up to 4 µg/mL colistin concentrations were chosen as previous studies suggested a mean serum colistin concentration of 2 µg/mL could efficiently eradicate gram-negative bacteria, and peak serum concentration is typically reaching 1-4 µg/mL in therapy (Lim *et al.* 2010; Tran *et al.* 2016).

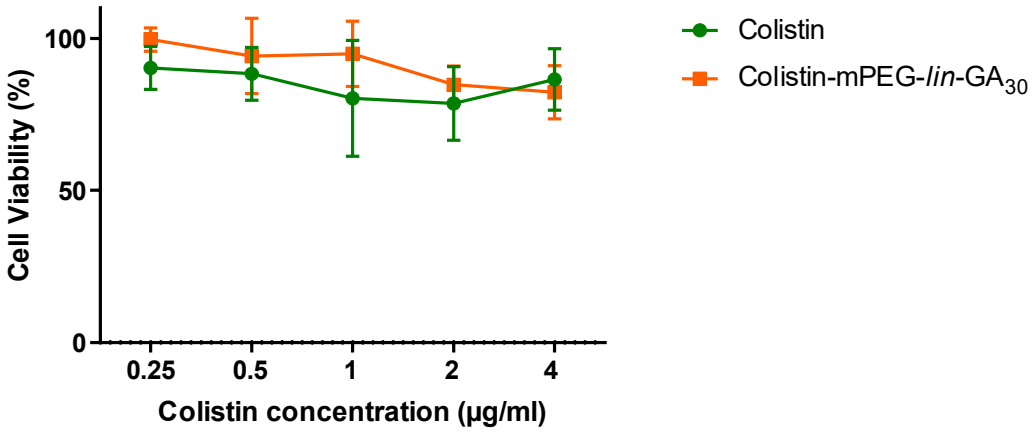


Figure 6.8 *Metabolic activity, as assessed by MTS assay, of A549 cells after 4 h of treatment with different concentration of free polymer mPEG-b-GA$_{30}$ and colistin:mPEG-b-GA$_{30}$ nanocomplexes. The error bar shown is the standard deviation of the mean. (N=3, n=3).*

These results are in agreement with a previous polymyxins toxicity studies on the human lung epithelial A549 cell line (Ahmed *et al.* 2017). In their study colistin applied at 2.0 mM caused apoptosis in about 20% of the cells following treatment for 24 h but did not

induce any significant cell death at concentration < 1.5 mM (1 mg/mL). The authors proposed that the hydrophobicity of position 6 in the polymyxin core structure is key for the apoptotic effect on A549 cells **(Figure 6.1)**. As the substituent in position 6 is the only difference between polymyxin B and colistin, the more hydrophobic D-phenylalanine at position 6 of polymyxin B may explain the greater magnitude of cell death and mitochondrial toxicity than that caused by colistin (D-Leucine at position 6). The net positive charge of polymyxins also appeared to be important for the apoptotic effect on A549 cells. Minimal cellular toxicity and mitochondrial oxidative stress in A549 cells were observed with the negatively charged prodrug CMS even at concentrations as high as 6.0 mM (Ahmed *et al.* 2017).

Another interesting observation described in that study is that with the same treatment of 100 μM polymyxin B for 24 h, the viability of kidney epithelial proximal tubule HK-2 (EC_{50} = 0.35 mM) cells decreased to approximately 55%, whereas the viability of A459 cells (EC_{50} = 1.74 mM) was not affected under same conditions. At higher polymyxin B concentration of 250 μM, cell death was > 80% for HK-2 cells at 24 h, while > 90% of the A549 cells remained viable. The main issue of polymyxins' toxicity in clinic is the associated nephrotoxicity which can occur in up to 60% of patients when the drug is administered intravenously; it is the major dose-limiting factor for their clinical use. The high tolerability of lung epithelial

cells to polymyxins, also observed in this study, compared to kidney cells further advocates the therapeutic potential of pulmonary administration of colistin; it could allow higher pulmonary dosing and in this way facilitate the safe use of inhaled polymyxins in patients to treat pulmonary infections (Ahmed *et al.* 2017).

Data from previous studies and the MTS experiment suggest colistin:mPEG$_{2k}$-*b*-GA$_{30}$ nanocomplexes given at colistin concentrations of 0.25 – 4 µg/mL were not toxic to A549 cells.

6.3.4 E. coli XL1 bacteria growth curve in the presence of nanocomplexes

Colistin is an antibiotic to treat Gram-negative infections; it displays *in vitro* activity against gram-negative bacteria such as *A. baumannii*, *P. aeruginosa*, *K. pneumoniae*, and *E. coli* (Li *et al.* 2005). *Escherichia coli* (*E. coli*) has a biosafety level of II and can be handled in our laboratory; hence was chosen in this study. In addition, *E. coli* strains are easily cultured with simple nutritional requirements and have a short generation time as little as ~20 minutes (Gibson *et al.* 2018).

The bacterial growth of a non-pathogenic strain of *E. coli* XL1 with or without treatment with colistin:mPEG$_{2k}$-*b*-GA$_{30}$ complexes is shown in **Figure 6.9**.

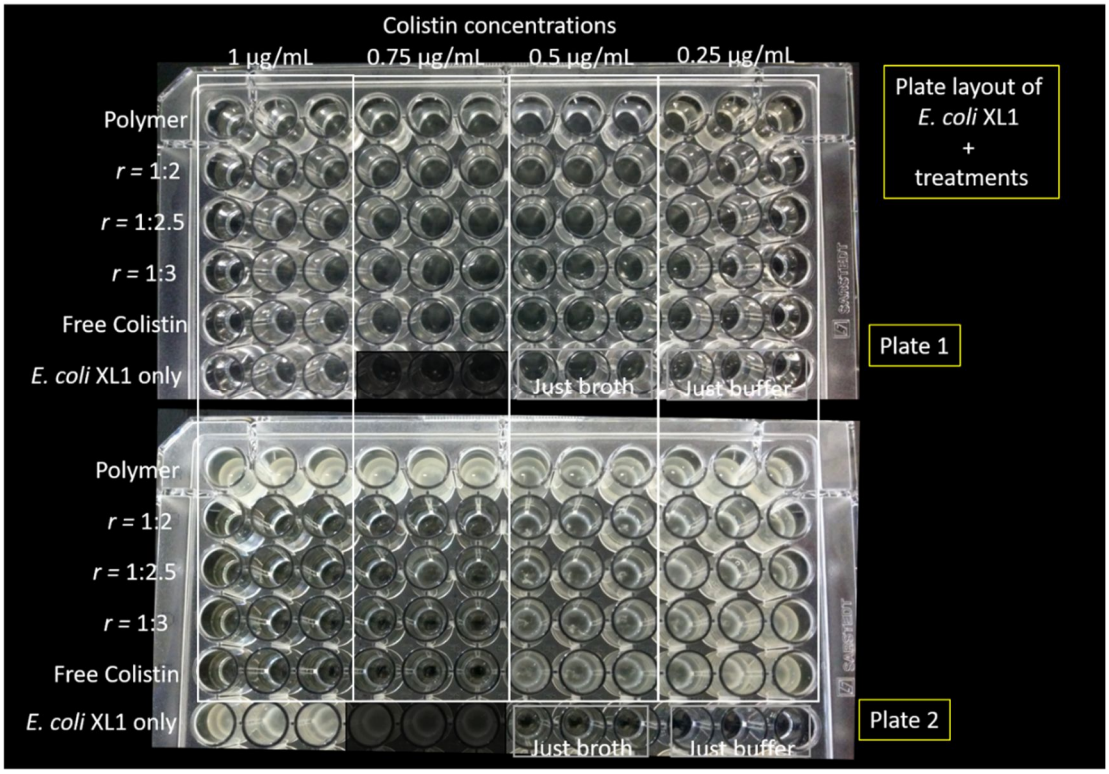


***Figure 6.9**. Bacteria growth test in 96 well plate. r = 1:2, 1:2.5 and 1:3 denotes colistin:mPEG$_{2k}$-b-GA$_{30}$ nanocomplexes prepared at molar charge ratio of 1:2, 1:2.5 and 1:3, respectively. Same number of bacteria were placed in each well. Free colistin and nanocomplexes with different r ratio at colistin concentrations or 0.25, 0.50, 0.75 and 1.0 were applied in triplicates. Polymer mPEG$_{2k}$-b-GA$_{30}$ were applied at concentrations matching polymer in r = 1:3 nanocomplexes as a control. Growth broth and 10 mM PB buffer were applied as contamination controls. Untreated E. coli XL1 were grown to produce control bacteria growth curve. Plate 1 contains test samples at time 0; plate 2 shows plate 1 post 20 h incubation at 37°C, opaque wells indicate high bacteria growth.*

The growth of *E. coli* XL1 presented the general growth curve pattern in line with the initial lag phase occurring between 0–2 h followed by the exponential (log) phase between 2–18 h and bacteria growth reached plateau thereafter **(Figure 6.10a)** (Wang *et al.* 2015; Allen and Waclaw 2019). The application of colistin significantly reduced *E. coli* growth at concentrations ≥ 0.50 µg/mL, whereby the reductions are positively proportional to increases in colistin

concentration at the concentrations tested. When colistin:mPEG$_{2k}$-*b*-GA$_{30}$ nanocomplexes prepared at different charge ratios (1:2 – 1:3) were applied (nanocomplexes suspension corresponding to 0.25 µg/mL – 1.0 µg/mL colistin concentration) a colistin concentration dependent reduction in *E. coli* growth over time is observed.

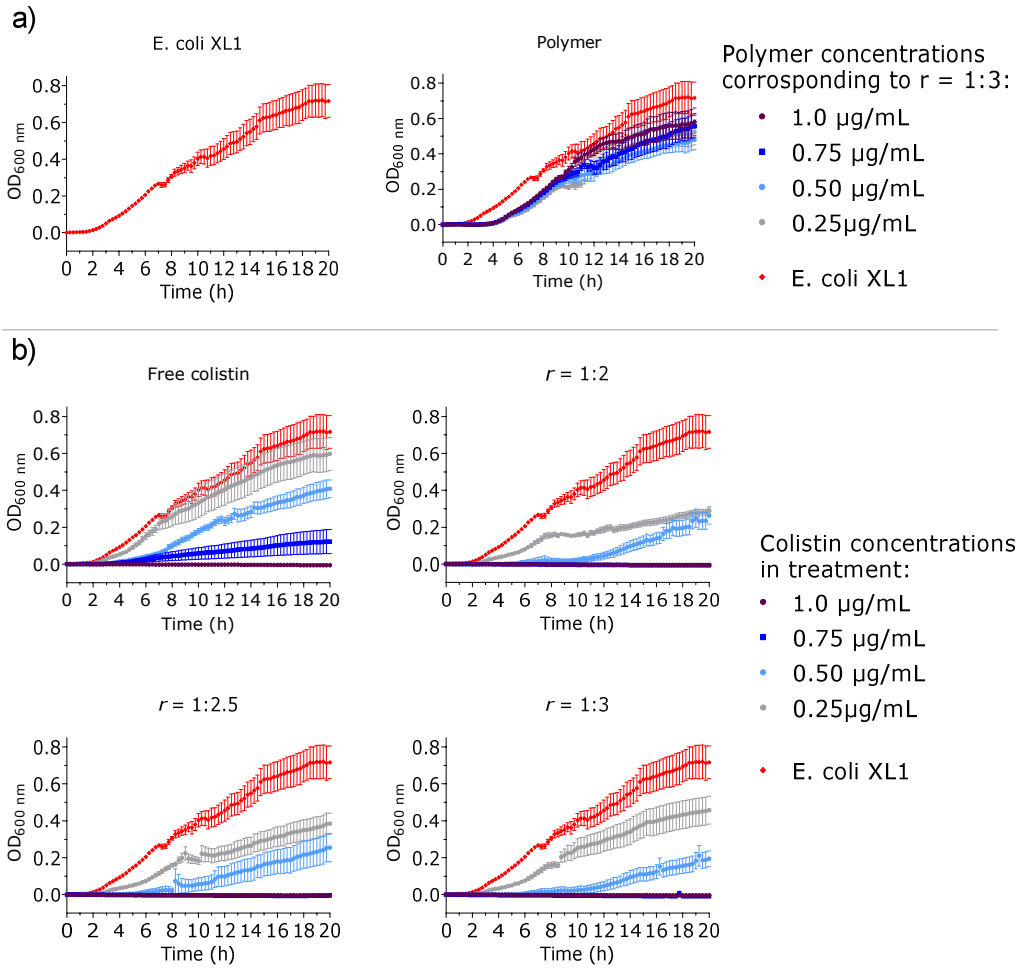


***Figure 6.10**. Growth curves of E. coli XL1 bacteria on application of different concentrations of colistin and colistin:mPEG$_{2k}$-b-GA$_{30}$ complexes suspensions measured by reading OD$_{600}$ as a function of time. a) Control E. coli XL1 growth curve and E. coli XL1 growth in suspensions containing mPEG$_{2k}$-b-GA$_{30}$ concentration corresponding to the amount of mPEG$_{2k}$-b-GA$_{30}$ in the r = 1:3 suspension. b) E. coli XL1 growth in suspensions containing free colistin, nanocomplexes with colistin:mPEG$_{2k}$-b-GA$_{30}$ charge ratio of 1:2, 1:2.5 and 1:3 at colistin concentrations of 0.25, 0.50, 0.75 and 1.0 µg/mL. The error bar shown is the standard error of the mean. (N=3, n=3).*

At the end of the 20 h incubation all 3 nanocomplex formulations with 0.75 μg/mL colistin concentration showed no *E. coli* growth compared to free colistin which had an overall bacteria growth rate of 0.239 **(Table 6.1)**.

Table 6.1. *Calculated E. coli XL1 bacteria growth rate over 20 h experiment based on OD_{600} readings. Bacteria treated with free colistin, free $mPEG_{2k}$-b-GA_{30} polymer, and colistin $mPEG_{2k}$-b-GA_{30} complexes at different r ratios achieving colistin concentrations between 0.25 to 1.0 μg/mL.*

Concentrations of colistin (μg/mL)	0.25	0.50	0.75	1.0
Polymer	0.313	0.309	0.316	0.318
Free colistin	0.316	0.300	0.239	0.000
r =1:2	0.284	0.272	0.000	0.000
r =1:2.5	0.297	0.276	0.000	0.000
r =1:3	0.306	0.263	0.000	0.000
Growth rate of *E. coli* XL 1 = 0.329				

The results from this part of the study provided evidence that for all colistin:$mPEG_{2k}$-*b*-GA_{30} nanocomplexes formulations *E. coli* XL1 growth rates are reduced, compared to corresponding concentration of colistin applied free in solution. Interestingly, at applied colistin concentration of 0.75 μg/mL, colistin:$mPEG_{2k}$-*b*-GA_{30} complexes at all ratios tested completely reduced the bacterial growth, whilst

the free colistin reduces the grow rate from 0.329 of untreated culture to 0.239 **Table 6.1**.

To exclude the possibility of $mPEG_{2k}$-*b*-GA_{30} copolymer, or its complexes with colistin, causing aggregation of broth ingredients, OD_{600} of $mPEG_{2k}$-*b*-GA_{30} and complexes added to the broth without bacteria was measured. The composition of the Mueller-Hinton broth used to includes beef infusion solids 2 g/L, starch 1.5 g/L and casein hydrolysate 17.5 g/L. Notably, casein hydrolysate is a complex mixture of 18 different amino acids, vitamins, calcium, phosphate, and several microelements (Bhatia 2015). Control experiments carried out shows no increase, or changes in OD_{600} for tested systems, indicating that OD_{600} profiles seen in **Figure 6.10** indeed arise from the *E. coli* XL1 growth, and the impact on the growth is caused by different treatments applied.

6.3.5 E. coli XL1 growth curve by colonies counting

After establishing that the colistin:$mPEG_{2k}$-*b*-GA_{30} nanocomplexes were more effective at reducing *E. coli* growth compared to free colistin, further experiments were carried out to assess the antibacterial effect of the nanocomplexes by counting bacteria colonies. Culture of *E. coli* XL1 were treated with the following: (i) untreated, (ii) $mPEG_{2k}$-*b*-GA_{30} polymer alone, (iii) free colistin, and (iv) colistin:$mPEG_{2k}$-*b*-GA_{30} complexes at ratio 1:2, (v) ratio 1:2.5,

and (vi) ratio 1:3. Untreated bacteria suspension and bacteria suspension containing $mPEG_{2k}$-*b*-GA_{30} polymer only was utilised as controls.

Figure 6.11 shows that the treatment with $mPEG_{2k}$-*b*-GA_{30} polymer only does not show statistically significant impact on reducing *E. coli* growth; the colony forming unit (CFU/mL) increased at the same rate as untreated bacteria. For colistin:$mPEG_{2k}$-*b*-GA_{30} nanocomplexes the trend follows results obtained in the growth curve experiment **(Figure 6.10)**. All nanocomplex formulations with colistin concentrations ≥ 0.50 μg/mL were effective at reducing bacteria growth. When assessed after 6 h, as the final time point of the experiment, all three nanocomplex formulations show statistically higher reduction in the bacterial growth relative to free colistin treatments at 0.50 and 0.75 μg/mL concentrations ($P \leq 0.0001$) **(Figure 6.12)**. At *r* = 1:2 the complexes show bacterial growth rate $\mu = -0.005$ and a superior, by extra 1 log, reduction in cell number compared to free colistin at 1.0 μg/mL ($\mu = 0.278$) **(Table 6.2)**.

Antibiotics can be classified as 'bactericidal' which kills bacteria or 'bacteriostatic' that inhibit bacterial growth which then requires immune system to clear the bacteria in clinical setting (Nemeth *et al.* 2014). The bacteria growth curve experiments in **Figure 6.10** confirmed the bacteriostatic effect of the nanocomplex formulations

on *E. coli* XL1 strain. Subsequent studies were conducted using colistin:mPEG$_{2k}$-*b*-GA$_{30}$ complexes at *r* 2:1, at 1.0 µg/mL colistin concentration as this nanocomplexes shows similar properties to those at the higher ratios, but contain lower proportion of polymeric material. To further explore the potential antibacterial effect of this colistin formulation, a pathogenic strain of *E. coli E2348/69* was employed. Research suggest *E. coli* population densities of up to ~ 10^9 cells *per* mL of culture medium could be used in lab experiments (Allen and Waclaw 2019).

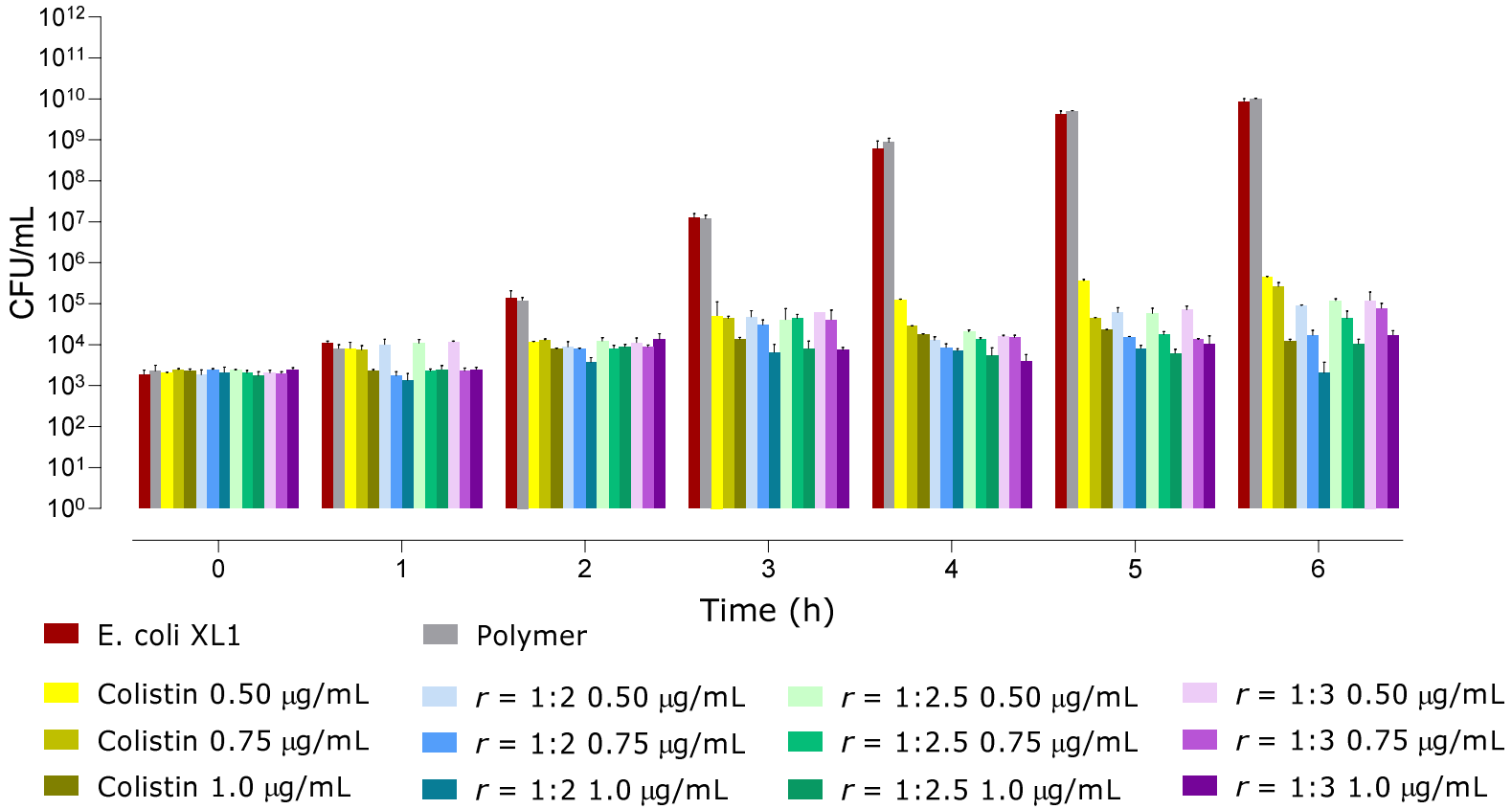


Figure 6.11. *Bacterial growth analysis by colonies counting. Cells of E. coli XL1 treated with different concentrations of colistin and colistin:mPEG$_{2k}$-b-GA$_{30}$ nanocomplex suspensions. The samples were serially diluted, plated onto agar plates and incubated at 37 °C. The colony count was expressed as log (CFU/ml). The experiment was performed in triplicates and the error bar represents their standard deviation of the mean.*

Table 6.2. *Table showing calculated E. coli XL1 bacteria growth rate over 6 h based on colony forming units (CFU/mL). Bacteria treated with free colistin, free $mPEG_{2k}$-b-GA_{30} polymer, and colistin:$mPEG_{2k}$-b-GA_{30} formulations at ratios 1:2, 1:2.5 and 1:3 at colistin concentrations between 0.50 to 1.0 µg/mL.*

Concentrations of colistin (µg/mL)	0.50	0.75	1.0
Free colistin	0.895	0.778	0.278
r = 1:2	0.478	0.323	-0.005
r = 1:2.5	0.652	0.513	0.300
r = 1:3	0.682	0.613	0.323
Growth rate of *E. coli* XL 1 = 2.557			
Growth rate of *E. coli* XL 1 at the presence of polymer = 2.555			

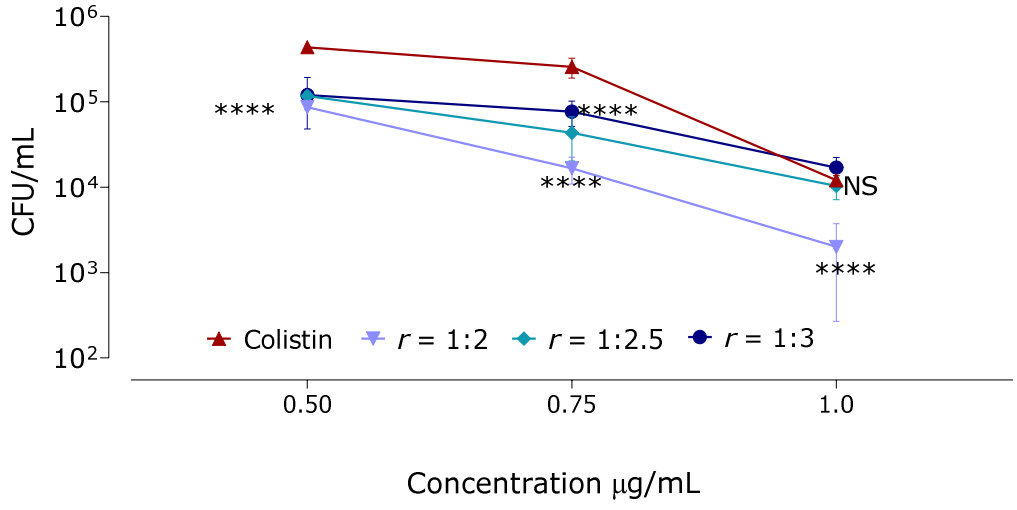


Figure 6.12. *Bacteria colony count expressed as log (CFU/mL) versus applied colistin concentration. Comparison of E. coli treated with colistin:mPEG$_{2k}$-b-GA$_{30}$ formulations to the corresponding colistin concentrations applied as 'free' colistin solution after 6 h incubation. Two-way ANOVA was used for statistical analysis. **** P ≤ 0.0001, NS not significant. The error bar represents their standard deviation of the mean.*

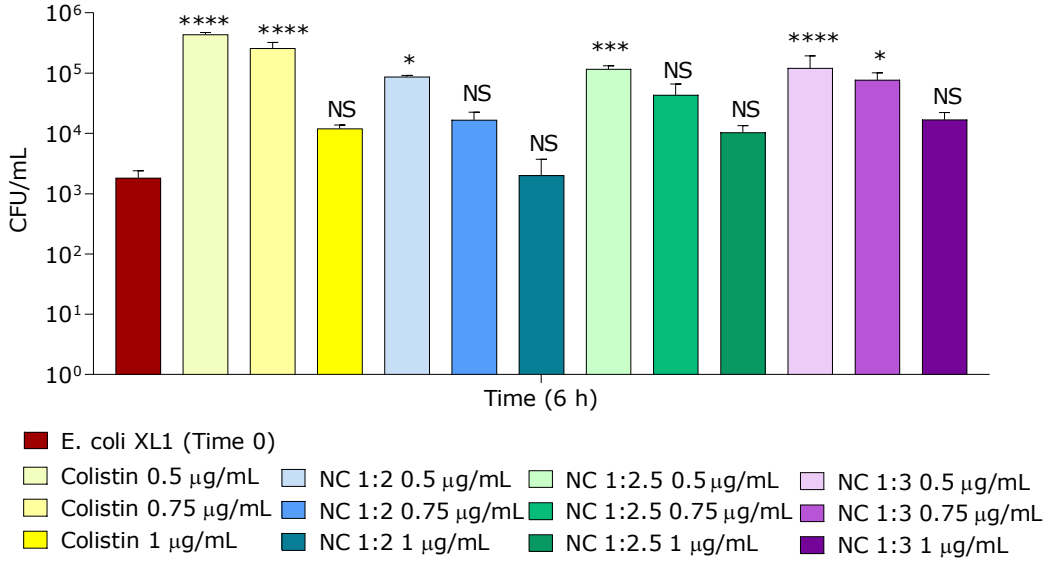


Figure 6.13. *Comparison of E. coli number between all antibiotic treatments at 6 h to time 0. One-way ANOVA was used for statistical analysis. *P ≤ 0.05, **P ≤ 0.01, ***P ≤ 0.001, **** P ≤ 0.0001, NS not significant. The error bar represents their standard deviation of the mean.*

6.3.6 Enteropathogenic Escherichia coli killing curve

E. coli can act as opportunistic pathogen and only in very rare instances can become a threat to normal individuals when the host have impaired immune defence (Kuhnert *et al.* 2000). However, some specific *E. coli* strains have an enhanced potential to cause disease. These pathogens have been broadly classified into two major categories: the enteric pathogens and the extraintestinal pathogens (Kuhnert *et al.* 2000). The enteric pathogenic *E.*

coli have been further divided into enterotoxigenic *E. coli* (ETEC), enteropathogenic *E. coli* (EPEC), Shiga toxin-producing *E. coli* (STEC), enteroinvasive *E. coli* (EIEC), enteroaggregative *E. coli* (EAEC), and diffusely adherent *E. coli* (DAEC) (Levine 1987). Enteropathogenic *E. coli* (EPEC) infections were historically treated with colistin (South 1971) and was therefore chosen as the pathogenic strain used in this study. Culture of EPEC was subjected to treatments with: (i) untreated with phosphate buffer only, (ii) free colistin, and (iii) colistin:mPEG$_{2k}$-*b*-GA$_{30}$ complexes at *r* = 2:1 and 1.0 µg/mL colistin concentration. The samples were drawn at different intervals, plated onto agar and incubated at 37 °C.

Figure 6.14 summarises the overall EPEC growth over 100 minutes expressed in log CFU/mL. Profiles show the growth lag phase at the initial 20 minutes, followed by an increase of 1 log between 20 and 40 minutes for untreated EPEC, whilst the cells treated with colistin and the colistin:mPEG$_{2k}$-*b*-GA$_{30}$ nanocomplexes were 'static' until 60 minutes of incubation. From the 60 minutes timepoint the treated EPEC show significant reduction in CFU/mL which continues to decrease to up to 2 log reduction in bacteria number for samples treated with colistin:mPEG$_{2k}$-*b*-GA$_{30}$ complexes 1:2 (bacteria growth rate µ= -2.6), and 1 log reduction for colistin treated cells (bacteria growth rate µ= -1.6) at 100 minutes time point **(Figure 6.14)**. These data show effective killing of EPEC by colistin:mPEG$_{2k}$-*b*-GA$_{30}$ complexes at *r* 1:2, and importantly a significantly higher activity

than free colistin applied at the same concentration in the same time period.

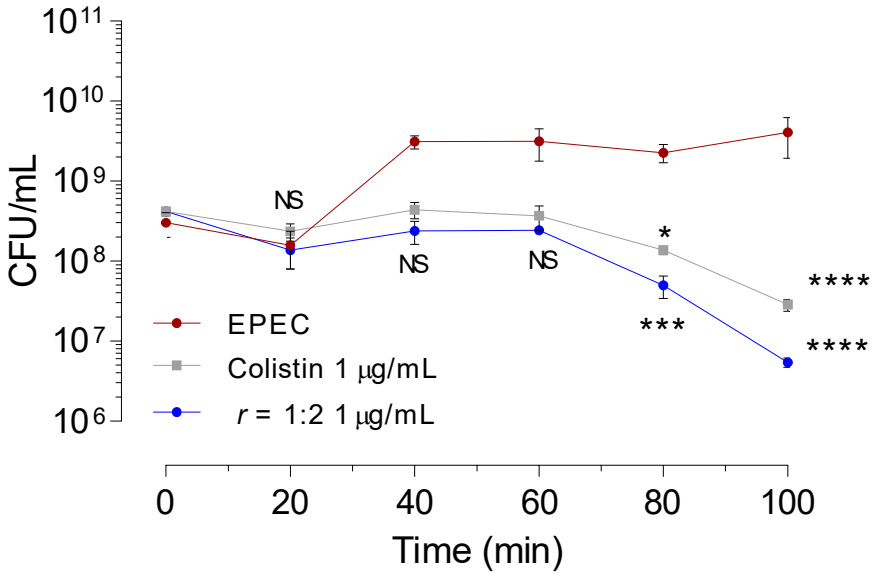


Figure 6.14. *Time-dependent growth of enteropathogenic Escherichia coli (EPEC) E2348/69 on treatment of colistin or colistin:mPEG$_{2k}$-b-GA$_{30}$ 1:2 nanocomplexes. The colony count is expressed as log (CFU/mL). CFU/mL of colistin and the nanocomplexes treatments samples were compared at different timepoints to EPEC at time 0. Two-way ANOVA was used for statistical analysis. *P ≤ 0.05, **P ≤ 0.01, ***P ≤ 0.001, **** P ≤ 0.0001, NS not significant. The error bar represents their standard deviation of the mean (N=4).*

6.3.7 Enteropathogenic Escherichia coli infection treatment

In further experiment colistin:mPEG$_{2k}$-*b*-GA$_{30}$ complexes at *r* = 1:2 were tested in *in vitro* EPEC infection of HeLa cells. EPEC E2348/69 is an extracellular pathogen that causes disease by attaching to the surface of host epithelial cells and forming a pore structure in the cell membrane, allowing the passage of virulence factors into the underlying cell (Vallance and Finlay 2000). EPEC E2348/69 infected HeLa cells have been shown to remain viable, but undergo changes

in filamentous actin distribution and cell morphology (Taylor *et al.* 1999). The experimental set up is illustrated in **Figure 6.15**.

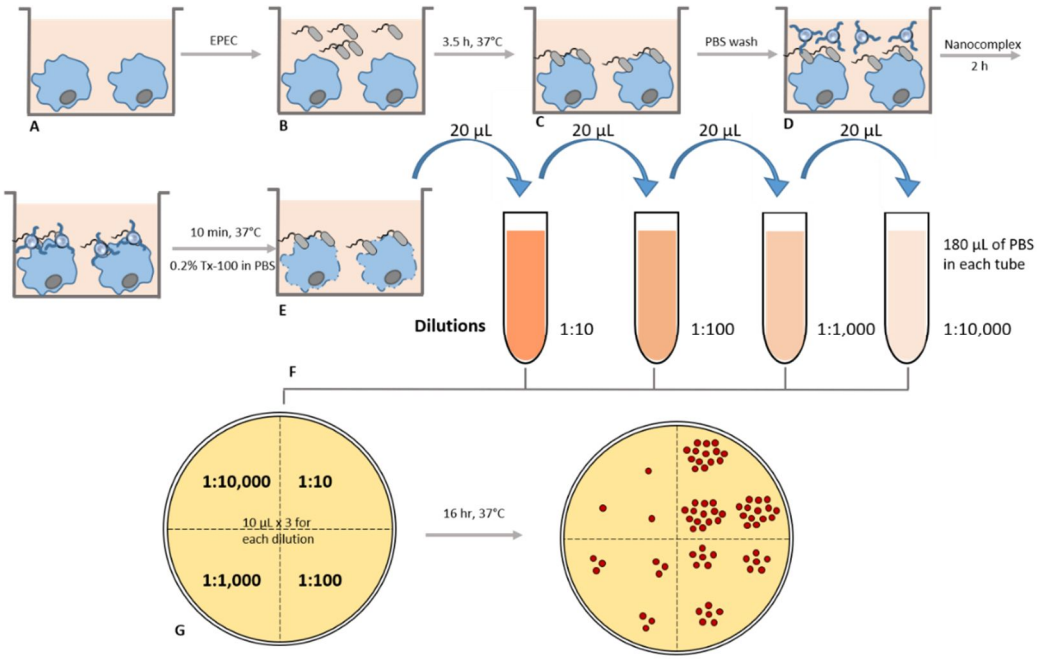


Figure 6.15. *EPEC E2348/69 infection assay procedures. A & B) HeLa-Mitotrap cells incubated in medium containing bacteria for 3.5 h. C) Cells are now infected with EPEC and washed with PBS. D) Cells were treated with i) medium (control), ii) 1 µg/mL free colistin, iii) 1 µg/mL of colistin in nanocomplex 1:2 and iv) equivalent of mPEG$_{2k}$-b-GA$_{30}$ polymer in medium, and incubated for 2 hours. E) Surviving bacteria were harvested by lysing the cells with 0.2% Triton X-100 in PBS for 10 min at 37°C. F & G) The supernatants were immediately serially diluted with PBS and spotted onto LB agar plates. After incubation for 16 h at 37°C, the numbers of bacterial colonies for each sample were counted and expressed as colony-forming units (CFU) per mL.*

Figure 6.16 shows the colony count - the number of bacteria that survived after 2 h of treatments. In the absence of colistin, mPEG$_{2k}$-*b*-GA$_{30}$ polymer does not statistically significantly impact on the growth of EPEC. 'Free' colistin treated EPEC infected cells had 2 log lower CFU/mL compared to the untreated cells. Nanocomplex 1:2 was significantly more effective at reducing bacteria number

compared to free colistin resulting in a 4 log reduction compared to untreated cells.

Figure 6.16 plots the EPEC E2348/69 colony counts. In the absence of colistin, mPEG$_{2k}$-*b*-GA$_{30}$ polymer does not statistically significantly impact on the growth of EPEC. 'Free' colistin treatment showed 2 log lower CFU/mL, compared to the untreated cells. Colistin:mPEG$_{2k}$-*b*-GA$_{30}$ complexes at *r* = 2:1 show a statistically significantly higher effect in reducing bacteria number compared to free colistin, resulting in a 4 log reduction compared to untreated cells.

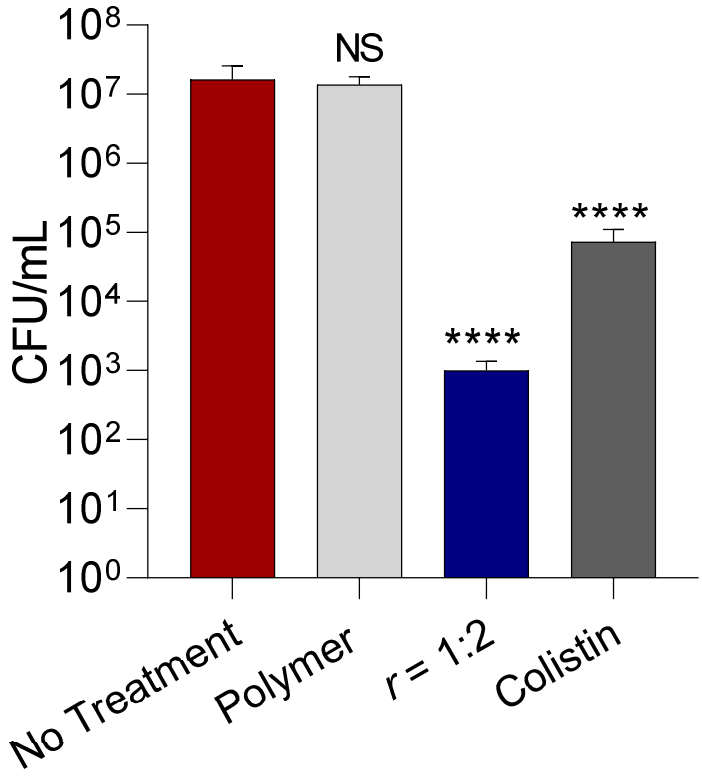


Figure 6.16. *Treatments of EPEC E2348/69 infected HeLa Mitotrap cells by colistin and colistin:mPEG$_{2k}$-b-GA$_{30}$ polymer r = 1:2. Results expressed as log (CFU/ml) showing colony counts of EPEC XX cells post treatment. CFU/mL of treatments with mPEG$_{2k}$-b-GA$_{30}$ polymer alone, colistin, and colistin:mPEG$_{2k}$-b-GA$_{30}$ polymer r = 1:2 were compared to EPEC infected cells without treatment. One-way ANOVA was used for statistical analysis. *P ≤ 0.05, **P ≤ 0.01, ***P ≤*

*0.001, **** P ≤ 0.0001, NS not significant. The error bar represents their standard deviation of the mean.*

The overall improvement in the antibacterial effect by the nanocomplexes compared to free colistin is an interesting finding. The mechanism of this noticeable improvement is not clear. The possible contribution to this effect may be arising from an increased 'local concentration' of the colistin that may be created by the complexes. Namely $mPEG_{2k}$-*b*-GA_{30} polymer used in this study contains 30 repeating units of glutamic acid, which complex with 5 positive charges on colistin surface at physiological pH. For the complexes prepared at the molar charge ratio between colistin and $mPEG_{2k}$-*b*-GA_{30} of 1:2, this equates to 3 colistin molecules *per* polymer chain. The nanocomplexes of around 100 nm **(Figure 6.5)** would consist of clusters of colistin and $mPEG_{2k}$-*b*-GA_{30} molecules. This could create, in a close proximity to the bacterial surface, an increased local concentration of colistin, compared to free colistin in solution. This local microenvironment with higher colistin concertation may in turn facilitate higher local effect of colistin on bacterial surface and LPS structure leading to higher antibacterial activity. This would be in line with published studies that have suggested that colistin resistance may be largely attributed to bacterial responses to environmental changes whereby cellular regulatory systems create bacterial resistance by lowering the

negative charge of the outer membrane and decreasing the number of binding sites for the cationic polymyxins (Mcphee *et al.* 2006; Gunn *et al.* 2000). It is possible that higher local colistin concentration overcomes this bacterial resistance.

Considering the mechanism of action as mentioned in the introduction, colistin interact with LPS on the bacteria surface through the positively charged amine groups which also act as interaction site for complexation with $mPEG_{2k}$-*b*-GA_{30}. For colistin to have antibacterial effect in the complexed form, the complexes would have to disassemble and may also reassemble spontaneously in a balanced manner at site of action. In **section 6.3.2**, the result suggested increase in ionic strength of the suspending buffer encourage disassembly of the complexes; this phenomenon can also be engaged here to hypothesis that the increase in availability of positively charged amine groups on colistin when present in complexed form in physiological environments.

6.4 Conclusions

In this chapter, colistin was successfully formulated into nanocomplexes with $mPEG_{2k}$-*b*-GA_{30} copolymer and complexation was confirmed by agarose electrophoresis and transmission electron microscopy. The polyelectrolyte nature of the complexes was probed and proved in a series of experiments in different ionic strength

buffers; 10 mM phosphate buffer and phosphate buffer saline. These experiments also illustrate that the nanocomplexes retain their integrity in PB and PBS after 7 days storage, with a higher population of fee colistin in the latter buffer.

In *in vitro* cell culture, free colistin and the nanocomplexes did not negatively impacted lung epithelial A549 cell viability up to the highest concentration tested of 4 μg/mL. It is noted that a full toxicity study is beyond the scope of this study and this would require testing on different cell lines, particularly models of renal and neurological toxicities.

All *in vitro* antimicrobial activity tests on both pathogenic E2348/69 and non-pathogenic XL1 *E. coli* strains suggest colistin formulated into colistin:mPEG$_{2k}$-*b*-GA$_{30}$ *r* = 1:2 nanocomplexes possess enhanced bacteriostatic effect in non-pathogenic *E. coli* XL1 and bactericidal activity in pathogenic *E. coli* E2348/69 compared to free colistin applied at the same concentration. It should be noted that colistin:mPEG$_{2k}$-*b*-GA$_{30}$ *r* = 1:2 formulation shows enhanced bactericidal effect in EPEC E2348/69 infection of HeLa cells, compared to free colistin by killing extra 2 logs of EPEC after 2 h treatment.

The low toxicity of the colistin nanocomplex to lung cells and improved antimicrobial activity may pave the path for the testing of this formulation as a viable drug candidate for lung administration

to treat respiratory infections. In addition, the self-assembly nature of the nanocomplex formulation and the absence of further chemical manipulation for release is also highly beneficial.

Future work needs to investigate the disassembly of the complexes in physiological condition and to consider the presence of potential interactions with pulmonary biomolecules, e.g. secretory mucin in sputum or epithelial mucin that lines airways at reducing free drug levels.

Overall, although further evaluation is needed to determine whether this activity profile extends to other Gram-negative species, we believe that due to the enhanced antimicrobial effect without the increase in toxicity, colistin:mPEG$_{2k}$-*b*-GA$_{30}$ nanocomplex has the potential to become a safer and more effective alternative to colistin and its derivatives.

Chapter 7. General discussions and future work

The field of biological therapeutics is one of the fastest growing sectors within the pharmaceutical industry; however, administration of biologics remains mostly limited to the parenteral route, with little advances in development of alternative delivery routes. Non-invasive strategies such as mucosal surface drug delivery face the challenge presented by the mucosae physiological barrier, which restricts the movement of material from the external milieu into the cells or systemic circulation (Leal *et al.* 2017). Taking advantage of the large potential drug absorption site and ability to bypass liver metabolism, pulmonary delivery is increasingly investigated as an non-invasive route for the delivery of protein and peptide therapeutics, to treat both local and systemic diseases (Agu *et al.* 2001). However, the lungs present different physiological and immunological barriers that need to be overcome to achieve effective drug delivery as discussed in Chapter 1. Many approaches have been investigated by drug delivery scientists with the aim to develop a mucosal delivery strategy based on systems that: i) exhibit no toxicity upon repeated administration, ii) preserve the biological function of the therapeutic molecule, and iii) achieve adequate bioavailability with minimal extra costs to the formulation (compared to parenteral systems) and which are amenable to different proteins or drugs.

Polymer-based nanosystems are proposed as valuable formulation

strategies in addressing the main challenges faced by low molecular weight drugs, and even biologicals (peptides, proteins, antibodies, oligonucleotides) in clinical development; namely, they can provide the following features: i) improve pharmacokinetic profile and increase plasma half-life; ii) allow to include targeting moieties for specific active targeting; and iii) stabilise and reduce immunogenicity of the bioactive compound and possess optimal size to allow better penetration (Kateb *et al.* 2011).

Poly(ethylene glycol) (PEG) has been covalently conjugated to a number of protein therapeutics with the earliest PEGylated macromolecular drugs entering the market over two decades ago (Davis 2002). However, this approach it is not suitable for all proteins as it can lead to reduced therapeutic efficacy. Within this context, this thesis has explored alternative approaches where the polymer and protein/drug would only conjugate temporarily upon administration, which ideally would be then released at the required bodily target.

Polymer therapeutics based on amino acids are excellent candidates for drug delivery; with their protein like structure they can be cleaved by proteolytic enzymes therefor biodegradable (Singer *et al.* 2003). Among them, polyglutamic acid (PGA) was chosen in the current project. PGA exists as polyanion at physiological pH, hence, can be used to complex proteins and peptides possessing multiple positively

charged units (mostly from Arg, Lys, *N*-terminal amine, and to a lesser extent His fragments). Furthermore, PGA is non immunogenic homopolymer that presents minimal antigenic epitopes (Apfelthaler *et al.* 2017). PGA-based polymer-drug conjugates and polymeric micelles have been utilised in various medical applications ranging from cancer to tissue regeneration (Canal *et al.* 2011). A PGA-paclitaxel conjugate Opaxio™ has advanced to Phase III trials for non-small cell lung cancer, ovarian cancer, and glioblastoma, which appears promising; if proven successful it could lead to the official FDA approval of PGA for carrier use in pharmaceutics (Ojima *et al.* 2016; Harshita *et al.* 2019).

With all that in mind, this thesis aimed to develop targeted PEG-*block*-poly(glutamic acid) (PEG-*b*-pGA) diblock copolymers to electrostatic interact with protein and small molecule drug forming complexes, for potential pulmonary delivery.

Among the techniques employed for the synthesis of polypeptides, the ring opening polymerization (ROP) of N-carboxyanhydrides (NCA) represents the most commonly applied polymerisation technique in producing polypeptide-based block copolymers on a multigram scale (Kricheldorf 2006; Hadjichristidis *et al.* 2009). This polymerisation technique can combine the use of functional and macromolecular initiators with non-natural amino acids to yield functional polypeptide-based homo- and multi-block copolymers,

with different architectures that acquires desired properties for biological applications. Previous project within the group have employed this technique and afforded both linear and star shaped PEG-*b*-pGA copolymers (Nieto-Orellana *et al.* 2017).

Studies have shown that nanocarriers conjugated with specific ligands can increase the interaction with epithelial cells, provided that suitable receptors can be identified (Tuma and Hubbard 2003; Russell-Jones *et al.* 1999). Preliminary research in our group indicated the potential of using the B12 pathway to increase the cellular uptake of B12 conjugated nanoparticles in the airway mucosa epithelium (Fowler *et al.* 2013), however research in the area of vitamin B_{12} transport mechanisms in the lung epithelium remain scarce and largely unexplored.

To this end, the present work started with confirmation at mRNA level, expression of cubilin (human CUBN gene), transcobalamin receptor (CD320 gene) and transcobalamin II protein (human TCN2 gene) that are all involved in B12 cellular uptake pathways. mRNA expression was confirmed for all the three genes tested but the expression of the cubilin receptor was found to be very low and unlikely to be adequate to provide cellular function. Hence, the data validated the Calu-3 cell model used in this study possess the functional components required for cellular internalisation of cobalamin (vitamin B_{12}) molecules *via* transcobalamin (CD320)

receptor-mediated transport.

Chapter 3 continues with work to confirm functional, endocytic activity of vitamin B_{12} receptors in Calu-3 lung epithelial model employed in this study. A novel low molecular weight B_{12}-fluorescent probe, pyr-B_{12}, was synthesised and used to probe the receptor function of cells to internalised B_{12} where it could be quantified by flow cytometry measuring the fluorescence level in the cells. This *O*-alkyl pyranine-based fluorescent compound (excitation/emission wavelengths of 390 nm/520 nm, respectively) (Tho and Škalko-Basnet 2016) was selected due to its structural similarity to Lucifer Yellow, which is known to have low cell membrane permeability, while possessing functionalities appropriate for conjugation to vitamin B_{12} (Zhao *et al.* 2019). The data showed a significant reduction of pyr-B_{12} cellular internalisation in the presence of an excess of 'free' vitamin B_{12} competitive ligand. This indicated a prominent, but not exclusive, role of B_{12}-specific transport in the cellular internalisation of pyr-B_{12} probe, likely occurring through TCN2 receptor-mediated transport.

Once the functionality of B_{12} receptor was confirmed in Calu-3 cell line used, work was carried out to synthesise B_{12}-targeted PEG-*b*-pGA deblock copolymer. The B_{12}-targeted copolymers, B_{12}-PEG-*b*-pGA, were produced through a modification of an approach we developed previously for synthesis of analogous non-targeted

counterparts (Nieto-Orellana *et al.* 2017). To improve the overall efficiency of preparation process, work in this thesis have successfully simplified the synthesis from a lengthy 5 step process to merely 3 steps excluding the chemical modification of the vitamin B_{12} ligand.

After successful formation of B_{12} targeted nanocomplex between model protein lysozyme and B_{12}-PEG_{3k}-p(GA) copolymers, cell studies demonstrated that vitamin B_{12}-conjugated nanocomplexes were internalised by the Calu-3 cells more efficiently compared to 'free' lysozyme and non-targeted nanocomplexes. The next part of the work included dry powder formulation of these nanocomplexes and *in vivo* studies and were carried out by collaborators (Dry powder work - Dr Alejandro Nieto-Orellana with assistance from Dr David Coghlan at project sponsor site Vectura group Plc, Chippenham, UK. *In vivo* work - Drs Remi Rosière, Nathalie Wauthoz and Karim Amighi at the Free University of Brussels (Belgium)). A brief summary of this work was included in this thesis for work completeness. With direct support from our industrial sponsor, dry powders with median particle size (D_{50}) < 5 μm for inhalation of the protein-polymer complexes were fabricated using a standard spray drying procedures. Results showed that the complexation protects the powder morphology on subsequent exposure to spraying, and B_{12}-targeted complexes can be released from dry powders formulations under aqueous conditions, to then be internalised by the epithelial

cells.

In vivo studies showed that the complexes did not induce an increased production of pro-inflammatory cytokines in chronic, repeated administration *via* endotracheal route studies over 3 weeks in heathy mice. Furthermore, no changes in cell count of alveolar macrophages, polymorphonuclear neutrophils and lymphocytes, relative to untreated control, were observed that would indicate development of an inflammation process in the lung. Hence, toxicity data demonstrated that PEG-*b*-pGA polymers based formulations are well tolerated in the lungs following chronic treatments, with no significant toxicity or lung inflammation indications. Additionally, the deposition data showed prolonged lung retention of the protein cargo at 14 hours after administration for targeted B_{12}-PEG-*b*-pGA:protein complexes, relative to non-targeted or 'free' protein formulations.

Taken together, these results strongly indicate that vitamin B_{12}-PEG-*b*-pGA copolymers have a potential as a new class of targeted 'excipients' for inhalation delivery of protein drugs to the lungs. To the best of our knowledge, this is the first example of ligand-targeted polymer-protein ionic complexes used for intracellular delivery of complexed protein. Despite the advantages offered by ligand targeted delivery, we have demonstrated the importance of different variables that must be considered during study design such as: the degree of receptor expression and whether the ligand is internalised

or not.

To expand the application of this delivery system, the use of a different targeting ligand in PEG-*b*-pGA complexing polymers was explored. Studies have suggested a potential use of another essential vitamin – biotin – as an alternative ligand suitable for cellular endocytosis targeting. Biotin receptor has been found overexpressed in cancer cells, relatively more than folate or vitamin B_{12} receptors; and biotin has been investigated as ligand for targeted delivery of nano-systems and prodrugs (Bhuniya *et al.* 2014; Santra *et al.* 2011). Furthermore, this vitamin is a promoter of cell growth in many cell types which does not limit this delivery system only to target cancer cells (Yang *et al.* 2009). This inspired the work in chapter 4 of the thesis to assess if biotin could be utilised for attachment to and targeting of PEG-*b*-pGA copolymer-based delivery systems.

To this aim we synthesised two biotin conjugated PEG_{2k}-*lin*-poly(glutamic acid) linear copolymers, with either 10 or 60 glutamic acid repeating units using commercially available Biotin-PEG_{2k}-amine suitable to act as a macroinitiator for *N*-carboxyanhydrides (NCA) ring opening polymerisation using the same principle as before with the B_{12} targeted B_{12}-PEG-*b*-pGA polymer synthesis. By varying the temperature during experiments, different glutamic acid repeating units were achieved. These were then used to assemble polymer–protein complexes and *in vitro* experiments were carried out to test

the ability of both polymers in aiding cellular uptake, exploiting the effect of different surface ligand densities. The difference of ligand surface density on nanoparticles was previously proven to effect cell receptor interaction with the ligand hence cellular internalisation of the nanoparticle (Moradi *et al.* 2012).

Flow cytometry data demonstrated statistically significant increased cellular internalisation by biotin receptor positive A549 cells of biotin-PEG_{2k}-*b*-$GA_{10/30}$:lysozyme nanocomplexes relative to non-biotin $mPEG_{2k}$-*b*-GA_{30}:lysozyme complexes or 'free' Cy5-lysozyme. Interestingly, no increased cellular internalisation was seen for the biotin-PEG_{2k}-*b*-$GA_{60/30}$:lysozyme nanocomplexes which has 6 times lower surface ligand density compared to biotin-PEG_{2k}-*b*-$GA_{10/30}$:lysozyme, indicating the importance of surface ligand density at decorating nanocomplexes for cellular recognition and delivery. Further studies would be required using a series of biotin-conjugated and non-conjugated PEG_{2k}-*b*-GA copolymers in order to define what may be the optimised formulation in respect to cellular internalisation, such as previous study on folate targeted nanoparticles (Moradi *et al.* 2012).

In the uptake experiment carried out in A549 cells, excess of either biotin or pantothenic acid, two known biotin receptor ligands, was employed in a competitive experiment with biotin-PEG_{2k}-*b*-$GA_{10/30}$:lysozyme complexes. Notably, cellular internalisation of

biotin-targeted complexes decreased significantly ($p < 0.0001$ or $p < 0.01$) in the presence of excess of 'free' biotin or 'free' pantothenic acid competitive ligands, respectively. The data would hence indicate a prominent role that biotin transport mechanism has in the internalisation of biotin-PEG_{2k}-*b*-$GA_{30/10}$:lysozime complexes by A459 cells. The current result parallels previous findings on the increase in uptake of vitamin B_{12} targeted protein complexes based on B_{12}-PEG_{2k}-*b*-GA copolymers compared to non-targeted complexes and non-complexed proteins (Nieto-Orellana *et al.* 2019) and further consolidates the utility of the PEG-*b*-pGA copolymers as a potential delivery system by forming non-covalent complexes with protein. As literature suggests that biotin receptors are overexpressed at higher levels compared to the folate and/or vitamin B_{12} receptors in many cancer cells (Santra *et al.* 2011; Bhuniya *et al.* 2014), this also widen the potential application of the current delivery system.

In addition to quantitative flow cytometry analysis, cellular internalisation of biotin-PEG_{2k}-*b*-$GA_{10/30}$:lysozyme complexes were visualised by confocal microscopy; images indicates that the labelled protein were indeed within cell cytoplasm and tend to be in close proximity of the nucleus. Further studies will be required to fully characterise the intracellular trafficking of these complexes, and co-localisation with specific organelles.

The stability data of B_{12}-PEG-*b*-pGA:lysozyme complex in cell culture

medium shown in Chapter 3 indicated the dissociation of nanocomplex to small extent over 3 h under cell culture condition. This prompted the investigation to assess if biotin-PEG_{2k}-*b*-GA_{10} that is fundamentally similar to the B_{12}-PEG_{2k}-*b*-GA_{30} complexes with lysozyme enter the cells as integral species, i.e. if the copolymers used in the complexation enter the cell together with the complexed protein. To this end, streptavidin-biotin interaction was exploited (Chivers *et al.* 2011); Alexa 488-labelled streptavidin was applied after polymer-protein were internalized by A549 cells and expected to bind to the exposed biotin from biotin-PEG_{2k}-*b*-GA_{10} copolymer used to complex lysozyme, hence provide information on the copolymer intracellular localisation.

The analysis of confocal images confirmed the intracellular presence of both labelled species; Cy5 lysozyme and Alexa 488 labelled streptavidin - the latter pointing to the intracellular localisation of biotin-PEG_{2k}-*b*-GA_{10} copolymer. Co-localisation analysis of the two fluorescently labelled entities using Pearson's correlation coefficient was performed on several confocal images and resulted in *r* value of ~ 0.5. The Pearson coefficient value of 0.5 indicates a positive relationship between the location of the labelled lysozyme and 'streptavidin detected' biotin-PEG_{2k}-*b*-GA_{10}. This finding indicated that at 1 h after the complexes were applied to, and internalised by the cells, the protein and biotin-PEG_{2k}-*b*-GA_{10} copolymers were co-localised. Taken together the data would indicate that biotin-PEG_{2k}-

b-$GA_{10/30}$ complexes with lysozyme enter A549 cells as integral species, with a prominent role of receptor mediated endocytosis in the process.

To the best of our knowledge this is the first study attempting to assess the intracellular location of polymers used in formation of targeted ionically interacting nanocomplexes, and their co-localisation with delivered cargo. Comparing to other studies that observed uptake of fluorescently labelled drugs or molecules in cells, the target agents were commonly chemically linked (*via* covalent linker) to the drug or molecule (Chen *et al.* 2010; Jung *et al.* 2014; Santra *et al.* 2011). The studies herein demonstrated that biotin-PEG_{2k}-*b*-$GA_{30/10}$:lysozyme nanocomplexes were internalised by A549 cells, driven by biotin receptor recognition *via* endocytosis mechanism. In a broader sense, the co-localisation study of polymer biotin-PEG_{2k}-*b*-GA_{10} and protein lysozyme in cells provided support that dynamically interacting complexes can maintain complex formation in biological environment enabling its cellular internalisation as intact entities. Taken together the study in Chapter 4 successfully provided an extension of the applicability of the PEG-*b*-pGA group of copolymers at delivering protein cargo to different cell types exploring targeting ligand approach to different receptor targets.

These promising preliminary results encouraged us for further *in*

vitro investigation in understanding the cellular internalisation mechanism that might be responsible for targeted polymer-protein complex uptake. Studies have demonstrated that ligand targeted formulations may not utilise the designated ligand-directed pathway, which means that some trafficking pathways can be pursued by synthetic nanoparticles in ways that differ from the transport activated by the ligand functionality alone (Tekle *et al.* 2008; Sayers *et al.* 2018). After extensive literature review, no known studies have investigated the endocytosis mechanisms of nanocomplex formed *via* self-assembled systems or exploring the difference regarding cellular internalisation of ligand targeted nanocomplex to non-targeted nanocomplex.

Studying the molecular and functional basis of endocytic mechanisms have important implications for the design of therapeutic delivery systems to improve therapy potentials, it provides basic concepts for improving the design parameters of delivery systems to improve efficiency and specificity of drug delivery (Sahay *et al.* 2013). In order to predict the success of the formulation, it is important to understand the cellular internalisation and their processing mechanisms of the delivery system in order to achieve efficient cellular uptake and avoid the destructive or recycling cellular pathways (Vranic *et al.* 2013). Therefore, work was carried out to probe the mechanisms of entry into the cells of targeted biotin-PEG_{2k}-*b*-$GA_{10/30}$:lysozyme nanocomplexes, and

whether it significantly differs to free lysozyme or non-targeted mPEG$_{2k}$-*b*-GA$_{30}$:lysozyme nanocomplexes. In this respect, a panel of pharmacological inhibitors was used to investigate which endocytic mechanisms were responsible for cellular uptake of the mentioned nanoparticles.

Dynamin functioning as a pair of molecular scissors for newly formed vesicles originating from the plasma membrane was found to play a major role in the uptake of all 3 nanomaterials, with lysozyme predominantly taken up via the clathrin mediated pathway while mPEG$_{2k}$-*b*-GA$_{30}$:lysozyme and biotin-PEG$_{2k}$-*b*-GA$_{10/30}$:lysozyme preferred the caveolae-mediated pathway; inhibiting the caveolae pathway had higher impact on the uptake of targeted biotin-PEG$_{2k}$-*b*-GA$_{10/30}$:lysozyme nanocomplexes. Further work can be carried out in the future to consolidate current findings, such as the use of molecular biological approaches include the use of dominant-negative mutants and RNA interference technology to compete with and downregulate the expression of endogenous proteins involved in specific endocytosis pathways. Overall, this work revealed a relatively unexplored route of polymer-protein complex cell internalisation and improved understanding of switching of cellular endocytosis mechanism due to cellular receptor involvement, with a potentially important impact in the area of mucosal delivery of nanocomplexes.

The promising results obtained from using PEG-*b*-pGA copolymer delivery system successfully complexing and delivering model protein lysozyme to epithelial cells *in vitro* and *in vivo* pave the way for further investigations, wherein the PEG-*b*-pGA copolymers can be used to deliver therapeutic drugs and maintain or improve the therapeutic effect. Furthermore, it was envisaged that the PEG-*b*-pGA copolymer delivery systems could potentially be applied not only to proteins but also small molecule therapeutics formulated in nano-sized entities, as long as they present a sufficient number of charged functionalities, which was explored the final chapter of this thesis.

After careful consideration, colistin, a member of the polymyxin family of antibiotics was chosen based on its amine group rich structure enabling electrostatic interaction with our polyanionic complexing polymers. Due to the emergence of drug-resistant Gram-negative bacteria coupled with scarce new antibiotics development, clinical interest in polymyxins has been growing over the last two decades (Nation *et al.* 2015). In clinical setting, colistin is commonly administered as CMS prodrug due to its lower toxicity, however CMS has reduced antibacterial activity compared to native colistin at the same concentration (Li *et al.* 2001; Bergen *et al.* 2006). The aim of the current work was to design a polymeric delivery system for colistin with similar, or ideally improved, antibacterial properties and better safety profile compared to current therapies.

The first task in this investigation was to establish and optimise a protocol for the complexation conditions between $mPEG_{2k}$-*b*-GA_{30} copolymer and colistin. This was achieved by optimisation of the formulation conditions, including the charge ratio between colistin to polymer and the buffer ionic strength used for complex formation. Later, colistin was successfully formulated into nanocomplexes with $mPEG_{2k}$-*b*-GA_{30} copolymer and complexation was confirmed by agarose electrophoresis and transmission electron microscopy. The polyelectrolyte nature of the complexes was probed and proved in a series of experiments in different ionic strength buffers; 10 mM phosphate buffer and phosphate buffer saline. These experiments also illustrated that the nanocomplexes retain their integrity in 10 mM phosphate buffer and phosphate buffer saline after 7 days storage at 4°C, with a higher population of free colistin in the latter buffer. In *in vitro* cell culture, free colistin and the nanocomplexes did not negatively impact lung epithelial A549 cell viability up to the highest concentration tested of 4 µg/mL. It is noted that a full toxicity study was beyond the scope of this study and this would require testing on different cell lines, particularly models of renal and neurological toxicities.

Colistin displays *in vitro* activity against gram-negative bacteria such as *A. baumannii*, *P. aeruginosa*, *K. pneumoniae*, and *E. coli* (Li *et al.* 2005). *Escherichia coli* (*E. coli*) has a biosafety level of II and can be handled in our laboratory; hence was chosen in this study.

Colistin:mPEG$_{2k}$-*b*-GA$_{30}$ complexes at different charge ratios were applied to E. coli and compared to free colistin. All *in vitro* antimicrobial activity tests on both pathogenic E2348/69 and non-pathogenic XL1 *E. coli* strains suggested colistin formulated into colistin:mPEG$_{2k}$-*b*-GA$_{30}$ *r* = 1:2 nanocomplexes possess enhanced bacteriostatic effect in non-pathogenic *E. coli* XL1 and bactericidal activity in pathogenic *E. coli* E2348/69 compared to free colistin applied at the same concentration. It should be noted that colistin:mPEG$_{2k}$-*b*-GA$_{30}$ *r* = 1:2 formulation shows enhanced bactericidal effect in EPEC E2348/69 infection of HeLa cells, compared to free colistin by killing extra 2 logs of EPEC after 2 h treatment. The possible contribution to this effect may be arising from an increased 'local concentration' of the colistin that may be created by the complexes. Namely mPEG$_{2k}$-*b*-GA$_{30}$ polymer used in this study contains 30 repeating units of glutamic acid, which complex with 5 positive charges on colistin surface at physiological pH. For the complexes prepared at the molar charge ratio between colistin and mPEG$_{2k}$-*b*-GA$_{30}$ of 1:2, this equates to 3 colistin molecules *per* polymer chain. This could create, in a close proximity to the bacterial surface, an increased local concentration of colistin, compared to free colistin in solution. This local microenvironment with higher colistin concertation may in turn facilitate higher local effect of colistin on bacterial surface and LPS structure leading to higher antibacterial activity.

The low toxicity of the colistin nanocomplex to lung cells and improved antimicrobial activity may pave the path for the testing of this formulation as a viable drug candidate for lung administration to treat respiratory infections. In addition, the self-assembly nature of the nanocomplex formulation and the absence of further chemical manipulation for release is also highly beneficial.

Further work is needed to investigate the disassembly of the complexes in physiological conditions and to consider the potential interactions of between the complex and pulmonary biomolecules, e.g. secretory mucin in sputum or epithelial mucin that lines airways at reducing free drug levels. Overall, although further evaluation is needed to determine whether this activity profile extends to other Gram-negative species, we believe that due to the enhanced antimicrobial effect without the increase in toxicity, colistin:mPEG$_{2k}$-*b*-GA$_{30}$ nanocomplex has the potential to become a safer and more effective alternative to colistin and its derivatives.

In conclusion it could be said that the results obtained so far, clearly point out that these PEG-*b*-pGA polymers are highly suitable to complex and facilitate the delivery of protein to epithelial cells. With the addition of targeting ligands, delivery of proteins was enhanced, and evidence shown a receptor mediated endocytosis route for the polymer-protein complexes for both B_{12} and biotin. Finally, it is important to note that, the applicability of the PEG-*b*-pGA polymer

delivery system could be easily directed towards complexing small molecule drug. With the use of antibiotic drug colistin in this thesis, complexation between PEG-*b*-pGA polymer and colistin provided higher antibiotic effectiveness compared to free colistin.

Appendix

1. Supporting information

1.1. Chapter 3

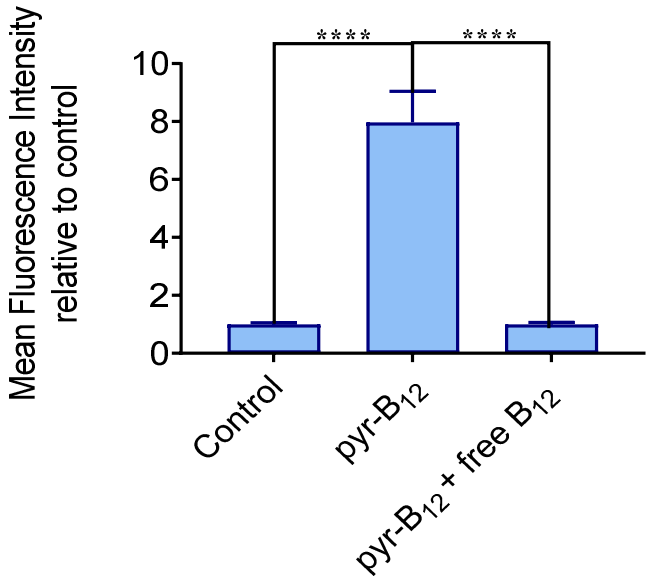


Figure S1 *Cellular internalization of pyr-B_{12} fluorescent probe by Caco-2 the presence or absence of free B_{12} competitive ligand, as assessed by flow cytometry. Control: untreated Caco-2 cells. One-way ANOVA was used for statistical analysis. *P ≤ 0.05, **P ≤ 0.01, ***P ≤ 0.001, **** P ≤ 0.0001. λ_{ex} : 401 nm and λ_{em} : 421 nm. Caco-2 cells are known to express both cubilin (Aseem, Barth et al. 2013) and TCN2 B_{12} (Bose, Seetharam et al. 1997) receptors, and 'free' B12 is a competitor to both transport mechanism. The error bar shown is the standard deviation of the mean. (N=3, n=3).*

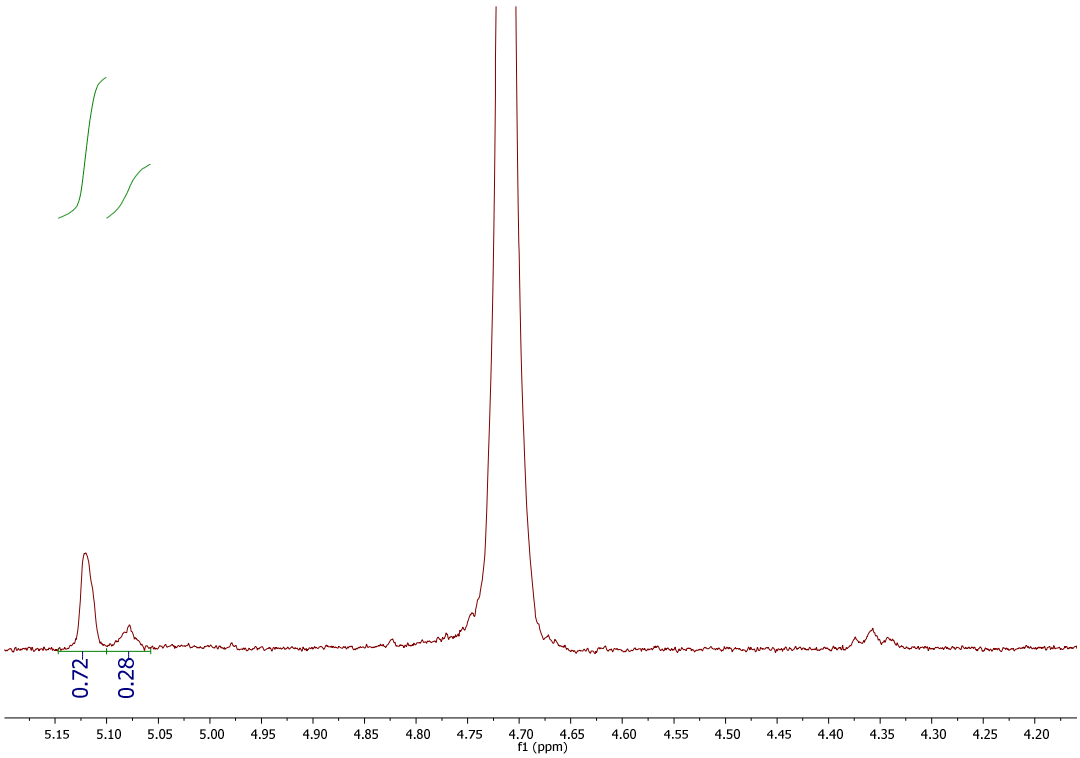


Figure S2 *^{1}H NMR spectrum of $mPEG_{2k}$-b-poly(glutamic acid)$_{30}$ in chloroform during the polymerisation on day 5, conversion were determined following the disappearance of the α-CH proton signal of the NCA monomer at 5.1 ppm.*

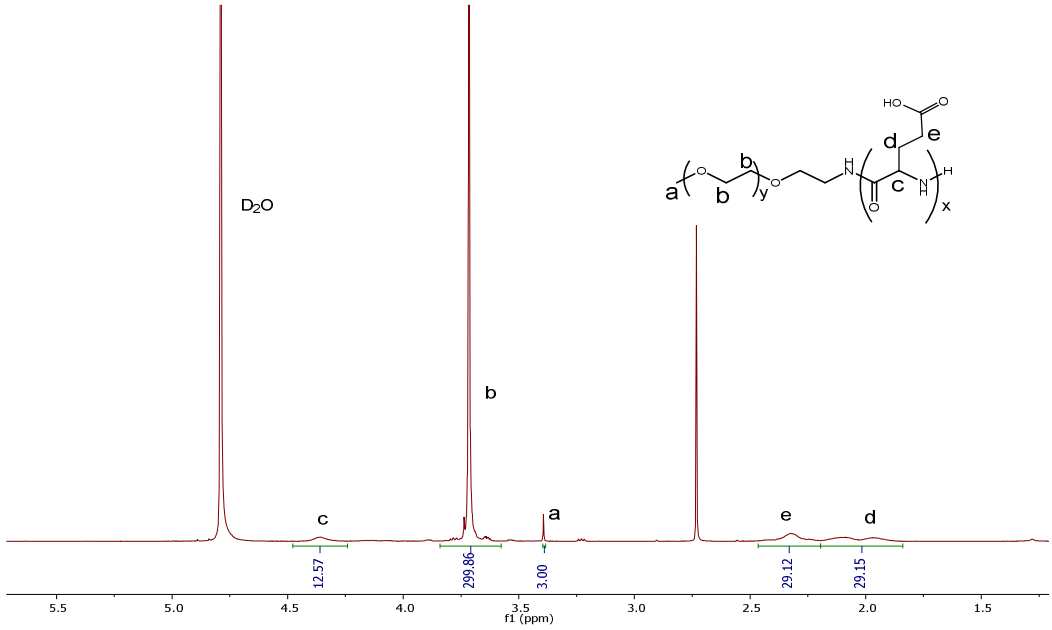


Figure S3 *^{1}H NMR spectrum of linear $mPEG_{2k}$-b-GA_{12} copolymer in D_2O.*

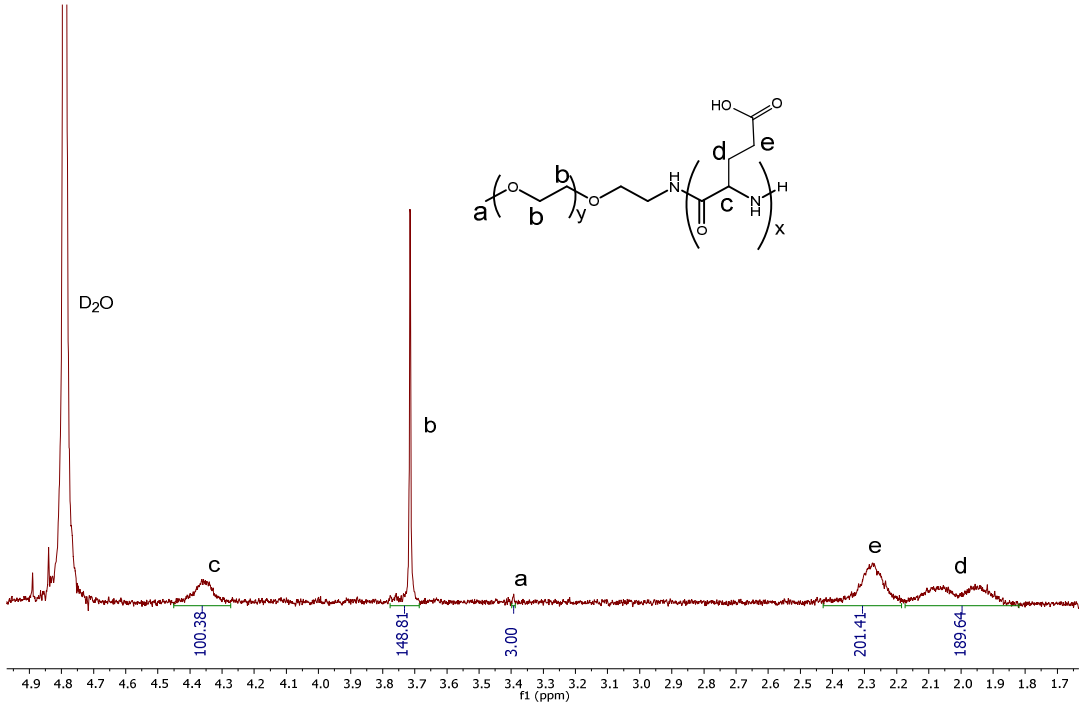


Figure S4 *^{1}H NMR spectrum of linear mPEG$_{2k}$-b-GA$_{100}$ copolymer in D$_2$O.*

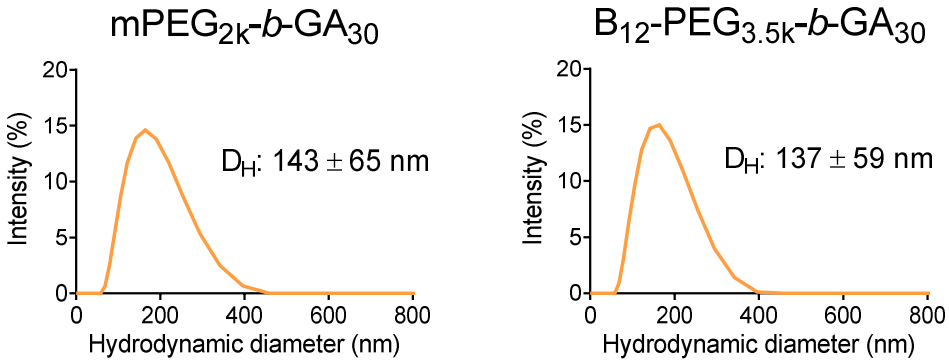


Figure S5 *Particle size distribution of lysozyme complexes assembled from non-targeted mPEG$_{2k}$-lin-GA$_{30}$ and B$_{12}$-PEG$_{3.5k}$-b-GA$_{30}$ as assessed by dynamic light scattering (DLS). B$_{12}$-PEG$_{3.5k}$-b-GA$_{30}$ refer to complexes assembled with 15:85 molar charge ratio of B$_{12}$-PEG$_{3.5k}$-b-GA$_{30}$ and mPEG$_{2k}$-b-GA$_{30}$ complexing copolymers. D$_H$ is the average hydrodynamic diameter (± SD) of polymer-protein complexes.*

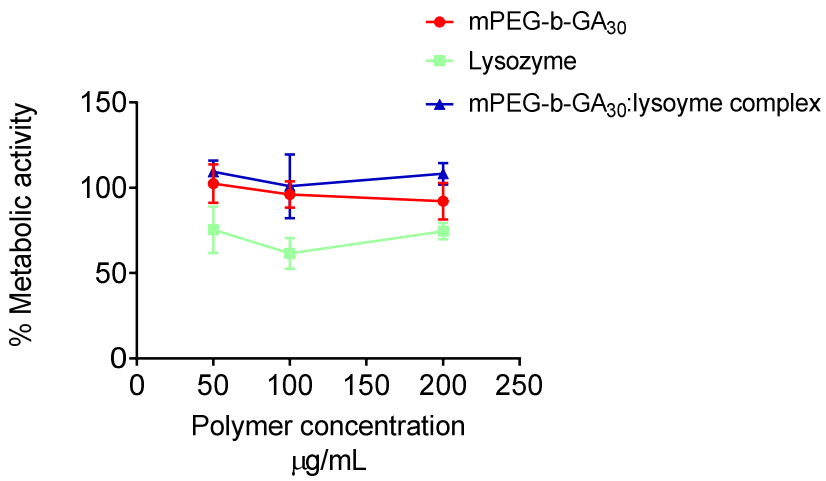


Figure S6 *Metabolic activity, as assessed by MTS assay, of Calu-3 cells after 4 h of treatment with different concentration of free polymer $mPEG_{2k}$-b-GA_{30}, free protein lysozyme and $mPEG_{2k}$-b-GA_{30}:lysozyme nanocomplexes. The error bar shown is the standard deviation of the mean. (N=3, n=3).*

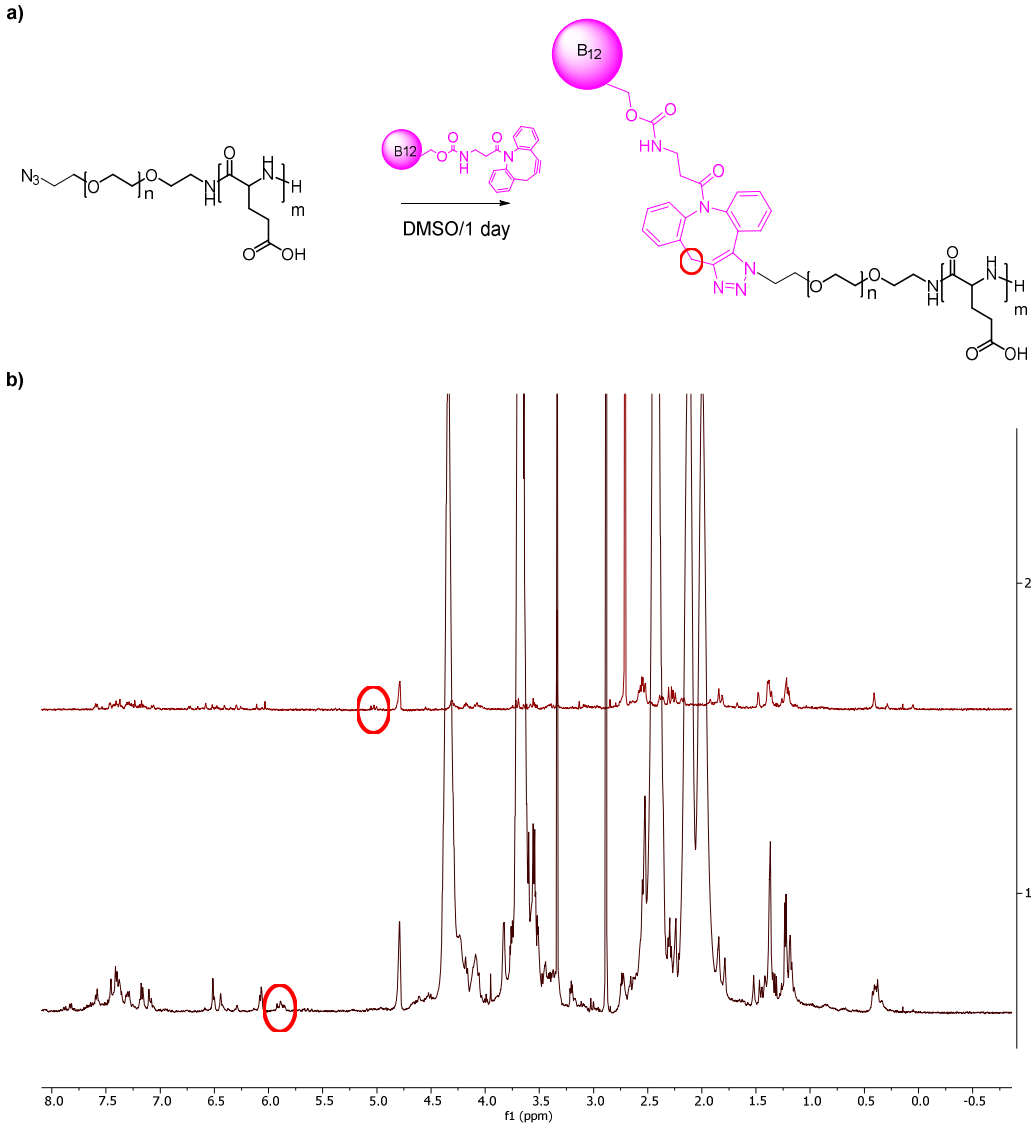


Figure S7 *Synthesis of B_{12}-$PEG_{3.5k}$-b-pGA a) reaction scheme b) ^1H NMR spectra of α-dibenzocyclooctyne-vitamin B_{12} starting material (top) and B_{12}-$PEG_{3.5k}$-b-pGA (bottom) in D_2O.*

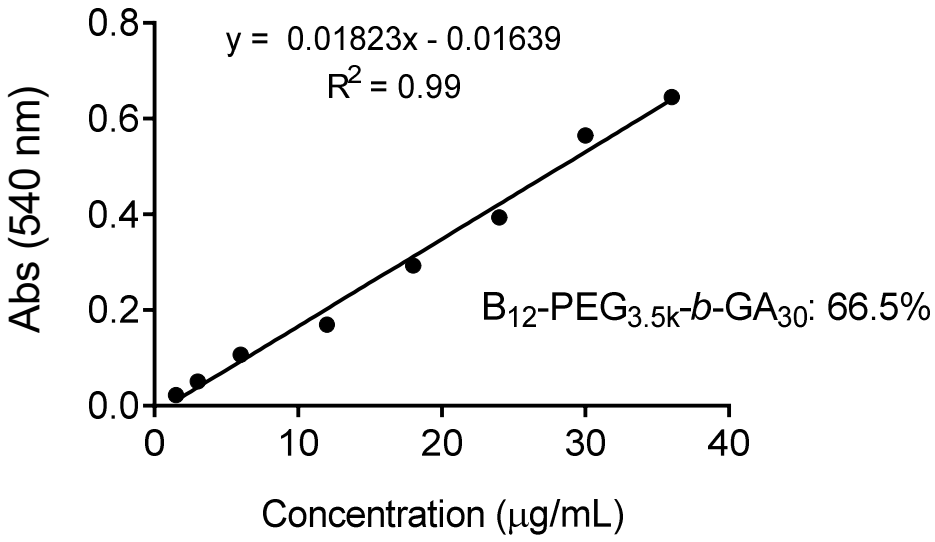


Figure S8 *Efficiency (%) of attachment of DBCO-B_{12} to azide-functional linear $mPEG_{3.5k}$-b-GA_{30} copolymer, was calculated by UV-vis analysis (λ = 540 nm), using deionised water as the solvent. The figures show the calibration curve utilised for this calculation, which was built using cyanocobalamin (B_{12}) solutions of known concentration.*

2.1. Chapter 4

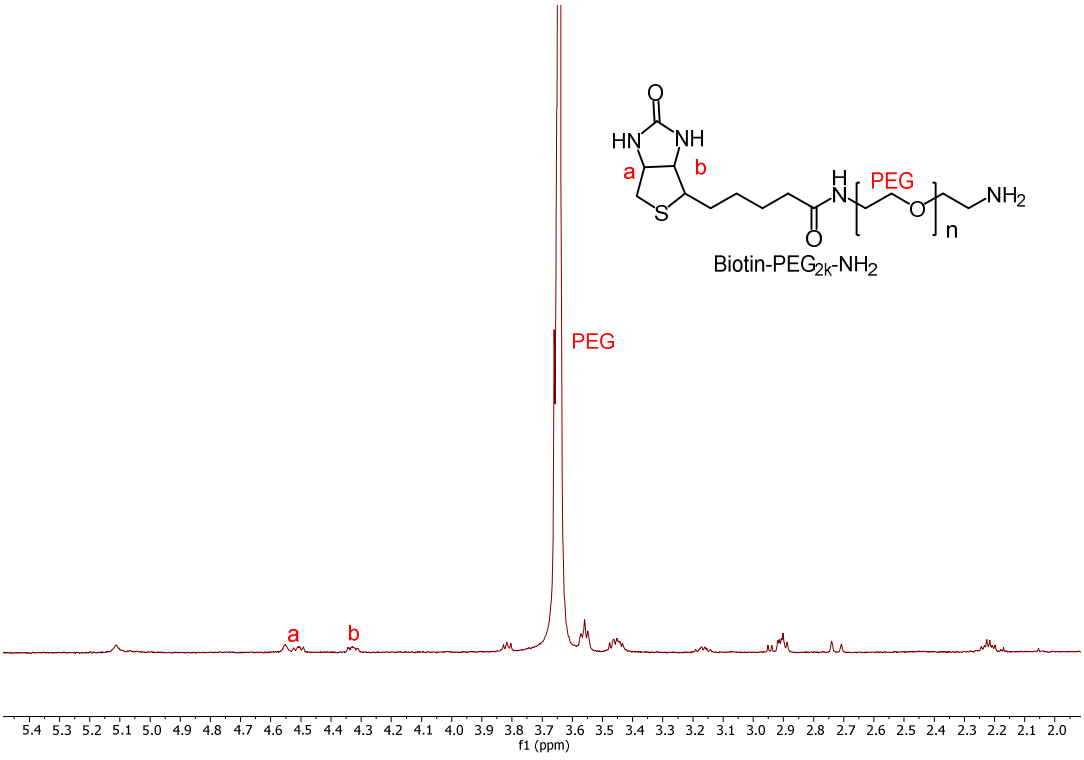


Figure S9. *^{1}H NMR spectrum of Biotin-PEG_{2k}-amine starting material in $CDCl_3$.*

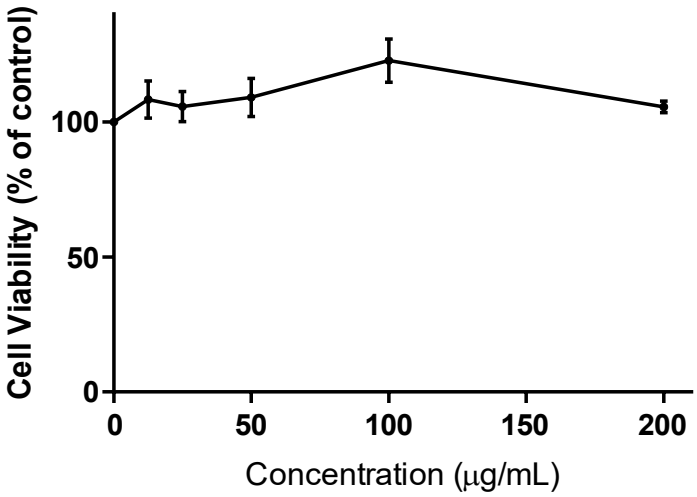


Figure S10 *MTS assay in A549 cells after 4 hours treatment with biotin-PEG$_{2k}$-b-GA$_{10/30}$: lysozyme nanocomplexes at r ratio of 2.5. Nanocomplexes with lysozyme concentration from 25 – 200 μg/mL were tested. The error bar shown is the standard deviation of the mean. (N=3, n=3).*

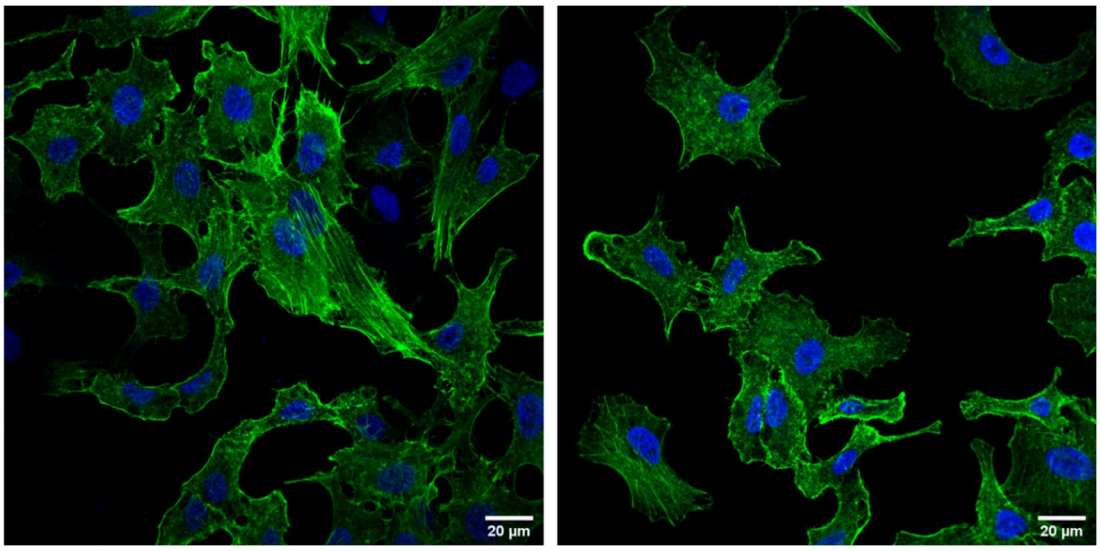


Figure S11. *Confocal microscopy images of A549 lung epithelial cells stained with actin cytoskeleton stain (green) and nuclear stain (DAPI, blue). On the left the cells were fixed using formaldehyde and on the left the cells were fixed and subsequently permeabilised using triton X before staining. Scale bars correspond to 20 μm.*

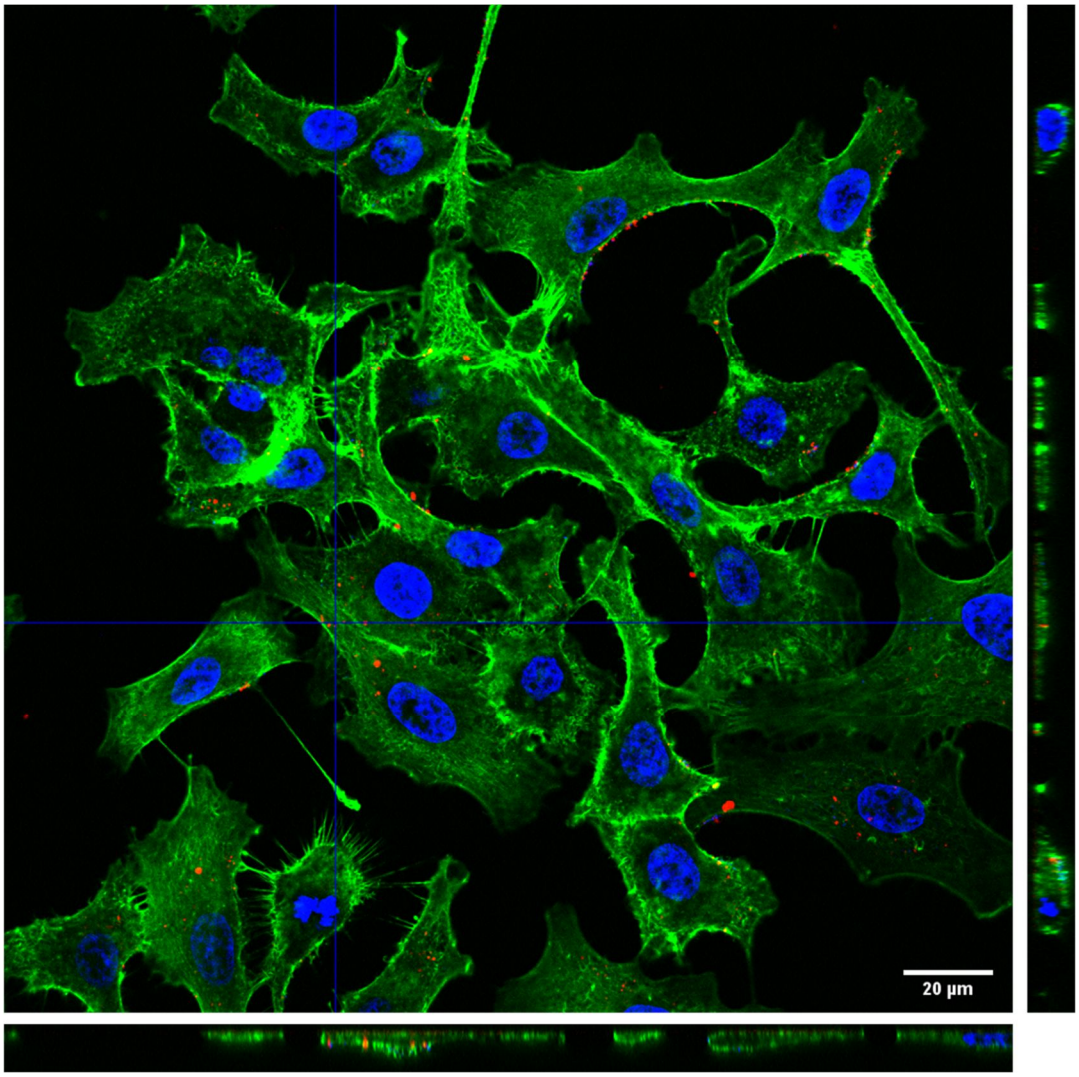


Figure S12. *Orthogonal view from different planes (x/y, x/z or y/z) of the confocal microscopy images of A549 lung epithelial cells incubated with 10 µg/mL 'free' lysozyme for 1 h, followed by a subsequent application of actin staining in fixed and permeabilized cells. Labelled protein (cy5-lysozyme, red); actin cytoskeleton stain (green) and nuclear stain (DAPI, blue). Scale bars correspond to 20 µm.*

3.1. Chapter 6

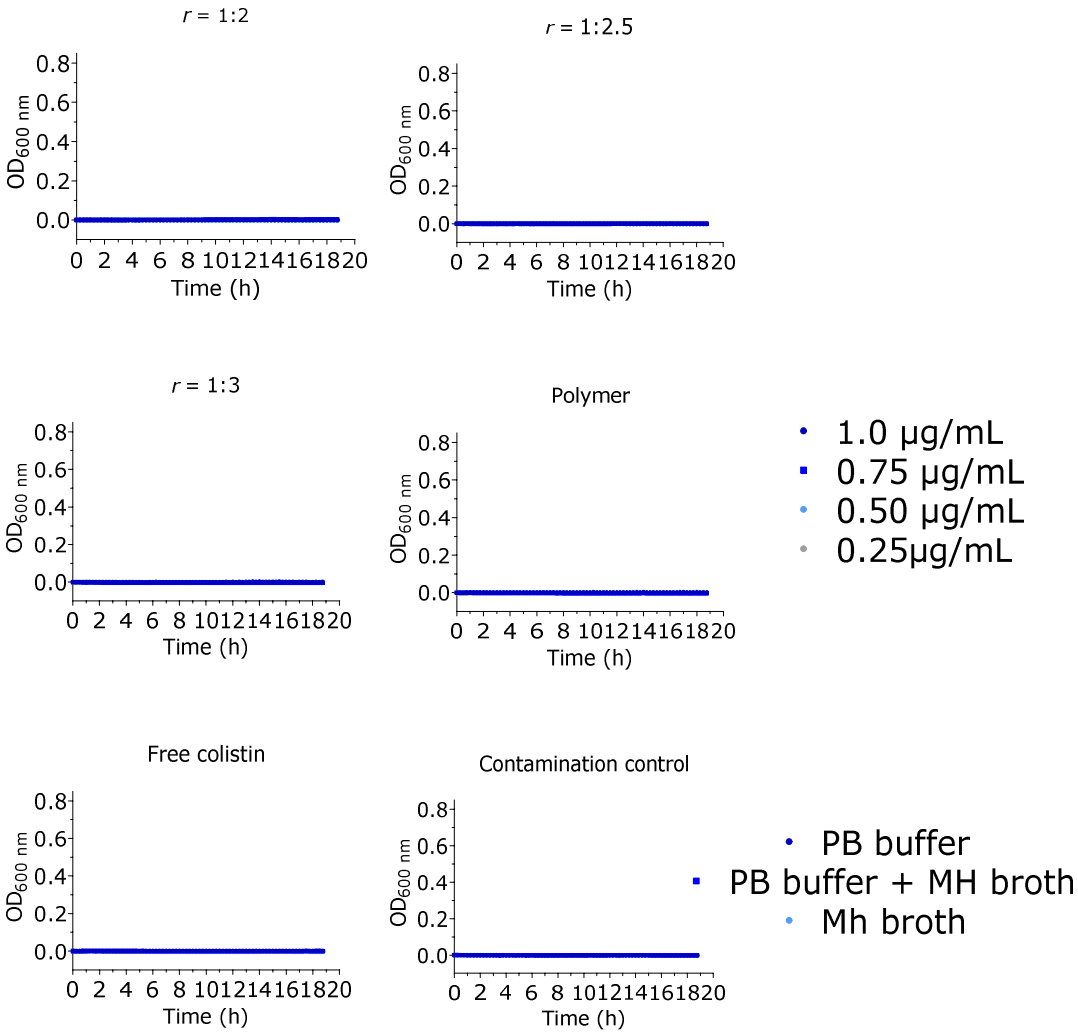


Figure S13. *Growth curves of E. coli XL1 bacteria on application of different control samples (as per Figure 6.9) measured by reading OD_{600} as a function of time. 'Contamination control' denotes OD_{600} of Mueller-Hinton broth over time without presence of bacteria.*

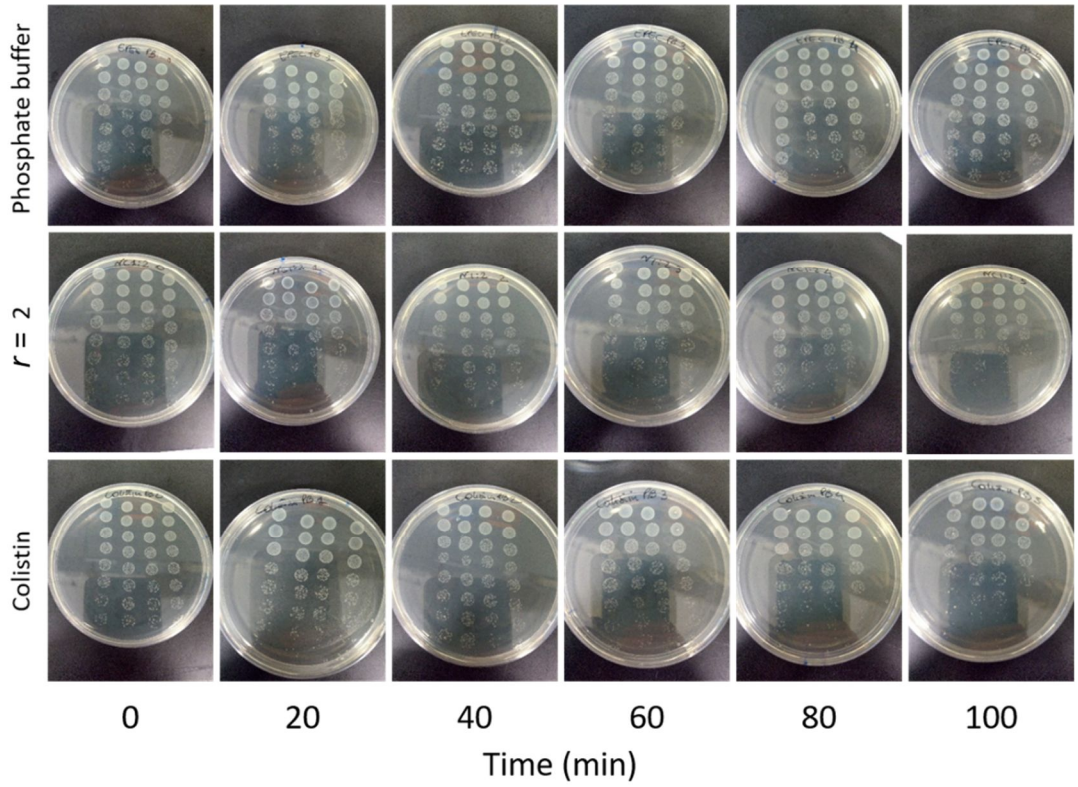


Figure S14. *Enteropathogenic Escherichia coli E2348/69 time kill curve plate layout showing colony forming units following treatment with colistin or colistin:mPEG$_{2k}$-b-GA$_{30}$ r = 2:1 nanocomplexes. The samples were serially diluted and plated onto agar plates and incubated at 37 °C. Control = 10 mM Phosphate buffer used to make nanocomplexes.*

References

Abuchowski, Van Es, Palczuk and Davis. 1977. 'Alteration of immunological properties of bovine serum albumin by covalent attachment of polyethylene glycol', *Journal of Biological Chemistry*, 252: 3578-81.

Agarwal, Iezhitsa, Agarwal, Abdul Nasir, Razali, Alyautdin and Ismail. 2016. 'Liposomes in topical ophthalmic drug delivery: An update', *Drug Delivery*, 23: 1075-91.

Agu, Ugwoke, Armand, Kinget and Verbeke. 2001. 'The lung as a route for systemic delivery of therapeutic proteins and peptides', *Respiratory Research*, 2: 198-209.

Ahmed, Velkov, Lin, Yun, Nowell, Zhou, Zhou, Chan, Azad and Li. 2017. 'Potential toxicity of polymyxins in human lung epithelial cells', *Antimicrobial Agents and Chemotherapy*, 61: e02690-16.

Ainsworth, Brown and Brownlee. 1947. 'Aerosporin, an antibiotic produced by bacillus aerosporus greer', *Nature*, 159: 263.

Alama, Kusamori, Morishita, Katsumi, Sakane and Yamamoto. 2019. 'Mechanistic studies on the absorption-enhancing effects of gemini surfactant on the intestinal absorption of poorly absorbed hydrophilic drugs in rats', *Pharmaceutics*, 11: 170.

Alconcel, Baas and Maynard. 2011. 'Fda-approved poly(ethylene glycol)–protein conjugate drugs', *Polymer Chemistry*, 2: 1442-48.

Aleandri, Bandera, Mezzenga and Landau. 2015. 'Biotinylated cubosomes: A versatile tool for active targeting and codelivery of paclitaxel and a fluorescein-based lipid dye', *Langmuir*, 31: 12770-76.

Alexander and Rietschel. 2001. 'Bacterial lipopolysaccharides and innate immunity', *Journal of Endotoxin Research*, 7: 167-202.

Alkilany, Zhu, Weller, Mews, Parak, Barz and Feliu. 2019. 'Ligand density on nanoparticles: A parameter with critical impact on nanomedicine', *Advanced Drug Delivery Reviews*, 143: 22-36.

Allen and Waclaw. 2019. 'Bacterial growth: A statistical physicist's guide', *Reports on progress in physics Physical Society (Great Britain)*, 82: 016601-01.

Alon, Bayer and Wilchek. 1993. 'Cell adhesion to streptavidin via rgd-dependent integrins', *European Journal of Cell Biology*, 60: 1-11.

Al-Qadi, Grenha, Carrión-Recio, Seijo and Remuñán-López. 2012. 'Microencapsulated chitosan nanoparticles for pulmonary protein delivery: In vivo evaluation of insulin-loaded formulations', *Journal of Controlled Release*, 157: 383-90.

Alshehri, Grabowska and Stolnik. 2018. 'Pathways of cellular internalisation of liposomes delivered sirna and effects on sirna engagement with target mrna and silencing in cancer cells', *Scientific Reports*, 8: 3748.

Ambrosio, Barattin, Bersani, Shubber, Uddin, Van Der Walle, Caliceti and Salmaso. 2016. 'A novel combined strategy for the physical pegylation of polypeptides', *Journal of Controlled Release*, 226: 35-46.

Anand, Kunnumakkara, Newman and Aggarwal. 2007. 'Bioavailability of curcumin: Problems and promises', *Molecular Pharmaceutics*, 4: 807-18.

Antonik, Eissa, Round, Cameron and Crowley. 2016. 'Noncovalent pegylation via lectin-glycopolymer interactions', *Biomacromolecules*, 17: 2719-25.

Apfelthaler, Anzengruber, Gabor and Wirth. 2017. 'Poly – (l) – glutamic acid drug delivery system for the intravesical therapy of bladder cancer using wga as targeting moiety', *European Journal of Pharmaceutics and Biopharmaceutics*, 115: 131-39.

Armstrong, Elliott, Ford, Gadsdon, Mccarthy, Rostron and Worsley. 1996. 'Poly-(d,l-lactic acid) microspheres incorporating histological dyes for intra-pulmonary histopathological investigations', *Journal of Pharmacy and Pharmacology*, 48: 258-62.

Aseem, Barth, Klatt, Smith and Argraves. 2013. 'Cubilin expression is monoallelic and epigenetically augmented via ppars', *BMC Genomics*, 14: 405.

Aseem, Obaidullah, Jeremy L. Barth, Sandra C. Klatt, Brian T. Smith and W. Scott Argraves. 2013. 'Cubilin expression is monoallelic and epigenetically augmented via PPARs', *BMC genomics*, 14: 405-05.

Atkinson andreu and Vicent. 2018. 'Polymer therapeutics: Biomarkers and new approaches for personalized cancer treatment', *Journal of personalized medicine*, 8: 6.

Ayame, Morimoto and Akiyoshi. 2008. 'Self-assembled cationic nanogels for intracellular protein delivery', *Bioconjugate Chemistry*, 19: 882-90.

Azarmi, Roa and Lobenberg. 2008. 'Targeted delivery of nanoparticles for the treatment of lung diseases', *Advanced Drug Delivery Reviews*, 60: 863-75.

Baek, Kim, Lee, Rhim, Eo and Kim. 2013. 'The cholesterol-binding antibiotic nystatin induces expression of macrophage inflammatory protein-1 in macrophages', *Biomolecules & Therapeutics*, 21: 42-48.

Bailey and Berkland. 2009. 'Nanoparticle formulations in pulmonary drug delivery', *Medicinal Research Reviews*, 29: 196-212.

Bajracharya, Song, Back and Han. 2019. 'Recent advancements in non-invasive formulations for protein drug delivery', *Computational and Structural Biotechnology Journal*, 17: 1290-308.

Baker, Reynolds, Lumicisi and Bryson. 2010. 'Immunogenicity of protein therapeutics: The key causes, consequences and challenges', *Self Nonself*, 1: 314-22.

Bannunah, Vllasaliu, Lord and Stolnik. 2014. 'Mechanisms of nanoparticle internalization and transport across an intestinal epithelial cell model: Effect of size and surface charge', *Molecular Pharmaceutics*, 11: 4363-73.

Bayer and Wilchek. 1980. 'The use of the avidin-biotin complex as a tool in molecular biology', *Methods of Biochemical Analysis*, 26: 1-45.

Behnke, Tranum-Jensen and Van Deurs. 1984. 'Filipin as a cholesterol probe. Ii. Filipin-cholesterol interaction in red blood

cell membranes', *European Journal of Cell Biology*, 35: 200-15.

Benoit, Stanton, Tartanian, Motzer, Mcgaughey, Bond and Brody. 2018. 'Functional and phylogenetic characterization of noncanonical vitamin b12–binding proteins in zebrafish suggests involvement in cobalamin transport', *Journal of Biological Chemistry*, 293: 17606-21.

Bergen, Li, Rayner and Nation. 2006. 'Colistin methanesulfonate is an inactive prodrug of colistin against pseudomonas aeruginosa', *Antimicrobial Agents and Chemotherapy*, 50: 1953-58.

Bertrand, Wu, Xu, Kamaly and Farokhzad. 2014. 'Cancer nanotechnology: The impact of passive and active targeting in the era of modern cancer biology', *Advanced Drug Delivery Reviews*, 66: 2-25.

Beule. 2010. 'Physiology and pathophysiology of respiratory mucosa of the nose and the paranasal sinuses', *GMC Current Topics in Otorhinolaryngology, Head and Neck Surgery*, 9: Doc07.

Beyerle, Braun, Banerjee, Ercal, Eickelberg, Kissel and Stoeger. 2011. 'Inflammatory responses to pulmonary application of pei-based sirna nanocarriers in mice', *Biomaterials*, 32: 8694-701.

Bhatia. 2015. 'Chapter 2 - plant tissue culture.' in Saurabh Bhatia, Kiran Sharma, Randhir Dahiya and Tanmoy Bera (eds.), *Modern applications of plant biotechnology in pharmaceutical sciences* (Academic Press: Boston).

Bhuniya, Maiti, Kim, Lee, Sessler, Hong and Kim. 2014. 'An activatable theranostic for targeted cancer therapy and imaging', *Angewandte Chemie, International Edition in English*, 53: 4469-74.

Biggar and Sturgess. 1977. 'Role of lysozyme in the microbicidal activity of rat alveolar macrophages', *Infection and Immunity*, 16: 974-82.

Biswas, Brunel, Dubus, Reynaud-Gaubert and Rolain. 2012. 'Colistin: An update on the antibiotic of the 21st century', *Expert Review of Anti-Infective Therapy*, 10: 917-34.

Bivas-Benita, Zwier, Junginger and Borchard. 2005. 'Non-invasive pulmonary aerosol delivery in mice by the endotracheal route', *European Journal of Pharmaceutics and Biopharmaceutics*, 61: 214-8.

Bose, Seetharam, Dahms and Seetharam. 1997. 'Bipolar functional expression of transcobalamin ii receptor in human intestinal epithelial caco-2 cells', *Journal of Biological Chemistry*, 272: 3538-43.

Bruno, Miller and Lim. 2013. 'Basics and recent advances in peptide and protein drug delivery', *Therapeutic Delivery*, 4: 1443-67.

Bui, Nicolas, Maksimenko, Desmaële and Couvreur. 2014. 'Multifunctional squalene-based prodrug nanoparticles for targeted cancer therapy', *Chemical Communications*, 50: 5336-38.

Bush, Nicholas, Pei, Kuipers, Cheng, Hamilton, Hegge, Li, Glebocka, Zhu, Chen, Kuehl, Schluep and Li. 2018. 'Targeting aenac with an epithelial rnai trigger delivery platform for the treatment of cystic fibrosis', *European Respiratory Journal*, 52: OA514.

Bustamante-Marin and Ostrowski. 2017. 'Cilia and mucociliary clearance', *Cold Spring Harbor Perspectives in Biology*, 9: a028241.

Cabral, Miyata, Osada and Kataoka. 2018. 'Block copolymer micelles in nanomedicine applications', *Chemical Reviews*, 118: 6844-92.

Canal, Sanchis and Vicent. 2011. 'Polymer--drug conjugates as nano-sized medicines', *Current Opinion in Biotechnology*, 22: 894-900.

Capel, Vllasaliu, Watts and Stolnik. 2016. 'Insight into the relationship between the cell culture model, cell trafficking and sirna silencing efficiency', *Biochemical and Biophysical Research Communications*, 477: 260-65.

Capel, Vllasaliu, Watts, Clarke, Luxton, Grabowska, Mantovani and Stolnik. 2018. 'Water-soluble substituted chitosan derivatives as technology platform for inhalation delivery of sirna', *Drug Delivery*, 25: 644-53.

Cefalu. 2004. 'Concept, strategies and feasibility of noninvasive insulin delivery', *Diabetes Care*, 27: 239-46.

Chakraborti, Sarkar, Pramanik and Chakraborti. 2017. 'Role of proteases in lung disease: A brief overview.' in, *Proteases in human diseases*.

Chalasani, Russell-Jones, Jain, Diwan and Jain. 2007. 'Effective oral delivery of insulin in animal models using vitamin b12-coated dextran nanoparticles', *Journal of Controlled Release*, 122: 141-50.

Chen, Einspanier and Schoen. 2015. 'Transepithelial electrical resistance (teer): A functional parameter to monitor the quality of oviduct epithelial cells cultured on filter supports', *Histochemistry and Cell Biology*, 144: 509-15.

Chen, Wang, Lu, Zhang, Fu and Luo. 2011. 'Cholesterol sequestration by nystatin enhances the uptake and activity of endostatin in endothelium via regulating distinct endocytic pathways', *Blood*, 117: 6392-403.

Chen, Zhao, Chen, Chen, Kuznetsova, Wong and Ojima. 2010. 'Mechanism-based tumor-targeting drug delivery system. Validation of efficient vitamin receptor-mediated endocytosis and drug release', *Bioconjugate Chemistry*, 21: 979-87.

Chivers, Koner, Lowe and Howarth. 2011. 'How the biotin-streptavidin interaction was made even stronger: Investigation via crystallography and a chimaeric tetramer', *The Biochemical journal*, 435: 55-63.

Commisso, Davidson, Soydaner-Azeloglu, Parker, Kamphorst, Hackett, Grabocka, Nofal, Drebin, Thompson, Rabinowitz, Metallo, Vander Heiden and Bar-Sagi. 2013. 'Macropinocytosis of protein is an amino acid supply route in ras-transformed cells', *Nature*, 497: 633-37.

Cooper. 2000. The cell: A molecular approach.

Coue and Engbersen. 2011. 'Functionalized linear poly(amidoamine)s are efficient vectors for intracellular protein delivery', *Journal of Controlled Release*, 152: 90-8.

Croyle, Patel, Tran, Gray, Zhang, Strong, Feldmann and Kobinger. 2008. 'Nasal delivery of an adenovirus-based vaccine bypasses pre-existing immunity to the vaccine carrier and improves the immune response in mice', *PloS One*, 3: e3548.

Dausend, Musyanovych, Dass, Walther, Schrezenmeier, Landfester and Mailänder. 2008. 'Uptake mechanism of oppositely charged fluorescent nanoparticles in hela cells', *Macromolecular Bioscience*, 8: 1135-43.

Davis. 2002. 'The origin of pegnology', *Advanced Drug Delivery Reviews*, 54: 457-8.

Dawson, Duda, Chae, Fukumura and Jain. 2009. 'Vegfr1 activity modulates myeloid cell infiltration in growing lung metastases but is not required for spontaneous metastasis formation', *PloS One*, 4: e6525.

De Carvalho and Quick. 2011. 'Surprising substrate versatility in slc5a6: Na+-coupled i- transport by the human na+/multivitamin transporter (hsmvt)', *Journal of Biological Chemistry*, 286: 131-7.

De Koker, De Geest, Cuvelier, Ferdinande, Deckers, Hennink, De Smedt and Mertens. 2007. 'In vivo cellular uptake, degradation and biocompatibility of polyelectrolyte microcapsules', *Advanced Functional Materials*, 17: 3754-63.

Delcour. 2009. 'Outer membrane permeability and antibiotic resistance', *Biochimica et Biophysica Acta*, 1794: 808-16.

Delos Santos, Bautista, Lucarelli, Bone, Dayam, Abousawan, Botelho and Antonescu. 2017. 'Selective regulation of clathrin-mediated epidermal growth factor receptor signaling and endocytosis by phospholipase c and calcium', *Molecular Biology of the Cell*, 28: 2802-18.

Depreter, Pilcer and Amighi. 2013. 'Inhaled proteins: Challenges and perspectives', *International Journal of Pharmaceutics*, 447: 251-80.

Dharmawardhane, Schürmann, Sells, Chernoff, Schmid and Bokoch. 2000. 'Regulation of macropinocytosis by p21-activated kinase-1', *Molecular Biology of the Cell*, 11: 3341-52.

Dix, Hassan, Obray, Shah and Wilson. 1990. 'The transport of vitamin b12 through polarized monolayers of caco-2 cells', *Gastroenterology*, 98: 1272-9.

Doherty and Mcmahon. 2009. 'Mechanisms of endocytosis', *Annual Review of Biochemistry*, 78: 857-902.

Dos Santos, Varela, Lynch, Salvati and Dawson. 2011. 'Effects of transport inhibitors on the cellular uptake of carboxylated polystyrene nanoparticles in different cell lines', *PloS One*, 6: e24438.

Dozier and Distefano. 2015. 'Site-specific pegylation of therapeutic proteins', *International Journal of Molecular Sciences*, 16: 25831-64.

Duncan and Gaspar. 2011. 'Nanomedicine(s) under the microscope', *Molecular Pharmaceutics*, 8: 2101-41.

Duncan and Vicent. 2013. 'Polymer therapeutics-prospects for 21st century: The end of the beginning', *Advanced Drug Delivery Reviews*, 65: 60-70.

Duncan, Ringsdorf and Satchi-Fainaro. 2006. 'Polymer therapeutics--polymers as drugs, drug and protein conjugates and gene delivery systems: Past, present and future opportunities', *Journal of Drug Targeting*, 14: 337-41.

Duncan. 2003. 'The dawning era of polymer therapeutics', *Nature Reviews Drug Discovery*, 2: 347-60.

Duncan. 2011. 'Polymer therapeutics as nanomedicines: New perspectives', *Current Opinion in Biotechnology*, 22: 492-501.

Duncan. 2014. 'Polymer therapeutics: Top 10 selling pharmaceuticals - what next?', *Journal of Controlled Release*, 190: 371-80.

Duret, Wauthoz, Merlos, Goole, Maris, Roland, Sebti, Vanderbist and Amighi. 2012. 'In vitro and in vivo evaluation of a dry powder endotracheal insufflator device for use in dose-dependent preclinical studies in mice', *European Journal of Pharmaceutics and Biopharmaceutics*, 81: 627-34.

Duro Castaño. 2015. 'Well-defined polyglutamates as carriers for the treatment of neurodegenerative diseases', http://purl.org/dc/dcmitype/Text, Universitat de València.

Duro-Castano, Conejos-Sánchez and Vicent. 2014. 'Peptide-based polymer therapeutics', *Polymers*, 6: 515-51.

Dutta and Donaldson. 2012. 'Search for inhibitors of endocytosis: Intended specificity and unintended consequences', *Cellular logistics*, 2: 203-08.

Dyawanapelly, Junnuthula and Singh. 2014. 'The holy grail of polymer therapeutics for cancer therapy: An overview on the pharmacokinetics and bio distribution', *Current Drug Metabolism*, 16.

Ekladious, Colson and Grinstaff. 2019. 'Polymer–drug conjugate therapeutics: Advances, insights and prospects', *Nature Reviews Drug Discovery*, 18: 273-94.

Elfinger, Maucksch and Rudolph. 2007. 'Characterization of lactoferrin as a targeting ligand for nonviral gene delivery to airway epithelial cells', *Biomaterials*, 28: 3448-55.

El-Sherbiny, El-Baz and Yacoub. 2015. 'Inhaled nano- and microparticles for drug delivery', *Global cardiology science & practice*, 2015: 2.

England, Conejos–Sánchez and Vicent. 2012. 'Chapter 8.2 drug delivery strategies: Polymer therapeutics.' in, *Nanostructured biomaterials for overcoming biological barriers* (The Royal Society of Chemistry).

Ernst, Klinger-Strobel, Arnold, Thamm, Hartung, Pletz, Makarewicz and Fischer. 2018. 'Polyester-based particles to overcome the obstacles of mucus and biofilms in the lung for tobramycin application under static and dynamic fluidic conditions', *European Journal of Pharmaceutics and Biopharmaceutics*, 131: 120-29.

Fahy and Dickey. 2010. 'Airway mucus function and dysfunction', *The New England journal of medicine*, 363: 2233-47.

Fazlollahi, Kim, Sipos, Hamm-Alvarez, Borok, Kim and Crandall. 2013. 'Nanoparticle translocation across mouse alveolar epithelial cell monolayers: Species-specific mechanisms', *Nanomedicine : nanotechnology, biology and medicine*, 9: 786-94.

Fielding and Fielding. 2000. 'Cholesterol and caveolae: Structural and functional relationships', *Biochimica et Biophysica Acta (BBA) - Molecular and Cell Biology of Lipids*, 1529: 210-22.

Fischer, Li, Ahlemeyer, Krieglstein and Kissel. 2003. 'In vitro cytotoxicity testing of polycations: Influence of polymer structure on cell viability and hemolysis', *Biomaterials*, 24: 1121-31.

Forstner. 1978. 'Intestinal mucins in health and disease', *Digestion*, 17: 234-63.

Foster, Langenback and Bergofsky. 1980. 'Measurement of tracheal and bronchial mucus velocities in man: Relation to lung clearance', *J Appl Physiol Respir Environ Exerc Physiol*, 48: 965-71.

Fowler, Vllasaliu, Falcone, Garnett, Smith, Horsley, Alexander and Stolnik. 2013. 'Uptake and transport of b(12)-conjugated nanoparticles in airway epithelium', *Journal of Controlled Release*, 172: 374-81.

Fowler, Vllasaliu, Trillo, Garnett, Alexander, Horsley, Smith, Whitcombe, Eaton and Stolnik. 2013b. 'Nanoparticle transport in epithelial cells: Pathway switching through bioconjugation', *Small*, 9: 3282-94.

Francia, Reker-Smit, Boel and Salvati. 2019. 'Limits and challenges in using transport inhibitors to characterize how nano-sized drug carriers enter cells', *Nanomedicine (Lond)*, 14: 1533-49.

Frokjaer and Otzen. 2005. 'Protein drug stability: A formulation challenge', *Nature Reviews: Drug Discovery*, 4: 298-306.

Fujita, Nelson, Daughton, Dobry, Spurzem, Irino and Rennard. 1990. 'Evaluation of elastase and antielastase balance in patients with chronic bronchitis and pulmonary emphysema', *American Review of Respiratory Disease*, 142: 57-62.

Gabay. 2006. 'Interleukin-6 and chronic inflammation', *Arthritis Research & Therapy*, 8: S3-S3.

Garcia-Verdugo, Descamps, Chignard, Touqui and Sallenave. 2010. 'Lung protease/anti-protease network and modulation of mucus production and surfactant activity', *Biochimie*, 92: 1608-17.

Garg, Tisdale, Haidari and Kokkoli. 2009. 'Targeting colon cancer cells using pegylated liposomes modified with a fibronectin-mimetic peptide', *International Journal of Pharmaceutics*, 366: 201-10.

Gauthier and Klok. 2010. 'Polymer-protein conjugates: An enzymatic activity perspective', *Polymer Chemistry*, 1: 1352-73.

Gekle, Drumm, Mildenberger, Freudinger, Gassner and Silbernagl. 1999. 'Inhibition of na+-h+ exchange impairs receptor-mediated albumin endocytosis in renal proximal tubule-derived epithelial cells from opossum', *Journal of Physiology*, 520 Pt 3: 709-21.

Gherasim, Lofgren and Banerjee. 2013. 'Navigating the b12 road: Assimilation, delivery and disorders of cobalamin', *Journal of Biological Chemistry*, 288: 13186-93.

Giannoni, Sawa, Allen, Wiener-Kronish and Hawgood. 2006. 'Surfactant proteins a and d enhance pulmonary clearance of pseudomonas aeruginosa', *American Journal of Respiratory Cell and Molecular Biology*, 34: 704-10.

Gibson, Wilson, Feil and Eyre-Walker. 2018. 'The distribution of bacterial doubling times in the wild', *Proceedings Biological sciences*, 285: 20180789.

Gizurarson, Marriott, Martin and Bechgaard. 1990. 'The influence of insulin and some excipients used in nasal insulin preparations on mucociliary clearance', *International Journal of Pharmaceutics*, 65: 243-47.

Grainger, Greenwell, Lockley, Martin and Forbes. 2006. 'Culture of calu-3 cells at the air interface provides a representative model of the airway epithelial barrier', *Pharmaceutical Research*, 23: 1482-90.

Grant and Donaldson. 2009. 'Pathways and mechanisms of endocytic recycling', *Nature reviews Molecular cell biology*, 10: 597-608.

Greco and Vicent. 2009. 'Combination therapy: Opportunities and challenges for polymer–drug conjugates as anticancer nanomedicines', *Advanced Drug Delivery Reviews*, 61: 1203-13.

Green, Allen, Bjørke-Monsen, Brito, Guéant, Miller, Molloy, Nexo, Stabler, Toh, Ueland and Yajnik. 2017. 'Vitamin b12 deficiency', *Nature Reviews Disease Primers*, 3: 17040.

Green. 1975. 'Avidin', *Advances in Protein Chemistry*, 29: 85-133.

Greenwald, Choe, Mcguire and Conover. 2003. 'Effective drug delivery by pegylated drug conjugates', *Advanced Drug Delivery Reviews*, 55: 217-50.

Groneberg, Witt, Wagner, Chung and Fischer. 2003. 'Fundamentals of pulmonary drug delivery', *Respiratory Medicine*, 97: 382-7.

Gunn, Ryan, Van Velkinburgh, Ernst and Miller. 2000. 'Genetic and functional analysis of a pmra-pmrb-regulated locus necessary for lipopolysaccharide modification, antimicrobial peptide resistance and oral virulence of salmonella enterica serovar typhimurium', *Infection and Immunity*, 68: 6139-46.

Guo, Zhang, Zheng, Zhang, Min, Wang, Cheon, Oak, Nah and Kim. 2015. 'Selectivity of commonly used inhibitors of clathrin-mediated and caveolae-dependent endocytosis of g protein-coupled receptors', *Biochimica et Biophysica Acta*, 1848: 2101-10.

Habibi, Kamaly, Memic and Shafiee. 2016. 'Self-assembled peptide-based nanostructures: Smart nanomaterials toward targeted drug delivery', *Nano today*, 11: 41-60.

Habraken, Heise and Thornton. 2012. 'Block copolypeptides prepared by n-carboxyanhydride ring-opening polymerization', *Macromolecular Rapid Communications*, 33: 272-86.

Habraken, Peeters, Dietz, Koning and Heise. 2010. 'How controlled and versatile is n-carboxy anhydride (nca) polymerization at 0

°C? Effect of temperature on homo-, block- and graft (co)polymerization', *Polymer Chemistry*, 1: 514-24.

Hadjichristidis, Iatrou, Pitsikalis and Sakellariou. 2009. 'Synthesis of well-defined polypeptide-based materials via the ring-opening polymerization of α-amino acid n-carboxyanhydrides', *Chemical Reviews*, 109: 5528-78.

Hamid-Akash, Rehman and Chen. 2015. 'Natural and synthetic polymers as drug carriers for delivery of therapeutic proteins', *Polymer Reviews*, 55: 371-406.

Harada and Kataoka. 1998. 'Novel polyion complex micelles entrapping enzyme molecules in the core: Preparation of narrowly-distributed micelles from lysozyme and poly(ethylene glycol)−poly(aspartic acid) block copolymer in aqueous medium', *Macromolecules*, 31: 288-94.

Harada-Shiba, Yamauchi, Harada, Takamisawa, Shimokado and Kataoka. 2002. 'Polyion complex micelles as vectors in gene therapy--pharmacokinetics and in vivo gene transfer', *Gene Therapy*, 9: 407-14.

Harris and Chess. 2003. 'Effect of pegylation on pharmaceuticals', *Nature Reviews: Drug Discovery*, 2: 214-21.

Harshita, Barkat, Beg, Pottoo and Ahmad. 2019. 'Nanopaclitaxel therapy: An evidence based review on the battle for next-generation formulation challenges', *Nanomedicine: Nanotechnology, Biology and Medicine*, 14: 1323-41.

He, Liu, Scally, Manaloto, Gunes, Ng, Maher, Tiwari, Byrne, Bourke, Tian, Cullen and Curtin. 2020. 'Cold atmospheric plasma stimulates clathrin-dependent endocytosis to repair oxidised membrane and enhance uptake of nanomaterial in glioblastoma multiforme cells', *Scientific Reports*, 10: 6985-85.

Healthcare. 2007. 'Pd-10 desalting columns', General Electric Company, Accessed 21st Feb. file:///C:/Users/paxhll/Downloads/PD10manual%20(1).pdf.

Heinemann, Klappoth, Rave, Hompesch, Linkeschowa and Heise. 2000. 'Intra-individual variability of the metabolic effect of

inhaled insulin together with an absorption enhancer', *Diabetes Care*, 23: 1343-7.

Hershfield, Buckley, Greenberg, Melton, Schiff, Hatem, Kurtzberg, Markert, Kobayashi, Kobayashi and Et Al. 1987. 'Treatment of adenosine deaminase deficiency with polyethylene glycol-modified adenosine deaminase', *New England Journal of Medicine*, 316: 589-96.

Hickey. 2003. Pharmaceutical inhalation aerosol technology (Taylor & Francis Group).

Hobro and Smith. 2017. 'An evaluation of fixation methods: Spatial and compositional cellular changes observed by raman imaging', *Vibrational Spectroscopy*, 91: 31-45.

Hoiby, Ciofu and Bjarnsholt. 2010. 'Pseudomonas aeruginosa biofilms in cystic fibrosis', *Future Microbiology*, 5: 1663-74.

Hollinshead, Sanderson and Vaux. 1997. 'Anti-biotin antibodies offer superior organelle-specific labeling of mitochondria over avidin or streptavidin', *Journal of Histochemistry and Cytochemistry*, 45: 1053-7.

Hua. 2019. 'Physiological and pharmaceutical considerations for rectal drug formulations', *Frontiers in Pharmacology*, 10: 1196-96.

Hussain, Arnold, Khan and Ahsan. 2004. 'Absorption enhancers in pulmonary protein delivery', *Journal of Controlled Release*, 94: 15-24.

Hussain, Leong, Ng and Chu. 2011. 'The essential role of clathrin-mediated endocytosis in the infectious entry of human enterovirus 71', *Journal of Biological Chemistry*, 286: 309-21.

Huth, Schubert and Peschka-Süss. 2006. 'Investigating the uptake and intracellular fate of ph-sensitive liposomes by flow cytometry and spectral bio-imaging', *Journal of Controlled Release*, 110: 490-504.

Illum. 2000. 'Transport of drugs from the nasal cavity to the central nervous system', *European Journal of Pharmaceutical Sciences*, 11: 1-18.

Itoh, Nishino and Hatabu. 2004. 'Architecture of the lung: Morphology and function', *Journal of Thoracic Imaging*, 19: 221-7.

Ivanov. 2008. 'Pharmacological inhibition of endocytic pathways: Is it specific enough to be useful?' in Andrei I. Ivanov (ed.), *Exocytosis and endocytosis* (Humana Press: Totowa, NJ).

Iversen, Skotland and Sandvig. 2011. 'Endocytosis and intracellular transport of nanoparticles: Present knowledge and need for future studies', *Nano today*, 6: 176-85.

Janoff, Raju and Dearing. 1983. 'Levels of elastase activity in bronchoalveolar lavage fluids of healthy smokers and nonsmokers', *American Review of Respiratory Disease*, 127: 540-4.

Jones, Jones, Riffo-Vasquez, Spina, Hoffman, Morgan, Patel, Page, Forbes and Dailey. 2014. 'Quantitative assessment of nanoparticle surface hydrophobicity and its influence on pulmonary biocompatibility', *Journal of Controlled Release*, 183: 94-104.

Jung, Maiti, Lee, Lee and Kim. 2014. 'Rational design of biotin–disulfide–coumarin conjugates: A cancer targeted thiol probe and bioimaging', *Chemical Communications*, 50: 3044-47.

Kaksonen and Roux. 2018. 'Mechanisms of clathrin-mediated endocytosis', *Nature Reviews: Molecular Cell Biology*, 19: 313-26.

Kalaydina, Bajwa, Qorri, Decarlo and Szewczuk. 2018. 'Recent advances in "smart" delivery systems for extended drug release in cancer therapy', *Int J Nanomedicine*, 13: 4727-45.

Kataoka, Matsumoto, Yokoyama, Okano, Sakurai, Fukushima, Okamoto and Kwon. 2000. 'Doxorubicin-loaded poly(ethylene glycol)-poly(beta-benzyl-l-aspartate) copolymer micelles: Their pharmaceutical characteristics and biological significance', *Journal of Controlled Release*, 64: 143-53.

Kateb, Chiu, Black, Yamamoto, Khalsa, Ljubimova, Ding, Patil, Portilla-Arias, Modo, Moore, Farahani, Okun, Prakash, Neman, Ahdoot, Grundfest, Nikzad and Heiss. 2011. 'Nanoplatforms for constructing new approaches to cancer treatment, imaging

and drug delivery: What should be the policy?', *Neuroimage*, 54 Suppl 1: S106-24.

Kim, Park, Kim, Chi, Lee, Song, Jiang, Lim, Youn and Lee. 2012. 'Low molecular weight (1 kda) polyethylene glycol conjugation markedly enhances the hypoglycemic effects of intranasally administered exendin-4 in type 2 diabetic db/db mice', *Biological and Pharmaceutical Bulletin*, 35: 1076-83.

Kisich, Heifets, Higgins and Diamond. 2001. 'Antimycobacterial agent based on mrna encoding human β-defensin 2 enables primary macrophages to restrict growth of mycobacterium tuberculosis', *Infection and Immunity*, 69: 2692-99.

Kissel and Werner. 1998. 'Nasal delivery of peptides: An in vitro cell culture model for the investigation of transport and metabolism in human nasal epithelium', *Journal of Controlled Release*, 53: 195-203.

Klok. 2005. 'Biological–synthetic hybrid block copolymers: Combining the best from two worlds', *Journal of Polymer Science Part A: Polymer Chemistry*, 43: 1-17.

Klonoff. 2014. 'Afrezza inhaled insulin: The fastest-acting fda-approved insulin on the market has favorable properties', *Journal of Diabetes Science and Technology*, 8: 1071-73.

Koch-Weser, Sidel, Frderman, Kanarek, Finer and Eaton. 1970. 'Adverse effects of sodium colistimethate: Manifestations and specific reaction rates during 317 courses of therapy', *Annals of Internal Medicine*, 72: 857-68.

Koivusalo, Welch, Hayashi, Scott, Kim, Alexander, Touret, Hahn and Grinstein. 2010. 'Amiloride inhibits macropinocytosis by lowering submembranous ph and preventing rac1 and cdc42 signaling', *The Journal of cell biology*, 188: 547-63.

Kompella and Lee. 2001. 'Delivery systems for penetration enhancement of peptide and protein drugs: Design considerations', *Advanced Drug Delivery Reviews*, 46: 211-45.

Kozyraki and Cases. 2013. 'Vitamin b12 absorption: Mammalian physiology and acquired and inherited disorders', *Biochimie*, 95: 1002-07.

Kricheldorf. 2006. 'Polypeptides and 100 years of chemistry of alpha-amino acid n-carboxyanhydrides', *Angewandte Chemie, International Edition in English*, 45: 5752-84.

Kuhn, Vanhecke, Michen, Blank, Gehr, Petri-Fink and Rothen-Rutishauser. 2014. 'Different endocytotic uptake mechanisms for nanoparticles in epithelial cells and macrophages', *Beilstein journal of nanotechnology*, 5: 1625-36.

Kuhnert, Boerlin and Frey. 2000. 'Target genes for virulence assessment of escherichia coli isolates from water, food and the environment', *FEMS Microbiology Reviews*, 24: 107-17.

Kumar, Dailey and Forbes. 2014. 'Lost in translation: What is stopping inhaled nanomedicines from realizing their potential?', *Therapeutic Delivery*, 5: 757-61.

Kurinomaru and Shiraki. 2015. 'Noncovalent pegylation of l-asparaginase using pegylated polyelectrolyte', *Journal of Pharmaceutical Sciences*, 104: 587-92.

Kurinomaru, Maruyama, Izaki, Handa, Kimoto and Shiraki. 2014. 'Protein–poly(amino acid) complex precipitation for high-concentration protein formulation', *Journal of Pharmaceutical Sciences*, 103: 2248-54.

Labiris and Dolovich. 2003. 'Pulmonary drug delivery. Part i: Physiological factors affecting therapeutic effectiveness of aerosolized medications', *British Journal of Clinical Pharmacology*, 56: 588-99.

Laffleur and Bernkop-Schnurch. 2013. 'Strategies for improving mucosal drug delivery', *Nanomedicine (Lond)*, 8: 2061-75.

Lam, Armes and Stolnik. 2011. 'The involvement of microtubules and actin filaments in the intracellular transport of non-viral gene delivery system', *Journal of Drug Targeting*, 19: 56-66.

Le and Nabi. 2003. 'Distinct caveolae-mediated endocytic pathways target the golgi apparatus and the endoplasmic reticulum', *Journal of Cell Science*, 116: 1059-71.

Leal, Smyth and Ghosh. 2017. 'Physicochemical properties of mucus and their impact on transmucosal drug delivery', *International Journal of Pharmaceutics*, 532: 555-72.

Lee, Loo, Traini and Young. 2015. 'Inhalation of nanoparticle-based drug for lung cancer treatment: Advantages and challenges', *Asian Journal of Pharmaceutical Sciences*, 10: 481-89.

Lee, Sahu, Jang and Tae. 2015. 'The effect of ligand density on in vivo tumor targeting of nanographene oxide', *Journal of Controlled Release*, 209: 219-28.

Lee, Wang, Ye, Yoon, Chan and Yang. 2008. 'Efficient intracellular delivery of functional proteins using cationic polymer core/shell nanoparticles', *Biomaterials*, 29: 1224-32.

Lehr, Bouwstra, Tukker and Junginger. 1990. 'Intestinal transit of bioadhesive microspheres in an in situ loop in the rat—a comparative study with copolymers and blends based on poly(acrylic acid)', *Journal of Controlled Release*, 13: 51-62.

Levine. 1987. 'Escherichia coli that cause diarrhea: Enterotoxigenic, enteropathogenic, enteroinvasive, enterohemorrhagic and enteroadherent', *Journal of Infectious Diseases*, 155: 377-89.

Li and Arakawa. 2019. 'Agarose native gel electrophoresis of proteins', *International Journal of Biological Macromolecules*, 140: 668-71.

Li, Li, Li, Zhang, Li and Chen. 2019. 'Fluorescent reconstitution on deposition of pm2.5 in lung and extrapulmonary organs', *Proceedings of the National Academy of Sciences of the United States of America*, 116: 2488-93.

Li, Nation, Milne, Turnidge and Coulthard. 2005. 'Evaluation of colistin as an agent against multi-resistant gram-negative bacteria', *International Journal of Antimicrobial Agents*, 25: 11-25.

Li, Nation, Turnidge, Milne, Coulthard, Rayner and Paterson. 2006. 'Colistin: The re-emerging antibiotic for multidrug-resistant gram-negative bacterial infections', *The Lancet Infectious Diseases*, 6: 589-601.

Li, Turnidge, Milne, Nation and Coulthard. 2001. 'In vitro pharmacodynamic properties of colistin and colistin methanesulfonate against pseudomonas aeruginosa isolates from patients with cystic fibrosis', *Antimicrobial Agents and Chemotherapy*, 45: 781-5.

Liechty, Kryscio, Slaughter and Peppas. 2010. 'Polymers for drug delivery systems', *Annual review of chemical and biomolecular engineering*, 1: 149-73.

Liechty, Kryscio, Slaughter and Peppas. 2010. 'Polymers for drug delivery systems', *Annual review of chemical and biomolecular engineering*, 1: 149-73.

Lim, Ly anderson, Yang, Macander, Jarkowski, Forrest, Bulitta and Tsuji. 2010. 'Resurgence of colistin: A review of resistance, toxicity, pharmacodynamics and dosing', *Pharmacotherapy*, 30: 1279-91.

Livnah, Bayer, Wilchek and Sussman. 1993. 'Three-dimensional structures of avidin and the avidin-biotin complex', *Proceedings of the National Academy of Sciences*, 90: 5076-80.

Lochhead and Thorne. 2012. 'Intranasal delivery of biologics to the central nervous system', *Advanced Drug Delivery Reviews*, 64: 614-28.

Lodish, Berk, Zipursky, Matsudaira, Baltimore and Darnell. 2000. *Molecular cell biology* (New York).

Loira-Pastoriza, Todoroff and Vanbever. 2014. 'Delivery strategies for sustained drug release in the lungs', *Advanced Drug Delivery Reviews*, 75: 81-91.

Lombry, Edwards, Preat and Vanbever. 2004. 'Alveolar macrophages are a primary barrier to pulmonary absorption of macromolecules', *American Journal of Physiology: Lung Cellular and Molecular Physiology*, 286: L1002-8.

Lorén, Hagman, Jonasson, Deschout, Bernin, Cella-Zanacchi, Diaspro, Mcnally, Ameloot, Smisdom, Nydén, Hermansson, Rudemo and Braeckmans. 2015. 'Fluorescence recovery after

photobleaching in material and life sciences: Putting theory into practice', *Quarterly Reviews of Biophysics*, 48: 323-87.

Lowery, Brubaker, Kuhlmann and Kovacs. 2013. 'The aging lung', *Clinical Interventions in Aging*, 8: 1489-96.

Lu, Zhang, Li, Luo, Wang, Guan, Ma, Zhao, Wei and Lei. 2017. 'Preparation and properties of reversible hydrogels based on triblock poly(amino acid)s with tunable ph-responsivity across a broad range', *Journal of Polymer Science Part A: Polymer Chemistry*, 55: 207-12.

Lumiprobe. 2018. 'Nhs ester labeling of amino biomolecules', Accessed 23 Jun. https://www.lumiprobe.com/protocols/nhs-ester-labeling.

Lv, Zhang, Wang, Cui and Yan. 2006. 'Toxicity of cationic lipids and cationic polymers in gene delivery', *Journal of Controlled Release*, 114: 100-09.

Macia, Ehrlich, Massol, Boucrot, Brunner and Kirchhausen. 2006. 'Dynasore, a cell-permeable inhibitor of dynamin', *Developmental Cell*, 10: 839-50.

Mahammad and Parmryd. 2015. 'Cholesterol depletion using methyl-β-cyclodextrin.' in Dylan M. Owen (ed.), *Methods in membrane lipids* (Springer New York: New York, NY).

Maiti, Park, Han, Jeon, Lee, Bhuniya, Kang and Kim. 2013. 'Gemcitabine–coumarin–biotin conjugates: A target specific theranostic anticancer prodrug', *Journal of the American Chemical Society*, 135: 4567-72.

Manzanares and Ceña. 2020. 'Endocytosis: The nanoparticle and submicron nanocompounds gateway into the cell', *Pharmaceutics*, 12: 371.

Mayor and Pagano. 2007. 'Pathways of clathrin-independent endocytosis', *Nature Reviews Molecular Cell Biology*, 8: 603-12.

Mcmahon. 2002. 'Biotin in metabolism and molecular biology', *Annual Review of Nutrition*, 22: 221-39.

Mcphee, Bains, Winsor, Lewenza, Kwasnicka, Brazas, Brinkman and Hancock. 2006. 'Contribution of the phop-phoq and pmra-pmrb two-component regulatory systems to mg2+-induced gene regulation in pseudomonas aeruginosa', *Journal of Bacteriology*, 188: 3995-4006.

Meng, Engbers and Feijen. 2004. 'Polyethylene glycol-grafted polystyrene particles', *Journal of Biomedical Materials Research, Part A*, 70: 49-58.

Menon, Ravikumar, Pise, Gyawali, Hsia and Nguyen. 2014. 'Polymeric nanoparticles for pulmonary protein and DNA delivery', *Acta Biomaterialia*, 10: 2643-52.

Meredith, Salameh and Banks. 2015. 'Intranasal delivery of proteins and peptides in the treatment of neurodegenerative diseases', *American Association of Pharmaceutical Scientists Journal*, 17: 780-7.

Merimsky, Gez, Weitzen, Nehushtan, Rubinov, Hayat, Peretz, Ben-Shahar, Biran, Katsenelson, Mermershtein, Loven, Karminsky, Neumann, Matcejevsky and Inbar. 2004. 'Targeting pulmonary metastases of renal cell carcinoma by inhalation of interleukin-2', *Annals of Oncology*, 15: 610-2.

Mero, Schiavon, Pasut, Veronese, Emilitri and Ferruti. 2009. 'A biodegradable polymeric carrier based on peg for drug delivery', *Journal of Bioactive and Compatible Polymers*, 24: 220-34.

Mettlen, Chen, Srinivasan, Danuser and Schmid. 2018. 'Regulation of clathrin-mediated endocytosis', *Annual Review of Biochemistry*, 87: 871-96.

Michael and Curiel. 1994. 'Strategies to achieve targeted gene delivery via the receptor-mediated endocytosis pathway', *Gene Therapy*, 1: 223-32.

Möller, Häussinger, Ziegler-Heitbrock and Heyder. 2006. 'Mucociliary and long-term particle clearance in airways of patients with immotile cilia', *Respiratory Research*, 7: 10-10.

Montaner, Da Silva, Sun, Sutterwala, Hollinshead, Vaux and Gordon. 1999. 'Type 1 and type 2 cytokine regulation of macrophage

endocytosis: Differential activation by il-4/il-13 as opposed to ifn-gamma or il-10', *Journal of Immunology*, 162: 4606-13.

Moradi, Vllasaliu, Garnett, Falcone and Stolnik. 2012. 'Ligand density and clustering effects on endocytosis of folate modified nanoparticles', *RSC Advances*, 2: 3025-33.

Morales, Fathe, Brunaugh, Ferrati, Li, Montenegro-Nicolini, Mousavikhamene, Mcconville, Prausnitz and Smyth. 2017. 'Challenges and future prospects for the delivery of biologics: Oral mucosal, pulmonary and transdermal routes', *American Association of Pharmaceutical Scientists Journal*, 19: 652-68.

Morello, Krone, Dickerson, Howerth, Germishuizen, Wong, Edwards, Bloom and Hondalus. 2009. 'Dry-powder pulmonary insufflation in the mouse for application to vaccine or drug studies', *Tuberculosis*, 89: 371-7.

Mostov, Su and Ter Beest. 2003. 'Polarized epithelial membrane traffic: Conservation and plasticity', *Nature Cell Biology*, 5: 287-93.

Motley , Bright , Seaman and Robinson 2003. 'Clathrin-mediated endocytosis in ap-2–depleted cells', *Journal of Cell Biology*, 162: 909-18.

Mueller, Capelle, Seyrek, Martel, Carrupt, Arvinte and Borchard. 2012. 'Noncovalent pegylation: Different effects of dansyl-, l-tryptophan–, phenylbutylamino-, benzyl- and cholesteryl-pegs on the aggregation of salmon calcitonin and lysozyme', *Journal of Pharmaceutical Sciences*, 101: 1995-2008.

Mukherjee, Morales-Scheihing, Butler and Soto. 2015. 'Type 2 diabetes as a protein misfolding disease', *Trends in Molecular Medicine*, 21: 439-49.

Murray, Attridge and Morona. 2003. 'Regulation of salmonella typhimurium lipopolysaccharide o antigen chain length is required for virulence; identification of fepe as a second wzz', *Molecular Microbiology*, 47: 1395-406.

Mutch, Howden, Jenner, Poulter and Rappoport. 2014. 'Polarised clathrin-mediated endocytosis of egfr during chemotactic invasion', *Traffic (Copenhagen, Denmark)*, 15: 648-64.

Narai, Arai and Shimizu. 1997. 'Rapid decrease in transepithelial electrical resistance of human intestinal caco-2 cell monolayers by cytotoxic membrane perturbents', *Toxicology in Vitro*, 11: 347-54.

Nation, Li, Cars, Couet, Dudley, Kaye, Mouton, Paterson, Tam, Theuretzbacher, Tsuji and Turnidge. 2015. 'Framework for optimisation of the clinical use of colistin and polymyxin b: The prato polymyxin consensus', *The Lancet Infectious Diseases*, 15: 225-34.

National-Cancer-Institute. 2017. Accessed 22 Jun. https://training.seer.cancer.gov/anatomy/respiratory/passages/.

Nemeth, Oesch and Kuster. 2014. 'Bacteriostatic versus bactericidal antibiotics for patients with serious bacterial infections: Systematic review and meta-analysis', *Journal of Antimicrobial Chemotherapy*, 70: 382-95.

Ng, Tang, Li, Ong, Yung and Bay. 2015. 'Clathrin-mediated endocytosis of gold nanoparticles in vitro', *Anat Rec (Hoboken)*, 298: 418-27.

Nicod. 2005. 'Lung defences: An overview', *European Respiratory Review*, 14: 45-50.

Nieto-Orellana, Coghlan, Rothery, Falcone, Bosquillon, Childerhouse, Mantovani and Stolnik. 2018. 'Dry-powder formulations of non-covalent protein complexes with linear or miktoarm copolymers for pulmonary delivery', *International Journal of Pharmacognosy*, 540: 78-88.

Nieto-Orellana, Di Antonio, Conte, Falcone, Bosquillon, Childerhouse, Mantovani and Stolnik. 2017. 'Effect of polymer topology on non-covalent polymer-protein complexation: Miktoarm versus linear mpeg-poly(glutamic acid) copolymers', *Polymer Chemistry*, 8: 2210-20.

Nieto-Orellana, Li, Rosiere, Wauthoz, Williams, Monteiro, Bosquillon, Childerhouse, Keegan, Coghlan, Mantovani and Stolnik. 2019. 'Targeted peg-poly(glutamic acid) complexes for inhalation protein delivery to the lung', *Journal of Controlled Release*, 316: 250-62.

Nikaido. 2003. 'Molecular basis of bacterial outer membrane permeability revisited', *Microbiology and Molecular Biology Reviews*, 67: 593-656.

Oberdorster, Oberdorster and Oberdorster. 2005. 'Nanotoxicology: An emerging discipline evolving from studies of ultrafine particles', *Environmental Health Perspectives*, 113: 823-39.

Oh, Horner, Witkiewicz and Schnitzer. 2012. 'Endothelin induces rapid, dynamin-mediated budding of endothelial caveolae rich in et-b', *Journal of Biological Chemistry*, 287: 17353-62.

Ojima, Lichtenthal, Lee, Wang and Wang. 2016. 'Taxane anticancer agents: A patent perspective', *Expert Opinion on Therapeutic Patents*, 26: 1-20.

Orlandi and Fishman. 1998. 'Filipin-dependent inhibition of cholera toxin: Evidence for toxin internalization and activation through caveolae-like domains', *Journal of Cell Biology*, 141: 905-15.

Owens, Zinman and Bolli. 2003. 'Alternative routes of insulin delivery', *Diabetic Medicine*, 20: 886-98.

Paranjpe and Müller-Goymann. 2014. 'Nanoparticle-mediated pulmonary drug delivery: A review', *International Journal of Molecular Sciences*, 15: 5852-73.

Parton, Joggerst and Simons. 1994. 'Regulated internalization of caveolae', *Journal of Cell Biology*, 127: 1199-215.

Pathak and Malviya. 2020. 'Introduction, theories and mechanisms of bioadhesion.' in.

Patil and Sarasija. 2012. 'Pulmonary drug delivery strategies: A concise, systematic review', *Lung India : Official Organ of Indian Chest Society*, 29: 44-49.

Patil, Freches, Karmani, Duncan, Ucakar, Suk, Hanes, Gallez and Vanbever. 2018. 'Fate of pegylated antibody fragments following delivery to the lungs: Influence of delivery site, peg size and lung inflammation', *Journal of Controlled Release*, 272: 62-71.

Patlolla, Swamy, Raju and Rao. 2004. 'Overexpression of caveolin-1 in experimental colon adenocarcinomas and human colon cancer cell lines', *Oncology Reports*, 11: 957-63.

Patton, Fishburn and Weers. 2004. 'The lungs as a portal of entry for systemic drug delivery', *Proceedings of the American Thoracic Society*, 1: 338-44.

Patwa and Shah. 2015. 'Anatomy and physiology of respiratory system relevant to anaesthesia', *Indian Journal of Anaesthesia*, 59: 533-41.

Pelkmans, Püntener and Helenius. 2002. 'Local actin polymerization and dynamin recruitment in sv40-induced internalization of caveolae', *Science*, 296: 535-39.

Peppas and Carr. 2009. 'Impact of absorption and transport on intelligent therapeutics and nano-scale delivery of protein therapeutic agents', *Chemical Engineering Science*, 64: 4553-65.

Pernodet, Maaloum and Tinland. 1997. 'Pore size of agarose gels by atomic force microscopy', *Electrophoresis*, 18: 55-58.

Pirooznia, Hasannia, Lotfi and Ghanei. 2012. 'Encapsulation of alpha-1 antitrypsin in plga nanoparticles: In vitro characterization as an effective aerosol formulation in pulmonary diseases', *J Nanobiotechnology*, 10: 20.

Pisal, Kosloski and Balu-Iyer. 2010. 'Delivery of therapeutic proteins', *Journal of Pharmaceutical Sciences*, 99: 2557-75.

Pluen, Netti, Jain and Berk. 1999. 'Diffusion of macromolecules in agarose gels: Comparison of linear and globular configurations', *Biophysical Journal*, 77: 542-52.

Prasad, Wang, Kekuda, Fujita, Fei, Devoe, Leibach and Ganapathy. 1998. 'Cloning and functional expression of a cdna encoding a mammalian sodium-dependent vitamin transporter mediating the uptake of pantothenate, biotin and lipoate', *Journal of Biological Chemistry*, 273: 7501-6.

Prompruk, Govender, Zhang, Xiong and Stolnik. 2005. 'Synthesis of a novel peg-block-poly(aspartic acid-stat-phenylalanine)

copolymer shows potential for formation of a micellar drug carrier', *International Journal of Pharmaceutics*, 297: 242-53.

Pubchem. 'Pubchem compound summary for cid 171548, biotin', National Center for Biotechnology Information, Accessed 20 Aug. https://pubchem.ncbi.nlm.nih.gov/compound/Biotin

Pubchem. 'Pubchem compound summary for cid 6613, pantothenic acid. ', National Center for Biotechnology Information (2020). Accessed 20 Aug. https://pubchem.ncbi.nlm.nih.gov/compound/Pantothenic-acid.

Quick and Shi. 2015. 'The sodium/multivitamin transporter: A multipotent system with therapeutic implications', *Vitamins and Hormones*, 98: 63-100.

Ramteke. 2012. 'Solid lipid nanoparticles: A review', *IOSR Journal of Pharmacy*.

Reddy and Low. 1998. 'Folate-mediated targeting of therapeutic and imaging agents to cancers', *Critical Reviews in Therapeutic Drug Carrier Systems*, 15: 587-627.

Rees, Clark and Morén. 1982. 'The importance of particle size in response to inhaled bronchodilators', *European Journal of Respiratory Diseases Supplement*, 119: 73-8.

Rejman, Oberle, Zuhorn and Hoekstra. 2004. 'Size-dependent internalization of particles via the pathways of clathrin- and caveolae-mediated endocytosis', *The Biochemical journal*, 377: 159-69.

Ren and Torres. 2009. 'Role of interleukin-1beta during pain and inflammation', *Brain Research Reviews*, 60: 57-64.

Ren, Han, Uhm, Jang, Kang, Kim and Kim. 2015. 'Recent development of biotin conjugation in biological imaging, sensing and target delivery', *Chemical Communications*, 51: 10403-18.

Rittig, Kaufmann, Robins, Shaw, Sprenger, Gemsa, Foulongne, Rouot and Dornand. 2003. 'Smooth and rough lipopolysaccharide phenotypes of brucella induce different intracellular trafficking and cytokine/chemokine release in

human monocytes', *Journal of Leukocyte Biology*, 74: 1045-55.

Rodal, Skretting, Garred, Vilhardt, Van Deurs and Sandvig. 1999. 'Extraction of cholesterol with methyl-beta-cyclodextrin perturbs formation of clathrin-coated endocytic vesicles', *Molecular Biology of the Cell*, 10: 961-74.

Rodriguez-Martinez, Sola, Castillo, Cintron-Colon, Rivera-Rivera, Barletta and Griebenow. 2008. 'Stabilization of alpha-chymotrypsin upon pegylation correlates with reduced structural dynamics', *Biotechnology and Bioengineering*, 101: 1142-9.

Rohatagi, Calic, Harding, Ozoux, Bouriot, Kirkesseli, Deleij and Jensen. 2000. 'Pharmacokinetics, pharmacodynamics and safety of inhaled cyclosporin a (adi628) after single and repeated administration in healthy male and female subjects and asthmatic patients', *Journal of Clinical Pharmacology*, 40: 1211-26.

Rosiere, Van Woensel, Mathieu, Langer, Mathivet, Vermeersch, Amighi and Wauthoz. 2016. 'Development and evaluation of well-tolerated and tumor-penetrating polymeric micelle-based dry powders for inhaled anti-cancer chemotherapy', *International Journal of Pharmacognosy*, 501: 148-59.

Rubin and Williams. 2014. 'Emerging aerosol drug delivery strategies: From bench to clinic', *Advanced Drug Delivery Reviews*, 75: 141-8.

Russell-Jones, Arthur and Walker. 1999. 'Vitamin b12-mediated transport of nanoparticles across caco-2 cells', *International Journal of Pharmacognosy*, 179: 247-55.

Russell-Jones, Mctavish, Mcewan, Rice and Nowotnik. 2004. 'Vitamin-mediated targeting as a potential mechanism to increase drug uptake by tumours', *Journal of Inorganic Biochemistry*, 98: 1625-33.

Russell-Jones, Westwood and Habberfield. 1995. 'Vitamin b12 mediated oral delivery systems for granulocyte-colony stimulating factor and erythropoietin', *Bioconjugate Chemistry*, 6: 459-65.

Russo, Davidson, Carlino-Macdonald, Helinski, Priore and Knight. 2003. 'The effects of escherichia coli capsule, o-antigen, host neutrophils and complement in a rat model of gram-negative pneumonia', *FEMS Microbiology Letters*, 226: 355-61.

Sabnis, Klöckner, Becce, Hagart, Evans, Furniss, Mavridou, Larrouy-Maumus, Stevens and Edwards. 2020. 'Colistin kills bacteria by targeting lipopolysaccharide in the cytoplasmic membrane', *bioRxiv*: 479618.

Saeed, Kolokoltsov, Albrecht and Davey. 2010. 'Cellular entry of ebola virus involves uptake by a macropinocytosis-like mechanism and subsequent trafficking through early and late endosomes', *PLoS Pathogens*, 6: e1001110.

Saeed, Magnusson, Moradi, Soliman, Wang, Stolnik, Thurecht, Howdle and Alexander. 2011. 'Modular construction of multifunctional bioresponsive cell-targeted nanoparticles for gene delivery', *Bioconjugate Chemistry*, 22: 156-68.

Sahay, Querbes, Alabi, Eltoukhy, Sarkar, Zurenko, Karagiannis, Love, Chen, Zoncu, Buganim, Schroeder, Langer and Anderson. 2013. 'Efficiency of sirna delivery by lipid nanoparticles is limited by endocytic recycling', *Nature Biotechnology*, 31: 653-58.

Sahay, Querbes, Alabi, Eltoukhy, Sarkar, Zurenko, Karagiannis, Love, Chen, Zoncu, Buganim, Schroeder, Langer and Anderson. 2013. 'Efficiency of sirna delivery by lipid nanoparticles is limited by endocytic recycling', *Nature Biotechnology*, 31: 653-58.

Sahib, Darwis, Peh, Abdulameer and Tan. 2011. 'Rehydrated sterically stabilized phospholipid nanomicelles of budesonide for nebulization: Physicochemical characterization and in vitro, in vivo evaluations', *Int J Nanomedicine*, 6: 2351-66.

Said and Nexo. 2018. 'Chapter 54 - intestinal absorption of water-soluble vitamins: Cellular and molecular mechanisms.' in Hamid M. Said (ed.), *Physiology of the gastrointestinal tract (sixth edition)* (Academic Press).

Said. 1999. 'Cellular uptake of biotin: Mechanisms and regulation', *The Journal of Nutrition*, 129: 490S-93S.

Salamat-Miller, Chittchang and Johnston. 2005. 'The use of mucoadhesive polymers in buccal drug delivery', *Advanced Drug Delivery Reviews*, 57: 1666-91.

Salmaso, Bersani, Mastrotto, Tonon, Schrepfer, Genovese and Caliceti. 2012. 'Self-assembling nanocomposites for protein delivery: Supramolecular interactions between peg-cholane and rh-g-csf', *Journal of Controlled Release*, 162: 176-84.

Salmaso, Bersani, Scomparin, Balasso, Brazzale, Barattin and Caliceti. 2014. 'A novel soluble supramolecular system for sustained rh-gh delivery', *Journal of Controlled Release*, 194: 168-77.

Sampath and Pollard. 1991. 'Effects of cytochalasin, phalloidin and ph on the elongation of actin filaments', *Biochemistry*, 30: 1973-80.

Sanchis, Canal, Lucas and Vicent. 2010. 'Polymer-drug conjugates for novel molecular targets', *Nanomedicine (Lond)*, 5: 915-35.

Sanders, Rudolph, Braeckmans, De Smedt and Demeester. 2009. 'Extracellular barriers in respiratory gene therapy', *Advanced Drug Delivery Reviews*, 61: 115-27.

Sandvig, Kavaliauskiene and Skotland. 2018. 'Clathrin-independent endocytosis: An increasing degree of complexity', *Histochemistry and Cell Biology*, 150: 107-18.

Santos, Ursu, Gaulton, Bento, Donadi, Bologa, Karlsson, Al-Lazikani, Hersey, Oprea and Overington. 2017. 'A comprehensive map of molecular drug targets', *Nature Reviews: Drug Discovery*, 16: 19-34.

Santra, Kaittanis, Santiesteban and Perez. 2011. 'Cell-specific, activatable and theranostic prodrug for dual-targeted cancer imaging and therapy', *Journal of the American Chemical Society*, 133: 16680-88.

Santra, Kaittanis, Santiesteban and Perez. 2011. 'Cell-specific, activatable and theranostic prodrug for dual-targeted cancer imaging and therapy', *Journal of the American Chemical Society*, 133: 16680-88.

Sayers, Magnusson, Moody, Mastrotto, Conte, Brazzale, Borri, Caliceti, Watson, Mantovani, Aylott, Salmaso, Jones and Alexander. 2018. 'Switching of macromolecular ligand display by thermoresponsive polymers mediates endocytosis of multiconjugate nanoparticles', *Bioconjugate Chemistry*, 29: 1030-46.

Scheinberg, Villa, Escorcia and Mcdevitt. 2010. 'Conscripts of the infinite armada: Systemic cancer therapy using nanomaterials', *Nature Reviews: Clinical Oncology*, 7: 266-76.

Schnitzer, Oh, Pinney and Allard. 1994. 'Filipin-sensitive caveolae-mediated transport in endothelium: Reduced transcytosis, scavenger endocytosis and capillary permeability of select macromolecules', *The Journal of cell biology*, 127: 1217-32.

Schuster, Suk, Woodworth and Hanes. 2013. 'Nanoparticle diffusion in respiratory mucus from humans without lung disease', *Biomaterials*, 34: 3439-46.

Scientific. 2011. "Calculate dye:Protein (f/p) molar ratios." In.: Thermo Fisher Scientific Inc.

Seliverstova and Prutskova. 2015. 'Receptor-mediated endocytosis of lysozyme in renal proximal tubules of the frog rana temporaria', *European Journal of Histochemistry*, 59: 2482.

Seubwai, Wongkham, Puapairoj, Khuntikeo and Wongkham. 2007. 'Overexpression of vitamin d receptor indicates a good prognosis for cholangiocarcinoma: Implications for therapeutics', *Cancer*, 109: 2497-505.

Shin, Han, Kumar, Lee, Sessler, Kim and Kim. 2016. 'Programmed activation of cancer cell apoptosis: A tumor-targeted phototherapeutic topoisomerase i inhibitor', *Scientific Reports*, 6: 29018-18.

Simons and Toomre. 2000. 'Lipid rafts and signal transduction', *Nature Reviews Molecular Cell Biology*, 1: 31-39.

Simpson. 2010. 'Rapid coomassie blue staining of protein gels', *Cold Spring Harb Protoc*, 2010: pdb.prot5413.

Singer, Baker, De Vries, Kumar, Shaffer, Vawter, Bolton and Garzone. 2003. "Poly-(l)-glutamic acid-paclitaxel (ct-2103)

[xyotax™], a biodegradable polymeric drug conjugate: Characterization, preclinical pharmacology and preliminary clinical data." In *Advances in Experimental Medicine and Biology*, 81-99.

Sivadas, O'rourke, Tobin, Buckley, Ramtoola, Kelly, Hickey and Cryan. 2008. 'A comparative study of a range of polymeric microspheres as potential carriers for the inhalation of proteins', *International Journal of Pharmacognosy*, 358: 159-67.

Smart and Anderson. 2002. 'Alterations in membrane cholesterol that affect structure and function of caveolae.' in Chandan K. Sen and Lester Packer (eds.), *Methods in enzymology* (Academic Press).

South. 1971. 'Enteropathogenic escherichia coli disease: New developments and perspectives', *Journal of Pediatrics*, 79: 1-11.

Steinman, Mellman, Muller and Cohn. 1983. 'Endocytosis and the recycling of plasma membrane', *The Journal of cell biology*, 96: 1-27.

Stellwagen. 2009. 'Chapter 23 gel filtration1.' in Richard R. Burgess and Murray P. Deutscher (eds.), *Methods in enzymology* (Academic Press).

Stolnik and Shakesheff. 2009. 'Formulations for delivery of therapeutic proteins', *Biotechnology Letters*, 31: 1-11.

Stone, Mercer, Gehr, Stockstill and Crapo. 1992. 'Allometric relationships of cell numbers and size in the mammalian lung', *American Journal of Respiratory Cell and Molecular Biology*, 6: 235-43.

Takano, Koyama, Nishikawa, Murakami and Yumoto. 2004. 'Segment-selective absorption of lysozyme in the intestine', *European Journal of Pharmacology*, 502: 149-55.

Taylor, Luther and Donnenberg. 1999. 'Expression of the espb protein of enteropathogenic escherichia coli within hela cells affects stress fibers and cellular morphology', *Infection and Immunity*, 67: 120-5.

Tekle, Deurs, Sandvig and Iversen. 2008. 'Cellular trafficking of quantum dot-ligand bioconjugates and their induction of changes in normal routing of unconjugated ligands', *Nano Letters*, 8: 1858-65.

Tho and Škalko-Basnet. 2016. '3.6 - cell-based in vitro models for vaginal permeability studies.' in Bruno Sarmento (ed.), *Concepts and models for drug permeability studies* (Woodhead Publishing).

Thorley and Tetley. 2007. 'Pulmonary epithelium, cigarette smoke and chronic obstructive pulmonary disease', *International Journal of Chronic Obstructive Pulmonary Disease*, 2: 409-28.

Tobio, Sanchez, Vila, Soriano, Evora, Vila-Jato and Alonso. 2000. 'The role of peg on the stability in digestive fluids and in vivo fate of peg-pla nanoparticles following oral administration', *Colloids and Surfaces B: Biointerfaces*, 18: 315-23.

Toremalm. 1960. 'The daily amoung of tracheo-bronchial secretions in man. A method for continuous tracheal aspiration in laryngectomized and tracheotomized patients', *Acta Oto-Laryngologica Supplementum*, 158: 43-53.

Torgersen, Skretting, Van Deurs and Sandvig. 2001. 'Internalization of cholera toxin by different endocytic mechanisms', *Journal of Cell Science*, 114: 3737-47.

Tran, Velkov, Nation, Forrest, Tsuji, Bergen and Li. 2016. 'Pharmacokinetics/pharmacodynamics of colistin and polymyxin b: Are we there yet?', *International Journal of Antimicrobial Agents*, 48: 592-97.

Tripodo, Mandracchia, Collina and Rossi. 2014. 'New perspectives in cancer therapy: The biotin-antitumor molecule conjugates', *Medicinal Chemistry*.

Tsiourvas, Sideratou, Sterioti, Papadopoulos, Nounesis and Paleos. 2012. 'Insulin complexes with pegylated basic oligopeptides', *Journal of Colloid and Interface Science*, 384: 61-72.

Tsujimoto, Gotoh and Nishino. 1999. 'Diffusion of macrolide antibiotics through the outer membrane of moraxella

catarrhalis', *Journal of Infection and Chemotherapy*, 5: 196-200.

Tuma and Hubbard. 2003. 'Transcytosis: Crossing cellular barriers', *Physiological Reviews*, 83: 871-932.

Turecek, Bossard, Schoetens and Ivens. 2016. 'Pegylation of biopharmaceuticals: A review of chemistry and nonclinical safety information of approved drugs', *Journal of Pharmaceutical Sciences*, 105: 460-75.

Uchida, Ito, Ohtsuki, Kubo, Suzuki and Terasaki. 2015. 'Major involvement of na+-dependent multivitamin transporter (slc5a6/smvt) in uptake of biotin and pantothenic acid by human brain capillary endothelial cells', *Journal of Neurochemistry*, 134: 97-112.

Ugwoke, Verbeke and Kinget. 2001. 'The biopharmaceutical aspects of nasal mucoadhesive drug delivery', *Journal of Pharmacy and Pharmacology*, 53: 3-21.

Valastyan and Lindquist. 2014. 'Mechanisms of protein-folding diseases at a glance', *Disease Models & Mechanisms*, 7: 9-14.

Vallance and Finlay. 2000. 'Exploitation of host cells by enteropathogenic escherichia coli', *Proceedings of the National Academy of Sciences*, 97: 8799-806.

Van Der Walle. 2011. *Peptide and protein delivery* (Academic Press: Boston).

Van Rijn. 2013. 'Polymer directed protein assemblies', *Polymers*, 5: 576.

Velino, Carella, Adamiano, Sanguinetti, Vitali, Catalucci, Bugli and Iafisco. 2019. 'Nanomedicine approaches for the pulmonary treatment of cystic fibrosis', *Front Bioeng Biotechnol*, 7: 406.

Velkov, Thompson, Nation and Li. 2010. 'Structure--activity relationships of polymyxin antibiotics', *Journal of Medicinal Chemistry*, 53: 1898-916.

Vercauteren, Vandenbroucke, Jones, Rejman, Demeester, De Smedt, Sanders and Braeckmans. 2010. 'The use of inhibitors

to study endocytic pathways of gene carriers: Optimization and pitfalls', *Molecular Therapy*, 18: 561-9.

Vila, Sanchez, Tobio, Calvo and Alonso. 2002. 'Design of biodegradable particles for protein delivery', *Journal of Controlled Release*, 78: 15-24.

Vllasaliu. 2010. 'In vitro investigation into strategies for mucosal delivery of proteins', the University of Nottingham.

Vranic, Boggetto, Contremoulins, Mornet, Reinhardt, Marano, Baeza-Squiban and Boland. 2013. 'Deciphering the mechanisms of cellular uptake of engineered nanoparticles by accurate evaluation of internalization using imaging flow cytometry', *Particle and Fibre Toxicology*, 10: 2.

Vyas, Singh and Sihorkar. 2001. 'Ligand-receptor-mediated drug delivery: An emerging paradigm in cellular drug targeting', *Critical Reviews in Therapeutic Drug Carrier Systems*, 18: 1-76.

Walker, Tarannum and Vivero-Escoto. 2016. 'Cellular endocytosis and trafficking of cholera toxin b-modified mesoporous silica nanoparticles', *Journal of Materials Chemistry B*, 4: 1254-62.

Wall and Lanutti. 1993. 'High levels of exopeptidase activity are present in rat and canine bronchoalveolar lavage fluid', *International Journal of Pharmaceutics*, 97: 171-81.

Wang, Fan, Chen and Terentjev. 2015. 'Bacterial growth, detachment and cell size control on polyethylene terephthalate surfaces', *Scientific Reports*, 5: 15159.

Wang, Henning and Heber. 2010. 'Limitations of mtt and mts-based assays for measurement of antiproliferative activity of green tea polyphenols', PloS One, 5: e10202-e02.

Wang, Rothberg and Anderson. 1993. 'Mis-assembly of clathrin lattices on endosomes reveals a regulatory switch for coated pit formation', *Journal of Cell Biology*, 123: 1107-17.

Wauthoz, Deleuze, Hecq, Roland, Saussez, Adanja, Debeir, Decaestecker, Mathieu, Kiss and Amighi. 2010. 'In vivo assessment of temozolomide local delivery for lung cancer

inhalation therapy', *European Journal of Pharmaceutical Sciences*, 39: 402-11.

Wibowo, Sulistio, Wong, Blencowe and Qiao. 2014. 'Polypeptide films via n-carboxyanhydride ring-opening polymerization (nca-rop): Past, present and future', *Chemical Communications (Cambridge, England)*, 50: 4971-88.

Widdel. 2007. 'Theory and measurement of bacterial growth', *Di dalam Grundpraktikum Mikrobiologie*, 4: 1-11.

Wilchek, Bayer and Livnah. 2006. 'Essentials of biorecognition: The (strept)avidin-biotin system as a model for protein-protein and protein-ligand interaction', *Immunology Letters*, 103: 27-32.

Wine. 1999. 'The genesis of cystic fibrosis lung disease', *Journal of Clinical Investigation*, 103: 309-12.

Wong, Scales and Reilly. 2007. 'DNA internalized via caveolae requires microtubule-dependent, rab7-independent transport to the late endocytic pathway for delivery to the nucleus', *Journal of Biological Chemistry*, 282: 22953-63.

Yamamoto, Hoshina, Kurashima, Takeuchi, Kawashima, Yokoyama and Tsujimoto. 2007. 'Engineering of poly(dl-lactic-co-glycolic acid) nanocomposite particles for dry powder inhalation dosage forms of insulin with the spray-fluidized bed granulating system', *Advanced Powder Technology*, 18: 215-28.

Yamamoto, Okumura, Fukuda, Fukui, Takahashi and Muranishi. 1997. 'Improvement of the pulmonary absorption of (asu1,7)-eel calcitonin by various absorption enhancers and their pulmonary toxicity in rats', *Journal of Pharmaceutical Sciences*, 86: 1144-7.

Yamanaka and Leong. 2008. 'Engineering strategies to enhance nanoparticle-mediated oral delivery', *Journal of Biomaterials Science, Polymer Edition*, 19: 1549-70.

Yang, Cheng, Xu, Wang and Wen. 2009. 'Targeting cancer cells with biotin–dendrimer conjugates', *European Journal of Medicinal Chemistry*, 44: 862-68.

Yang, Peters and Williams. 2008. 'Inhaled nanoparticles--a current review', *International Journal of Pharmacognosy*, 356: 239-47.

Youn, Jeon, Chae, Lee and Lee. 2008. 'Pegylation improves the hypoglycaemic efficacy of intranasally administered glucagon-like peptide-1 in type 2 diabetic db/db mice', *Diabetes, Obesity & Metabolism*, 10: 343-6.

Youn, Kwon, Na, Chae, Lee and Lee. 2008. 'Improved intrapulmonary delivery of site-specific pegylated salmon calcitonin: Optimization by peg size selection', *Journal of Controlled Release*, 125: 68-75.

Yumoto, Suzuka, Oda, Nagai and Takano. 2012. 'Endocytic uptake of fitc-albumin by human alveolar epithelial cell line a549', *Drug Metabolism and Pharmacokinetics*, 27: 336-43.

Zempleni and Mock. 1998. 'Uptake and metabolism of biotin by human peripheral blood mononuclear cells', *American Journal of Physiology*, 275: C382-8.

Zempleni and Mock. 1999. 'Human peripheral blood mononuclear cells:: Inhibition of biotin transport by reversible competition with pantothenic acid is quantitatively minor', *The Journal of Nutritional Biochemistry*, 10: 427-32.

Zhang, Chen, Feng, Shao, Liu, Zhang, Pang and Jiang. 2014a. 'Intranasal nanoparticles of basic fibroblast growth factor for brain delivery to treat alzheimer's disease', *International Journal of Pharmaceutics*, 461: 192-202.

Zhang, Liu and Wan. 2014b. 'Discussion about several potential drawbacks of pegylated therapeutic proteins', *Biological and Pharmaceutical Bulletin*, 37: 335-9.

Zhang, Wu, Chan and Watanabe. 2011. 'Formation, characterization and fate of inhaled drug nanoparticles', *Advanced Drug Delivery Reviews*, 63: 441-55.

Zhao, Fang, Wang, Tang and Wang. 2010. 'Involvement of type ii pneumocytes in the pathogenesis of chronic obstructive pulmonary disease', *Respiratory Medicine*, 104: 1391-95.

Zhao, Han, Bae and Manickam. 2019. 'Lucifer yellow - a robust paracellular permeability marker in a cell model of the human blood-brain barrier', *J Vis Exp*.

Zihni, Mills, Matter and Balda. 2016. 'Tight junctions: From simple barriers to multifunctional molecular gates', Nature Reviews Molecular Cell Biology, 17: 564-80.